

**M A S A R Y K O V A  
U N I V E R Z I T A**

LÉKAŘSKÁ FAKULTA

**Kontinuálně rostoucí  
řezáky a morfogeneze  
zubu**

Habilitační práce

Mgr. Jan Křivánek, Ph.D.

Obor: Anatomie, Histologie a Embryologie

Brno 2022



**MUNI**  
MED

## Bibliografický záznam

**Autor:** Mgr. Jan Křivánek, Ph.D.  
Lékařská fakulta  
Masarykova univerzita  
Ústav histologie a embryologie

**Obor:** Anatomie, Histologie a Embryologie

**Název práce česky:** Kontinuálně rostoucí řezáky a morfogeneze zubu

**Rok:** 2022

**Počet stran:** 175

**Klíčová slova:** Kontinuálně rostoucí řezáky, Morfogeneze, Odontogeneze, Zuby, Kmenové buňky, Dentin, Sklovina

## Bibliographic record

**Author:** Mgr. Jan Křivánek, Ph.D.  
Faculty of Medicine  
Masaryk University  
Department of Histology and Embryology

**Field:** Anatomy, Histology and Embryology

**Title of Thesis:** Continuously growing incisors and tooth morphogenesis

**Year:** 2022

**Number of Pages:** 175

**Keywords:** Continuously growing incisors, Morphogenesis, Odontogenesis, Teeth, Stem cells, Dentin, Enamel

## Anotace

Studium biologie kmenových buněk, vývoje a morfogeneze jednotlivých částí organismu je základním předpokladem pro vytvoření nových terapeutických přístupů regenerativní medicíny. Tato práce shrnuje a komentuje ucelený soubor autorských prací, které se věnují vývoji, růstu, buněčnému složení a vnitřní mikrostruktuře tvrdých zubních tkání u několika organismů. Jako výchozí modelový systém zde slouží kontinuálně rostoucí myši řezáky. Tento zajímavý typ zubů umožňuje sledovat nejen tvorbu dentinu a skloviny od její samotné iniciace, ale zejména přináší možnost studovat niche kmenových buněk, které stojí za jejím neustálým růstem.

## **Abstract**

The study of stem cell biology, development, and morphogenesis of different parts of the organism is a basic prerequisite for the development of new therapeutic approaches in regenerative medicine. This work summarizes and comments on comprehensive research focused on the development, growth, cellular composition, and microstructure of hard dental tissues in several organisms. As the main model system serves here continuously growing mouse incisors. This peculiar tooth type allows not only to follow the formation of dentin and enamel from its initiation, but in particular brings the possibility to study the stem cell niche responsible for its continuous growth.



## Čestné prohlášení

Prohlašuji, že jsem habilitační práci na téma **Kontinuálně rostoucí řezáky a morfogeneze zubu** zpracoval sám. Veškeré prameny a zdroje informací, které jsem použil k sepsání této práce, byly citovány v textu a jsou uvedeny v seznamu použitých pramenů a literatury.

V Brně 8. dubna 2022

.....  
Mgr. Jan Křivánek, Ph.D.



## Poděkování

Rád bych využil tohoto prostoru, abych poděkoval všem lidem, s nimiž se střetly naše pracovní nebo osobní cesty a bez kterých bych tuhle práci nikdy nepsal. Předně se jedná o mou rodinu, a to hlavně manželku Katku a syna Františka, kteří mi každý den přinášejí lásku, radost, štěstí a nekonečnou podporu. Dále bych z celého srdce rád poděkoval svým rodičům, kteří za mnou vždy stáli a byli mi oporou, bráchovi a všem ostatním.

Během svého dosavadního pracovního života jsem měl tu čest poznat celou řadu vynikajících výzkumníků a lidí, kteří mi často byli inspirací a jejich práce velkou motivací. Ačkoliv tento prostor není dostatečně dlouhý na to, abych všechny vyjmenoval, a protože bych určitě na někoho zapomněl, nebudu se o to ani pokoušet. Přesto bych však rád zmínil tři klíčové osoby, které hrály a hrají důležitou roli v mém pracovním životě a kterým bych rád upřímně poděkoval (v abecedním pořadí). Jsou to Igor Adameyko, v jehož laboratoři jsem mohl strávit několik skvělých let a který mi byl a je nekonečnou inspirací i podporou. Dále bych rád poděkoval Marcelle Buchtové za její vytrvalost, nezlomnost a za naše společné diskuse, jež mě vždy dokáží motivovat. V neposlední řadě bych rád srdečně poděkoval Aleši Hamplovi za to, že mě provází od samotného počátku mého vědeckého života a za to, že mi vždy poskytoval skvělé pracovní zázemí i osobní podporu.

Mé velké díky samozřejmě náleží i všem kolegům a přátelům, s nimiž nejen spolupracujeme, pijeme kávu, ale věnujeme si vzájemně svůj čas i mimo práci. Závěrem bych rád poděkoval všem členům naší výzkumné skupinky, bez kterých by to nešlo. Vážím si vaší práce a děkuji vám za ni.

Úplně na závěr děkuji všem mým múzám, jež mě provází životem.

**Děkuji!**

# Obsah

<b>Seznam obrázků</b>	<b>13</b>
<b>Seznam pojmů a zkratk</b>	<b>14</b>
<b>1 Úvod</b>	<b>15</b>
<b>2 Teoretický úvod</b>	<b>16</b>
2.1 Zuby a dentice .....	16
2.2 Vývoj zubu .....	16
2.2.1 Morfogeneze zubních tkání.....	17
2.1 Mechanismus tvorby hlavních tvrdých tkání zubu a vznik kořene .....	22
2.1.1 Vznik skloviny .....	22
2.1.2 Vznik dentinu .....	24
2.1.3 Vznik kořene .....	25
2.2 Kontinuálně rostoucí zuby .....	27
2.3 Niche kmenových buněk.....	29
2.3.1 Kmenové buňky a „ <i>lineage tracing</i> “ .....	31
2.3.2 Epiteliální a mezenchymální kmenové buňky.....	32
2.3.3 Využití metody scRNA-seq ve studiu kmenových buněk .....	33
<b>3 Komentáře k přiloženým publikacím</b>	<b>37</b>
3.1 Komentář k přiložené publikaci číslo 1 .....	37
3.2 Komentář k přiložené publikaci číslo 2 .....	40
3.3 Komentář k přiložené publikaci číslo 3 .....	41
3.4 Komentář k přiložené publikaci číslo 4 .....	42
3.5 Komentář k přiložené publikaci číslo 5 .....	43
3.6 Komentář k přiložené publikaci číslo 6 .....	44
3.7 Komentář k přiložené publikaci číslo 7 .....	46
<b>4 Závěr</b>	<b>47</b>
<b>Použité zdroje</b>	<b>48</b>

## 5 Přílohy

Chyba! Záložka není definována.

5.1	Příloha A – Publikace číslo 1.....	<b>Chyba! Záložka není definována.</b>
5.2	Příloha B – Publikace číslo 2.....	85
5.3	Příloha C – Publikace číslo 3.....	110
5.4	Příloha D – Publikace číslo 4.....	121
5.5	Příloha E – Publikace číslo 5.....	134
5.6	Příloha F – Publikace číslo 6.....	146
5.7	Příloha G – Publikace číslo 7.....	159



## Seznam obrázků

**Obrázek 1:** Schéma vývoje zubu.

**Obrázek 2:** Tři různé typy prvních dolních molárů podle výšky korunky.

**Obrázek 3:** Organizace apikální růstové části kontinuálně rostoucího myšího řezáku.

## Seznam pojmů a zkratk

Brachyodontní zuby	- Typ zubů s nízkou korunkou a omezeným růstem
<i>Cre</i> rekombináza	- Enzym zprostředkávající rekombinaci mezi loxP místy
Cuboidal layer	- Vrstva kubických buněk pod ameloblasty nacházející se ve vrstvě stratum intermedium
DEJ	- Dentino-sklovinná hranice; Dentin-enamel junction
Dentální lamina	- Dentální lišta; epiteliální záhyb stojící na počátku vývoje zubu
Dentice	- Chrup; soubor zubů v ústní dutině
ECM	- Extracelulární matrix; Mezibuněčná hmota
ERM	- Malassezovy epiteliální zbytky; Epithelial rests of Malassez
FACS	- Fluorescenčně aktivované třídění buněk; Fluorescence-activated cell sorting
HERS	- Hertwigova epitelová kořenová pochva; Hertwig's epithelial root sheath
Hypselodontní zuby	- Typ zubů s kontinuálním růstem
Hypsodontní zuby	- Typ zubů s vysokou korunkou a prodlouženým růstem
IHC	- Imunohistochemie
ISH	- In situ hybridizace
Lineage tracing	- Metoda genetického označení za účelem sledování vývojového osudu buněk
Niche kmenových buněk	- Nika, mikroprostředí kmenových buněk
Monofyodontní dentice	- Jednogeneční chrup - v průběhu života není první generace zubů nahrazena
scRNA-seq	- Transkriptomika na úrovni jednotlivých buněk; single-cell RNA-sequencing
Tamoxifen	- Látka, která umožňuje časování genetické rekombinace u fúzního cre-ER systému
Transkriptom	- Soubor všech RNA transkriptů

# 1 Úvod

Zuby jsou často chápány jako jednoduché zvápenaté útvary nacházející se na začátku trávicí trubice s jedinou funkcí – mechanické rozmělnění potravy. Opak je však pravdou. Zuby vykazují velice komplexní vnitřní uspořádání, které jim jednak umožňuje aktivně reagovat na změny vnějšího prostředí a jednak jim dává vlastnosti, které zabezpečují jejich dlouhodobou životaschopnost, často trvajících i několik desítek let. Když vezmeme v potaz, že se vlastní tvrdé tkáně zubu průběžně nepřestavují, tak jako je tomu u kosti, jde o pozoruhodné vlastnosti.

Kromě zmíněných vlastností těchto tvrdých zubních tkání, které umožňují dlouhodobou životnost a udržení správné funkce zubů, se uvnitř každého zdravého zubu nachází živá zubní pulpa, jejímž prostřednictvím je zub inervován a vyživován. Tato část zubu přitahuje zvláštní pozornost, protože se obecně má za to, že se zde nachází kmenové buňky s širokým diferenciačním potenciálem. Studium zubní pulpy na buněčné úrovni tak může v budoucnu poskytnout cenný zdroj buněk s kmenovými vlastnostmi použitelnými v regenerativní medicíně.

V následující práci jsou sumarizovány dosavadní ucelené výsledky bádání věnující se vývoji zubu, kmenovým buňkám, morfogenezi skloviny a dentinu na mikroskopické úrovni nebo studiu složení a funkce zubu na buněčné úrovni za využití pokročilých technik. Většinu těchto komentovaných prací spojuje využití permanentně rostoucího myšího řezáku při studiu výše zmíněných jevů. Využití tohoto modelového orgánu s sebou přináší četné výhody, kterých je v prezentovaných pracích různými způsoby využito. Kromě myších řezáků je však pozornost věnována i jiným typům zubů, jako jsou myší nebo lidské moláry, a dentici jiných modelových organismů.

Studium a porovnání fungování a vývoje zubu u prezentovaných organismů tak přináší širší kontext umožňující zobecnění separátně pozorovaných jevů.

## 2 Teoretický úvod

### 2.1 Zuby a dentice

Zuby jsou vysoce specializované, mineralizované útvary umístěné na samém počátku trávicí soustavy. Celkový soubor zubů v ústní dutině se nazývá chrup neboli dentice. Ačkoliv primární funkcí dentice je získávání a prvotní mechanické zpracování potravy, slouží i jako důležitý prvek při sociálních interakcích a v některých případech i jako senzorický orgán.

Z evolučního pohledu bylo vyvinutí zubů zásadním vývojovým milníkem, který je spolu s několika dalšími důležitými vývojovými novinkami neoddělitelně spojený s neurální lištou (Gans and Northcutt, 1983). Vznik tohoto souboru buněk zapříčinil vývoj mnoha zcela nových struktur a orgánů. Zuby tak společně s ostatními deriváty neurální lišty poskytly jejich vlastníkům schopnost rychlého přizpůsobení měnícím se vnějším podmínkám a v konečném důsledku i nový způsob života – predaci (Bronner and LeDouarin, 2012; Le Douarin and Dupin, 2018, 2012). Vznikly tak obratlovci, nová a velmi rozmanitá skupina živočichů, jež osídlila prakticky všechny ekologické niky a stala se dominantními a nejvíce vyvinutými organismy.

Od doby vývoje prvních zubů došlo adaptací k pozoruhodné specializaci funkce, tvarů, počtu, ukotvení v čelisti, schopnosti obnovy nebo vnitřní mikrostruktury zubů napříč různými druhy živočichů.

### 2.2 Vývoj zubu

Zuby se stejně jako několik dalších struktur v těle vyvíjí vzájemnou interakcí mezi epitelem a ektomezenchymem. Ze zubního epitelu, který pochází z ektodermu (případně endodermu), vzniká jednak sklovinu tvořící sklovinný orgán a jednak transienční epiteliální záhyb, podléjící se na tvorbě kořene (Fraser et al., 2010; Krivanek et al., 2017; Soukup et al., 2008). Z ektomezenchymu, který pochází

z neurální lišty, vzniká jak vnitřní část zubu – zubní pulpa včetně odontoblastů a dentinu, tak i celé blízké okolí zubu včetně cementu, periodoncia a alveolární kosti. Na finální stavbě a funkci zubu se kromě těchto dvou hlavních struktur podílí ještě buňky nervového systému – axony s asociovanými gliovými buňkami, krevní cévy s asociovanými perivaskulárními buňkami a buňky imunitního systému z nichž, jak bylo ukázáno, mnohé vystupují z krevního řečiště a trvale osidlují tkáň uvnitř zubu i v jeho okolí (Krivanek et al., 2020, 2017).

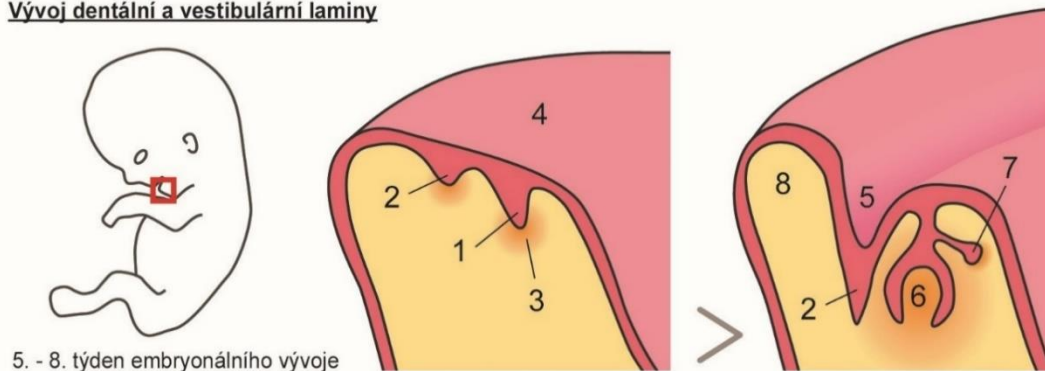
Ačkoliv je mezidruhová variabilita ve stavbě, geometrii, funkci nebo mechanismech růstu a obnovy zubu/dentice obrovská, zůstávají vývojové mechanismy na molekulární i buněčné úrovni velmi podobné. Finální rozdíly jsou dány spíše lehkou modifikací v jednotlivých signalizačních drahách než fundamentálně rozdílnými vývojovými procesy (Tummers and Thesleff, 2009). Evoluční konzervace mechanismů vývoje zubu může být ukázkově prezentována nejen u jednotlivých skupin obratlovců majících zuby (savci, plazi, obojživelníci, ryby), ale i u třídy ptáků, kteří ztratili zuby před 70–80 miliony let (Krivanek et al., 2017). Kokultivační experimenty ukázaly, že ptačí embryonální epitel může po společné kultivaci s myším ektomezenchymem iniciovat vývoj zubu a stejně tak tomu je i v opačném případě (Mitsiadis et al., 2003; Wang et al., 1998). Molekulární procesy, které zapříčiňují interakci mezi těmito dvěma tkáněmi, jsou tak desítky milionů let konzervované a principiálně se nezměnily. Tyto procesy zahrnují prakticky všechny hlavní skupiny signalizačních drah jako jsou: WNT, FGF, BMP nebo SHH (Balic and Thesleff, 2015; Thesleff, 2015).

### **2.2.1 Morfogeneze zubních tkání**

Vývoj zubu je schematicky prezentován na příkladu lidské dentice v obrázku 1. Prochází přes několik charakteristických stádií: Stádium zubní plakody, pupene, čepičky, zvonku a apozice (produkce tvrdých zubních tkání). Iniciací vývoje zubu a plynulý přechod mezi jednotlivými stádii je zprostředkován vzájemnou interakcí mezi

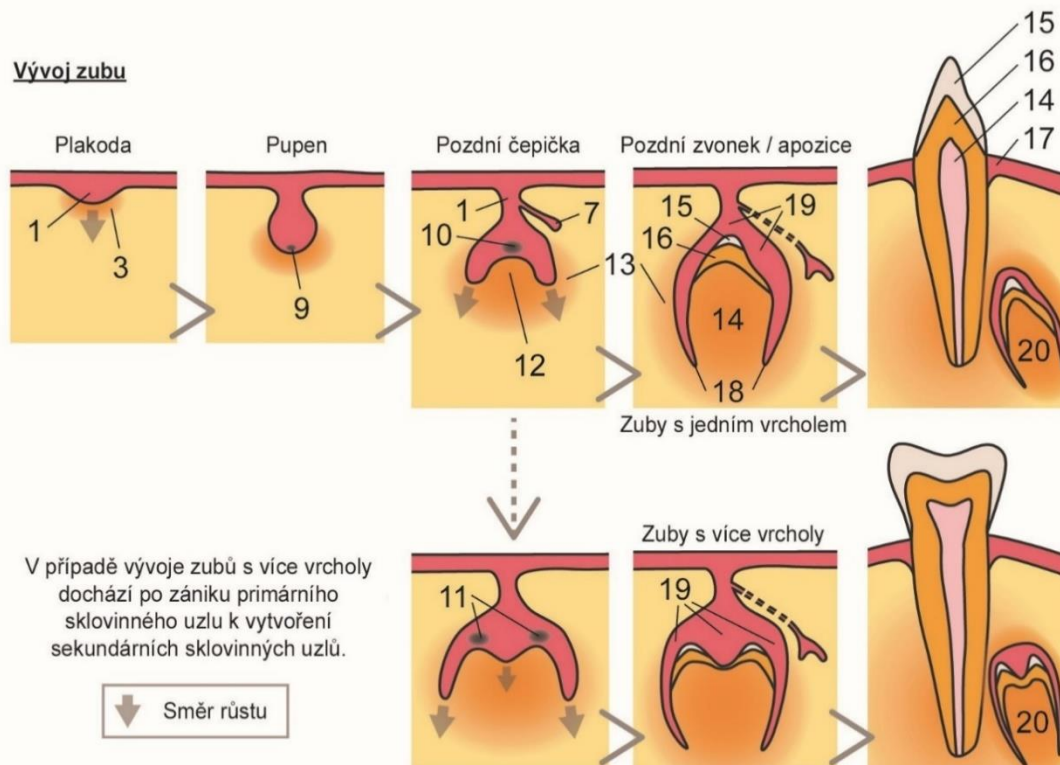
(orálním) epitelem a přiléhajícím ektomezenchymem, podobně, jak je tomu při vývoji mnoha jiných struktur, jako jsou například vlasové folikuly, peří nebo slinné a mléčné žlázy (Dassule and McMahon, 1998; Sanders, 2011).

Vývoj dentální a vestibulární laminy



5. - 8. týden embryonálního vývoje

Vývoj zubu



**Obrázek 1: Schéma vývoje zubu.** (1) Zubní lišta, (2) vestibulární lišta, (3) kondenzovaný ektomezenchym (původem z neurální lišty), (4) orální epitel, (5) vestibulum oris, (6) základ zubu primární dentice, (7) náhradní zubní lišta (základ pro zub trvalé dentice), (8) vyvíjející se ret, (9) vznikající primární sklovinný uzal, (10) primární sklovinný uzal, (11) sekundární sklovinné uzly, (12) zubní papila, (13) zubní folikul, (14) zubní pulpa, (15) sklovina, (16) zubovina – dentin, (17) dásněň, (18) cervikální epitelové kličky (HERS – Hertwigova epitelální kořenová pochva), (19) sklovinný orgán, (20) vyvíjející se zub sekundární dentice. Autor: Jan Křivánek.

Na samém počátku vývoje zubu dochází k migraci buněk neurální lišty pod orální epitel. Buňky epitelu jsou stimulovány k proliferaci a vytváří se tak dentální lamina (dentální lišta), první epiteliální záhyb, který tvoří společný základ celé dentice. V místech vzniku jednotlivých zubů pak dochází k zesílení epitelu a na protilehlé straně i k proliferaci přilehlých mezenchymálních buněk. Vzniká tak prvotní zubní základ, zubní plakoda. Další proliferací buněk epitelu se zubní plakoda mění v jednoduchý epitelový útvar vrůstající do mezenchymu – zubní pupen. Následuje stádium čepičky, které se od pupene morfologicky liší tím, že jeho okraje přerůstají střed (někdejší vrchol pupene) a začíná se tak utvářet mezenchymální zubní papila. Toto přerůstání epitelu je spíše než zrychlením proliferace periferních částí čepičky způsobeno zastavením proliferace vrcholu pupene a vytvořením důležitého signálního centra – primárního sklovinného uzlu (Obrázek 1). V tomto okamžiku dochází v mezenchymální části zubu k prvotní specializaci buněk, vnořením mezenchymálních buněk mezi přerůstající zubní epitel. Dochází tak k diferenciaci částí mezenchymu na zubní papilu a zubní folikul. Ze zubní papily se vytvoří zubní pulpa s odontoblasty (produkující dentin) a ze zubního folikulu pak vznikají části závěsného aparátu zubu: periodontální ligamenta, cement a alveolární kost

Dalším prodlužováním periferních částí epitelu dochází k formování zubního pohárku, ve kterém je již jasně patrná stratifikace epitelu i diferenciaci mezenchymu. Z epitelu se tak formuje sklovinný orgán, v němž již mohou být rozlišeny čtyři základní vrstvy: vnitřní sklovinný epitel, vnější sklovinný epitel, hvězdicové retikulum a *stratum intermedium*. Vnitřní sklovinný epitel a vnější sklovinný epitel se navzájem potkávají v záhybu cervikální kličky. Mezi těmito dvěma hraničními vrstvami leží hvězdicové retikulum, které je charakteristické svou řídkou a neuspořádanou strukturou, v níž nacházíme buňky hvězdicovitého tvaru. Charakter této zvláštní struktury je zapříčiněn desmosomálními spoji, držícími buňky vzájemně pohromadě, a zároveň vysokým obsahem extracelulární matrix, která je těmito buňkami produkována (Nanci and TenCate, 2018; Sasaki et al., 1984). Bylo také ukázáno, že hvězdicové retikulum u kontinuálně rostoucích zubů poskytuje zdroj kmenových buněk nezbytných pro

regeneraci ameloblastů (Juuri et al., 2012). Poslední vrstva, *stratum intermedium*, se nachází mezi hvězdicovým retikulem a vrstvou vnitřního sklovinného epitelu. Její funkce tkví zejména v poskytování podpory budoucím ameloblastům, jež se diferencují z vnitřního sklovinného epitelu.

V naší práci byla vrstva *stratum intermedium* dále detailněji stratifikována objevením a popisem nové vrstvy nazvané „*cuboidal layer*“ (Krivanek et al., 2020). Jedná se o jednovrstevnou strukturu nacházející se hned pod vrstvou ameloblastů v jejich neaktivnější části života. Tato struktura byla prvně predikována s využitím metody scRNA-seq (single-cell RNA-sequencing; transkriptomika na jednobuněčné úrovni) a následně validována pomocí imunohistochemického *in vivo* barvení díky specifické expresi genu *Thbd*. Kromě tohoto charakteristického genu byla zjištěna zvýšená exprese několika dalších význačných genů, které souvisí s transportem kyslíku a iontů (*Cygb*, *Nphs*), mají strukturní funkci (*Kirrel2*, *Jph4*) nebo mohou mít podpůrnou roli při diferenciaci ameloblastů (*Gnrh1*, *Paqr5*). Na základě těchto zjištění byla „*cuboidal layer*“ identifikována jako buněčná vrstva nezbytná pro správný vývoj i funkci ameloblastů.

Z celého sklovinného orgánu je vnitřní sklovinný epitel (resp. ameloblasty, které jej tvoří), jedinou vrstvou, jež aktivně produkuje sklovinu. Kromě tvorby skloviny je vnitřní sklovinný epitel nezbytným interakčním partnerem pro buňky zubní papily. Vlivem vzájemné interakce se přilehlá svrchní vrstva zubní papily začne diferencovat v preodontoblasty a buňky vnitřního sklovinného epitelu do preameloblastů (Balic and Thesleff, 2015; Krivanek et al., 2017; Nanci and TenCate, 2018). Tím je započata fáze apozice – produkce tvrdých zubních tkání.

### **Souvislost s publikační aktivitou**

- V našem originálním vědeckém článku „***Dental cell type atlas reveals stem and differentiated cell types in mouse and human teeth***“ jsme objevili a popsali nové struktury a buněčné typy během vývoje zubu. Jedná se například o novou stratifikaci vrstvy *stratum intermedium*, nový typ ameloblastů

s potenciálně mechanosenzorickou funkcí nebo nové typy kmenových buněk v epitelové i mezenchymové části (Krivanek et al., 2020).

**Viz příložená publikace číslo 1.**

- V našem originálním vědeckém článku „*Developmental mechanisms driving complex tooth shape in reptiles*“ jsme ukázali důležitost sklovinného uzlu, jeho zánik apoptózou a molekulární signalizace během formování vnitřního sklovinného epitelu během morfogeneze zubu chameleona (Landova Sulcova et al., 2020).

**Viz příložená publikace číslo 2.**

### **Edukativní materiály a přehledové články**

- V naší kapitole s názvem „*Dental stem cells: Developmental aspects*“ publikované v knize „*Cell-to-cell communication: Cell-atlas – Visual biology in oral medicine*“ jsme prezentovali vývoj zubu v kontextu funkce kmenových buněk a některých souvisejících patologických stavů (Gruber et al., 2022).

**Viz příložená publikace číslo 3.**

- V našem přehledovém článku „*Heterogeneity and developmental connections between cell types inhabiting teeth*“ jsme prezentovali a diskutovali nejnovější poznatky o buněčném složení zubu, a to jak v dospělém brachyodontním zubu, v zubu hypselodontního typu, tak i během jejich vývoje (Krivanek et al., 2017).

**Viz příložená publikace číslo 4.**

- V učebním materiálu „*Cytologický a embryologický atlas*“ sestaveného doc. RNDr. Petrem Vaňharou, Ph.D. a MUDr. Janou Dumkovou, Ph.D. jsem přispěl vytvořením schématu které vysvětluje vývoj zubu (Obrázek 1). Toto schéma jsem zde prezentoval společně s mikroskopickými fotografiemi názorně popisujícími různá stádia vývoje zubu včetně jejich detailně stratifikace.

## 2.1 Mechanismus tvorby hlavních tvrdých tkání zubu a vznik kořene

Od iniciálního kontaktu dentálního epitelu a ektomezenchymu, který se do budoucího místa pozice zubů dostal migrací buněk neurální lišty, dochází k jejich interakci na molekulární úrovni a postupné diferenciaci (Balic and Thesleff, 2015). Tato diferenciaci graduje při vzniku dentin-tvořících odontoblastů na mezenchymální straně a sklovinu-tvořících ameloblastů na epiteliální straně. Epitelo-mezenchymální interakce při vývoji zubu jsou dobře studovanou problematikou, na níž měly v uplynulých několika desetiletích zásadní podíl zejména četné objevné práce prof. Army Thesleff a jejího týmu (Balic and Thesleff, 2015; Jernvall and Thesleff, 2012; Thesleff et al., 2001; Thesleff and Hurmerinta, 1981; Thesleff and Tummers, 2008; Tummers and Thesleff, 2009), ale i mnozí další.

### 2.1.1 Vznik skloviny

Sklovina je nejvíce mineralizovanou a zároveň nejtvrdější tkání lidského těla i těl obratlovců obecně (Lacruz et al., 2017). Výjimečná tvrdost skloviny je způsobena především vysokým zastoupením anorganických látek, jež ve finálně vytvořené sklovině dosahují až 96–98 %. Fyzikální vlastnosti skloviny však nejsou určeny pouze množstvím anorganických látek. Důležitou roli zde hraje i složité vnitřní uspořádání krystalů hydroxyapatitu a sklovinných prismatic, které úzce souvisí s mechanismem formování této tvrdé tkáně (Bajaj and Arola, 2009; Smith, 1998; Smith et al., 2019).

Celý proces tvorby skloviny mají na starosti jediné buňky, ameloblasty, které se během svého života zásadním způsobem proměňují, aby finálně vytvořená sklovina získala požadované fyzikální vlastnosti a vytvořila svou specifickou vnitřní mikrostrukturu. Její vývoj probíhá v několika krocích. V raných fázích tvorby skloviny nejprve dochází k formování proteinové kostry, jež je však následně enzymaticky degradována a nahrazována anorganickými látkami (Smith, 1998).

V první fázi se nediferencované buňky vnitřního sklovinného epitelu polarizují a diferencují v presekreční preameloblasty, které se následně mění v metabolicky velmi

aktivní, protáhlé sekreční ameloblasty. Ty jsou zodpovědné za vytvoření proteinové kostry skloviny a na straně přivrácené k již vytvořenému (pre)dentinu začínají tvořit sklovinná prismata. Tím se od sebe postupně začínají ameloblasty a odontoblasty oddalovat a místo jejich někdejšího rozhraní se mění v DEJ (dentino-sklovinná hranice; dentin-enamel junction). V další fázi přechází ameloblasty do maturační fáze, kdy dochází k degradaci proteinové kostry a postupně k plné mineralizaci. Důležité je zmínit, že k mineralizaci dochází ve směru uložení proteinové kostry. Je tak zachována charakteristická prismatická struktura skloviny, kdy každý ameloblast dává vzniknout jednomu protáhlému sklovinnému prismatu, který prochází celou tloušťkou skloviny od DEJ až po vnější hranici zubu. V závěrečné fázi ameloblasty postupně degradují, až nakonec na povrchu zubu vytvoří pouze tenkou epiteliální vrstvu, která je finálně odstraněna při erupci (Nanci and TenCate, 2018).

### **Souvislost s publikační aktivitou**

- V současné době se náš tým aktivně věnuje studiu mechanismů vzniku prismatického uspořádání skloviny a specificky vzniku dekusačního charakteru u skloviny hlodavců. Výsledky našeho výzkumu v tomto poli jsme recentně prezentovali na několika významných mezinárodních univerzitách a konferenci.
  - Enamel seminar series, 2021 – **Zvaná přednáška** – online.
  - UMKC Oral and Craniofacial Virtual Seminar Series, 2021 – **Zvaná přednáška** – online.
  - Visegrad Group Society for Developmental Biology meeting, Szeged Hungary, 2021 – **Posterová prezentace** (prezentováno Bc. Vladislavem Rakultsevem).

## 2.1.2 Vznik dentinu

Dentin je narozdíl od skloviny živou a aktivní tkání, schopnou reagovat na podněty přicházející z vnějšího prostředí, jako je změna teploty, poranění nebo infekce (Khatibi Shahidi et al., 2015). Díky úzkému strukturnímu a funkčnímu propojení mezi pulpou a dentinem, které je zprostředkované odontoblasty, je dentin spolu s pulpou někdy jednotně nazýván jako dentino-pulpální komplex (Sloan, 2015). Odontoblasty narozdíl od ameloblastů nezanikají a za fyziologických podmínek vystylají vnitřek pulpy po celý život zubu. Zásadní strukturní prvek, jímž se dentin liší od skloviny, je síť dentinových tubulů obsahující dlouhé výběžky odontoblastů a zprostředkovávající tak vzájemné propojení pulpy a dentinu.

Ačkoliv se dentin nedokáže remodelovat (jak je tomu u kosti), neustává jeho produkce ani po dokončení vývoje korunky a kořene a je produkován během celého života. Dochází tak k postupnému zmenšování objemu pulpy a jejímu nahrazování touto tvrdou tkání.

V průběhu raného vývoje zubu se odontoblasty od zbytku pulpy začínají odlišovat během fáze pozdní čepičky, v době tvorby zubní papily. Jednobuněčná vrstva, která přiléhá k vnitřnímu sklovinnému epitelu, zde postupně dává vzniknout pseudoepitelové vrstvě odontoblastů. Tyto mezenchymální buňky se nejprve začínají polarizovat a orientovat svá jádra opačným směrem k budoucímu DEJ. Vznikají tak preodontoblasty. Tyto buňky poté na základě interakce s přilehlým epitelem začínají tvořit první predentin, který je postupně mineralizován a vzniká z něj dentin. Dávají tak vzniknout DEJ a z preodontoblastů se stávají odontoblasty. V počátku tvorby predentinu mají odontoblasty desítky úzkých výběžků, jež zasahují až těsně k DEJ. Vlivem následné další depozice (pre)dentinu se teprve utváří jeden hlavní výběžek (Tomesovo vlákno), který se s nabýváním tloušťky dentinu částečně prodlužuje a jeho část je tak ponechána uvnitř dentinové matrix ve svém kanálku (Khatibi Shahidi et al., 2015). Časový průběh celého vývoje dentinu je tak zakonzervován v jeho vnitřním uspořádání ve směru od DEJ do pulpy a umožňuje jeho studium.

## Souvislost s publikační aktivitou

- V našem originálním vědeckém článku „*Three-dimensional imaging reveals new compartments and structural adaptations in odontoblasts*“ jsme pomocí metod *lineage tracingu*, imunohistochemického barvení, konfokální mikroskopie a trojrozměrné elektronové mikroskopie (FIB-SEM) detailně popsali diferenciaci odontoblastů, její vztah ke vnitřní mikrostruktuře dentinu a objevili nové strukturní a molekulární aspekty těchto buněk (Khatibi Shahidi et al., 2015).
- V našem originálním vědeckém článku „*Generation and characterization of DSPP-Cerulean/DMP1-Cherry reporter mice*“ jsme vytvořili a charakterizovali nový geneticky upravený myší kmen, který exprimuje modrý a červený fluorescenční protein společně s expresí dvou genů (*Dspp* a *Dmp1*), jejichž exprese je charakteristická pro odontoblasty. Tento myší kmen umožňuje studium různých mikrostrukturních aspektů odontoblastů a zjednodušuje testování diferenciačního potenciálu do tohoto buněčného typu (Vijaykumar et al., 2019). Tento myší kmen hojně využíváme i v našem současném výzkumu.

**Viz příložená publikace číslo 5.**

### 2.1.3 Vznik kořene

Iniciace buněčné diferenciace a následně prvotní tvorba dentinu a skloviny vždy probíhá nejprve v místě budoucích zubních vrcholků korunky. Tato místa jsou charakteristická přítomností sklovinných uzlů – hlavních epiteliálních signálních center během ranného vývoje zubu, jejichž aktivita indukuje diferenciaci odontoblastů (Thesleff et al., 2001). Odtud se diferenciační vlna šíří dál směrem k cervikálním kličkám, a nakonec k budoucím/u kořenům/u.

Jak již bylo výše zmíněno, je vznik dentinu vždy iniciován interakcí mezi mezenchymem s epitelem. Ačkoliv během vývoje nebyly popsány zásadní rozdíly mezi

interagujícím mezenchymem papily korunky a kořene, vykazuje na druhé straně interagující epitel v těchto dvou lokacích zásadní rozdíl. Zatímco při tvorbě korunky se přilehlý epitel diferencuje ve sklovinu-produkující ameloblasty, epitel, který se účastní tvorby kořene, se rozpadá a přímo nedává vzniknout žádné funkční tvrdé matrix. Místo, kde dochází k přehybu epitelu a které se zároveň účastní tvorby kořene se nazývá HERS (Hertwigova epitelová kořenová pochva; Hertwig's epithelial root sheath). Jakmile se přilehlé mezenchymální buňky ve vznikající pulpě začnou diferencovat v odontoblasty a tvořit dentinovou matrix, HERS se rozpadá a v místě budoucího periodontia z ní zůstanou pouze malé epitelové ostrůvky – ERM (Malassezovy epitelové zbytky; Epithelial rests of Malassez) (Xiong et al., 2013). Role těchto útvarů zatím není zcela objasněna, ale zřejmě se podílí na regeneraci struktur v periodontálním prostoru (Rincon et al., 2006).

Dospělý zub tvoří ještě třetí tvrdá tkáň, zubní cement, který se po utvoření kořene podílí na uchycení zubu v zubním lůžku. Ačkoliv je cement velmi důležitý pro správnou funkci zubu, tvoří jen poměrově malou část z tvrdých zubních tkání a jeho studium nebylo přímo součástí mého výzkumu.

### **Souvislost s publikační aktivitou**

- V našem originálním vědeckém článku „*The development of dentin microstructure is controlled by the type of adjacent epithelium*“ jsme popsali rozdílnou strukturu dentinu v korunkové a kořenové části zubu iniciovanou jiným typem přilehlého epitelu. Pomocí geneticky upravených myších kmenů a funkčních experimentů jsme popsali a kvantifikovali rozdílný průběh výběžků odontoblastů, navrhli molekulární podstatu stojící za vytvoření těchto odlišností a určili rozdílné prvkové složení u těchto dvou sledovaných typů dentinu (Lavicky et al., 2021).

**Viz přiložená publikace číslo 6.**

## 2.2 Kontinuálně rostoucí zuby

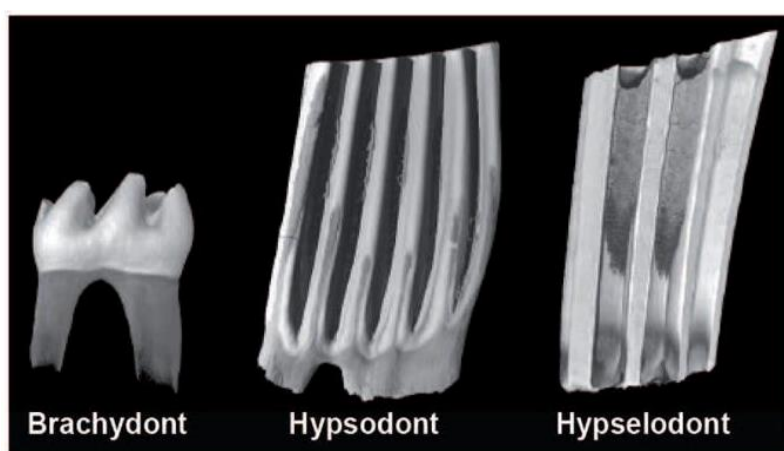
V průběhu evoluce obratlovců došlo u zubů k několika zásadním inovacím, zapříčiněným tlakem na přizpůsobení se okolním podmínkám a spojených s měnícím se způsobem života. Jednou ze zajímavých inovací byl vývin hypsodontních zubů s vysokými korunkami (například kůň, tur) a následně hypselodontních – konstantně rostoucích zubů (například hlodavci). Tyto nové adaptace dentice se mnohokrát konvergentně vyvinuly u různých živočichů u všech typů zubů – u řezáků, špičáků, premolárů i molárů (Renvoisé and Michon, 2014; von Koenigswald, 2011). Tyto nové typy zubů jsou často, avšak ne vždy, spojeny s vysoce abrazivními stravovacími zvyky a přinesly jejich držitelům zásadní evoluční výhodu. Mezi hypselodontní adaptace zubů, jež nejsou přímo spojené se zpracováním potravy, můžeme jmenovat jejich využití pro boj nebo jako znak dominance (například slon, prase divoké) nebo jako senzorického orgánu (narval jednorohý) (Nweeia et al., 2014; Renvoisé and Michon, 2014).

U brachyodontních zubů (zuby s nízkou korunkou, například lidské) dochází při jejich vývoji na okrajích ke vzniku epitelového záhybu (epitelové kličky), který se dále prodlužuje, mění v HERS a utváří tak základ pro tvořící se kořen, jak bylo popsáno výše. Jakmile je vývoj kořene dokončen, aktivita HERS se zastavuje, a nakonec tato struktura degraduje. Zub je tak plně vytvořen a ztrácí schopnost dalšího růstu.

U hypsodontních zubů trvá aktivita cervikálních kliček podstatně delší dobu. HERS tak vzniká později a dále díky zvýšené proliferační aktivitě epitelu dochází kromě prerůstání periferních částí i k zanořování epitelu v centrálních částech budoucího zubu. Závěrem, s utichající proliferační aktivitou epitelu se vytvoří HERS a krátký kořen. Zub tak má během života dostatečný prostor pro postupnou abrazi a zároveň se díky rozdílnému složení korunky na příčném řezu obrušuje nerovnoměrně. To má za důsledek zvýšenou třecí plochu vhodnou pro zpracování těžce stravitelné potravy (Renvoisé and Michon, 2014; Tapaltsyan et al., 2016).

Evolučně nejpozději vyvinutým typem zubu z hlediska výšky korunky (resp. proliferační aktivity korunku-tvořícího epitelu) je typ hypselodontní (Tapaltsyan et al.,

2015). U hypselodontních zubů, narozdíl od hypsodontních, nedochází vůbec k utlumení proliferací aktivity epitelu a zub roste kontinuálně po celý život. Takové zuby mohou dorůstat různého tvaru a velikosti a mohou se lišit svým složením na průřezu i funkcí (von Koenigswald, 2011). Ačkoliv zde není vytvořen pravý kořen, můžeme u nich někdy rozlišovat kořenovou a korunkovou stranu v závislosti na tom, která strana je nebo není kryta sklovinou (Lavický et al., 2021). Rozdíly mezi zuby brachyodontními, hypsodontními a hypselodontními jsou zobrazeny v obrázku 2.



**Obrázek 2: Tři různé typy prvních dolních molárů podle výšky korunky, resp. podle způsobu růstu a aktivity kmenových buněk.** Hypselodontní zub (vpravo) za fyziologických podmínek nikdy nezastavuje svůj růst. Zleva: *Mus musculus*, *Ondatra zibethicus* a *Lemmus lemmus*. Upraveno podle: (Tapaltsyan et al., 2016).

U živočichů, kteří stálerostoucí zuby obušují, se takové zuby kompletně zregenerují mnohokrát během jejich života. Kromě zjevných zvýhodnění, jež takové zuby přináší svým držitelům, tato zvláštní vývojová adaptace poskytuje četné benefity i pro vědecký výzkum. Jedním z hlavních důvodů, proč kontinuálně rostoucí zuby přitahují pozornost vědecké komunity, je, že se jedná o komplexní, inervovaný a vaskularizovaný orgán epitelo-mezenchymálního původu, který neustále roste, a můžeme v něm tak v jakémkoliv období života nalézt různě diferencované buněčné typy počínaje kmenovými buňkami a konče buňkami tvořícími sklovinu nebo dentin (An et al., 2018; Juuri et al., 2012; Krivanek et al., 2017; Zhao et al., 2014). Hypselodontní zuby tak umožňují studovat mechanismy udržování a funkce niche kmenových buněk, epitelo-mesenchymální interakce, mechanismy buněčné diferenciacce nebo způsob, jak jsou tvořeny tvrdé zubní tkáně. Tato celá vývojová

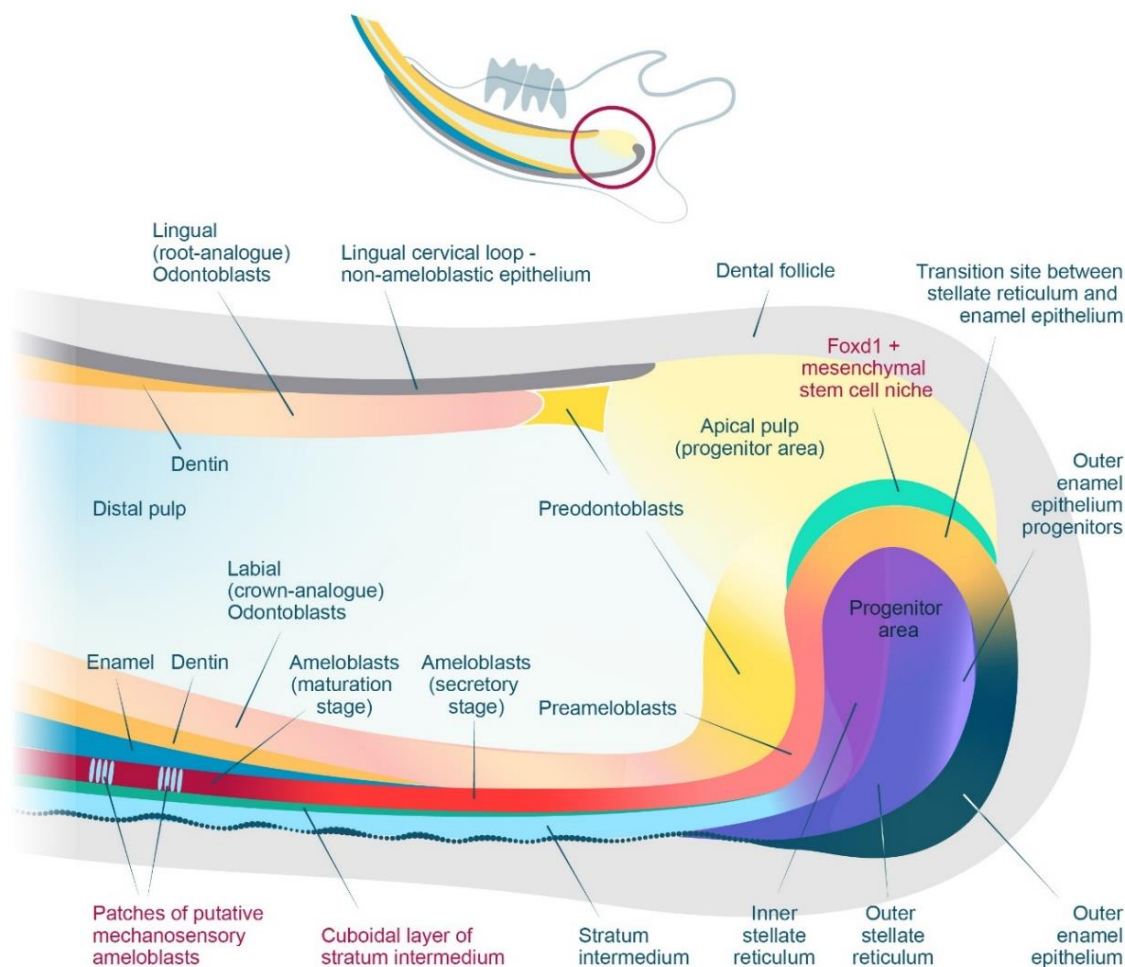
historie se přitom naráz odehrává v rámci jednoho zubu plně dospělého organismu. Kontinuálně rostoucí zuby jsou tak jedinečným a těžko nahraditelným modelem oboru vývojové biologie.

Nejčastěji zkoumaným typem hypselodontních zubů jsou myší řezáky. Existuje pro to několik důvodů. Myš (*Mus musculus*) má nezastupitelnou úlohu jako modelový organismus v rámci savců. Důvody jsou relativně snadný chov, krátká generační doba, větší množství mláďat ve vrhu, relativní příbuznost s člověkem, ale zejména tisíce dostupných geneticky modifikovaných kmenů. Myší dentice je monofyodontní (jednogenerační) a skládá se v každém kvadrantu ze třech brachyodontních molárů a jednoho hypselodontního řezáku. Moláry jsou svou strukturou, typem růstu i ukotvením v čelisti podobnější zubům lidské dentice, čehož je často využíváno pro studium terciární dentinogeneze, aktivity kmenových buněk zubní pulpy nebo pro studium ukotvení a pohybů zubu (Dosedělová et al., 2015; Neves et al., 2020; Nottmeier et al., 2020; Vidovic et al., 2017). Myší řezáky naopak poskytují všechny výše zmíněné výhody a jejich studiu je věnována značná pozornost (An et al., 2018; Beertsen and Niehof, 1986; Harada et al., 1999; Juuri et al., 2012; Krivanek et al., 2020; Lavicky et al., 2021; Sharir et al., 2019; Yu and Klein, 2020; Zhao et al., 2014).

### 2.3 Niche kmenových buněk

Jeden z hlavních důvodů atraktivity kontinuálně rostoucích zubů ve výzkumu je přítomnost stabilního niche kmenových buněk. Protože u těchto zubů nedochází po jejich vývinu k zastavení růstu, přechází již během raného života takového jedince vývoj zubu volně v jeho stabilní růst. Je tak těžké určit jasnou hranici těchto dvou procesů. Narozdíl od ostatních tkání, kde je udržována vysoká aktivita kmenových buněk (hematopoéza, střevní epitel apod.), u zubu spolu nejenže interaguje epitel a mezenchym, ale obě tyto prostorově oddělené části dávají vzniknout funkčním tkáním. Můžeme zde tak nalézt obnovující se mezenchymální i epiteliální niche kmenových buněk, které jsou spolu ve vzájemném kontaktu a aktivně interagují. Ačkoliv jsou

vlastnosti kmenových buněk u hypselodontních zubů po dekády objektem velkého zájmu, tak charakter jejich udržování ani následné diferenciační kaskády nejsou stále zcela objasněny. Růstová část myšního řezáku, obsahující epiteliální i mezenchymální kmenové niche, ze kterého je zub neustále obnovován, se nachází v jeho apikální části. Jednotlivé části a celková stratifikace tohoto místa je znázorněna v obrázku 3.



**Obrázek 3: Organizace apikální růstové části kontinuálně rostoucího myšního řezáku.** Za neustálou obnovu myšního řezáku je zodpovědná jeho apikální část, ve které spolu interaguje dentální epitel a mezenchym a nachází se zde niche kmenových buněk. Za pozornost stojí rozdílná struktura na lingvální (v horní části obrázku) a labiální (ve spodní části obrázku) straně. Červeně jsou znázorněny nové struktury a buněčné typy recentně popsané v naší práci (Krivánek et al., 2020). Autoři: Jan Křivánek a Olga Kharchenko.

Lokalizace epiteliálních kmenových buněk má ze své podstaty jasnější ohraničení než její mezenchymální protějšek. Na molekulární úrovni byla v této nejapikálnější části zubu popsána aktivita mnoha různých rodin genů, jako tomu je při vývoji brachyodontního zubu (Harada et al., 1999; Laphanasupkul et al., 2012; Suomalainen and Thesleff, 2010; Thesleff and Tummers, 2008; Wang et al., 2007). U několika z nich bylo zároveň prokázáno narušení funkce růstu, porucha asymetrie nebo jiné defekty v souvislosti s jejich vyřazením z funkce (Cao et al., 2010; Klein et al., 2008; Kwon et al., 2015; Kyrylkova et al., 2012; Thesleff and Tummers, 2008).

Všechny tyto dosavadní práce se však poměrně nespécificky zaměřují na popis kmenového niche jako celku – bez specifického zaměření na konkrétní typy kmenových buněk. Biologií samotných jednotlivých kmenových buněk, jež jsou zodpovědně za kontinuální obnovu, se začínají zabývat až některé recentní studie.

### 2.3.1 Kmenové buňky a „*lineage tracing*“

Až metody *lineage tracingu* umožnily spolehlivě identifikovat různé populace kmenových buněk v obou částech zubu. Nejrozšířenější metodou je využití genetické modifikace, během které se do genomu cílového organismu vnese gen kódující specifickou rekombinázu (nejčastěji *Cre*) exprimovanou pod kontrolou vybraného promotoru. Dochází tak k její konstitutivní, tkáňově-specifické expresi. Tato rekombináza následně způsobí vystřížení nebo inverzi dalšího, uměle vloženého úseku DNA označeného vloženými *LoxP* sekvencemi. Obvykle dochází k vystřížení STOP kodonu, což následně způsobí expresi vložené sekvence kódující vybraný fluorescenční protein.

Protože se jedná o trvalou genetickou změnu, jsme nejen schopni fluorescenčně označit a sledovat vybrané buňky, ale díky výše uvedené metodě můžeme sledovat i všechny dceřiné buňky, které vzniknou z původně označené mateřské buňky (VanHorn and Morris, 2021). Tento mechanismus tak například umožňuje odhalit kmenové buňky a sledovat jejich diferenciační trajektorii.

Užitečnou modifikací je úprava *Cre* rekombinázy její fúzí s estrogen-vázající doménou *ERT2* (Indra et al., 1999; Zhang et al., 1996). Tato modifikace sice nemění expresi *Cre* rekombinázy, ale pro její aktivaci (tj. umožnění transportu vytvořené rekombinázy po její translaci do jádra a provedení změny v DNA) je potřeba aktivace tamoxifenem. Bez externího podání tamoxifenu, který je v těle metabolizován na svou aktivovanou formu 4-hydroxytamoxifen, nedochází k vystřížení ani inverzi *LoxP*-označených míst v sekvenci DNA. Podáním tamoxifenu tak můžeme indukovat cílenou genetickou změnu v konkrétní čas u konkrétního buněčného typu. Tato technologie otevírá možnost zkoumat chování konkrétních buněčných typů v přesně stanoveném okamžiku vývoje, a to včetně embryonálního vývoje.

### 2.3.2 Epiteliální a mezenchymální kmenové buňky

Mezi první identifikované a nejdříveji akceptované typy dentálních epiteliálních kmenových buněk náleží buňky charakteristické expresí genu *Sox2* (Juuri et al., 2012). Pomocí *lineage tracingu* bylo prokázáno, že *Sox2*-exprimující buňky dlouhodobě zůstávají uvnitř labiální cervikální kličky a dokáží diferencovat do všech typů zubního epitelu včetně ameloblastů. Později byla popsána řada dalších genů, které taktéž označují zubní epiteliální kmenové buňky, jako například: *Bmi1*, *Lrig1*, *Gli1*, *Meis1*, *Igfbp5* nebo *Lgr5* (Krivanek et al., 2020; Sanz-Navarro et al., 2019; Seidel et al., 2017; Zhao et al., 2014).

Narozdíl od dentálního epitelu, který je jasně ohraničenou strukturou, do níž přímo nezasahují nervy ani cévy, je dentální mezenchym místem značné rozmanitosti a buněčné plasticity. Identifikace zdejšího kmenového niche je tak podstatně složitější záležitostí. Již dříve bylo popsáno, že niche mezenchymálních kmenových buněk v řezáku je značně heterogenní, co se týká pozice kmenových buněk i jejich exprese (Feng et al., 2011; Kaukua et al., 2014; Krivanek et al., 2017; Sharpe, 2016; Zhao et al., 2014). Kmenové buňky zodpovědné za růst mezenchymální části zubu a za postupnou diferenciaci do dospělých buněk pulpy a odontoblastů se nachází v apikální části

řezáku, kde jsou ohraničeny cervikálními kličkami a distálně jsou protáhlé kolem neurovaskulárního svazku. Ačkoliv se má obecně za to, že původ mezenchymálních kmenových buněk v zubu vývojově náleží do ektomezenchymu (neurální lišty), není jisté, kdy dochází k ustálení finální populace těchto kmenových buněk a jakou roli zde hrají perivaskulární buňky, u kterých byla taktéž prokázána jejich kmenovost (Vidovic et al., 2017; Zhao et al., 2014). *Lineage tracing* s využitím genu *Thy1-cre* zde prokázal stabilně označenou populaci kmenových buněk, jež zaujímal asi 10–20 % všech odontoblastů a buněk pulpy (Krivanek et al., 2017; Pang et al., 2016; Sharpe, 2016). Jedním z dalších charakteristických znaků mezenchymálního kmenového niche je exprese genu *Gli1* (Zhao et al., 2014). *Lineage tracing* s užitím *Gli1-creERT2* zde prokázal robustní označení apikální části zubu a časově závislé postupné označení prakticky všech buněk pulpy i odontoblastů. Ačkoliv tyto analýzy potvrzují kmenové vlastnosti niche v apikální části řezáku, geny použité při *lineage tracingu* (*Thy1*, *Gli1*) stále označují poměrně rozsáhlou a zřejmě i heterogenní buněčnou populaci v apikální části řezáku. Rekombinace v kmenových buňkách (a jejich genetické označení), tak může být způsobená i rozsáhlejším označením různých (i nekmenových) buněk této oblasti.

### 2.3.3 Využití metody scRNA-seq ve studiu kmenových buněk

Díky rychlému technologickému pokroku v posledních několika letech se v současné době dostávají do popředí nové techniky umožňující provést různé „-omic“ analýzy z odebraných vzorků tkáně, a to i na jednobuněčné úrovni. Jednou z možností, jak nezaujatým způsobem identifikovat rozdílné buněčné populace, je metoda scRNA-seq. Tato a příbuzné technologie recentně zásadním způsobem akcelerovaly výzkum biologie zubu s dosud nemyslitelnou přesností (Chiba et al., 2020; Fresia et al., 2021; Krivanek et al., 2020; Pagella et al., 2021a; Sharir et al., 2019; Yianni and Sharpe, 2020). Metoda scRNA-seq umožňuje přečíst expresní profil (transkriptom) z každé jednotlivé analyzované buňky ve studované tkáni.

Stručný postup této metody spočívá v několika po sobě jdoucích krocích. Po izolaci tkáně z organismu je z ní enzymatickou a mechanickou cestou připravena suspenze jednotlivých buněk (Krivanek et al., 2021; Pagella et al., 2021b). Následně s využitím rozdílných technik dochází k přípravě knihoven a jejich samotnému osekvenování.

Posledním krokem, který je nezbytný pro zpřístupnění získaných dat, je bioinformatická analýza. Tyto typy analýz mohou buď následovat standardizované algoritmy, ale často je samotná analýza rozsáhlou vědeckou prací přesahující rámec rutinních postupů. Bioinformatika, zvláště ve spojitosti s „-omics“ přístupy se tak stává samostatným vědním oborem (Kharchenko, 2021; La Manno et al., 2018). Prostřednictvím těchto analýz jsou z experimentu *in silico* odstraněny buňky/události nevhodné k další analýze. Jedná se například o mrtvé buňky, dublety (dvě nebo víc buněk, které prošly analýzou společně) nebo buňky s velmi nízkou hladinou exprese. Finálně získáváme informace, které nám umožní roztrždit buňky do skupin na jednotlivé populace a subpopulace, detailně je charakterizovat, lépe určit jejich funkci, odhalit potenciální interakce mezi jednotlivými buněčnými typy, identifikovat nové buněčné typy nebo mapovat vývoj a diferenciaci (Kharchenko, 2021; Krivanek et al., 2020; La Manno et al., 2018; Soldatov et al., 2019).

Díky využití technologie „*smart-seq2*“, jedné z metod scRNA-seq umožňující hlubokou analýzu genové exprese na jednobuněčné úrovni, a následným pokročilým bioinformatickým analýzám se nám recentně podařilo odhalit nové typy kmenových buněk v kontinuálně rostoucím myším řezáku (Krivanek et al., 2020; La Manno et al., 2018; Picelli et al., 2014). V dentálním mezenchymu tak například byla *in silico* navržena minoritní populace *Foxd1*<sup>+</sup> kmenových buněk. Následná *in vivo* analýza pomocí *in situ* hybridizace a *lineage tracingu* za využití *Foxd1*<sup>CreERT2</sup> myšího kmene zkříženého s reportérovými kmeny, potvrdila vysokou specificitu této populace kmenových buněk a lokalizovala je do těsné blízkosti cervikální kličky. Kmenovost a vysoká prostorová i časová stabilita niche *Foxd1*<sup>+</sup> buněk byla potvrzena dlouhodobým *lineage tracingem*. Tyto experimenty prokázaly, že *Foxd1*<sup>+</sup> buňky dlouhodobě

perzistují v mezenchymální oblasti kolem labiální cervikální kličky i po tom, co je zub několikrát kompletně obnoven. Tyto kmenové buňky se pomalu dělí a jejich dceřiné buňky diferencují do buněk pulpy i funkčních odontoblastů (Krivanek et al., 2020). Narozdíl od dříve popsaných markerů dentálních mezenchymálních kmenových buněk, jako například dříve zmíněných *Thy1* nebo *Gli1*, je exprese *Foxd1* charakteristická pouze pro velmi úzkou populaci buněk. Metodou jejich označení pomocí *lineage tracingu* tak dochází k označení pouze této, velmi specifické populace, a nikoliv jejího širšího okolí. Zajímavostí je, že tyto kmenové buňky dávají vzniknout pouze buňkám zubní pulpy a odontoblastům na labiální straně řezáku, přičemž na lingvální straně nebyly pozorovány žádné nebo pouze velmi raritně značené buňky. Toto zjištění otevírá hypotézu, že v mezenchymální části řezáku se vyskytuje heterogenní niche kmenových buněk se specializovanou, prostorově oddělenou funkcí. Zůstává otázkou, jestli tato heterogenita může v konečném důsledku způsobovat jinou mikrostrukturu dentinu na labiální a lingvální straně, jak bylo v naší práci nedávno ukázáno (Lavicky et al., 2021).

U zubního epitelu jsme pomocí metody scRNA-seq odhalili kompaktní buněčnou populaci, která sdílela některé dříve popsané molekulární znaky epiteliálních kmenových buněk, jako je například exprese *Lgr5*, *Lrig1* nebo *Sox2* (Barker et al., 2007; Juuri et al., 2012; Seidel et al., 2017). Zjistili jsme však, že tyto geny, a zvláště pak *Sox2*, který značí populaci dříve popsaných všeobecně uznávaných kmenových buněk, jsou exprimovány podstatně širěji, než jen v předpokládané populaci kmenových buněk. Exprese *Sox2* sahá až k progenitorovým a přechodně rychle se dělícím buňkám. Pro potvrzení kmenovosti navržené populace jsme vybrali další ze specificky exprimovaných genů: *Acta2*, u něhož jsme v labiální cervikální kličce pomocí imunohistochemie lokalizovali buňky, které ho exprimují. S využitím *lineage tracingu* pomocí kmene *Acta2<sup>CreERT2</sup>* jsme potvrdili jejich kmenový charakter (Krivanek et al., 2020).

## Souvislost s publikační aktivitou

- V našem originálním vědeckém článku „**Dental cell type atlas reveals stem and differentiated cell types in mouse and human teeth**“ jsme popsali nové typy kmenových buněk v zubním epitelu i mezenchymu kontinuálně rostoucích řezáků. Tyto kmenové buňky byly objeveny a potvrzeny díky celkové analýze transkriptomu na jednobuněčné úrovni, pokročilým bioinformatickým analýzám a následnou *in vivo* validací pomocí *in situ* hybridizace, imunohistochemie a *lineage tracingu* (Krivanek et al., 2020).

**Viz přiložená publikace číslo 1.**

- V našem metodologicky zaměřeném článku „**Rapid isolation of single cells from mouse and human teeth**“ jsme prezentovali detailní protokol zaměřený na získání suspenze jednotlivých živých buněk z myších i lidských, čerstvě extrahovaných zubů. Efektivní, rychlé a šetrné získání živých buněk z tkáně je zásadním iniciálním krokem pro získání spolehlivých dat metodou scRNA-seq (Krivanek et al., 2021).

**Viz přiložená publikace číslo 7.**

## 3 Komentáře k přiloženým publikacím

### 3.1 Komentář k přiložené publikaci číslo 1

#### **Dental cell type atlas reveals stem and differentiated cell types in mouse and human teeth**

Originální vědecký článek  
Nature Communications, 2020; Q1, IF: 14,92

*Jan Krivanek, Ruslan A Soldatov, Maria Eleni Kastriti, Tatiana Chontorotzea, Anna Nele Herdina, Julian Petersen, Bara Szarowska, Marie Landova, Veronika Kovar Matejova, Lydie Izakovicova Holla, Ulrike Kuchler, Ivana Vidovic Zdrilic, Anushree Vijaykumar, Anamaria Balic, Pauline Marangoni, Ophir D Klein, Vitor C M Neves, Val Yianni, Paul T Sharpe, Tibor Harkany, Brian D Metscher, Marc Bajénoff, Mina Mina, Kaj Fried, Peter V Kharchenko, Igor Adameyko*

Pochopení dynamiky obnovy buněčného složení zubu na úrovni jednotlivých buněk je základním předpokladem při vývoji nových metod v oboru regenerativní zubní medicíny. Tato myšlenka nás motivovala při práci na tvorbě a validaci atlasu buněčných typů v zubu, kdy jsme detailně popsali několik dosud neznámých faktů o kmenových buňkách nebo diferenciacních drahách a umožnili využití našich dat pro širokou vědeckou veřejnost.

Základní část této práce tvoří nezaujatá analýza buněčného složení myších řezáků a molárů a jejich porovnání s buněčným složením lidských dospělých a rostoucích zubů. Abychom zjistili informace o všech buněčných typech těchto typů zubů, metodou analýzy genové exprese na úrovni jednotlivých buněk (scRNA-seq) jsme nezávisle charakterizovali všechny izolované buňky zubu a jeho nejbližšího okolí. Následně jsme pomocí pokročilých bioinformatických analýz jednotlivé populace a subpopulace charakterizovali *in silico*. Objevili jsme tak některé nové buněčné typy a popsali jejich expresní profil, zmapovali diferenciacní trajektorie vedoucí k vytvoření odontoblastů a ameloblastů z nediferencovaných buněk, objevili nové typy kmenových buněk a porovnali buněčné složení zubů modelového organismu s lidskými zuby. Data

získaná z těchto analýz jsme následně zpětně pomocí různých technik validovali *in vivo*.

V první části výsledků naší práce jsme se věnovali myšímu řezáku. Myší řezák, jakožto základní modelový systém využívaný pro studium vývoje, růstu a kmenových buněk zubů, zároveň představuje hlavní studovaný orgán v této práci. V této části charakterizujeme pomocí scRNA-seq analýz genovou expresi hlavních buněčných populací tvořících zub. Tyto populace jsme následně díky známým i nově objeveným charakteristickým expresním znakům validovali pomocí imunohistochemie.

Dále jsme se separátně detailně věnovali epiteliální a mezenchymální části zuby. V zubním epitelu jsme popsali 13 jednotlivých subpopulací, tvořících sklovinný orgán kontinuálně rostoucího řezáku, z nichž některé buněčné typy byly popsány zcela nově. Jedná se zejména o cluster č. 1, který byl následně s využitím informace o expresi *Thbd* metodou IHC identifikován jako nová vrstva náležící mezi *stratum intermedium*. Podle charakteristického kubického tvaru jsme tuto vrstvu pojmenovali jako „*Cuboidal layer*“. Dále cluster č. 3, který jsme díky informaci o expresi genu *Ryr2* následně metodou IHC charakterizovali jako nový specifický podtyp ameloblastů. Exprese dalších genů v tomto clusteru napovídá, že se může jednat o buňky s mechanosenzorickými vlastnostmi. Tyto buňky tak mohou reagovat na mechanické stimuly přicházející z vnějšího prostředí. V rámci epitelu jsme popsali celou diferenciační trajektorii vedoucí od progenitorových buněk až po ameloblasty v maturační fázi. V jednotlivých fázích jsme identifikovali transkripční faktory, jež se mohou podílet na řízení této diferenciace. Se specifickým zaměřením jsme se věnovali niche kmenových buněk. Cluster č. 13 byl na základě exprese dříve potvrzených genů specifických pro kmenové buňky identifikován jako potenciální zdroj epiteliálních kmenových buněk. Nezávislou metodou hledání podobných expresních znaků jsme prezentovali 20 genů s nejpodobnější expresí a stanovili tak další potenciální geny specificky se exprimující u kmenových buněk. Jeden z těchto znaků, *Acta2*, byl využit pro potvrzení kmenovosti tohoto clusteru s využitím metod *lineage tracingu*.

V rámci zubního mezenchymu jsme identifikovali tři základní vývojové trajektorie vedoucí do: a) distální pulpy, b) apikální pulpy a c) odontoblastů. Metodou *RNA-velocity* byl potvrzen navržený směr diferenciaci a následně metodami „*stability individualních komponent*“ byla v předpokládané progenitorové oblasti stanovena buněčná populace s kmenovým potenciálem. Jedním z charakteristických znaků této populace byla exprese genu *Foxd1*. *Lineage tracing* potvrdil kmenovost a vysokou stabilitu a specificitu této populace na labiální straně v apikální části řezáku. Následně jsme separátně analyzovali diferenciační trajektorii odontoblastů a potvrdili ji *in vivo* metodou ISH. Ukázalo se, že dříve identifikované populace kmenových buněk charakteristické expresí *Thy1* nebo *Gli1* poměrně nespecificky značí i mnohé ostatní buňky apikální pulpy. Dále byl na expresní i histologické úrovni lépe stratifikován přechod mezi apikální pulpou a zubním folikulem a rozlišena zubní pulpa na lingvální a labiální straně.

Následně byly na expresní úrovni popsány jednotlivé populace buněk v pulpě u lidských, plně vyvinutých zubů moudrosti a u buněk izolovaných z apikální papily rostoucích zubů téhož typu. Jednotlivé populace byly s využitím nově zjištěných, charakteristicky exprimovaných genů následně identifikovány *in vivo* pomocí metod IHC.

Závěrem bylo popsáno zastoupení jednotlivých buněk imunitního systému v zubu. Nové zjištění v tomto směru bylo zejména rozdělení populace makrofágů na expresní i prostorové úrovni v dospělých i rostoucích zubech. Byla popsána nová subpopulace makrofágů charakteristická expresí genu *Lyve1*. Tato populace byla koncentrována spíše do středu pulpy a neosidlovala okrajové části pulpy ani vrstvu odontoblastů. Toto zjištění bylo konzistentní u myších i lidských zubů.

Kromě dat prezentovaných v této rozsáhlé práci jsme vytvořili interaktivní, veřejně přístupné online stránky obsahující expresní informace z jednotlivých vzorků, včetně analýzy jednotlivých hlavních skupin.

## 3.2 Komentář k přiložené publikaci číslo 2

### Developmental mechanisms driving complex tooth shape in reptiles

Originální vědecký článek  
Developmental dynamics, 2020; Q1, IF: 3,78

*Marie Landova Sulcova, Oldrich Zahradnicek, Jana Dumkova, Hana Dosedelova, **Jan Krivanek**, Marek Hampl, Michaela Kavkova, Tomas Zikmund, Martina Gregorovicova, David Sedmera, Jozef Kaiser, Abigail S Tucker, Marcela Buchtova*

Ačkoliv jsou základní principy řídící morfogenezi jednotlivých zubů napříč obratlovci fundamentálně podobné, vyzývá rozmanitá různorodost ve tvarech zubů u různých druhů k hledání příčin zodpovědných za tato přizpůsobení. Role sklovinných uzlů při formování zubů savců je dobře popsáným jevem řídícím hlavní vývoj korunky. U některých plazů se však vyskytuje zvláštní morfologický útvar na samém vrcholku zubu: sklovinná rýha (*enamel groove*) ohraničený ostrými sklovinnými hřebeny (*enamel ridges*). Mechanismus vzniku tohoto útvaru a role sklovinných uzlů při morfogenezi zubu u plazů není dosud dobře popsán.

Tato práce detailně charakterizuje strukturu, funkci a molekulární signalizaci sklovinných uzlů u vybraných plazů (*Chamaeleo calypttratus*, *Paroedura picta* a *Crocodylus siamensis*). V oblasti sklovinných uzlů byly objeveny podobné signální dráhy jako jsou ty, které řídí morfogenezi savčích zubů (*Shh* nebo *Fgf4*), a bylo rovněž pozorováno zastavení buněčné proliferace a detekována apoptóza. Na základě experimentálních výsledků dosažených různými metodami byl v této práci navržen mechanismus, jakým přítomnost (i postupná degradace) sklovinných uzlů řídí specifickou morfogenezi korunkové části zubu, což vede k formování sklovinné rýhy a sklovinných hřebenů u plazů.

Tato práce tak odhaluje nové mechanismy zodpovědné za přesnou finální morfogenezi korunkové části zubu konzervované u různých plazů.

### 3.3 Komentář k přiložené publikaci číslo 3

#### **Dental stem cells: Developmental aspects**

publikované v knize

#### **Cell-to-cell communication: Cell-atlas – Visual biology in oral medicine**

Kapitola v knize

2022

*Jan Krivanek, Kaj Fried*

Kniha „*Cell-to-cell communication: Cell-atlas – Visual biology in oral medicine*“ jako celek, ve 21 kapitolách edukativním způsobem představuje zub z pohledu jednotlivých buněčných populací, které ho utváří. Zvláštní důraz je zde kladen na grafickou stránku a klinické souvislosti. Tím tak kniha zpřístupňuje často poměrně abstraktní témata i pro studenty nebo klinické pracovníky.

Kapitola „*Dental stem cells: Developmental aspects*“ se zaměřuje nejen na fungování kmenových buněk v zubu, ale zvláště klade důraz na vývoj a interakci jednotlivých buněčných typů a objasnění příčin některých souvisejících vrozených onemocnění. Úvodní část, zaměřená na vývoj zubu, je doplněna několika fotografiemi různých stádií vyvíjejícího se myšího zubu, pořízenými pomocí skenovacího elektronového mikroskopu, a přináší tak netypický pohled na vývoj zubu. V části zaměřené na mezenchymální a epitelální kmenové buňky jsou prezentovány recentní poznatky zjištěné u kontinuálně rostoucích myších řezáků. Je zde přehledně znázorněna dynamika jejich obnovy a buněčného přispění vedoucímu k růstu zubu. Následuje část zaměřena na molekulární signalizaci zejména mezi mezenchymem a epitelem a také na identifikaci jednotlivých genů charakteristických pro kmenové buňky v zubu. Klinická část se věnuje některým vybraným patologiím, které jsou způsobeny špatnou kontrolou iniciální části vývoje a související deregulací kmenových buněk v dospělosti. Celou kapitolu následně uzavírají vyhlídky do budoucnosti, kde je diskutována zejména přicházející éra regenerativní zubní medicíny.

### 3.4 Komentář k přiložené publikaci číslo 4

#### **Heterogeneity and developmental connections between cell types inhabiting teeth**

Přehledový vědecký článek (review)  
Frontiers in Physiology, 2017; Q1, IF: 3,39

*Jan Krivanek, Igor Adameyko, Kaj Fried*

Ačkoliv hlavní funkce zubů (mechanické zpracování potravy) je spojená spíše s fyzikálními vlastnostmi tvrdých zubních tkání, mají všechny tyto tři základní typy tkání (sklovina, dentin a cement) svůj buněčný původ a jejich mikrostruktura i funkce vyplývá z buněk, které je tvoří.

Cílem této práce bylo diskutovat buněčné složení zubu na různých úrovních. Práce je tematicky rozdělena do jednotlivých kapitol, v nichž jsou postupně diskutována tato témata: heterogenita buněk epiteliálního původu, heterogenita buněk mezenchymálního původu, buněčné typy tvořící zubní folikul a podílející se na tvorbě kořene, buněčné typy spojené s inervací a vaskularizací, diverzita imunitních buněk obývajících zub a v závěrečné kapitole pak evoluční pohled na heterogenitu buněčných typů v zubu.

Zvláštní důraz je zde kladen na porovnání morfologické stavby brachyodontního typu zubu (např. lidské zuby) a hypselodontního typu zubu (kontinuálně rostoucí myší řezáky). Práce funkčně reflektuje časový vývoj brachyodontních zubů do různých částí kontinuálně rostoucích zubů a představuje tak hypselodontní zub jako ukázkový případ umožňující pozorování a studium diferenciačních buněčných procesů nebo procesů tvorby skloviny a dentinu. Paralelně jsou zde popsány různé buněčné typy, které se na vývoji nebo kontinuálním růstu podílí, a to včetně funkce kmenových buněk. Zvláštní pozornost je věnována obnově a stabilitě epiteliálního a mezenchymálního kmenového niche a s tím související novotvorbě dentinu a skloviny.

Celkově se jedná o ucelenou práci, poskytující komplexní přehled o buněčném složení, vývoji a obnově zubu v souvislosti s evolučními aspekty.

### 3.5 Komentář k přiložené publikaci číslo 5

#### **Generation and characterization of DSPP-Cerulean/DMP1-Cherry reporter mice**

Originální vědecký článek  
Genesis, 2019; Q2, IF: 1,76

*Anushree Vijaykumar, Sean Ghassem-Zadeh, Ivana Vidovic-Zdrilic, Karren Komitas, Igor Adameyko, Jan Krivanek, Yu Fu, Peter Maye, Mina Mina*

Různá transgenní zvířata mají v současném vědeckém bádání nezastupitelnou roli při zkoumání nejrůznějších strukturních, vývojových nebo funkčních vlastností genů, buněk, tkání nebo organismu jako celku. Zvláště důležitým milníkem, který umožnil geneticky značit a následně vizualizovat specifické buněčné typy, bylo využití fluorescenčních proteinů. Geny, kódující tyto proteiny, byly „zkopírovány“ z jiných organismů a metodami genového inženýrství „vloženy“ do cílového zkoumaného organismu.

V této práci byl vytvořen nový myší reportérový kmen (*DSPP-Cerulean/DMP1-Cherry*), který umožňuje fluorescenčně rozlišit buňky exprimující gen *Dspp* (*Dentin Sialophosphoprotein*) a/nebo *Dmp1* (*Dentin Matrix Protein 1*) jejich označením modrým fluorescenčním proteinem (*Dspp*) a červeným fluorescenčním proteinem (*Dmp1*). Specifita exprese uměle vnesených fluorescenčních proteinů byla potvrzena korelací s analýzou genové exprese *Dmp1* a *Dspp*. Byl tak vytvořen zcela nový, unikátní myší kmen, díky kterému mohou být jednak vizualizovány a analyzovány funkční odontoblasty *in vivo*, ale také explantáty z tohoto kmene mohou sloužit v dalším *in vivo* výzkumu, jak bylo v této práci dále ukázáno. Součástí práce je detailní konfokální analýza takto označených odontoblastů během vývoje i v plně vyvinutém zubu, což odhaluje nové strukturní aspekty těchto důležitých buněk při formování dentinu.

Celkově tato práce prezentuje nový, jedinečný reportérový myší kmen, který je v současné době hojně využíván nejen naší laboratoří.

### 3.6 Komentář k přiložené publikaci číslo 6

#### **The development of dentin microstructure is controlled by the type of adjacent epithelium**

Originální vědecký článek  
Journal of Bone and Mineral Research, 2021; Q1, IF: 6,741

*Josef Lavicky, Magdalena Kolouskova, David Prochazka, Vladislav Rakultsev, Marcos Gonzalez-Lopez, Klara Steklikova, Martin Bartos, Anushree Vijaykumar, Jozef Kaiser, Pavel Pořízka, Maria Hovorakova, Mina Mina, **Jan Krivanek***

Dentin je objemově nejvíce zastoupenou tvrdou tkání tvořící zub. Tato tkáň jako první vzniká i mineralizuje a tvoří tak strukturní i funkční základ každého zubu. Dentin je zároveň, narozdíl od skloviny, v celém svém objemu protkán složitou sítí tubulů, vyplněných dentinovou tekutinou. Uvnitř tubulů se pak nachází dlouhé výběžky odontoblastů. Tato mikrostruktura tak z dentinu dělá živou tkáň, schopnou reagovat na různé podněty přicházející z vnějšího prostředí. Vývojově dentin (resp. odontoblasty, které ho tvoří) vzniká z ektomezenchymu interakcí s přilehlým dentálním epitelem, který je přítomný jak v korunce (vznikají z něj ameloblasty), tak v kořenu (tvoří HERS). Ačkoliv se ví o odlišnostech těchto dvou typů dentálních epitelů, nebyl dosud jejich rozdílný vliv na formování přilehlého dentinu popsán.

V této práci jsme se věnovali vnitřní mikrostruktuře dentinu ve vztahu k jeho poloze a vývoji. Pro studium jsme využili jednak myší řezáky, u kterých byla dříve identifikována kořenová a korunková strana zubu a zároveň je u nich možné detailně studovat vývoj, a jednak myší moláry, které svou stavbou lépe odpovídají lidským zubům. U obou typů zubu naše výsledky konzistentně prokázaly zásadní roli typu přilehlého epitelu během vývoje na budoucí mikrostrukturu dentinových tubulů. Pro detailní studium mikrostruktury dentinu jsme využili geneticky fluorescenčně značený

myší kmen *DSPP-Cerulean/DMP1-Cherry*, který nám umožnil studovat mikrostrukturu dentinu a zároveň vztah vnitřního uspořádání k expresi dvou zásadních genů pro formování dentinu: *Dspp* a *Dmp1*. Naše výsledky z konfokální mikroskopie a následné kvantifikační analýzy ukázaly, že výběžky odontoblastů mají v korunkové části rovnější průběh, mají užší průměr a tvoří hustší síť než v části kořenové. Následně jsme provedli analýzu prvkového složení různých částí dentinu metodou LIBS (Laser-induced breakdown spectroscopy), která ukázala, že lingvální (kořenová) a labiální (korunková) část řezáku se liší v obsahu vápníku a hořčíku, což může dále poukazovat na odlišné mechanické vlastnosti dentinu v různých částech zubu. Pro potvrzení naší hypotézy o rozdílném indukčním vlivu různých typů zubních epitelů jsme využili kmen *Spry2<sup>+/-</sup>;Spry4<sup>-/-</sup>*, který má ektopicky vyvinutou sklovinu i na lingvální (kořenové) straně řezáku. Tyto výsledky odhalily, že pokud se v místě, které odpovídá zubnímu kořenu, vytvoří sklovina, dojde zároveň k zásadnímu ovlivnění mikrostruktury přilehlého dentinu. Takový dentin se bude více podobat dentinu v korunkové části zubu. Znamená to tedy, že došlo k časnému ovlivnění odontoblastů typem epitelu, se kterým během svého brzkého raného vývoje interagovaly, a že tyto odontoblasty si získané vlastnosti ponechávají i během dalšího vývoje. Na molekulární úrovni jsme zjistili, že jednotlivé typy dentin-tvořících odontoblastů se liší v expresi několika vývojově významných genů, a odhalili jsme tak možnou účast Wnt signalizace při formování mikrostruktury dentinu.

Tato práce díky komplexnímu metodologickému přístupu a funkčním analýzám odhaluje odlišnou mikrostrukturu dentinu v korunkové a kořenové části zubu a zároveň jako první navrhuje mechanismy, které tuto rozdílnost způsobují.

### 3.7 Komentář k přiložené publikaci číslo 7

#### **Rapid isolation of single cells from mouse and human teeth**

Originální vědecký článek  
Journal of Visualized Experiments, 2021; Q3, IF: 1,36

*Jan Krivanek, Josef Lavicky, Thibault Boudierlique, Igor Adameyko*

Metoda analýzy genové exprese na úrovni jednotlivých buněk je principiálně závislá na vstupní kvalitě buněk izolovaných z živé tkáně. Nešetrná nebo naopak pomalá disociace tkáně zájmu s sebou přináší nedostatečný výtěžek buněk, vysoký počet umírajících a mrtvých buněk nebo ovlivnění genové exprese v analyzované buněčné populaci. Situace je ještě komplikovanější, pokud je potřeba izolovat buňky z tvrdých tkání, jako jsou kosti nebo zuby.

V této práci přinášíme protokol vyvinutý pro rychlou, efektivní a zároveň šetrnou izolaci jednotlivých buněk z myších i lidských zubů. Připravená buněčná suspenze je vhodná pro zpracování pomocí různých metod analýzy genové exprese na úrovni jednotlivých buněk, ale i pro další využití, jako je například FACS (Fluorescence-activated cell sorting; Fluorescenčně aktivované třídění buněk) nebo *in vitro* kultivace. Prezentovaný protokol je rozdělen do několika částí: a) vyjmutí tkáně z organismu, b) mechanická fragmentace tkáně, c) enzymatické štěpení extracelulární matrix, d) příprava buněčné suspenze a případně e) FACS. Celková doba a způsob izolace je zásadní pro získání kvalitní suspenze buněk, která nebude mít izolací změněnou genovou expresi. Trvání prvních čtyřech kroků proto bylo optimalizováno celkem na 35–45 minut. Závěrem byla prezentována vhodná strategie pro FACS a kvantifikováno zastoupení imunitních buněk v připraveném vzorku i ve finálních datech.

Tento protokol byl úspěšně aplikován při tvorbě „Atlasu zubních buněk“ (viz. publikace číslo 1) a to jak pro metodu smart-seq2, tak pro 10x. V souhrnu zde prezentujeme ověřený protokol pro získání kvalitní suspenze jednotlivých buněk ze zubu. Předpokládáme, že tento protokol bude možné aplikovat i na další typy tkání.

## 4 Závěr

Neustále se zdokonalující technologický vývoj se ruku v ruce pojí s pronikáním do větších a větších zákoutí a detailů fungování organismů. Nemusí se však vždy jednat o zjištěný (nebo také aplikovaný) výzkum. Samotná zvědavost a snaha o pochopení toho, jak věci fungují ve své nejbazálnější rovině, s sebou přináší radost a často i novou inspiraci, již později může (anebo nemusí) být využito.

Tato práce sumarizuje výsledky, které využívají nových technologických přístupů k zodpovídání těchto principů. Paralelně s tím však naše bádání otevírá desítky nových témat, jimž se v budoucnu budeme my nebo možná jiní výzkumníci věnovat. Věřím, že výsledky naší práce poskytnou důležitý vědomostní základ v našem oboru a snad i otevřou nové perspektivy pro čerstvá vědecká témata, která budou nejen cílit na poznání jako takové, ale bude díky nim umožněno aplikovat výsledky naší práce v metodách regenerativní medicíny.

Podstata naší práce i práce ostatních badatelů této doby však zatím stále spočívá v pečlivém zkoumání jednotlivých dílčích komponent (ať už se jedná o orgány, buňky, geny nebo jednotlivé molekuly), které tvoří organismus jako celek. To je bohužel často umožněno pouze destruktivním rozložením celkově fungujícího organismu na jeho jednotlivé části a následně jejich separátním studiem. Tento způsob práce tak pomáhá odhalit pouze jednu malou část z fungujícího celku. Je proto důležité stále nezapomínat na enormní komplexitu a původ i důvod celého organismu i života jako celku. Jedině to nám může poskytnout odpovědi na otázky, které zatím stále unikají našemu chápání.

*I když některým věcem zatím nerozumíme, vše má svůj čas, místo a smysl.*

## Použité zdroje

- An, Z., Sabalic, M., Bloomquist, R.F., Fowler, T.E., Streelman, T., Sharpe, P.T., 2018. A quiescent cell population replenishes mesenchymal stem cells to drive accelerated growth in mouse incisors. *Nat. Commun.* 9, 378. <https://doi.org/10.1038/s41467-017-02785-6>
- Bajaj, D., Arola, D., 2009. Role of prism decussation on fatigue crack growth and fracture of human enamel. *Acta Biomater.* 5, 3045–3056. <https://doi.org/10.1016/j.actbio.2009.04.013>
- Balic, A., Thesleff, I., 2015. Tissue Interactions Regulating Tooth Development and Renewal. *Curr. Top. Dev. Biol.* 115, 157–186. <https://doi.org/10.1016/bs.ctdb.2015.07.006>
- Barker, N., van Es, J.H., Kuipers, J., Kujala, P., van den Born, M., Cozijnsen, M., Haegbarth, A., Korving, J., Begthel, H., Peters, P.J., Clevers, H., 2007. Identification of stem cells in small intestine and colon by marker gene *Lgr5*. *Nature* 449, 1003–1007. <https://doi.org/10.1038/nature06196>
- Beertsen, W., Niehof, A., 1986. Root-analogue versus crown-analogue dentin: a radioautographic and ultrastructural investigation of the mouse incisor. *Anat. Rec.* 215, 106–118. <https://doi.org/10.1002/ar.1092150204>
- Bronner, M.E., LeDouarin, N.M., 2012. Evolution and Development of the Neural Crest: An Overview. *Dev. Biol.* 366, 2–9. <https://doi.org/10.1016/j.ydbio.2011.12.042>
- Cao, H., Wang, J., Li, X., Florez, S., Huang, Z., Venugopalan, S.R., Elangovan, S., Skobe, Z., Margolis, H.C., Martin, J.F., Amendt, B.A., 2010. MicroRNAs play a critical role in tooth development. *J. Dent. Res.* 89, 779–784. <https://doi.org/10.1177/0022034510369304>
- Chiba, Y., Saito, K., Martin, D., Boger, E.T., Rhodes, C., Yoshizaki, K., Nakamura, T., Yamada, A., Morell, R.J., Yamada, Y., Fukumoto, S., 2020. Single-Cell RNA-Sequencing From Mouse Incisor Reveals Dental Epithelial Cell-Type Specific Genes. *Front. Cell Dev. Biol.* 8, 841. <https://doi.org/10.3389/fcell.2020.00841>
- Dassule, H.R., McMahon, A.P., 1998. Analysis of epithelial-mesenchymal interactions in the initial morphogenesis of the mammalian tooth. *Dev. Biol.* 202, 215–227. <https://doi.org/10.1006/dbio.1998.8992>
- Dosedělová, H., Dumková, J., Lesot, H., Glocová, K., Kunová, M., Tucker, A.S., Veselá, I., Krejčí, P., Tichý, F., Hampl, A., Buchtová, M., 2015. Fate of the molar dental lamina in the monophyodont mouse. *PloS One* 10, e0127543. <https://doi.org/10.1371/journal.pone.0127543>
- Feng, J., Mantesso, A., De Bari, C., Nishiyama, A., Sharpe, P.T., 2011. Dual origin of mesenchymal stem cells contributing to organ growth and repair. *Proc. Natl. Acad. Sci. U. S. A.* 108, 6503–6508. <https://doi.org/10.1073/pnas.1015449108>

- Fraser, G.J., Cerny, R., Soukup, V., Bronner-Fraser, M., Streelman, J.T., 2010. The Odontode Explosion: The origin of tooth-like structures in vertebrates. *BioEssays News Rev. Mol. Cell. Dev. Biol.* 32, 808–817. <https://doi.org/10.1002/bies.200900151>
- Fresia, R., Marangoni, P., Burstyn-Cohen, T., Sharir, A., 2021. From Bite to Byte: Dental Structures Resolved at a Single-Cell Resolution. *J. Dent. Res.* 100, 897–905. <https://doi.org/10.1177/00220345211001848>
- Gans, C., Northcutt, R.G., 1983. Neural crest and the origin of vertebrates: a new head. *Science* 220, 268–273. <https://doi.org/10.1126/science.220.4594.268>
- Gruber, R., Stadlinger, B., Terheyden, H., 2022. Cell-to-Cell Communication: Cell-Atlas - Visual Biology in Oral Medicine.
- Harada, H., Kettunen, P., Jung, H.-S., Mustonen, T., Wang, Y.A., Thesleff, I., 1999. Localization of Putative Stem Cells in Dental Epithelium and Their Association with Notch and Fgf Signaling. *J. Cell Biol.* 147, 105–120.
- Indra, A.K., Warot, X., Brocard, J., Bornert, J.-M., Xiao, J.-H., Chambon, P., Metzger, D., 1999. Temporally-controlled site-specific mutagenesis in the basal layer of the epidermis: comparison of the recombinase activity of the tamoxifen-inducible Cre-ERT and Cre-ERT2 recombinases. *Nucleic Acids Res.* 27, 4324–4327. <https://doi.org/10.1093/nar/27.22.4324>
- Jernvall, J., Thesleff, I., 2012. Tooth shape formation and tooth renewal: evolving with the same signals. *Dev. Camb. Engl.* 139, 3487–3497. <https://doi.org/10.1242/dev.085084>
- Juuri, E., Saito, K., Ahtiainen, L., Seidel, K., Tummers, M., Hochedlinger, K., Klein, O.D., Thesleff, I., Michon, F., 2012. Sox2+ stem cells contribute to all epithelial lineages of the tooth via Sfrp5+ progenitors. *Dev. Cell* 23, 317–328. <https://doi.org/10.1016/j.devcel.2012.05.012>
- Kaukua, N., Shahidi, M.K., Konstantinidou, C., Dyachuk, V., Kaucka, M., Furlan, A., An, Z., Wang, L., Hultman, I., Ahrlund-Richter, L., Blom, H., Brismar, H., Lopes, N.A., Pachnis, V., Suter, U., Clevers, H., Thesleff, I., Sharpe, P., Ernfors, P., Fried, K., Adameyko, I., 2014. Glial origin of mesenchymal stem cells in a tooth model system. *Nature* 513, 551–554. <https://doi.org/10.1038/nature13536>
- Kharchenko, P.V., 2021. The triumphs and limitations of computational methods for scRNA-seq. *Nat. Methods* 18, 723–732. <https://doi.org/10.1038/s41592-021-01171-x>
- Khatibi Shahidi, M., Krivanek, J., Kaukua, N., Ernfors, P., Hladik, L., Kostal, V., Masich, S., Hampl, A., Chubanov, V., Gudermann, T., Romanov, R.A., Harkany, T., Adameyko, I., Fried, K., 2015. Three-dimensional Imaging Reveals New Compartments and Structural Adaptations in Odontoblasts. *J. Dent. Res.* 94, 945–954. <https://doi.org/10.1177/0022034515580796>

- Klein, O.D., Lyons, D.B., Balooch, G., Marshall, G.W., Basson, M.A., Peterka, M., Boran, T., Peterkova, R., Martin, G.R., 2008. An FGF signaling loop sustains the generation of differentiated progeny from stem cells in mouse incisors. *Development* 135, 377–385. <https://doi.org/10.1242/dev.015081>
- Krivanek, J., Adameyko, I., Fried, K., 2017. Heterogeneity and Developmental Connections between Cell Types Inhabiting Teeth. *Front. Physiol.* 8. <https://doi.org/10.3389/fphys.2017.00376>
- Krivanek, J., Lavicky, J., Boudierlique, T., Adameyko, I., 2021. Rapid Isolation of Single Cells from Mouse and Human Teeth. *J. Vis. Exp. JoVE.* <https://doi.org/10.3791/63043>
- Krivanek, J., Soldatov, R.A., Kastriti, M.E., Chontorotzea, T., Herdina, A.N., Petersen, J., Szarowska, B., Landova, M., Matejova, V.K., Holla, L.I., Kuchler, U., Zdrilic, I.V., Vijaykumar, A., Balic, A., Marangoni, P., Klein, O.D., Neves, V.C.M., Yianni, V., Sharpe, P.T., Harkany, T., Metscher, B.D., Bajénoff, M., Mina, M., Fried, K., Kharchenko, P.V., Adameyko, I., 2020. Dental cell type atlas reveals stem and differentiated cell types in mouse and human teeth. *Nat. Commun.* 11, 4816. <https://doi.org/10.1038/s41467-020-18512-7>
- Kwon, H.J.E., Park, E.K., Jia, S., Liu, H., Lan, Y., Jiang, R., 2015. Deletion of *Osr2* Partially Rescues Tooth Development in *Runx2* Mutant Mice. *J. Dent. Res.* 94, 1113–1119. <https://doi.org/10.1177/0022034515583673>
- Kyrylkova, K., Kyryachenko, S., Biehs, B., Klein, O., Kioussi, C., Leid, M., 2012. BCL11B regulates epithelial proliferation and asymmetric development of the mouse mandibular incisor. *PloS One* 7, e37670. <https://doi.org/10.1371/journal.pone.0037670>
- La Manno, G., Soldatov, R., Zeisel, A., Braun, E., Hochgerner, H., Petukhov, V., Lidschreiber, K., Kastriti, M.E., Lönnerberg, P., Furlan, A., Fan, J., Borm, L.E., Liu, Z., van Bruggen, D., Guo, J., He, X., Barker, R., Sundström, E., Castelo-Branco, G., Cramer, P., Adameyko, I., Linnarsson, S., Kharchenko, P.V., 2018. RNA velocity of single cells. *Nature* 560, 494–498. <https://doi.org/10.1038/s41586-018-0414-6>
- Lacruz, R.S., Habelitz, S., Wright, J.T., Paine, M.L., 2017. Dental Enamel Formation and Implications for Oral Health and Disease. *Physiol. Rev.* 97, 939–993. <https://doi.org/10.1152/physrev.00030.2016>
- Landova Sulcova, M., Zahradnicek, O., Dumkova, J., Dosedelova, H., Krivanek, J., Hampl, M., Kavkova, M., Zikmund, T., Gregorovicova, M., Sedmera, D., Kaiser, J., Tucker, A.S., Buchtova, M., 2020. Developmental mechanisms driving complex tooth shape in reptiles. *Dev. Dyn. Off. Publ. Am. Assoc. Anat.* 249, 441–464. <https://doi.org/10.1002/dvdy.138>
- Lapthanasupkul, P., Feng, J., Mantesso, A., Takada-Horisawa, Y., Vidal, M., Koseki, H., Wang, L., An, Z., Miletich, I., Sharpe, P.T., 2012. Ring1a/b polycomb proteins regulate the mesenchymal stem cell niche in continuously growing incisors. *Dev. Biol.* 367, 140–153. <https://doi.org/10.1016/j.ydbio.2012.04.029>

- Lavicky, J., Kolouskova, M., Prochazka, D., Rakultsev, V., Gonzalez-Lopez, M., Steklikova, K., Bartos, M., Vijaykumar, A., Kaiser, J., Pořizka, P., Hovorakova, M., Mina, M., Krivanek, J., 2021. The Development of Dentin Microstructure Is Controlled by the Type of Adjacent Epithelium. *J. Bone Miner. Res.* jbmr.4471. <https://doi.org/10.1002/jbmr.4471>
- Le Douarin, N.M., Dupin, E., 2018. The “beginnings” of the neural crest. *Dev. Biol., The Neural Crest: 150 years after His’ discovery* 444, S3–S13. <https://doi.org/10.1016/j.ydbio.2018.07.019>
- Le Douarin, N.M., Dupin, E., 2012. The neural crest in vertebrate evolution. *Curr. Opin. Genet. Dev.* 22, 381–389. <https://doi.org/10.1016/j.gde.2012.06.001>
- Mitsiadis, T.A., Chéraud, Y., Sharpe, P., Fontaine-Pérus, J., 2003. Development of teeth in chick embryos after mouse neural crest transplantations. *Proc. Natl. Acad. Sci. U. S. A.* 100, 6541–6545. <https://doi.org/10.1073/pnas.1137104100>
- Nanci, A., TenCate, A.R., 2018. Ten Cate’s oral histology: development, structure, and function, 9th edition. ed. Elsevier, St. Louis, Missouri.
- Neves, V.C.M., Yianni, V., Sharpe, P.T., 2020. Macrophage modulation of dental pulp stem cell activity during tertiary dentinogenesis. *Sci. Rep.* 10, 20216. <https://doi.org/10.1038/s41598-020-77161-4>
- Nottmeier, C., Decker, M.G., Luther, J., von Kroge, S., Kahl-Nieke, B., Amling, M., Schinke, T., Petersen, J., Koehne, T., 2020. Accelerated tooth movement in *Rsk2*-deficient mice with impaired cementum formation. *Int. J. Oral Sci.* 12, 35. <https://doi.org/10.1038/s41368-020-00102-4>
- Nweeia, M.T., Eichmiller, F.C., Hauschka, P.V., Donahue, G.A., Orr, J.R., Ferguson, S.H., Watt, C.A., Mead, J.G., Potter, C.W., Dietz, R., Giuseppetti, A.A., Black, S.R., Trachtenberg, A.J., Kuo, W.P., 2014. Sensory ability in the narwhal tooth organ system. *Anat. Rec. Hoboken NJ* 2007 297, 599–617. <https://doi.org/10.1002/ar.22886>
- Pagella, P., de Vargas Roditi, L., Stadlinger, B., Moor, A.E., Mitsiadis, T.A., 2021a. A single-cell atlas of human teeth. *iScience* 24, 102405. <https://doi.org/10.1016/j.isci.2021.102405>
- Pagella, P., Stadlinger, B., Mitsiadis, T.A., 2021b. Isolation of dental pulp and periodontal cells from human teeth for single-cell RNA sequencing. *STAR Protoc.* 2, 100953. <https://doi.org/10.1016/j.xpro.2021.100953>
- Pang, Y.W., Feng, J., Daltoe, F., Fatscher, R., Gentleman, E., Gentleman, M.M., Sharpe, P.T., 2016. Perivascular Stem Cells at the Tip of Mouse Incisors Regulate Tissue Regeneration. *J. Bone Miner. Res. Off. J. Am. Soc. Bone Miner. Res.* 31, 514–523. <https://doi.org/10.1002/jbmr.2717>
- Picelli, S., Faridani, O.R., Björklund, Å.K., Winberg, G., Sagasser, S., Sandberg, R., 2014. Full-length RNA-seq from single cells using Smart-seq2. *Nat. Protoc.* 9, 171–181. <https://doi.org/10.1038/nprot.2014.006>

- Renvoisé, E., Michon, F., 2014. An Evo-Devo perspective on ever-growing teeth in mammals and dental stem cell maintenance. *Front. Physiol.* 5, 324. <https://doi.org/10.3389/fphys.2014.00324>
- Rincon, J.C., Young, W.G., Bartold, P.M., 2006. The epithelial cell rests of Malassez – a role in periodontal regeneration? *J. Periodontal Res.* 41, 245–252. <https://doi.org/10.1111/j.1600-0765.2006.00880.x>
- Sanders, E.J., 2011. The roles of epithelial–mesenchymal cell interactions in developmental processes. *Biochem. Cell Biol.* <https://doi.org/10.1139/o88-063>
- Sanz-Navarro, M., Delgado, I., Torres, M., Mustonen, T., Michon, F., Rice, D.P., 2019. Dental Epithelial Stem Cells Express the Developmental Regulator Meis1. *Front. Physiol.* 10, 249. <https://doi.org/10.3389/fphys.2019.00249>
- Sasaki, T., Segawa, K., Takiguchi, R., Higashi, S., 1984. Intercellular junctions in the cells of the human enamel organ as revealed by freeze-fracture. *Arch. Oral Biol.* 29, 275–286. [https://doi.org/10.1016/0003-9969\(84\)90101-8](https://doi.org/10.1016/0003-9969(84)90101-8)
- Seidel, K., Marangoni, P., Tang, C., Houshmand, B., Du, W., Maas, R.L., Murray, S., Oldham, M.C., Klein, O.D., 2017. Resolving stem and progenitor cells in the adult mouse incisor through gene co-expression analysis. *eLife* 6, e24712. <https://doi.org/10.7554/eLife.24712>
- Sharir, A., Marangoni, P., Zilionis, R., Wan, M., Wald, T., Hu, J.K., Kawaguchi, K., Castillo-Azofeifa, D., Epstein, L., Harrington, K., Pagella, P., Mitsiadis, T., Siebel, C.W., Klein, A.M., Klein, O.D., 2019. A large pool of actively cycling progenitors orchestrates self-renewal and injury repair of an ectodermal appendage. *Nat. Cell Biol.* 21, 1102–1112. <https://doi.org/10.1038/s41556-019-0378-2>
- Sharpe, P.T., 2016. Dental mesenchymal stem cells. *Dev. Camb. Engl.* 143, 2273–2280. <https://doi.org/10.1242/dev.134189>
- Sloan, A.J., 2015. Chapter 29 - Biology of the Dentin-Pulp Complex, in: Vishwakarma, A., Sharpe, P., Shi, S., Ramalingam, M. (Eds.), *Stem Cell Biology and Tissue Engineering in Dental Sciences*. Academic Press, Boston, pp. 371–378. <https://doi.org/10.1016/B978-0-12-397157-9.00033-3>
- Smith, C.E., 1998. Cellular and chemical events during enamel maturation. *Crit. Rev. Oral Biol. Med. Off. Publ. Am. Assoc. Oral Biol.* 9, 128–161. <https://doi.org/10.1177/10454411980090020101>
- Smith, C.E., Hu, Y., Hu, J.C.-C., Simmer, J.P., 2019. Characteristics of the transverse 2D uniserial arrangement of rows of decussating enamel rods in the inner enamel layer of mouse mandibular incisors. *J. Anat.* 235, 912–930. <https://doi.org/10.1111/joa.13053>
- Soldatov, R., Kaucka, M., Kastriti, M.E., Petersen, J., Chontorotzea, T., Englmaier, L., Akkuratova, N., Yang, Y., Häring, M., Dyachuk, V., Bock, C., Farlik, M., Piacentino, M.L., Boismoreau, F., Hilscher, M.M., Yokota, C., Qian, X., Nilsson, M., Bronner, M.E., Croci, L., Hsiao, W.-Y., Guertin, D.A., Brunet, J.-F., Consalez,

- G.G., Ernfors, P., Fried, K., Kharchenko, P.V., Adameyko, I., 2019. Spatiotemporal structure of cell fate decisions in murine neural crest. *Science* 364, eaas9536. <https://doi.org/10.1126/science.aas9536>
- Soukup, V., Epperlein, H.-H., Horáček, I., Cerny, R., 2008. Dual epithelial origin of vertebrate oral teeth. *Nature* 455, 795–798. <https://doi.org/10.1038/nature07304>
- Suomalainen, M., Thesleff, I., 2010. Patterns of Wnt pathway activity in the mouse incisor indicate absence of Wnt/beta-catenin signaling in the epithelial stem cells. *Dev. Dyn. Off. Publ. Am. Assoc. Anat.* 239, 364–372. <https://doi.org/10.1002/dvdy.22106>
- Tapaltsyán, V., Charles, C., Hu, J., Mindell, D., Ahituv, N., Wilson, G.M., Black, B.L., Viriot, L., Klein, O.D., 2016. Identification of novel Fgf enhancers and their role in dental evolution: Novel Fgf enhancers and their role in dental evolution. *Evol. Dev.* 18, 31–40. <https://doi.org/10.1111/ede.12132>
- Tapaltsyán, V., Eronen, J.T., Lawing, A.M., Sharir, A., Janis, C., Jernvall, J., Klein, O.D., 2015. Continuously growing rodent molars result from a predictable quantitative evolutionary change over 50 million years. *Cell Rep.* 11, 673–680. <https://doi.org/10.1016/j.celrep.2015.03.064>
- Thesleff, I., 2015. Chapter 22 - Molecular Genetics of Tooth Development, in: Moody, S.A. (Ed.), *Principles of Developmental Genetics* (Second Edition). Academic Press, Oxford, pp. 393–405. <https://doi.org/10.1016/B978-0-12-405945-0.00022-3>
- Thesleff, I., Hurmerinta, K., 1981. Tissue Interactions in Tooth Development. *Differentiation* 18, 75–88. <https://doi.org/10.1111/j.1432-0436.1981.tb01107.x>
- Thesleff, I., Keränen, S., Jernvall, J., 2001. Enamel knots as signaling centers linking tooth morphogenesis and odontoblast differentiation. *Adv. Dent. Res.* 15, 14–18. <https://doi.org/10.1177/08959374010150010401>
- Thesleff, I., Tummers, M., 2008. Tooth organogenesis and regeneration, in: *StemBook*. Harvard Stem Cell Institute, Cambridge (MA).
- Tummers, M., Thesleff, I., 2009. The importance of signal pathway modulation in all aspects of tooth development. *J. Exp. Zool. B Mol. Dev. Evol.* 312B, 309–319. <https://doi.org/10.1002/jez.b.21280>
- VanHorn, S., Morris, S.A., 2021. Next-Generation Lineage Tracing and Fate Mapping to Interrogate Development. *Dev. Cell* 56, 7–21. <https://doi.org/10.1016/j.devcel.2020.10.021>
- Vidovic, I., Banerjee, A., Fatahi, R., Matthews, B.G., Dymant, N.A., Kalajzic, I., Mina, M., 2017.  $\alpha$ SMA-Expressing Perivascular Cells Represent Dental Pulp Progenitors In Vivo. *J. Dent. Res.* 96, 323–330. <https://doi.org/10.1177/0022034516678208>
- Vijaykumar, A., Ghassem-Zadeh, S., Vidovic-Zdrilic, I., Komitas, K., Adameyko, I., Krivanek, J., Fu, Y., Maye, P., Mina, M., 2019. Generation and characterization of DSPP-Cerulean/DMP1-Cherry reporter mice. *Genes*. N. Y. N 2000 57, e23324. <https://doi.org/10.1002/dvg.23324>

- von Koenigswald, W., 2011. Diversity of hypsodont teeth in mammalian dentitions – construction and classification. *Palaeontogr. Abt. A* 294, 63–94. <https://doi.org/10.1127/pala/294/2011/63>
- Wang, X.-P., Suomalainen, M., Felszeghy, S., Zelarayan, L.C., Alonso, M.T., Plikus, M.V., Maas, R.L., Chuong, C.-M., Schimmang, T., Thesleff, I., 2007. An Integrated Gene Regulatory Network Controls Stem Cell Proliferation in Teeth. *PLOS Biol.* 5, e159. <https://doi.org/10.1371/journal.pbio.0050159>
- Wang, Y.H., Upholt, W.B., Sharpe, P.T., Kollar, E.J., Mina, M., 1998. Odontogenic epithelium induces similar molecular responses in chick and mouse mandibular mesenchyme. *Dev. Dyn. Off. Publ. Am. Assoc. Anat.* 213, 386–397. [https://doi.org/10.1002/\(SICI\)1097-0177\(199812\)213:4<386::AID-AJA4>3.0.CO;2-2](https://doi.org/10.1002/(SICI)1097-0177(199812)213:4<386::AID-AJA4>3.0.CO;2-2)
- Xiong, J., Gronthos, S., Bartold, P.M., 2013. Role of the epithelial cell rests of Malassez in the development, maintenance and regeneration of periodontal ligament tissues. *Periodontol.* 2000 63, 217–233. <https://doi.org/10.1111/prd.12023>
- Yianni, V., Sharpe, P.T., 2020. Transcriptomic Profiling of Dental Pulp Pericytes: An RNAseq Approach. *Front. Dent. Med.* 1, 6. <https://doi.org/10.3389/fdmed.2020.00006>
- Yu, T., Klein, O.D., 2020. Molecular and cellular mechanisms of tooth development, homeostasis and repair. *Dev. Camb. Engl.* 147. <https://doi.org/10.1242/dev.184754>
- Zhang, Y., Riesterer, C., Ayrall, A.-M., Sablitzky, F., Littlewood, T.D., Reth, M., 1996. Inducible Site-Directed Recombination in Mouse Embryonic Stem Cells. *Nucleic Acids Res.* 24, 543–548. <https://doi.org/10.1093/nar/24.4.543>
- Zhao, H., Feng, J., Seidel, K., Shi, S., Klein, O., Sharpe, P., Chai, Y., 2014. Secretion of shh by a neurovascular bundle niche supports mesenchymal stem cell homeostasis in the adult mouse incisor. *Cell Stem Cell* 14, 160–173. <https://doi.org/10.1016/j.stem.2013.12.013>

## 5 Přílohy

### 5.1 Příloha A – Publikace číslo 1

# **Dental cell type atlas reveals stem and differentiated cell types in mouse and human teeth**

*Jan Krivanek, Ruslan A Soldatov, Maria Eleni Kastriti, Tatiana Chontorotzea, Anna Nele Herdina, Julian Petersen, Bara Szarowska, Marie Landova, Veronika Kovar Matejova, Lydie Izakovicova Holla, Ulrike Kuchler, Ivana Vidovic Zdrilic, Anushree Vijaykumar, Anamaria Balic, Pauline Marangoni, Ophir D Klein, Vitor C M Neves, Val Yianni, Paul T Sharpe, Tibor Harkany, Brian D Metscher, Marc Bajénoff, Mina Mina, Kaj Fried, Peter V Kharchenko, Igor Adameyko*

# Dental cell type atlas reveals stem and differentiated cell types in mouse and human teeth

Jan Krivanek <sup>1,2,18</sup>, Ruslan A. Soldatov<sup>3,18</sup>, Maria Eleni Kastri<sup>1,4</sup>, Tatiana Chontorotzea<sup>1</sup>, Anna Nele Herdina<sup>4</sup>, Julian Petersen <sup>1,4</sup>, Bara Szarowska<sup>1</sup>, Marie Landova<sup>5</sup>, Veronika Kovar Matejova<sup>6</sup>, Lydie Izakovicova Holla <sup>6</sup>, Ulrike Kuchler<sup>7,8</sup>, Ivana Vidovic Zdrilic<sup>9</sup>, Anushree Vijaykumar <sup>9</sup>, Anamaria Balic <sup>10</sup>, Pauline Marangoni<sup>11</sup>, Ophir D. Klein <sup>11,12</sup>, Vitor C. M. Neves<sup>13</sup>, Val Yianni <sup>13</sup>, Paul T. Sharpe <sup>13</sup>, Tibor Harkany<sup>1,14</sup>, Brian D. Metscher <sup>15</sup>, Marc Bajénoff<sup>16</sup>, Mina Mina<sup>9</sup>, Kaj Fried<sup>14</sup>, Peter V. Kharchenko <sup>3</sup>✉ & Igor Adameyko <sup>1,4,17</sup>✉

Understanding cell types and mechanisms of dental growth is essential for reconstruction and engineering of teeth. Therefore, we investigated cellular composition of growing and non-growing mouse and human teeth. As a result, we report an unappreciated cellular complexity of the continuously-growing mouse incisor, which suggests a coherent model of cell dynamics enabling unarrested growth. This model relies on spatially-restricted stem, progenitor and differentiated populations in the epithelial and mesenchymal compartments underlying the coordinated expansion of two major branches of pulpal cells and diverse epithelial subtypes. Further comparisons of human and mouse teeth yield both parallelisms and differences in tissue heterogeneity and highlight the specifics behind growing and non-growing modes. Despite being similar at a coarse level, mouse and human teeth reveal molecular differences and species-specific cell subtypes suggesting possible evolutionary divergence. Overall, here we provide an atlas of human and mouse teeth with a focus on growth and differentiation.

<sup>1</sup> Department of Molecular Neuroscience, Center for Brain Research, Medical University of Vienna, Vienna, Austria. <sup>2</sup> Department of Histology and Embryology, Faculty of Medicine, Masaryk University, Brno, Czech Republic. <sup>3</sup> Department of Biomedical Informatics, Harvard Medical School, Boston, MA, USA. <sup>4</sup> Department of Physiology and Pharmacology, Karolinska Institutet, Stockholm, Sweden. <sup>5</sup> Institute of Animal Physiology and Genetics, CAS, Brno, Czech Republic. <sup>6</sup> Clinic of Stomatology, Institution Shared with St. Anne's Faculty Hospital, Faculty of Medicine, Masaryk University, Brno, Czech Republic. <sup>7</sup> Department of Oral Biology, Medical University of Vienna, Vienna, Austria. <sup>8</sup> Department of Oral Surgery, Medical University of Vienna, Vienna, Austria. <sup>9</sup> Department of Craniofacial Sciences, School of Dental Medicine, University of Connecticut Health Center, Farmington, CT, USA. <sup>10</sup> Research Program in Developmental Biology, Institute of Biotechnology, University of Helsinki, Helsinki, Finland. <sup>11</sup> Program in Craniofacial Biology and Department of Orofacial Sciences, University of California, San Francisco, CA, USA. <sup>12</sup> Department of Pediatrics and Institute for Human Genetics, University of California, San Francisco, CA, USA. <sup>13</sup> Centre for Craniofacial and Regenerative Biology, Faculty of Dentistry, Oral & Craniofacial Sciences, King's College London, London, UK. <sup>14</sup> Department of Neuroscience, Karolinska Institutet, Stockholm, Sweden. <sup>15</sup> Department of Evolutionary Biology, University of Vienna, Vienna, Austria. <sup>16</sup> Centre d'Immunologie de Marseille-Luminy, Aix Marseille Université, INSERM, CNRS UMR, Marseille, France. <sup>17</sup> Department of Neuroimmunology, Center for Brain Research, Medical University of Vienna, Vienna, Austria. <sup>18</sup> These authors contributed equally: Jan Krivanek, Ruslan A. Soldatov. ✉email: [peter.kharchenko@post.harvard.edu](mailto:peter.kharchenko@post.harvard.edu); [igor.adameyko@ki.se](mailto:igor.adameyko@ki.se)

Mammalian teeth are formed by the ectoderm of the first pharyngeal arch and neural crest-derived ectomesenchyme. Developmental interactions between these tissue types enable the construction of solid dental structures composed of epithelium-derived crown enamel and ectomesenchyme-derived dentin<sup>1–4</sup>. In humans, teeth primordia are formed in utero and complete their growth before adulthood, at which point the progenitor populations disappear. In contrast to this, in mice and many other species, teeth can continue to grow throughout life, providing the major model system to study progression of various tooth cell lineages from the dental stem-cell populations located in the apical end of the tooth. In mice, the incisor stem-cell population continuously self-renews and replenishes tissues that are lost due to gnawing, making this model attractive for studies of stem-cell generation, cell differentiation, homeostasis, and injury-induced regeneration. In addition, the mouse incisor represents a model of continuously self-renewing organ with cell dynamics conceptually similar to gut epithelium, hair follicles, and nails. Even though major tooth cell types have long been identified, the spectrum of rare and transient cell populations and interactions that enable tooth growth remain poorly understood. The identity of epithelial and mesenchymal stem populations and their possible spatial and functional diversity remains unresolved, especially when it comes to such populations in growing and nongrowing human teeth. Besides, whether rodent teeth represent a bioequivalent model system for studying specific aspects of human tooth development and physiology is not yet clear. The long held-view is that the human teeth contain mesenchymal stem cells analogous to mouse incisor mesenchymal stem cells<sup>5–8</sup>. However, at this point, no clear consensus has been reached about the molecular identity of such cells in vivo<sup>6,9</sup>. In addition, the role and population structure of other cell types, such as resident cells of the immune system, is unclear in relation to the maintenance of local tissue homeostasis and beyond their major protective function in teeth. There is growing evidence that macrophages are important constituents influencing the stem-cell compartments, for instance, in control of the intestinal stem-cell niche or in promoting wound-induced hair follicle regeneration<sup>10,11</sup>.

Towards answering these questions, we applied single-cell transcriptomics and lineage tracing techniques with a specific aim to examine the organizational complexity and self-renewal of growing mouse incisor, contrasting it with nongrowing mouse molars, and evaluating the extent to which the mouse model reflects the growth of human teeth. Our data revealed stem and differentiated cell subtypes in epithelial and mesenchymal compartments and heterogeneity of tissue-residential immune cells in mouse incisor. We provide a comparative map of cell types inhabiting mouse and human growing vs. nongrowing teeth.

## Results

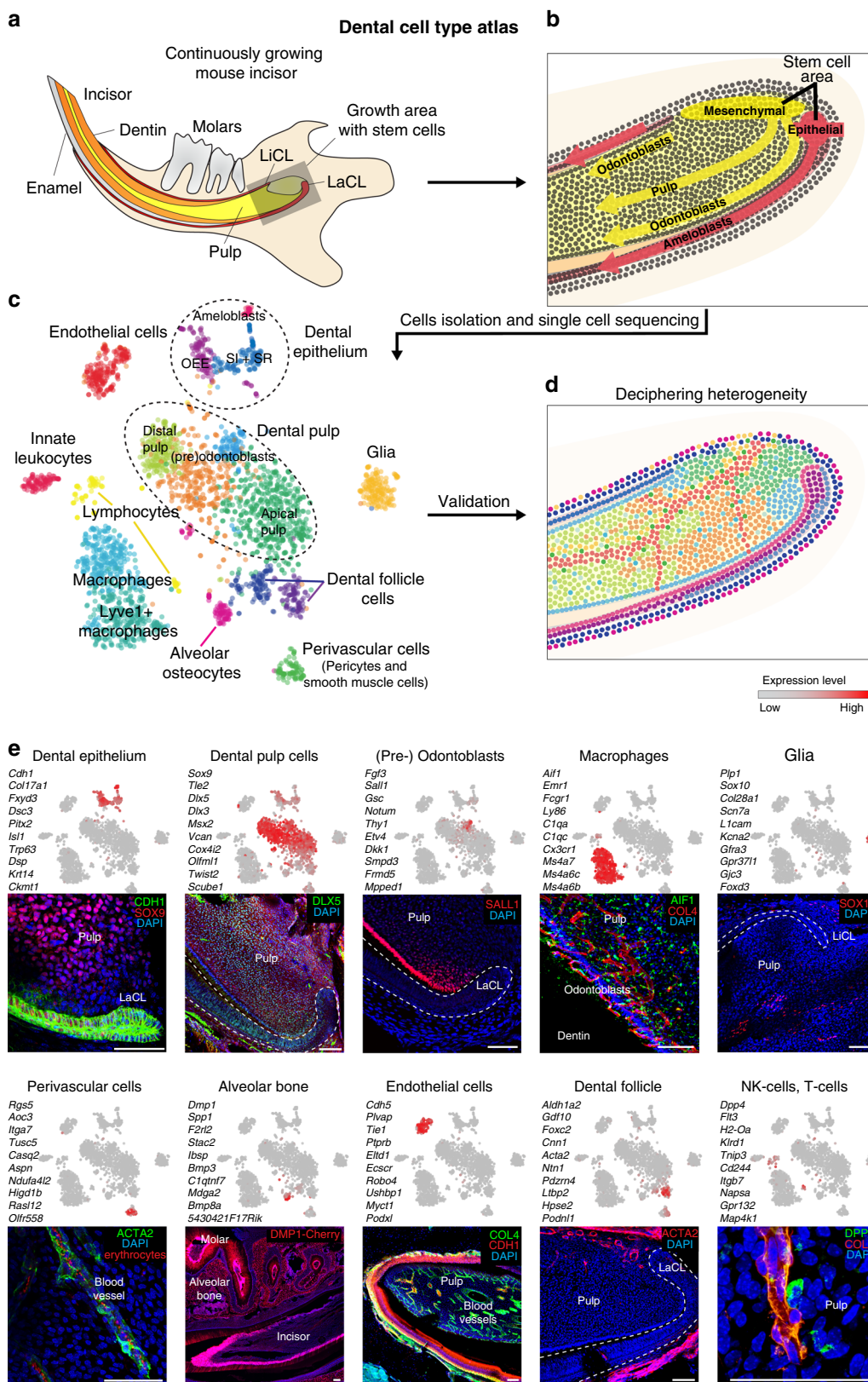
**sc-RNA-seq reveals cell heterogeneity of the self-renewing mouse incisor.** To address the entire course of differentiation of cell types in the tooth during self-renewal, we first isolated all dental tissues from the adult mouse incisor and sequenced individual cell transcriptomes with the Smart-seq2 protocol to obtain high sequencing depth<sup>12</sup> (Fig. 1a, b). Clustering using PAGODA revealed 17 major cell subpopulations (Fig. 1c–e; Supplementary Figs. 1–3 and Supplementary table 1,2,3 and Supplementary Data File 1), including the major immune, epithelial, and mesenchymal compartments. The relative in vivo cell-type abundances might not be reflective of clusters proportions due to cell isolation biases and strategies<sup>13</sup>. All general cell types show considerable degree of internal heterogeneity (Supplementary Figs. 1e–g, i, 3) emphasizing complexity of interactions and physiological processes in a

growing and self-renewing tooth. We next focused on the most striking aspects of population complexity of epithelial (Figs. 2–4) and mesenchymal (Figs. 5–7) compartments, their human analogues (Figs. 8, 9), and finally immune (Fig. 10) populations.

### Heterogeneity of the epithelial compartment in mouse incisor.

The epithelial compartment of the tooth is essential to generate the enamel, as well as for the morphogenetic guidance of tooth development and self-renewal. Focused reanalysis of the epithelial (*Krt14* and *Cdh1* co-expressing) subpopulation showed a complex mixture of at least 13 distinct epithelial clusters (Fig. 2a). These include mature subpopulations, such as enamel-generating ameloblasts, and a heterogeneous pool of stem/progenitor cells. During sequencing, we enriched for epithelial progenitors by using *Sox2*-driven GFP in *Sox2*<sup>GFP</sup> animals and subsequent FACS of fluorescent cells. Ameloblasts and enamel development in the incisor is not restricted to early developmental stages as it is in molars. Continuous replenishing of enamel is essential for the incisor growth. Thus, we can find all the ameloblasts' stages: closer to the labial cervical loop we can find early stages and closer to the tip more differentiated stages. Differentiation of ameloblasts starts at the preameloblast stage (early fate decision and first differentiation), then continues through secretory stage during which the enamel backbone is formed. Subsequently, the secretory ameloblasts are further differentiated in a maturation phase during which the first enamel backbone is fully calcified<sup>2</sup>. During the last phase, known as a postmaturation phase, the enamel epithelium diminishes and enamel production is completed. Consistent with these stages, we observed spatially separated stages of ameloblast differentiation, including preameloblasts (*Shh*<sup>+</sup> cluster 11), secretory (*Enam*<sup>+</sup> cluster 5), maturation (*Klk4*<sup>+</sup> cluster 10) and postmaturation (*Gm17660*<sup>+</sup> cluster 6) stages (Fig. 2a, e, Fig. 4a, c, h, i)<sup>14–16</sup>. Our results show that transitions in gene expression profiles between the canonical stages are rather abrupt, consistent with the fact that the stages were previously characterized based on significant morphological and functional changes during ameloblast differentiation. The data show progressive modulation of transcription factor expression during different stages of ameloblast development (Fig. 4d–f), connecting known spatial and morphological transitions associated with the ameloblast differentiation with previously uncharacterized intermediate transcriptional states. In addition to these spatially separated populations, we observed a subset of RYR2<sup>+</sup> cells scattered in the ameloblasts layer (cluster 3) (Fig. 2a, b). The function of these cells is unknown, however this population expresses different mechanotransduction-related genes: *Piezo2*, *Trpm2*, *Trpm3*, and *Trpm6* cation channels, as well as calcium-dependent genes (*Itpr1*, *Ryr1*, and *Ryr2*) (Fig. 3b and Supplementary Table 1)<sup>17–19</sup>. To clarify if these cells can respond by changing their numbers to the lack of mechanical load, we clipped the incisor on one side of the jaw to prevent the usage of this tooth for a significant period of time. This unilateral tooth clipping experiment did not reveal any changes in the number and distribution of RYR2<sup>+</sup> cells (Fig. 3i).

Other mature populations in the tooth epithelium included stratum intermedium (clusters 8, 9, and 1) and outer enamel epithelium (cluster 4), whose functions are poorly understood (Fig. 2a). The identity of cluster 1 was unclear, but immunohistochemistry using THBD as a marker specific to this population, revealed that these previously uncharacterized cells reside in a distinct anatomical structure that we named the cuboidal layer of stratum intermedium (Figs. 2b, 3g, h). The broader gene expression signature of these cells (*Cygb*, *Nphs1*, and *Rhcg*) suggested that they maintain the functional interphase between blood vessels and metabolically active ameloblasts<sup>20–23</sup>.



Such function might be important for proper ameloblasts' activity essential for the efficient enamel synthesis.

The repertoire of stem and progenitor cells supporting these diverse tooth epithelial populations is poorly characterized. A combination of putative markers for dental epithelial stem cells (*Sox2*, *Lrig1*, *Bmi1*, *Gli1*, *Igfbp5*, and *Lgr5*) identified from studies of

late embryogenesis<sup>24–28</sup>, showed most consistent expression in a subset of cluster 13 (Figs. 2a, 4b, c, g). Even this small subpopulation, however, was heterogeneous. For instance, *Sox2*, *Acta2* and many other genes were specifically co-expressed in a single cell from the stem-cell subcluster, suggesting a distinct stem-cell subtype. Indeed, lineage tracing with *Acta2*<sup>CreERT2/R26</sup><sup>tdTomato</sup>

**Fig. 1 Unbiased identification, validation, and spatial mapping of major dental cell types and subpopulations.** **a** Schematic drawing of continuously growing mouse incisor with highlighted stem-cell area. **b** Cell dynamics during self-renewal and growth based on the activity of the dental epithelial and mesenchymal stem cells. **c** Unbiased identification of dental cell types and subpopulations. t-SNE dimensional reduction visualizes the similarity of the expression profiles of 2889 single cells (individual points). Colors demonstrate 17 clusters as defined by PAGODA clustering. All major clusters correspond to cell types in the mouse incisor, defined by expression of known markers. **d** Schematic drawing summarizing validation and mapping of the observed cellular subpopulations back onto the incisor tissue preparations. **e** Validations and mapping of unbiasedly identified populations based on the expression of selected marker genes. All validations were performed by immunohistochemistry except of alveolar bone panel where *DSPC<sup>Creulean</sup>/DMP1<sup>Cherry</sup>* mice was used (only red channel showed). Note. SOX9 is well-known marker for pulp cells, COL4 for blood vessels, CDH1 for epithelium, and ACTA2 for dental follicle (and perivascular cells). All these marker genes are highly and specifically expressed in corresponding clusters (Supplementary Table 1), but do not belong to top10 genes shown in plots above the images. (LiCL Lingual Cervical Loop, LaCL Labial Cervical Loop, SI Stratum Intermedium, SR Stellate reticulum, OEE Outer Enamel Epithelium). Scale bars: 50  $\mu$ m.

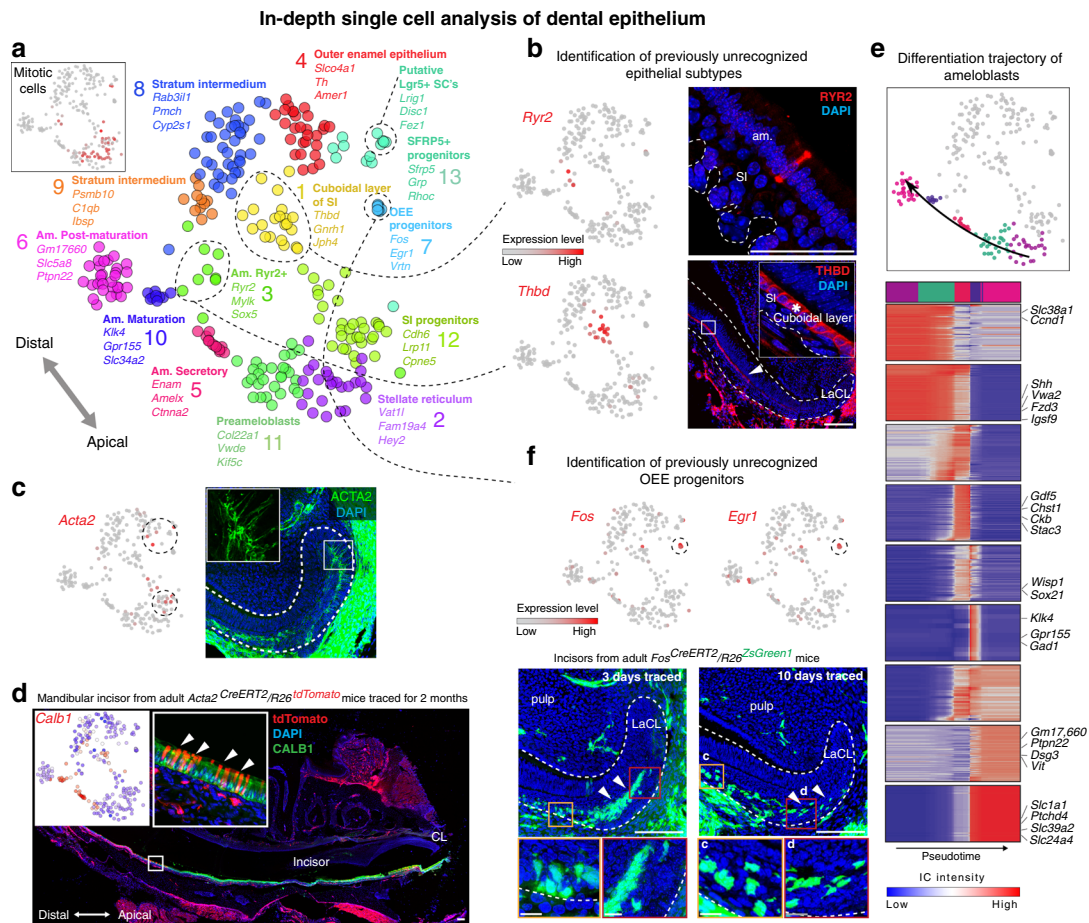


**Fig. 2 In-depth single-cell analysis of dental epithelium.** **a** t-SNE dimensional reduction shows subpopulations of 268 single epithelial cells. 13 unbiased clusters (colors) reveal previously unrecognized stem, progenitor and mature epithelial subtypes. Inset: mitotic signature as defined by average expression of cell-cycle-related genes. **b** Identification of a previously unrecognized cellular subtypes of epithelial layer. RYR2<sup>+</sup> cells in ameloblasts' layer and THBD<sup>+</sup> subpopulation of stratum intermedium organized into cuboidal layer found by immunohistochemistry. **c** Panel on the right shows localization of ACTA2-expressing cells inside the labial cervical loop (immunohistochemistry) and corresponding expression of *Acta2* predicted from RNA-seq analysis (left panel). **d** Long-term (2 months) lineage tracing of a *Acta2<sup>CreERT2</sup>/R26<sup>tdTomato</sup>* dental epithelial stem cells shows the traced cells in both apical (near the cervical loop) and distal ameloblasts. Ameloblast character was proved both morphologically and by expression of CALB1 (immunohistochemistry). **e** Transcriptional program of ameloblasts differentiation. Four clusters corresponding to different stages of ameloblasts maturation (upper). Transcriptional states of ameloblasts progenitors were modeled as a single trajectory, which reveals sequence of cell state transitions and linked activity developmental gene modules (bottom). Heatmap: the cells (columns) are arranged according to estimated pseudotime, genes (rows) were clustered in nine modules. Smoothed gene expression profiles are shown. **f** Transient progenitor population found in labial cervical loop is demarcated by the expression of *Egr1* and *Fos*. Panels in the bottom part shows the lineage tracing of *Fos<sup>CreERT2</sup>/R26<sup>ZsGreen1</sup>*. Insets show the lineage traced cells in outer enamel epithelium. Of note, *Fos<sup>CreERT2</sup>/R26<sup>ZsGreen1</sup>* traced cells in epithelial and mesenchymal compartments are of distinct origins since compartments are spatially separated. (LaCL Labial Cervical Loop, SI Stratum Intermedium, Am. Ameloblasts). Scale bars: **b, d, e**: 50  $\mu$ m; **c** and insets of **e**: 10  $\mu$ m.

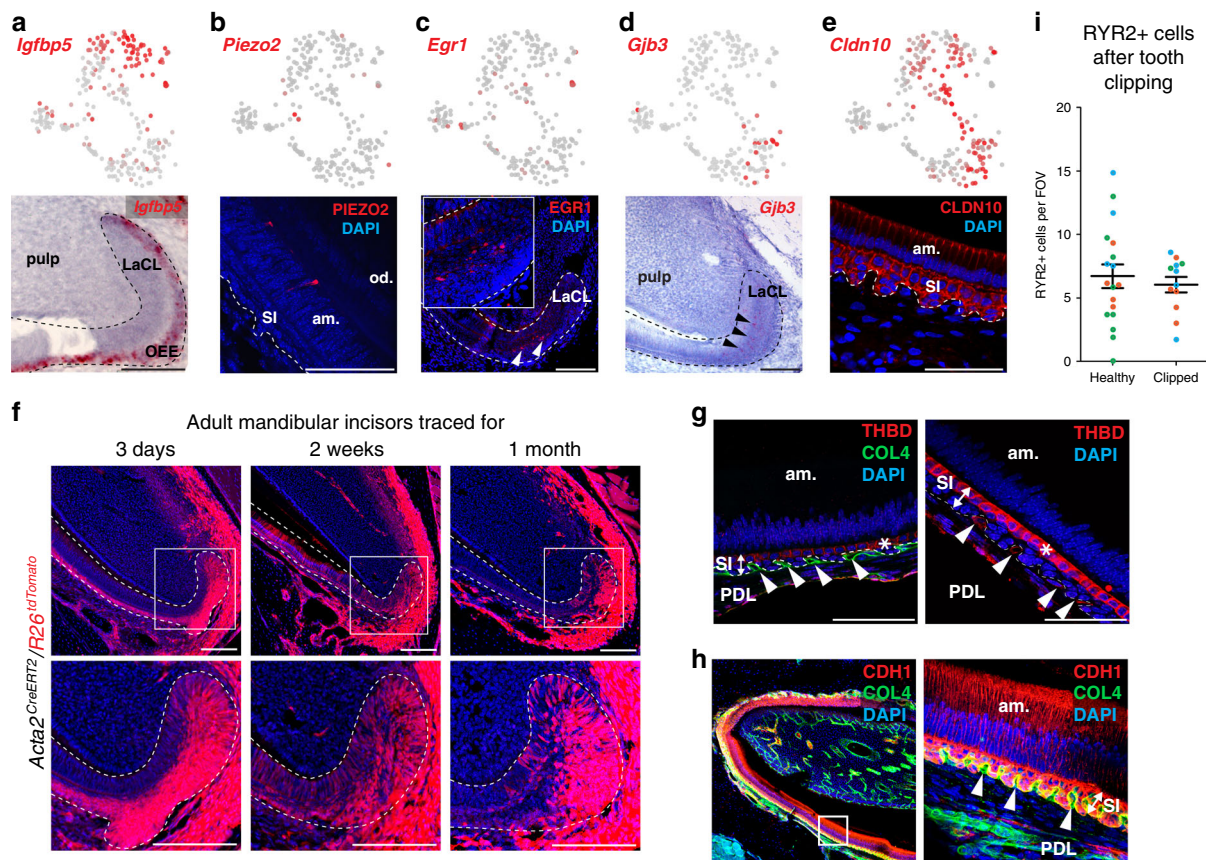
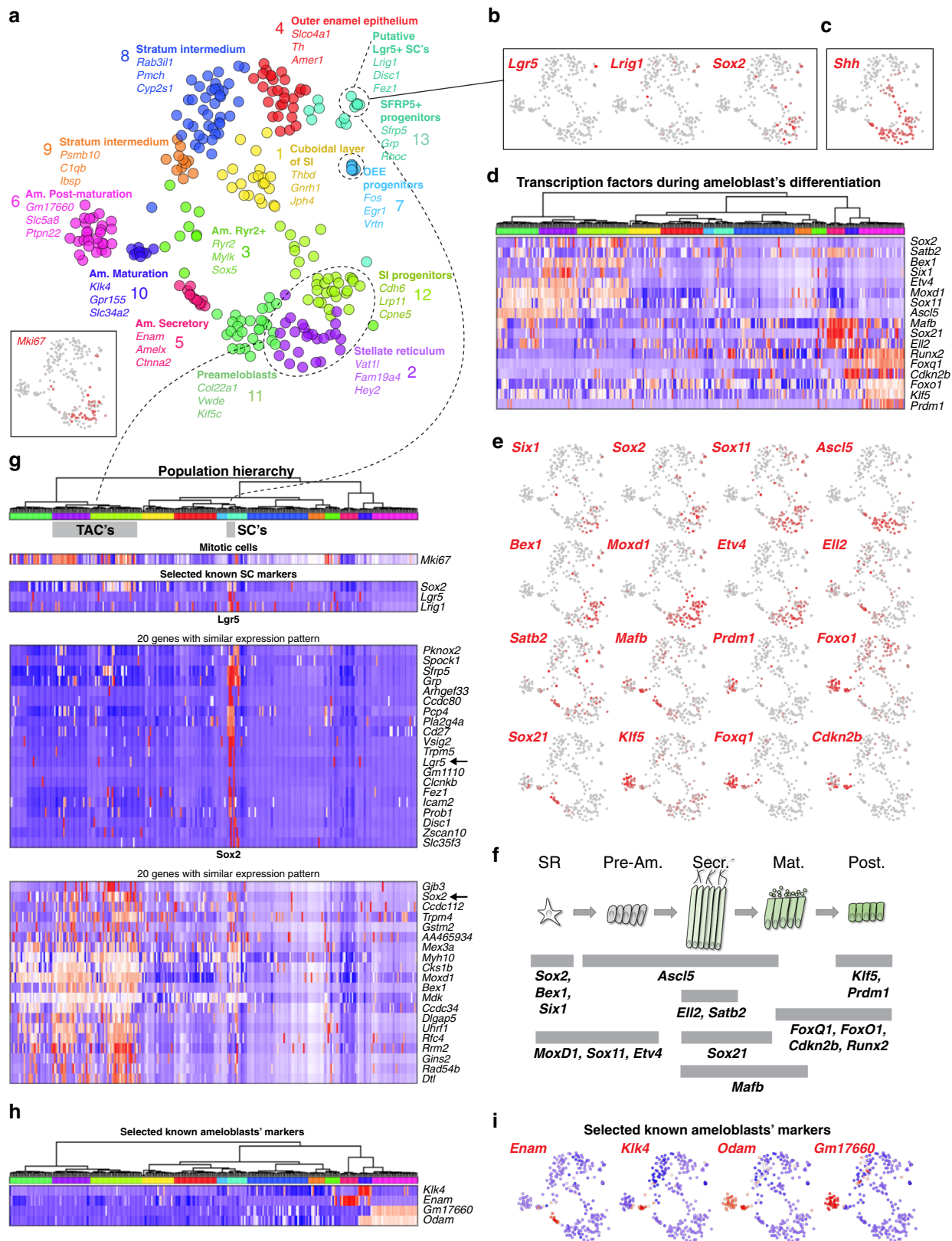


**Fig. 3 Identification of previously unrecognized cell types in dental epithelium and stem cells. a–e** In situ hybridization (*Igfbp5*, *Gjb3*) and immunohistochemistry (PIEZO2, EGR1, and CLDN10) validations of selected markers demarcating different progenitor and differentiated states in epithelial layer. Note: Validation of expression of *Igfbp5* enables identification of outer enamel epithelium clusters on a t-SNE representation (**a**). Validation of PIEZO2-expressing cells shows sporadic cells inside the ameloblast layer (**b**). *Egr1*<sup>+</sup> cells are present in the progenitor area on the edge of stellate reticulum and outer enamel epithelium (**c**). Mapping of *Gjb3* on the section tissue consistently reveals the position in stellate reticulum within the labial cervical loop (**d**). Validation of *Cldn10* expression helps to outline all non-ameloblastic parts of epithelial differentiation including developing stratum intermedium and outer enamel epithelium (**e**). **f** *Acta2*<sup>CreERT2</sup>/*R26*<sup>tdTomato</sup> genetic tracing shows significant contribution of *Acta2*<sup>+</sup> cells of the labial cervical loop to more differentiated cell types of dental epithelium including ameloblasts, stellate reticulum, outer enamel epithelium, and stratum intermedium after 3 days, 2 weeks, and 1 month long tracing period. **g, h** Immunohistochemistry identification of the Cuboidal layer of stratum intermedium (expressing THBD) and spatial relation to the neighboring blood vessels submerged into the papillary structure of stratum intermedium. COL4 expression characterizes the blood vessels on left panel. **h** Papillary structure of stratum intermedium with submerged blood vessels (COL4) and CDH1 expressing ameloblasts and cells from stratum intermedium. Note. Cuboidal layer characterized by THBD expression (**g**) forms subpopulation of stratum intermedium cells (**h**). Immunohistochemistry. **i** Comparison of RYR2<sup>+</sup> ameloblasts in healthy (mean 6.71 ± 0.93 SEM per FOV, Field Of View) and unilaterally clipped (mean 6.04 ± 0.61 SEM per FOV) mouse incisor. Counts of RYR2<sup>+</sup> ameloblasts per FOV are plotted, and the color-code of dots corresponds to 3 individual animals per healthy or clipped condition. (am. ameloblasts, od. odontoblasts, LaCL Labial Cervical Loop, SI stratum intermedium, OEE Outer Enamel Epithelium, am. Ameloblasts, PDL periodontal ligamentum). Scale bars: 50 μm.

mice traced ameloblasts and other cell types of dental epithelium in adult animals after 3 days, 2 weeks, 1 month and 2 months after tamoxifen injection (Figs. 2d and 3f). The presence of ACTA2<sup>+</sup> cells was confirmed by immunohistochemistry (Fig. 2c) in the outer half of stellate reticulum, outer enamel epithelium and dental follicle. Lineage tracing data using the *Acta2*<sup>CreERT2</sup>/*R26*<sup>tdTomato</sup> mice appeared consistent with this immunohistochemical staining. In the short-term lineage tracing experiment (3 days), numerous cells appeared traced within dental epithelium. However, the mature ameloblasts were not traced, which is different from long-term lineage tracings (1–2 months), where mature ameloblasts are robustly detected (Figs. 2d, 3f). At the same time, the overall numbers of all traced cells decreases over time because these cells are being replaced by the progeny of non-labeled stem cells. Only a small fraction representing traced epithelial cells is derived from ACTA2<sup>+</sup> epithelial stem cells, which retain self-renewing capacity

and can produce a minor proportion of epithelial progeny constantly during incisor self-renewal.

The expression patterns of the epithelial stem-cell markers show partial overlap with diverse clusters of proliferating progenitors. These include *Shh*<sup>+</sup> cells<sup>25,29</sup> (*Sox2*<sup>+</sup>/*Shh*<sup>+</sup> clusters 12 and 2, as well as more differentiated *Sox2*<sup>-</sup>/*Shh*<sup>+</sup> clusters 11, 5, 1, 13; Figs. 2a, 4c). Expression of *Egr1* and *Fos* in cluster 7 suggested a distinct type of an epithelial progenitor. Immunohistochemistry labelling showed that *Egr1*<sup>+</sup> epithelial cells were positioned adjacent to the stem-cell niche (Figs. 2f, 3c). Lineage tracing in *Fos*<sup>CreERT2</sup>/*R26*<sup>ZsGreen1</sup> mice revealed epithelial progeny inside the cervical loop, and predominantly in the outer enamel epithelium 10-days after the induction of lineage tracing in *Fos*<sup>CreERT2</sup>/*R26*<sup>ZsGreen1</sup> mice (Fig. 2f). These *Egr1*<sup>+</sup>/*Fos*<sup>+</sup> cells, thus, although being *Sox2* negative, represent a long-lasting progenitors that disappear after 1 month of the lineage tracing from the cervical



loop, and that are fate-biased towards outer enamel epithelium. Overall, our analysis of the epithelial compartment revealed a complexity of stem, progenitor and mature cell types, many of which were previously unknown and provide opportunities for further characterization.

**Heterogeneity of the mesenchymal compartment in mouse incisor.** Mesenchymal cell types in teeth build cementum, dentin, and soft tissue of pulpal cavity, and have diverse spatial localizations inside and around the tooth. Our data revealed that the tooth is surrounded by two subtypes of the dental follicular cells

**Fig. 4 Extended analysis of the heterogeneity of dental epithelial subtypes.** **a** t-SNE dimensional reduction visualizes the similarity of the expression profiles of 268 single dental epithelial cells. Thirteen unbiased clusters shown by different colors including revealed stem, progenitor and mature epithelial subtypes. **b** Previously unrecognized identified stem-cell subpopulation shows expression of *Lgr5*, *Lrig1*, and *Sox2*. Unlike *Lgr5* and *Lrig1*, *Sox2* is more widely expressed also in TAC's (also shown in panel **g**). **c** *Shh* is expressed in the progenitor populations including the stellate reticulum, stratum intermedium progenitors or preameloblasts (clusters 2, 11, and 12). **d–f** Transcriptional factor code associated with ameloblasts differentiation. **f** Schematic drawing summarizing expression of various selected transcription factors in different stages of ameloblasts development. **g** Heatmap showing the expression of mitotic and stem-cell markers within identified clusters of dental epithelial cells. Population hierarchy axis colors resemble the same populations on tSNE from panel **a**. Note that some of previously described stem-cell markers: *Lrig1*, *Sox2*, *Bmi1*, *Glil*, *Lgr5*, or *Igfbp5* are co-expressed only within a subcluster of cluster 13. This subcluster possesses a unique and extensive multigenic signature, including previously unknown markers *Pknox2*, *Zfp273*, *Spock1*, and *Pcp4*. The putative DESCs from cluster 13 might represent one type of epithelial stem cells in the tooth. The listed stem-cell markers show reasonably large and partly overlapping domains of expression that coincide with clusters containing proliferating progenitors. *Sox2*<sup>+</sup> DESCs give rise to *Shh*<sup>+</sup> populations including transient amplifying cells (TAC's) in the epithelial compartment. In agreement with that, we observe that the *Sox2*<sup>+</sup>/*Shh*<sup>+</sup> clusters 12 and 2 contain the majority of TAC's and most likely represent less differentiated states as compared to *Sox2*<sup>+</sup>/*Shh*<sup>+</sup> clusters 11, 5, 1, and 13. **h, i** Expression of well-known markers corresponding to a different ameloblast stage proving the gradual differentiation from secretory ameloblasts stage (*Enam*<sup>+</sup>) through maturation ameloblast stage (*Klk4*<sup>+</sup>, *Odam*<sup>+</sup>) into postmaturation ameloblast stage (*Gm17660*<sup>+</sup>).

and is encapsulated by the alveolar bone (Fig. 6e–h, Supplementary Fig. 3a, and Supplementary Table 1)<sup>27,30,31</sup>. The dental follicle populations express *Aldh1a2* - the key enzyme for retinoic acid production (Supplementary Fig. 3a, b). Retinoic acid, being a key morphogen, is known to control dental development and self-renewal<sup>32,33</sup>. Correspondingly, complementary receptor genes *Rara*, *Rarb*, and *Rarg* are expressed in some of the major populations of the tooth itself (Supplementary Fig. 3a, b). This suggests previously unanticipated crosstalk between retinoic acid producing and sensing populations in incisor growth and maintenance.

Inside, the incisor contains a continuously replenished mesenchymal compartment, comprised of odontoblasts producing dentin (the most abundant type of hard matrix in teeth), and heterogeneous sets of pulp cells whose role and subtypes remain to be understood from the functional point of view. Smart-seq2 data showed at least three major mesenchymal populations inside of the mouse incisor: odontoblasts and two distinct pulp subtypes, all connected by a continuum of transient cell states (Fig. 5a, b). The first pulp subtype, constitutively expressing *Smoc2* and *Sfrp2*, is localized specifically to the apical pulp in the area between cervical loops according to validation experiments (Fig. 6d, f). Expression of genes linked to self-renewal properties in the incisor mesenchyme (*Thy1* and *Glil*) was restricted to cells of apical subtype (Fig. 6a)<sup>27,34</sup>. However, dividing cells (*Mki67*<sup>+</sup>) are mostly segregated to a distinct heterogeneous transcriptional subpopulation localized in the pulp near the cervical loops, as evident from *Fgf3* and *Foxd1* expression (Fig. 6a–c). This indicates that apical pulp subtypes include diverse pools of quiescent stem cells and stromal cells likely supporting the stem-cell niche. The other pulp subtype corresponded to incrementally differentiating distal pulp cells finally labelled by the expression of *Igfbp5* and *Syt6* (Fig. 6d). Transcriptional trajectory modelling of the three mesenchymal populations, predicted a central branchpoint at a subpopulation with a strong mitotic signature, suggesting a likely active pool of stem/progenitor cells within the mesenchymal compartment (Figs. 5a–c, 6g)<sup>27,35</sup>. The potential area of active progenitors was corroborated by RNA velocity (Fig. 5b)<sup>36</sup>.

To improve the resolution of the active stem/progenitor subpopulation, we profiled mouse incisor by sequencing a larger number of cells using the 10× Chromium platform, which recovered the same mesenchymal landscape and overall population structure (Supplementary Fig. 4e, h). Branch analysis showed that transcriptional programs of the three populations were activated in a mutually exclusive manner in individual cells, without a notable multilineage primed state (Fig. 6h)<sup>37</sup>. A small fraction of the dividing cells showed activation of population-specific transcriptional biases, including an odontoblastic program. Obtaining cells of odontoblast sublineage became possible

because we enriched for it by using *Dspp*<sup>cerulean</sup>/*Dmp1*<sup>Cherry</sup> transgenic animals<sup>38</sup>. The immunohistochemistry confirmed activation of early odontoblast markers *Notum* and *Sall1* in the near cervical loop mesenchymal area, indicating that odontoblast fate selection happens before embedding into the odontoblastic layer (Figs. 5g, i, 7g). However, it is not clear if all *Notum*- and *Sall1*-expressing progenitor cells always irreversibly and selectively commit to the odontoblast fate or these factors convey a strong bias towards odontoblast differentiation. This goes in-line with the previously established fact that proximity of a stem cell to the epithelial compartment was shown to modulate selection of odontoblast fate, indicating the extrinsic signal from epithelium might induce odontoblast program<sup>39</sup>. This initial fate selection step, as well as clear transcriptional progression through at least three spatially separated stages of odontoblast differentiation provide a useful resource for ongoing efforts for targeted differentiation of odontoblasts (Fig. 5g, 7e–i).

Analysis of the apical progenitor subpopulation demarcated several axes of transcriptional heterogeneity that could identify programs specific to progenitor pools, one of which is marked by *Foxd1* expression (Figs. 5d, 7a–c). In situ hybridization confirmed the expression of *Foxd1* exclusively near the labial cervical loop area (Fig. 5d). A fraction of these cells is mitotic (Fig. 7d). To test whether *Foxd1* expression designates a functionally distinct subpopulation of biased stem cells residing in apical area, we performed lineage tracing using *Foxd1*<sup>CreERT2</sup>/*R26*<sup>tdTomato</sup>. Indeed, we found that *Foxd1*-traced cells gave rise predominantly to periodontoblastic pulp cells and dentin-secreting odontoblasts (Fig. 5e, f). Even after 3-months-long tracing, *Foxd1*-traced cells in the apical stem-cell area were detected only near the labial cervical loop revealing a spatially restricted structure of self-renewal pathway in the mouse incisor (Fig. 5e). Thus, the initial position of stem cells along the central-periodontoblastic axis is associated with its transcriptional state, migratory trajectory, and fates of progeny (Fig. 5c).

**Comparisons of composition of growing vs. nongrowing mouse teeth.** Although the mouse incisor stands as a model for a growing tooth, molecular features that distinguish it from nongrowing teeth remain unexplored. Therefore, we generated single-cell transcriptional snapshots of a nongrowing adult mouse molar using both 10X Chromium and Smart-seq2 platforms. To leverage total scale of multiple datasets, we analysed them jointly and together with self-renewing incisor datasets using Conos data integration strategy (Supplementary Fig. 4)<sup>40</sup>. Coarse-grained cell-type composition appeared similar between molar and incisor, except for the lack of epithelial populations in adult molars (Supplementary Fig. 4a–c). However, molar pulp appeared

## In-depth single cell analysis of dental mesenchyme

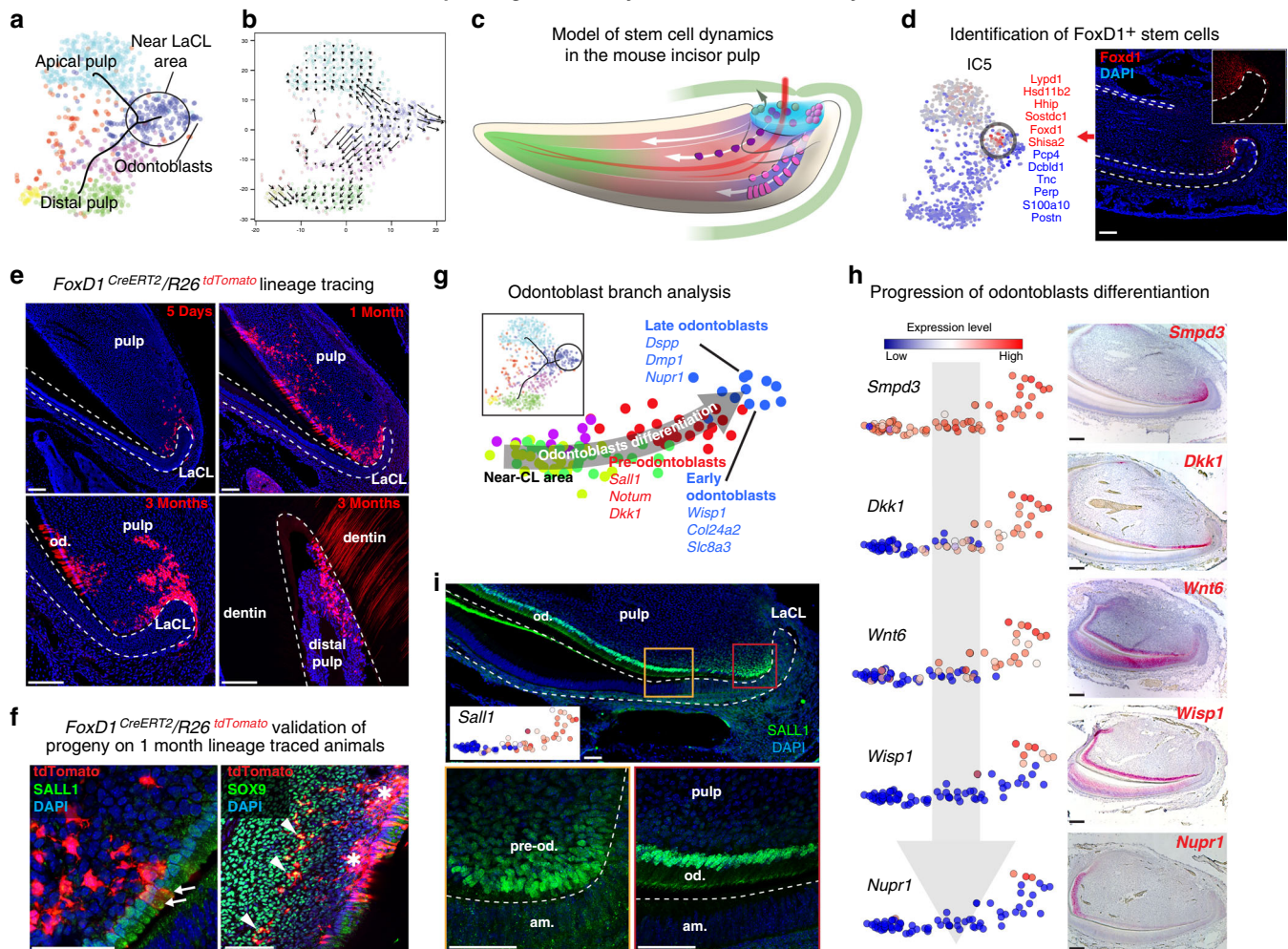


**Fig. 5 Developmental dynamics of dental mesenchyme.** **a** Analysis of mouse-incisor dental mesenchymal cells isolated for separate analysis from general dataset. Colors show unbiased clusters. The principal tree correctly captures positions of mature mesenchymal derivative and progenitor populations. **b** Analysis of RNA velocity shows major directions of cell progression in the transcriptional space. The arrow start- and endpoints indicate current and predicted future cell states. **c** Model of stem-cell dynamics in mesenchymal compartment with relation to dental follicle. **d** Prediction and validation of spatially restricted *Foxd1*<sup>+</sup> stem cells. The *Foxd1*-associated axis was selected for validation, and is shown on t-SNE (genes with the strongest positive and negative associations are shown in red and blue respectively). *Foxd1*<sup>+</sup> cells (in situ hybridization) are located in the mesenchyme surrounding the labial cervical loop. **e** Lineage tracing of *FoxD1*<sup>CreERT2</sup>/*R26*<sup>tdTomato</sup> strain confirmed the predicted stem-cell nature of *Foxd1*<sup>+</sup> mesenchymal cells. In short-term tracing (5 days) *tdTomato*<sup>+</sup> cells are predominantly around LaCL in contrast to long-term (1-month-long and 3 months) tracing where pulp and odontoblast progeny are observed. Importantly, *tdTomato*<sup>+</sup> cells are maintained in their original position in the long-term manner (3 months) and at the same time point *tdTomato*<sup>+</sup> distally located odontoblasts can be observed supporting the theory of *Foxd1*<sup>+</sup> cells being a long-living mesenchymal stem cells. **f** Nature of *Foxd1*<sup>+</sup> cells progeny confirmed by a combination of *FoxD1*<sup>CreERT2</sup>/*R26*<sup>tdTomato</sup> tracing and SALL1 and SOX9 immunohistochemical stainings. *FoxD1*<sup>CreERT2</sup>/*R26*<sup>tdTomato</sup>-traced cells contribute to both the SALL1<sup>+</sup> odontoblasts (arrows) and SOX9<sup>+</sup> pulp cells (arrowheads). Asterisks show the of subodontoblast layer *FoxD1*<sup>CreERT2</sup>/*R26*<sup>tdTomato</sup> traced cells. **g** Variability of cells assigned to a branch leading to odontoblasts (inset) was reanalysed using principal component analysis. Colors mark five clusters obtained by unbiased hierarchical clustering. Left-right axis reflects developmental stages of odontoblasts. **h** Gradual odontoblast differentiation (suggested in **g**) from near-CL area into fully differentiated odontoblasts. Left: expression pattern acquired from scRNA-seq, right: in situ hybridization-based histological validations of the proximal part of the mouse incisor proving suggested gradual transition. **i** Spatial pattern of a discovered (pre)odontoblast transcription factor—SALL1 (Immunohistochemistry). (LaCL Labial Cervical Loop, pre-od. preodontoblasts, Od. Odontoblasts, Am. Ameloblasts). Scale bars: 50 μm.

significantly more homogeneous as compared to the pulpal populations of the incisor given the resolution of the current measurements. Joint Conos clustering of incisor and molar datasets shows that molar mesenchyme falls into a single cluster shared with the distal mouse-incisor pulp (Supplementary Fig. 4a, b). Analysis of mesenchyme heterogeneity using separately 10× and Smart-seq2 platforms corroborated the heterogeneous population structure of mouse incisor and homogeneous distal-like population of mouse molar (Supplementary Fig. 4d, e). At the

same time, gene expression programs of mouse molar and distal incisor pulp have noticeable expression differences in 379 genes ( $p$  value  $< 10^{-2}$ ,  $t$ -test group means comparison and at least two fold change in both Smart-seq2 and 10× Chromium datasets) (Supplementary Fig. 4f). Mouse-incisor apical genes tend to show high expression in a *Smoc2*<sup>+</sup> compared to *Smoc2*<sup>-</sup> human apical papilla. On the other hand, mouse-incisor distal genes tend to show high expression in a *Smoc2*<sup>-</sup> and not *Smoc2*<sup>+</sup> human apical papilla. In adult teeth, mouse-incisor distal genes are uniformly

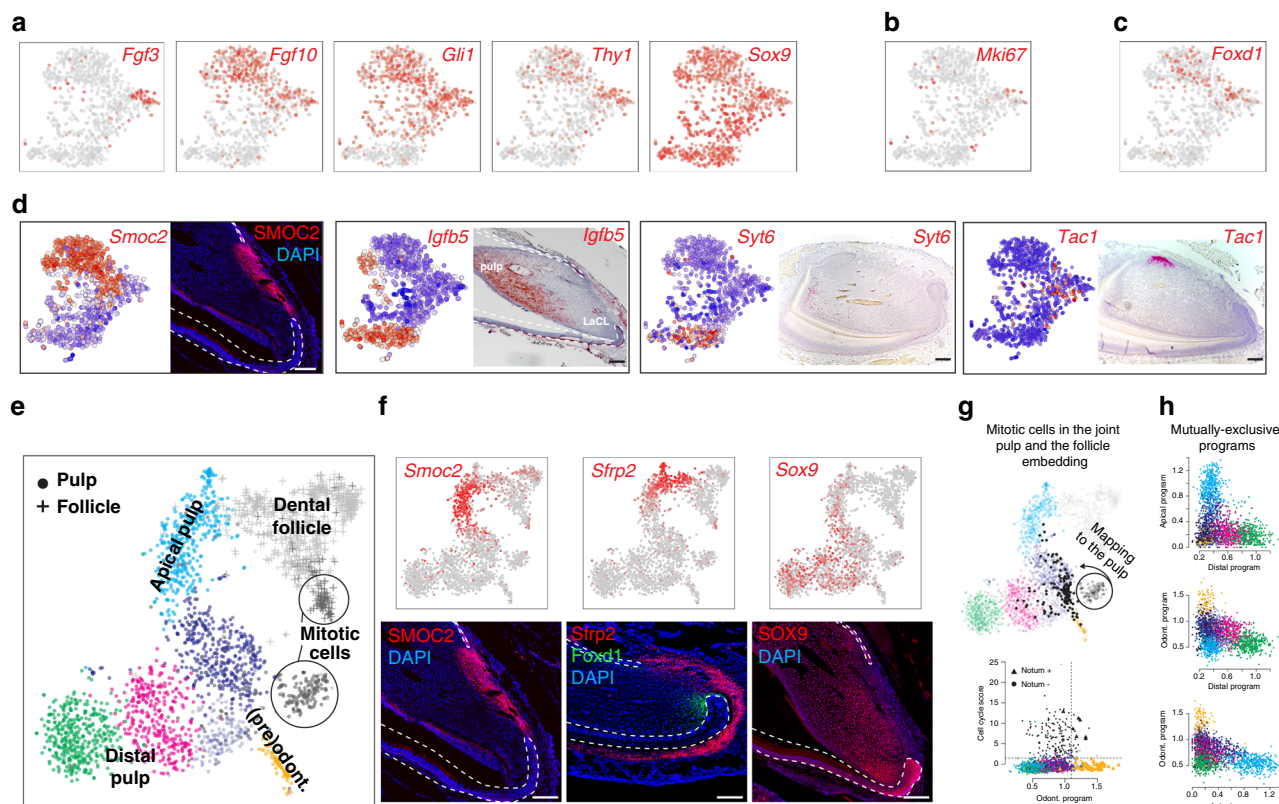


**Fig. 6** Portrait of transcriptional heterogeneity in dental mesenchymal populations. **a** t-SNE representations of selected, previously known marker genes. **b** t-SNE representation showing position of *Mki67*<sup>+</sup> cells. **c** t-SNE representation showing position of *Foxd1*<sup>+</sup> cells. **d** Immunohistochemistry (SMOC2) and in situ hybridization (*Igfb5*, *Syt6*, and *Tac1*) characterization of key populations in the mesenchymal population. Importantly, *Igfb5* and *Syt6* demarcate more distal pulp and *Tac1* is a unique marker for dental pulp attached to the lingual cervical loop. **e** Landscape of mesenchymal cells of dental pulp (dots) and follicle (crosses) is reproduced and extended with 10× Chromium. t-SNE embedding shows 2552 mesenchymal cells grouped in clusters, where clusters colours reflect colours of annotated Smart-seq2 pulp clusters (see Fig. 3a). Of note, cells from apical pulp gradually extend into cells of dental follicle. **f** Experimental validations of gradual spatio-transcriptional gradient from apical pulp to dental follicle. Immunohistochemistry of SMOC2 highlights the position of the apical pulp state, corroborated by Smart-seq2 and 10× Chromium single-cell datasets. In situ hybridization of *Sfrp2*, consistent with 10× Chromium and Smart-seq2 t-SNE representations, labels coherent states between apical pulp and dental follicle. Immunohistochemistry for SOX9 labels all pulp cells but not odontoblasts or dental follicle. **g** In silico mapping of mitotic cells onto non-mitotic landscape pinpoints progenitor states of active cell division (upper). To remove effect of mitotic program, mitotic cells were re-positioned as average of 10 transcriptionally similar non-mitotic cells. Comparison of intensity of odontoblast (lower, X-axis) and cell cycle (lower, Y-axis) programs in each cell reveals a subset of mitotic cells with activated odontoblast program (lower). Dashed lines demarcate cells with active programs. **h** Mutually exclusive activation of fate-specific programs (odontoblasts, distal and apical fates). An estimate of activity of fate-specific programs in each cell was based on average expression of 20 fate-specific markers. Comparison of pairs of fates (three panels of fate pairs) shows activation of only one of fates indicating lack of noticeable multilineage priming.

expressed in all populations, but incisor apical genes show the affinity to the periodontoblastic pulp. The meaning of this heterogeneity is unknown and requires further investigation. Altogether, these results support aetiology of the apical subtype in the incisor as stromal and quiescent cells of the niche, the structure absent in the nongrowing molar. We thus, suggest that the distal-like subtype is a constitutive terminally differentiated population, while the apical pulp state is an emergent property of growing mesenchymal dental tissue. Importantly, the apical incisor pulp shows a coherent expression of genes involved in regenerative response in a tooth and production of a hard matrix in case of physical damage (*Sfrp2*, *Lef1*, *Fzd1*, *Sfrp1*, *Rspo1*, *Trabd2b*, *Gli1*, and *Wif1*)<sup>41</sup>, which is much less present in the pulp populations found in molars (Supplementary Fig. 4d, e).

**Parallels and differences between growing and nongrowing human teeth.** The studies of mouse incisor are generally motivated by the translational insights on human tooth development. In humans, the growth of teeth stops postnatally after permanent teeth erupt between 6–21 years of age (eruption of the 3rd molar

is variable). To determine the extent to which the observed pulp contrast between growing and nongrowing teeth in mouse reflects human biology, we conducted single-cell profiling of 39,095 cells from healthy nongrowing and growing wisdom teeth in humans (Figs. 8, 9). To focus on the growth-relevant populations, the cells were isolated from the apical papilla located in most apical part of developing wisdom tooth where the tooth is still growing. The analysis revealed that human teeth contain cell types analogous to those in mice, including vascular and perivascular cells, glia and immune populations, and distinct subpopulations of pulp cells (Figs. 8a–d, 9a, b).

Human pulp cells significantly differ between the growing apical papilla and nongrowing molar, and form at least several transcriptionally distinct subpopulations (Fig. 8c, d). In that regard, the pulp of human nongrowing molars appeared to be much more transcriptionally diverse compared to the mouse nongrowing molars. In particular, human molar contained a pulp subpopulation that was spatially localized in the periodontoblastic layer, previously morphologically described as cell-free and cell-rich zones, which are absent in mouse (Fig. 8i)<sup>42</sup>. We detected a group of proliferative cells

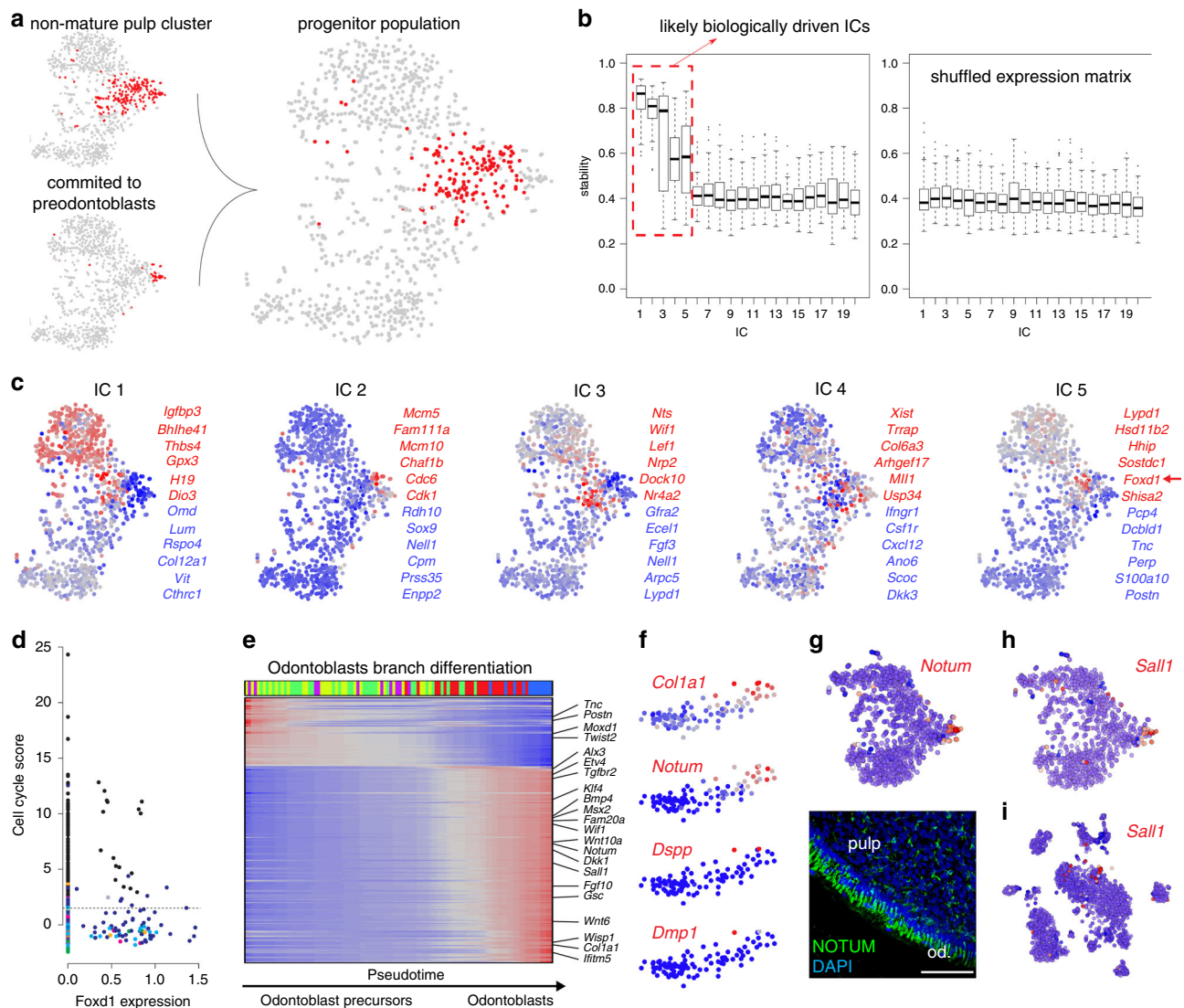
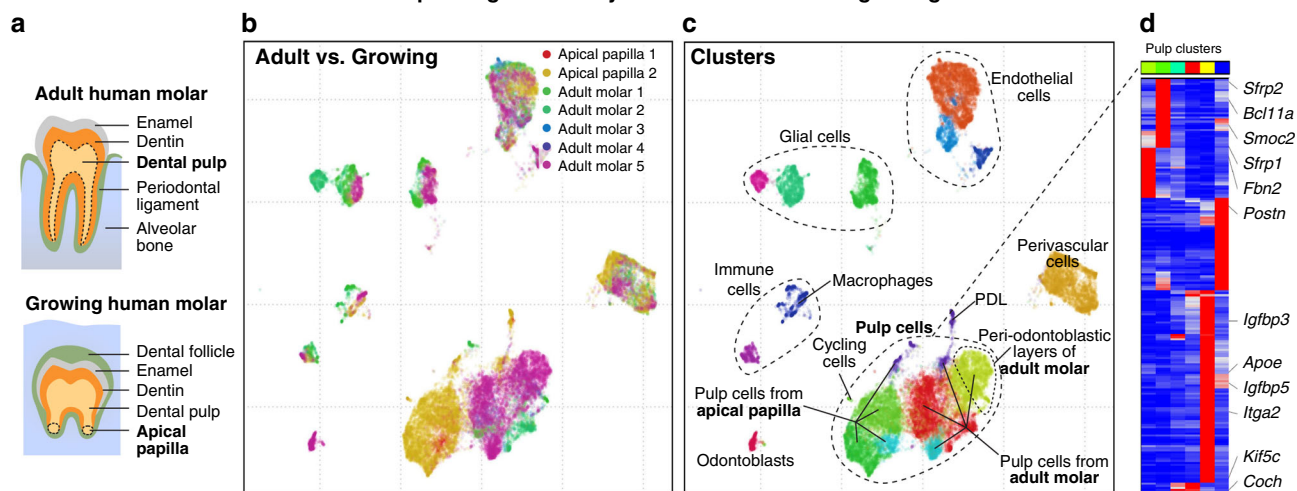


**Fig. 7 Detailed analysis of mesenchymal branching point and odontoblast lineage.** **a** Selection of non-mature subpopulation. An unbiased cluster of cells that do not represent mature pulp populations was selected (left, upper), and preodontoblasts (left, lower), were excluded from it, resulting in non-mature subpopulation (right). **b** Analysis of ICs stability reveals five biologically driven aspects of heterogeneity of non-mature subpopulation. Average correlation of ICs to the most similar ICs across 100 runs of subsamplings of 70% of cells (right) reveals 5 out of 20 ICs with stability substantially higher than expected from shuffled control (left). Stability of all ICs of control shuffled matrix and 15 ICs of original matrix are around 0.4 indicating background expectations of spurious components. **c** Five ICs of non-mature subpopulation reveal processes related to (from left to right) apical gradient (IC 1), cell cycle (IC 2), *Fgf3*-mediated (IC 3), and *Foxd1*-mediated (IC 5) heterogeneity restricted to the progenitor states. Colors show intensities of identified ICs. Genes that have the highest (red) and lowest (blue) associations with corresponding IC are shown. **d** Graph showing cells expressing *Foxd1* in comparison to cell-cycle score. **e** Transcriptional events during pulp differentiation trajectories. Each trajectory encompasses cell states from progenitor, as identified from analysis of preodontoblasts, to mature states with cells arranged by pseudotime reflecting maturation process. The black cells belong to the trajectory being shown, while other cells are shown in light gray (upper panels). Heatmap shows smoothed gene expression profiles with cells arranged by pseudotime and genes (rows) arranged by pseudotime of maximal expression (lower panels). **f–i** Expression analysis of the selected genes determining odontoblasts (*Col1a1*, *Dmp1*, and *Dspp*) and together with previously unrecognized identified odontoblast marker genes (*Notum* and *Sall1*). *Notum* expression is visualized on t-SNE embedding of the pulp dataset and immunohistochemistry proves NOTUM to be expressed in odontoblasts (**g**). *Sall1* expression is visualized on t-SNE embeddings of the both pulp (**h**) and complete incisor dataset (**i**). Scale bars: 50  $\mu$ m.

in a growing human apical papilla, which showed pronounced transcriptional similarity to a *Smoc2*<sup>-</sup> human apical papilla pulp, and dissimilarity with any subpopulations of nongrowing human molars (Figs. 8e–g, 9e, g). To explore similarity of genetic programs in a mesenchymal compartment of human and mouse teeth, we compiled a set of marker genes that are differentially expressed between apical and distal mouse-incisor subtypes in both Chromium 10x and Smart-seq2 datasets (Supplementary Table 4). Assessment of average expression of marker genes of apical and

distal incisor pulp subtypes showed their preferential expression in corresponding populations of human pulp cells (Fig. 9f, h). In particular, similar to incisor apical pulp, *Smoc2*<sup>+</sup> human pulp cluster tends to express apical incisor markers and repress distal incisor markers. Immunostaining reveals localization of *Smoc2*<sup>+</sup> human subtype to mesenchymal regions demarcating apical papilla around the Hertwig epithelial root sheath (Fig. 8e, f). Overall, these data indicate that *Smoc2*<sup>-</sup> and *Smoc2*<sup>+</sup> human pulp subtypes might form a maturation hierarchy similar to that in mouse incisor.

In-depth single cell analysis of human adult and growing molar



Validation of human tooth subpopulations

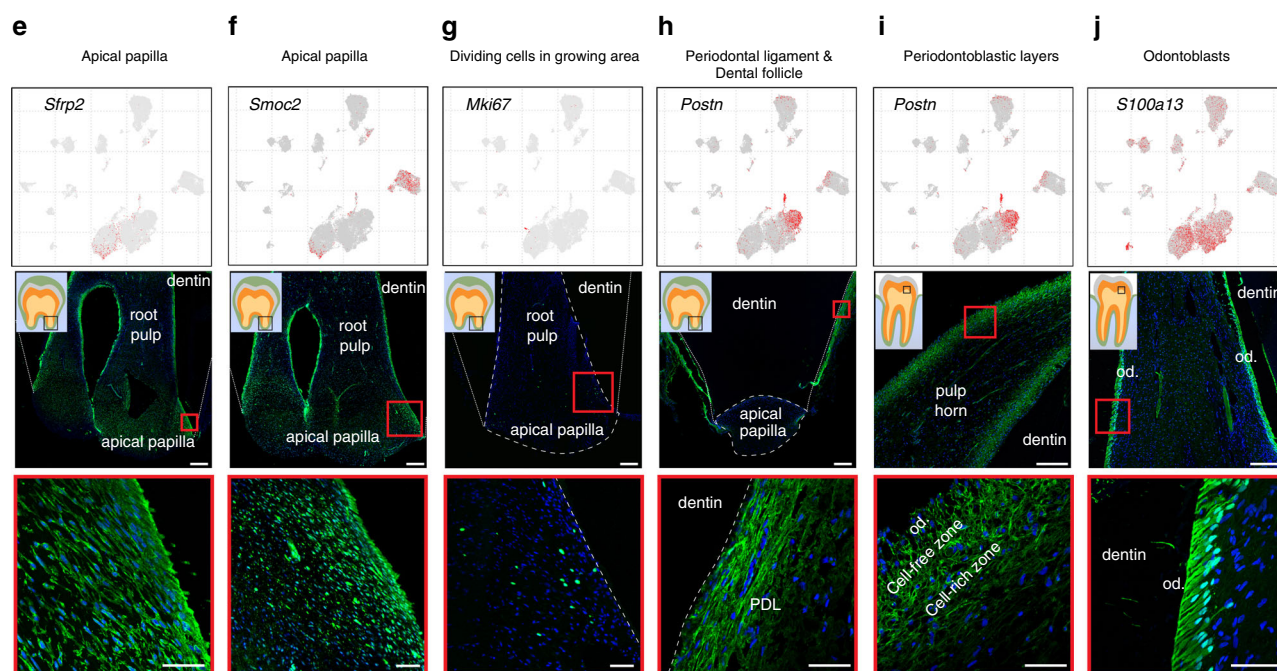


**Fig. 8** Single-cell analysis of human adult and growing teeth. **a** Scheme of pulp regions isolated for single-cell RNA-seq from adult human molars and apical papillae of growing human molars (dotted regions). **b** Characterization of cell composition across five adult and two growing human molars using scVI deep learning framework. UMAP dimensionality reduction visualizes similarity of expression profiles of 39,095 single cells. Colors correspond to individual datasets and indicate clustering by cell types. **c** Characterization of dental cell types in human teeth. Colors demonstrate 17 clusters as defined by leiden clustering. Major clusters are defined by expression of known markers. **d** Human dental pulp have at least six transcriptionally distinct states. Top color bar reflects colors of clusters shown in **c**. Top 198 genes enriched in each cluster are shown (maximum to medium expression across clusters is at least four-fold and  $p$  value  $< 10^{-50}$ , one-way ANOVA test). **e, f** Identification of apical-like-mouse-incisor regions in the growing apical papilla of human molar shown by the expression of SFRP2 and SMOC2 (immunohistochemistry) in the growing region of apical papilla. **g** Dividing, MKI67<sup>+</sup> cells are positioned in the growing part of the apical papilla. **h, i** Expression of *POSTN* shows very regionalized pattern in two main clusters: periodontal ligament (PDL) on the samples from apical papillae (**h**), but also demarcate the periodontal layers of adult dental pulp previously recognized as a cell-rich and cell-free zones (**i**). Immunohistochemical *POSTN* staining. **j** *S100A13* was proposed as a marker of human odontoblasts. This gene is highly overexpressed in one of the subclusters, which is on t-SNE located in the close proximity to dental pulp. *S100A13* was proved to be expressed in odontoblasts by immunohistochemistry. (Od. Odontoblasts; PDL periodontal ligament). Scale bars: 50  $\mu$ m, insets: 250  $\mu$ m.

However, individual genes inside both apical and distal incisor pulp modules often have incoherent patterns across human pulp subtypes (Fig. 9c, d). This suggests an evolutionary divergence between mouse and human gene expression programs governing development and

homeostasis of dental pulp tissue (Fig. 9c, d) and precludes establishing the homologous fine subtypes between mouse and human pulp. Thus, some human pulp subpopulations do not appear to have clear parallel in mouse teeth.

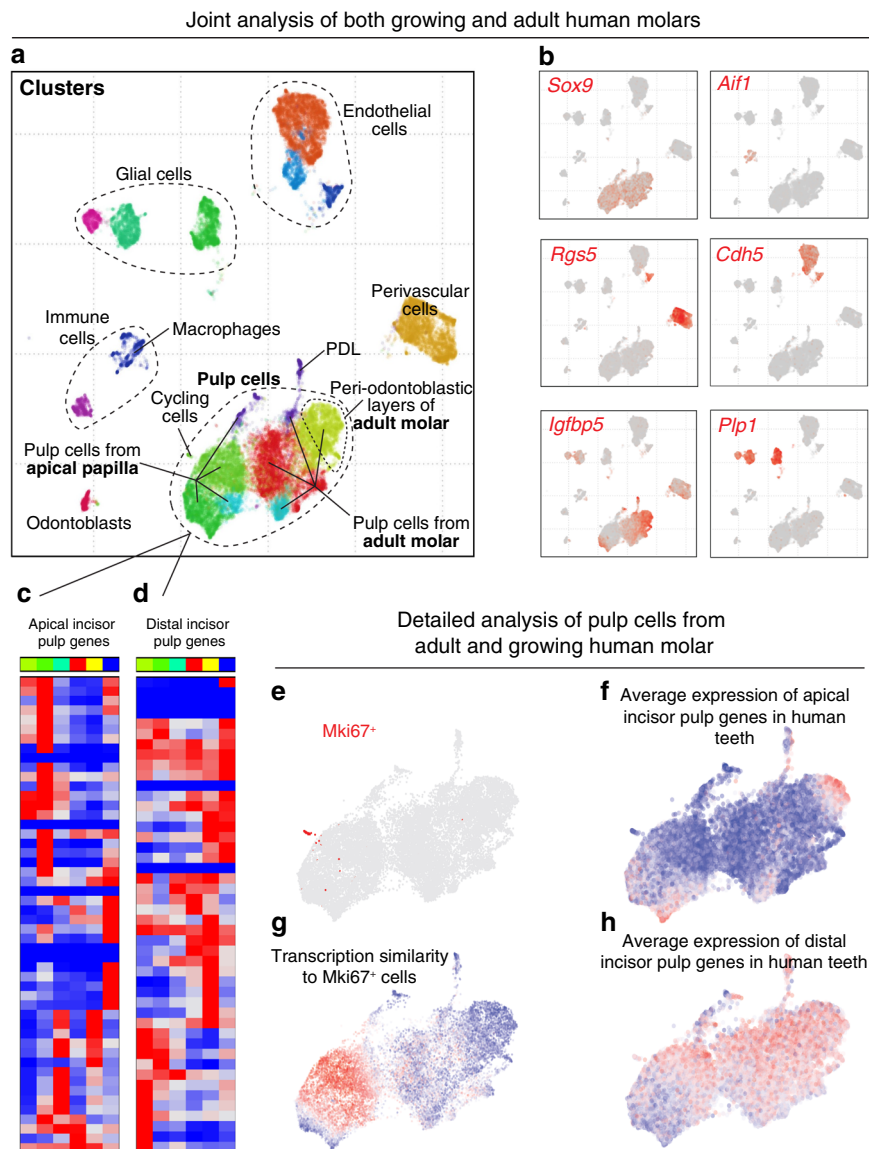


**Fig. 9 Analysis of adult and growing human molars.** **a** Dental cell types in human teeth, see Fig. 4. **b** Expression of selected marker genes. **c, d** Expression of genes coordinately active in apical (51 genes, **c**) or distal (48 genes, **d**) incisor pulp across clusters of human mesenchyme reveals divergence of pulp expression programs. Apical incisor genes were defined as at least three-fold and significantly ( $p < 10^{-10}$ , two-sided  $t$ -test) overexpressed in apical compared to distal incisor pulp in both 10 $\times$  Chromium and Smart-seq2 datasets. The same for distal incisor genes. **e** Expression of *MKI67* in cells of human pulp shows a group dividing cells. **f** Transcriptional similarity of the group of dividing cells to individual nondividing mesenchyme cells. **g, h** Average expression of apical incisor genes (**g**) and distal incisor genes (**h**) in cells of human mesenchyme outline tendency to expression in complementary cell states.

**Heterogeneity of tissue-residential immune cells in mouse incisor.** Immune cells are the first responders to any infection invading the pulp cavity<sup>43</sup>. Understanding the organization and diversity of the dental immune system can help develop approaches to improve dental treatments to preserve dental pulp and odontoblasts. We observed eight well-defined immune cell populations in the mouse incisor, dominated by an extensive repertoire of macrophages and other innate immune cells including intravascular and tissue-resident DPP4<sup>+</sup> natural killer (NK) cells (Fig. 10a, c; Supplementary Fig. 5a, b, e and Supplementary Table 1).

The population of macrophages and dendritic cells contained three subclusters (Fig. 10a). The most evident was presence of *Aif1*<sup>+</sup>/*Lyve1*<sup>+</sup> and *Aif1*<sup>+</sup>/*Lyve1*<sup>-</sup> populations (Fig. 10, Supplementary Fig. 5a, b and Supplementary Table 1) Unexpectedly,

immunohistochemistry demonstrated regional specificity of LYVE1<sup>+</sup> and LYVE1<sup>-</sup> macrophage subpopulations: while LYVE1<sup>+</sup> macrophages resided in the pulp distant from odontoblast layers, LYVE1<sup>-</sup> macrophages were scattered ubiquitously and penetrated the odontoblast layer (Fig. 10c, Supplementary Fig. 5c, d). Given the importance of the tooth immune system in preventing caries, we tested whether similar patterns are also present in human teeth. Indeed, examination of analogous macrophage populations in the human dentition confirmed regional specificity of the LYVE1<sup>+</sup> population across species (Supplementary Fig. 5f). Interestingly, the density of macrophages in an intact mouse unerupted incisor was much higher than in the surrounding tissues (Supplementary Fig. 5c) and this tooth shows the same patterns as fully developed adult incisor in presence of *Aif1*<sup>+</sup>/*Lyve1*<sup>+</sup> and *Aif1*<sup>+</sup>/*Lyve1*<sup>-</sup> macrophage populations.

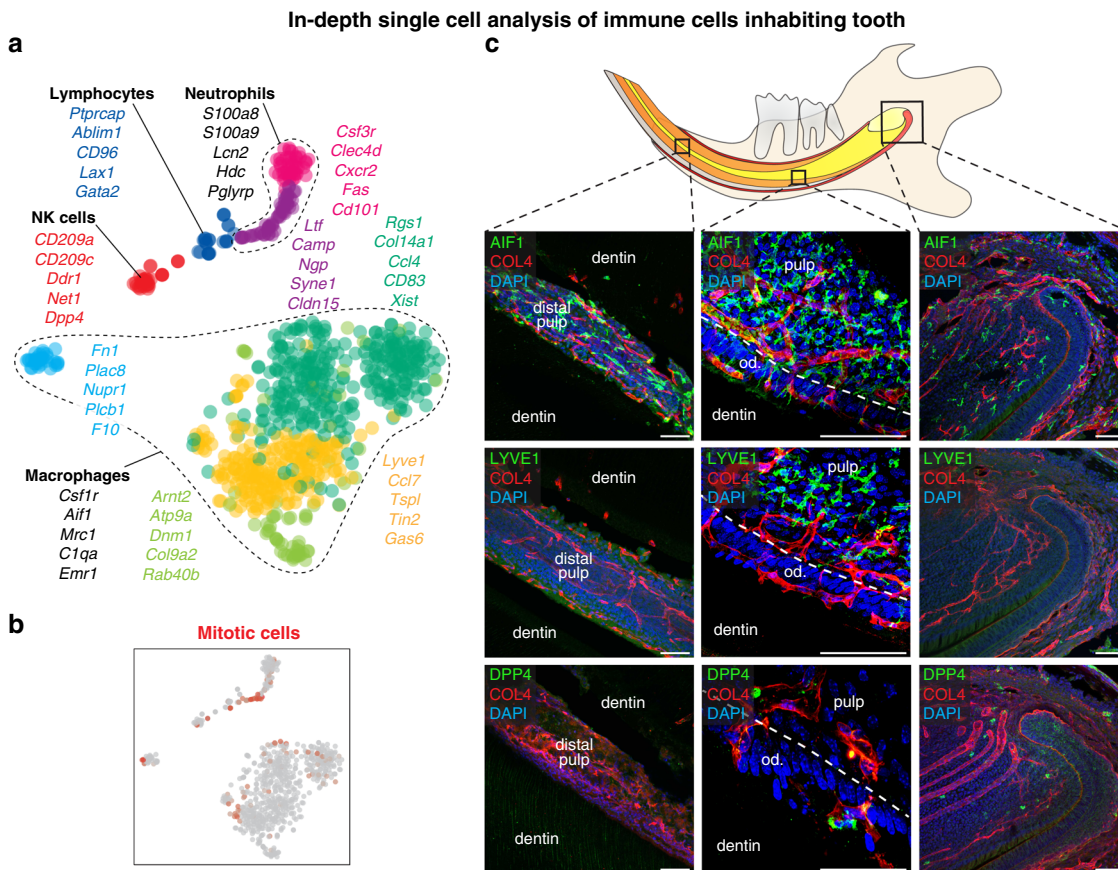


**Fig. 10 Heterogeneity of immune cells in mouse incisor.** **a** t-SNE dimensional reduction shows ten identified populations of immune cells. **b** Position of mitotic cells in the immune cluster. **c** Location of tissue-residential immune cells in the different parts of mouse incisor. AIF1<sup>+</sup> macrophages are located in the whole incisor including apical pulp, cervical loop, odontoblast layer, and distal pulp in contrast to LYVE<sup>+</sup> macrophages which mostly resides in the middle part of the pulp, but not inside the odontoblast layer. DPP4<sup>+</sup> immune cells are sporadically located in the apical part of the tooth and odontoblast layer. COL4 immunohistochemical staining visualize the blood vessels. (Od. Odontoblasts), Scale bars: 50 μm.

**Discussion**

Coordination of mesenchymal and epithelial compartments is a common feature of self-renewing and developing tissues and organs. Continuously growing mouse incisor has been widely used as a model of tooth development as well as a model of self-renewing organ in general<sup>44,45</sup>. Earlier studies, using bulk RNA-seq, have elucidated some of the transcriptional complexity, characterizing differentiated and progenitor cells in stem-cell niches<sup>27</sup>. Our results based on a single-cell transcriptomics go further to reveal previously unappreciated complexity of the terminal and transient cell states that altogether enable self-renewal and growth of mammalian teeth.

In addition to the previous lineage tracing studies revealing the nature of the Sox2<sup>+</sup>, Bmi1<sup>+</sup>, and Lrig1<sup>+</sup> dental epithelial stem cells<sup>24,25,27</sup>, we identified stem population of Acta2<sup>+</sup> cells in the labial cervical loop. The lineage tracing experiments presented here or published by other authors never showed the entire population of ameloblasts to be traced. Instead, the epithelial progeny appears in characteristic patches, supporting the diversity of epithelial stem cells. Furthermore, we identified Egr1<sup>+</sup> long-lasting epithelial progenitors, which appeared to be similar to a concept of short-living stem cells. Thus, the progenitor area might rely on functional diversification of different stem cells with a stemness gradation. Such diversity of epithelial progenitor cell subtypes might also reflect the remarkable plasticity noted by earlier studies<sup>35,46</sup>.

Aside from the discovered epithelial stem-cell types, our unbiased scRNA-seq approach uncovered different subtypes within incisor epithelium including the subtypes of stratum intermedium or a population of ameloblasts that expresses some mechanotransduction-related genes. Future research is required to clarify a precise role of this population. Although the functional and histological structure of mouse-incisor enamel organ was previously extensively investigated<sup>25,27,46</sup>, we introduced a sublayer of stratum intermedium—cuboidal layer, which is positioned immediately underneath the ameloblast layer. The in-depth characterization of a transition from progenitors to mature ameloblasts may benefit ongoing attempts to establish a system of ameloblast differentiation in vitro or to grow dental organoids.

Although our Smart-seq2-based analysis provided a sequencing depth allowing to find populations with fine transcriptional differences, it is laborious and expensive, which precludes the analysis of large cell numbers. Complementary to our Smart-seq2-based study of the epithelial compartment, Sharir and co-authors addressed heterogeneity and the plasticity of the incisor epithelium at a single-cell level<sup>46</sup>. In addition to major epithelial groups, also described in their single-cell study, we identified a number of small subpopulations with finer transcriptional differences, including cuboidal epithelial layer, Ryr2<sup>+</sup> population and subtypes of stem or progenitor cells (Acta2<sup>+</sup>, Egr1<sup>+</sup>). Sharir et al. demonstrated the capacity of Notch1-expressing cells to convert into ameloblasts upon injury, which significantly extends

our results in a domain of dental regenerative response. Compared to other single-cell studies, we characterized also heterogeneity of all cellular subtypes of mouse and human teeth.

Although several dental mesenchymal stem-cell markers had been previously presented<sup>27,34,39,47,48</sup>, in all cases they are not specific to mark the stem cells only as they are expressed in wider population extending in the area between the cervical loops or along the neurovascular bundle. Here we present a spatially completely segregated and specific subtype of multipotent long-lasting *Foxd1*<sup>+</sup> mesenchymal stem cells attached to the labial cervical loop. These stem cells contribute to odontoblasts, subodontoblastic subtype of pulp cells and other populations of dental pulp. We identified this population based on the in-depth scRNA-seq analysis and proved their functionality by the lineage tracing. Next to a stem-cell niche, odontoblast and pulp fates demonstrated unexpectedly fast separation occurring in a spatially restricted manner, which suggests cell–cell interaction between odontoblast fate-inclining cells with the epithelial layer (Supplementary Fig. 4). We further run a separate analysis of pulp branch and subsequently odontoblast branch only. By doing this we were able to map a complete differentiation pathway of odontoblasts differentiation which was subsequently proved by in situ hybridization. Whereas the previous studies utilized the bulk sequencing providing only a fraction of specific marker genes<sup>27</sup>, our approach enables to obtain the complete picture of transcriptional states across the entire differentiation timeline of odontoblasts.

The comparison between mouse growing and nongrowing tooth showed high homogeneity of mouse molar pulp populations. Therefore, the diversity of mesenchymal populations in the self-renewing incisor can be largely explained by the necessity to maintain growth and self-renewal. Despite mouse molar pulp homogeneous appearance, human nongrowing molar pulp showed a clear presence of several distinct subpopulations, which differed by the specialized matrix production and some other parameters. For instance, the apical papilla part, being the growing region of an unerupted human tooth, demonstrated corresponding growth-related cell-type heterogeneity. At the same time, the fully grown and erupted human molar teeth also preserved apical pulp-like transcriptional aspects in some pulp subpopulations, which, for instance, might be taken advantage of during reparative response. Thus, the preservation of some residual apical-distal or growth-related heterogeneity aspects in growing and fully grown human molar teeth highlights the key aspects of heterogeneity of human dental pulp transcriptional states. The functional meaning of these growth-related aspects will require further analysis in experimental ex vivo and in vivo settings. At this point, our data of such heterogeneity markers (also including signatures for proliferative populations) can serve as a guide for the isolation and culture of mesenchymal stem cells for tissue engineering and fundamental understanding of different pulp cell subtypes.

Finally, we addressed the heterogeneity of immune cells in mouse and human teeth including macrophages. The analysis revealed the human-specific aspects of macrophage localization, which suggest better protection of mouse teeth versus human. The predominant concentration of human macrophages in odontoblastic and periodontoblastic space suggests the existence of unknown cell–cell interactions and heterogeneously distributed homing factors that can be potentially tackled for increasing the protection of our teeth against infections.

Overall, we hope that the presented detailed and validated map of dental cell types, supplemented by human comparison, will serve as a key resource stimulating further studies of cell dynamics in tooth morphogenesis, also including reparative and regenerative therapies.

## Methods

**Animals and human tissue.** All animal experiments were approved by the Ethik-Kommission der MedUni Wien zur Beratung und Begutachtung von Forschungsprojekten am Tier in Austria as well as Ethical Committee on Animal Experiments (Stockholm North Committee) in Sweden and performed according to the Austrian, UK, Swedish and international regulations. All mice were kept under SPF conditions in 12/12 light/dark cycle, 18–23 °C and 40–60% humidity. Experiments with human samples were performed with the approval of the Committees for Ethics of the Medical Faculty, Masaryk University Brno & St. Anne's Faculty Hospital (No. 13/2013) and Ethik-Kommission der Medizinischen Universität Wien (No. 018/03/2018, 631/2007). Written informed consent was obtained from all participants, in-line with the Declaration of Helsinki. *Fos*<sup>CreERT2</sup>/*R26*<sup>ZsGreen1</sup> strain was used for genetic tracing of outer enamel epithelium progenitor cells. *DMP1-Cherry*/*DSPP-creulean* mice were used for visualization of alveolar bone<sup>38,49</sup>. *Acta2*<sup>CreERT2</sup>/*R26*<sup>tdTomato</sup> mice were used for lineage tracing of *Acta2*<sup>+</sup> dental epithelial stem cells in cervical loop<sup>31</sup>. *Sox2-GFP* animals were used to enrich epithelial stem cells population for single-cell sequencing<sup>25</sup>. *Foxd1*<sup>CreERT2</sup>/*Ai9* mice were used for lineage tracing of dental mesenchymal stem cells<sup>50</sup>. Mice used for all experiments were sacrificed by an isoflurane (Baxter KDG9623) overdose. Human teeth were extracted for clinically relevant reasons at Clinic of Stomatology, St. Anne's Faculty Hospital, Brno, Czech Republic or Department of Oral Surgery, Medical University of Vienna, Austria.

**Tissue handling and staining.** Mice used for all experiments were sacrificed by an isoflurane (Baxter KDG9623) overdose, mandibles were carefully dissected out, fixed in 4% paraformaldehyde pH 7.4 for 5–15 h, decalcified in 10% EDTA pH 7.4 for 7 days at +4 °C, cryopreserved in 30% sucrose overnight at +4 °C and embedded in OCT medium (Tissue-Tek, 4583) on dry ice. Samples were cut on cryostat (Leica CM1850UV) in sagittal orientation as 14-µm thick sections. Human teeth extracted for clinically relevant reasons were fixed in 4% paraformaldehyde pH 7.4 for overnight, decalcified in 10% EDTA pH 7.4 for 7 days at +4 °C and paraffin embedded. Samples were cut on microtome (Leica SM2000R) as 2-µm thick sections. Before antibody staining antigen retrieval was performed (Dako S1699). Staining with primary antibodies was performed overnight at room temperature followed by Alexa-conjugated secondary antibodies staining at room temperature for 1 h (Invitrogen, 1:1000) or HRP-conjugated streptavidin-biotin antibody and immunoreactivity was visualized with ImmPACT DAB Peroxidase (Vector Laboratories, SK4105). Used antibodies: ACTA2 (Protein Tech, 23081-1-AP; 1:500), AIF1 (Novus, NB100-1028; 1:500), CALB1 (Swant; CB-38a; 1:500); COL4 (AbD Serotec, 2150-1470; 1:500), CDH1 (Novus, Af748; 1:500), CSF1 (NSJ, R31901; 1:200), CLDN10 (Sigma–Aldrich, HPA042348; 1:200), DLX5 (LSbio, LS-C352119; 1:200), DPP4 (Novus, AF954; 1:200), EGR1 (Cell Signalling, 4154; 1:200), F4/80 (Abcam, ab6640; 1:200), LYVE1 (Novus, AF2125; 1:200), MKI67 (Zytemed, RBK027-05; 1:200), NOTUM (Sigma–Aldrich, HPA023041; 1:200), PIEZO2 (Sigma–Aldrich, HPA040616; 1:200), POSTN (Novus, NBP1-30042; 1:200), RYR2 (ThermoFisher, PA5-36121; 1:200), S100A13 (DAKO; IS504; 1:500), SALL1 (Abcam, ab31526; 1:200), SMOC2 (MyBioSource, MBS2527784; 1:200), SOX9 (Sigma–Aldrich, HPA001758; 1:200), SOX10 (Santa cruz, sc-365692; 1:200), THBD (RnD systems, MAB3894; 1:200). Cell nuclei counterstaining was performed with DAPI (Sigma–Aldrich, D9542) diluted 1:1000 in PBS + 0.1% Tween 20 (Sigma–Aldrich, P9416) and slides were mounted with 87% glycerol (Merck, 104094) or Fluoromount Aqueous Mounting Medium (Sigma–Aldrich, F4680). Imaging was performed using Zeiss LSM880 laser scanning confocal microscope and Lightsheet Z.1 microscope. ZEN2.1 (ZEISS) and Imaris (Bitplane) software was used for image processing. Conventional histological staining after Clodrosome or Encapsome treatments was performed after 4 weeks decalcification of dissected mandibles in 19% EDTA. Mandibles were embedded in wax blocks and sectioned using 8µm thickness. Sections were stained using Masson's Trichrome.

**RNAscope.** *C56Bl6/J* mice (7 days to 4 month old) were used to verify scRNA-seq candidate gene expression. Dissected mouse mandibles were fixed in 4% paraformaldehyde pH 7.4 overnight, decalcified in 10% EDTA for 7 days at +4 °C for 7 days (*Foxd1*, *Sfrp2*) or in 0.5 M EDTA at +4 °C for 20 days (*Gjb3*, *Krt15*, and *Igfbp5*). All samples were embedded in paraffin and sectioned at 7 µm. Tissue were subsequently processed using the RNAscope multiplex fluorescent detection reagents v2 (ACD, 323110) (*Foxd1*, *Sfrp2*) or RNAscope 2.5 HD Assay-RED detection kit (ACD, 322350, 322360) (*Gjb3* (508841), *Igfbp5* (425731), *Smpd3* (815591), *Dkk1* (402521), *Wnt6* (401111), *Wisp1* (501921), *Nupr1* (434811), *Syt6* (449641), *Tac1* (410351)) according to the manufacturer's instructions. Notably, slides were boiled in the target retrieval buffer and incubated in Protease Plus solution at 40 °C for 15 min before probes were incubated at 40 °C for 2 h. The following probes were used: *Foxd1* (495501), *Gjb3* (508841), *Igfbp5* (425731), *Sfrp2* (400381). Samples were counterstained either with DAPI for 30 s (*Sfrp2* and *Foxd1*) or with Hematoxylin Gills #2 (20% dilution) for 15 s, followed by 10 s in ammonium hydroxide. Imaging was performed using a Leica DM5000 B (*Gjb3*, *Igfbp5*) or Zeiss LSM880 laser scanning confocal microscope (*Foxd1*, *Sfrp2*).

**Statistics and reproducibility.** Images: 1e; 2b–d, f; 3a–k; 5d, e, f, i; 6d, f; 7g; 8e–j; 10c, d and Supplementary Fig. 5c–f were selected as a representative pictures. The same or similar results were obtained in >3 independent experiments.

**Single-cell preparation.** *Mouse:* Wild-type *C56Bl6*, and *Sox2-GFP* mice were used for cell isolation from mandibular incisors for single-cell transcriptomics experiments. Age of all mice used for single-cell experiments was between 2 and 4 months. Mice were sacrificed by isoflurane overdose. Mandibles were carefully dissected and under stereomicroscope and surrounding soft tissue was removed. Using scalpel and scissors mandibular bone was gradually removed to obtain separated incisor. Particularly careful handling was performed in the soft area around the most proximal part of incisor where cervical loops. Both epithelial and mesenchymal parts from the whole of incisor were together dissected and processed as described further.

*Human:* Tissue from adult human healthy molar pulp, adult human molar pulp with caries and apical papilla from growing human molar was harvested for isolation of cells for RNA-seq analysis. Adult human healthy molar and adult human molar with caries were sectioned carefully to avoid damaging pulp using dental drill through enamel and part of dentin in mesial-distal direction. Dental pulps from adult molar and dental papilla were harvested, sectioned on petri dish in droplet of HBSS (Sigma–Aldrich, H6648) on ice into small pieces and further processed in the same way as mouse tissue.

Human tissue or mouse dental pulps with dental epithelium and surrounding dental follicle were isolated, cut into small pieces, transferred to 15 mL falcon tube with 2.5 mL Collagenase P (3 U/mL; Sigma–Aldrich, COLLA-RO ROCHE) dissolved in HBSS and incubated for 20–30 min at 37 °C shaking (120 rpm). During enzymatic digestion, tissue pieces were homogenized three times using 1 mL pipet. After incubation, the suspension was finally homogenized using pipet and 10 mL of 2% FBS (ThermoFisher Scientific, 10500064) in HBSS were slowly added. The suspension was centrifuged in 4 °C precooled centrifuge for 10 min at 300 × g. After centrifugation, supernatant was removed, the pellet was resuspended in 1 mL 2% FBS in HBSS, suspension was filtered using Tubes with Cell Strainer Snap Cap (Corning, 352235) and FACS (BD FACSAria III; software used: BD FACSDiva 8.0.1) was performed. All the work (except of enzymatic digestions at 37 °C) was performed on ice.

**Numbers of used mice for single-cell RNA-seq analyses.** For analysis of adult healthy mouse-incisor 78 mandibular incisors were used out of 39 animals in total. For analysis of mouse molar pulps 48 first molars out of 12 adult animals were used in total. For adult human tooth analyses 7 wisdom molars out of 7 healthy randomly selected males and females of age 18–31 were used and 6 apical papillae out of 3 patients/teeth were used.

**Single-cell sorting and single-cell transcriptomics.** All the sortings were performed on BD FACSAria III Cell Sorter into pre-prepared 384-well plates with lysis buffer. To minimize time of the cells outside the body no viability staining was performed. Three gating aspects were selected for isolation of non-traced cells: (a) SSC-A/FSC-A, (b) FSC-A/FSC/W, (c) SSC-A/SSC/W and strict gates were applied to remove debris, dead cells, and doublets. When genetically traced organisms were used the fourth gate (d) was applied during FACS sorting. Negative control using wild-type organism was applied to make a correct gating (e). After sorting, plates were frozen on dry ice and until being processed kept at –80 °C. Single-cell sequencing was performed according to smart-seq2 protocol following published guidelines<sup>12</sup>.

**Flow cytometry.** P7 incisor pulp was extracted in ice cold PBS and cut into small pieces using a fine scissor. The pulp was then resuspended in 5 ml of Collagenase D (0.5U/ml, Roche, 11088866001) and Dispase II (1.5U/ml, Roche, 4942078001). The tissue was allowed to dissociate by incubating the suspension in a cell culture incubator at 37 °C in 5% CO<sub>2</sub> for 30 minutes. Following enzymatic digestion the cell suspension was filtered through a 70-um Falcon Cell Strainer (Falcon, 352350) and the enzyme reaction quenched using 10 ml of ice cold PBS. Cells were centrifuged at 300 × g for 10 minutes, and resuspended in 200 ul of FACS staining buffer (BioLegend, 420201). 0.10 ug of rat anti mouse Gr-1—Alexa Fluor 488 conjugated (108417, BioLegend), and rat anti mouse F4/80—APC conjugated (123116/BioLegend) were added to the cell suspension. Cells were incubated with the antibodies on ice for 30 min. Excess staining buffer was added to quench the reaction and cells were centrifuged twice as before to remove excess antibody. Following the final centrifugation, cells were resuspended in 500 ul of staining buffer and 1.5 ug of DAPI (D1306, Invitrogen) added to be used as a dead cell exclusion marker. Samples were then analyzed on BD FACSAria III fusion machine. Data analysis was performed on FlowJo v10 software. Cells were gated based on size using standard SSC-A and FSC-A parameters so that debris is excluded. Following gating of cells, we focused on single cells and excluded doublets using SSC-A and SSC-W parameters. Live cells were then selected as cells identified to be dimly fluorescing in DAPI. Appropriate gating strategies were then used to select cells positive for the antibodies being used as deducted from the use of unstained controls.

**Data processing of mouse incisor.** The reads were aligned to the UCSC mm10 genome assembly, and per-gene read counts in each cell were determined using feature Counts software. STAR aligner was used to align scRNA-seq reads. The cells were filtered to exclude those with fewer than 800 detected genes resulting in 2889 out of 3312 cells for further analysis. Only genes that had at least 60 reads in at least 30 cells were considered for downstream processing. The data were analysed using PAGODA using k-nearest neighbour error models ( $k = 20$  and plain batch correction across samples). Gene expression levels were normalized per mean expression level in every cell and log<sub>10</sub> transformed (abbreviated below as fpm). Annotated Gene Ontology (GO) categories and de-novo gene clusters showing statistically significant overdispersion ( $z$ -score > 2.3) were clustered to determine the top aspects of transcriptional heterogeneity. Mitotic signature was removed from gene expression values by regressing out the mitotic expression signature, as previously described using a set of cell-cycle-related genes from<sup>6,31</sup>. The cells were grouped in 17 clusters using unbiased clustering as determined by PAGODA. t-SNE embedding was generated using *Rtsne* package and PAGODA-based cell–cell distance with perplexity = 25. Expression of a set of genes, where it is shown, was defined as their average expression for each cell.

To characterize gene modules controlling cell-type identities, we selected genes that have at least 2 fpm difference between maximum and mean average expression among clusters. For supplementary heatmap of general dataset genes were clustered using *hclust()* and *cutree()* R functions in 20 clusters using hierarchical clustering with Euclidean distance between gene expression profiles using Ward's linkage and cells were arranged using PAGODA clustering described above. Similar procedure was used to characterize gene modules separately in epithelial (552 genes) and other compartments using different cutoffs of 1.5 and 0.5 fpm difference on expression between maximum and mean average expression among clusters.

**Epithelial compartment.** Three epithelial clusters comprising 268 cells altogether were identified based on high expression of *Krt14* and reanalyzed separately. Gene expression levels in epithelial cells were adjusted to account for variance-mean trend in cell–cell expression variability as defined by PAGODA ( $k_{nn} = 40$ ). Epithelial cells were grouped in 13 clusters by hierarchical clustering with Ward linkage using correlation-based cell–cell distance of expression levels of 10410 the most variable genes (standard deviation variance-adjusted expression levels >0.8) in epithelial compartment. t-SNE embedding was generated using the same cell–cell distance and perplexity = 20. Mitotic signature was calculated as average expression of mitotic genes.

Five clusters representing progressive ameloblast differentiation were identified based on known markers of respective stages. Heterogeneity of ameloblasts cells was modelled as a principal trajectory using *crestree* R package approach<sup>51</sup>, with parameters ( $\lambda = 100$ ,  $\sigma = 0.03$ ,  $M = 100$ ) and cosine-based cell–cell distance. Root of the reconstructed trajectory was selected to biologically correspond to progenitor population of ameloblasts and each cell was assigned pseudotime as a distance from the root along the trajectory. Gene expression levels were modeled as a function of pseudotime using splines of the fifth degree with *gam* function from *mgcv* R package. Significance of association was calculated as Benjamini–Hochberg adjusted *gam* estimates of spline  $p$  value. Fitted gene expression levels were used to estimate magnitude of expression levels variation along the trajectory and downstream clustering. Five hundred and fifty-six genes that had more than 100-fold magnitude differences along the trajectory and adjusted  $p$  value <  $10^{-5}$  were clustered in nine clusters using hierarchical clustering with Ward linkage based on Euclidean distance.

**Mesenchymal compartment.** Four mesenchymal clusters of the general dataset comprising 1111 cells were reanalyzed separately. Only genes that had at least 20 reads in at least 10 cells were considered for downstream processing using PAGODA ( $k = 20$  and plain batch correction across wells). Mitotic signature was regressed out and top aspects of transcriptional heterogeneity were determined as for general dataset. The cells were grouped in five clusters using unbiased clustering as determined by PAGODA and t-SNE embedding was generated using PAGODA-based cell–cell distance with perplexity = 20. To clean up non-mesenchymal admixture of cells from other populations, only 1042 cells that had mean correlation of more than 0.2 to 200 the most correlated cells were retained for further analysis.

Transcriptional states of mesenchymal cells were modelled as a principal tree using our *crestree* R package based on the SimplePPT approach<sup>51,52</sup>. Briefly, given a set of data points  $x_1, \dots, x_N$  in  $M$ -dimensional space, a set of principal points  $z_1, \dots, z_K$  are arranged and are connected as a tree in the same space. Positions of principal points and tree structure are learned as alternate convex optimization problem that balances overall proximity of principal tree to data points and stringency of the tree. Tree was learned with parameters ( $\lambda = 2000$ ,  $\sigma = 0.03$ ,  $M = 200$ ) and cosine-based cell–cell distance. Principal tree contained three major branches and a few small sporadic branches that were removed.

For analysis of odontoblasts differentiation, cells assigned to a branch leading to mature odontoblasts were isolated and projected to the first two principal component using *pacMethods* R package. PCA was performed using 259 the most overdispersed genes (standard deviation variance-adjusted expression levels >1.3) whose expression was adjusted to account for variance-mean trend as described in PAGODA. The first principal component (PC1) corresponded to transition of

progenitor population to odontoblasts and was used as cell pseudotime. To identify differentiation-associated genes, expression levels were modeled as described for epithelial trajectory modeling. For heatmap visualization 252 genes that had magnitude of fitted expression levels of more than 1 fpm difference along PC1 and adjusted  $p$  value  $< 10^{-5}$  were arranged by pseudotime of maximum expression and pseudotime of the first derivative pass of ratio of expression magnitude to pseudotime magnitude. Sharp transition in expression pattern along pseudotime marked transition point from progenitor population to preodontoblasts and was used to separate progenitor population. To identify genes associated with distant and periodontoblastic pulp trajectories, cells assigned to one of pulp branches and cells of progenitor population from odontoblastic branch were arranged by pseudotime defined for the whole tree. Expression levels were modeled by a function of pseudotime as described above. For each of two pulp trajectories 100 genes with the highest magnitude along pseudotime and adjusted  $p$  value  $< 10^{-4}$  are shown.

To identify sources of heterogeneity in progenitor mesenchymal cells, all mature populations were removed using the following procedure: first, we selected the only one of five unbiased clusters does not represent mature pulp populations; second, we removed preodontoblasts from the cluster (Suppl. Fig. 4B) thus retaining only progenitor or immature committed cells (immature subpopulation below). Only 5343 the most overdispersed genes (standard deviation variance-adjusted expression levels across progenitor  $> 0.9$ ) in immature subpopulation were considered and their expression levels were normalized to zero mean and unit dispersion among immature cells. Independent components (ICs) of transcriptional variability were identified by independent component analysis (ICA) using *icafast()* function from *ica* R package. The number of statistically meaningful components was identified by comparison of components stability with that of control expression matrix, the latter obtained by shuffling of expression levels among immature cells independently for each gene. Twenty components of ICA were calculated for full original and control matrices and for their 100 subsamplings of 70% of cells. Stability of an IC of full matrix is estimated as the average correlation with the most similar components among 100 subsamplings. It reveals that all ICs of control matrix and 15 ICs of original matrix have stability of about 0.4, while 5 ICs of original matrix have substantially higher stability indicating confident statistical signal behind them. Final five ICs were predicted by running ICA with  $nc = 5$ .

We next analysed larger sample of 2552 mesenchymal cells profiled with 10x Chromium. Mesenchymal cells were isolated as clusters among 10x Chromium mouse-incisor populations expressing known mesenchymal marker, excluding minor admixture of epithelial cells in clusters based on expression of *Epcam*, *Krt14*, or *Cdh1*. The cells were reanalysed using standard PAGODA2 processing, including normalization of expression levels per mean in every cell, log10 transform and dimensionality reduction to 20 principal components (conducted with correction of expression levels for mean-variance trend). Mesenchymal cells were grouped in 12 clusters using default PAGODA2 multilevel community detection method. Three follicle clusters were merged, while nine dental pulp clusters were coloured to reflect the most similar cluster colour of Smart-seq2 annotation (see Fig. 4a). For analysis of fate-specific expression programs, 20 genes of each fate that have the largest mean expression difference between a fate cluster (e.g. apical, distal and pre-odontoblastic clusters) and progenitor clusters were considered as fate-specific markers. Intensity of fate-specific expression program in each cell was estimated as mean expression among 20 fate-specific genes. Cell-cycle score was defined as first principal component of cells transcriptional variability based on cell-cycle-annotated genes from. Cells from a cluster of mitotic cells were projected onto t-SNE embedding of non-mitotic mesenchymal landscape as a mean position of 10-nearest neighbours non-mitotic cells, where neighbours were defined using cosine-based distance in dimensionally reduced space of 20 PCs.

**Immune cluster analysis.** We isolated four clusters of cells representing immune subpopulations, partitioned them in eight clusters using hierarchical clustering with Ward linkage and visualized using t-SNE with perplexity = 20. For clustering and visualization 1-corr(.) cell-cell distance was used restricted to 1739 the most overdispersed genes (standard deviation variance-adjusted expression levels across progenitor  $> 1.1$ ) in immune compartment as estimated by standard deviation of mean-variance trend adjusted expression levels.

**Pericytes, glia, and endothelium analysis.** Subpopulations of pericytes and endothelial cells were partitioned in three groups each, while glial cells were partitioned in two groups using hierarchical clustering with Ward linkage. Clustering, t-SNE visualization and PCA were based on mean-variance-adjusted expression levels restricted to the most overdispersed genes in each compartment (glia: 873 genes, endothelium: 1878 genes, pericytes: 2110 genes; standard deviation variance-adjusted expression levels across progenitor  $> 1.5$  for glia, 1 for endothelium, 1 for pericytes). 1-corr(.) cell-cell distance was used for clustering and t-SNE (perplexity = 20).

**Assessment of cell quality.** Cell quality was additionally probed using metrics reflecting expression complexity, mitochondrial content and doublet probabilities.

Toward that goal, we assessed tradeoffs between number of expressed genes and UMIs (or reads for Smart-seq2) per cells, fraction of total reads from mitochondrial genes and cell doublet probabilities estimated using Scrublet with default parameters<sup>53</sup>. We estimated and explored these metrics for four datasets and manually excluded one cluster that had low number of genes compared to UMIs (it was a cluster of spike-in cells, see below) and a number of clusters of joint human analysis that were likely doublets (see Extended Data Fig. 2e-h).

**Data preprocessing of 10x Chromium samples.** Cell Ranger- 10x Chromium software was used to perform alignment to GRCh38 human genome or mm10 mouse genome assemblies, filtering, barcode counting and UMI counting. For Apical papilla 1, Adult molar 3, Adult molar 4, incisor (10x), mouse molar 1 (10x) datasets preprocessing was performed using Cell Ranger-2.2.0 following by filtering of cells having less than 500 UMIs. For other datasets datasets preprocessing was performed using Cell Ranger 3.0.2 following by default Cell Ranger 3.0.2 filtering of cells. Additionally, a protocol of library preparation used by the facility included spike-in of Jurkat and 32D cells of human and mouse species. Spike-in cells were not used for data processing or analysis and were excluded as *Hbb*<sup>+</sup> clusters; they are also easily detectable as having low complexity and forming a separate outlier transcriptional cluster.

**Joint analysis of mouse datasets.** Two mouse-incisor datasets (10x Chromium, 4236 cells, and Smart-seq2, 2889 cells) and three mouse molar datasets (two 10x Chromium, 1460 and 384 cells, and Smart-seq2, 195 cells), each composed of multiple teeth (see chapter “Numbers of used mice for single-cell RNA-seq analyses” in materials and methods and Supplementary Table 2), were processed independently using PAGODA2 R package<sup>13</sup> routine *basicP2proc()*, which performs normalization, log transformation, correction for mean-variance trend of expression levels, dimensionality reduction via PCA and clustering. After filtration of spike-in clusters identified through expression of *Hbb*, processed datasets were then jointly analysed using CONOS R package, which enables integrative analysis of single-cell datasets across samples and conditions<sup>40</sup>. Joint graph of 9164 cells from all datasets was constructed using CONOS routine *buildGraph()* with nearest neighbour parameters  $k = 15$ ,  $k.self = 15$ ,  $k.self.weight = 0.1$  in space of 10 common principal components (CPCA) estimated using 1000 overdispersed genes for each pair of samples. Joint graph was layout in 2D using UMAP method through CONOS routine *embedGraph()* with parameters  $spread = 1$  and  $min.dist = 0.05$ . Graph-based leiden community method with resolution = 1.0 was used to partition cells in 22 clusters.

To provide additional statistical support for reproducible structure of mesenchymal incisor populations and homogeneous distal-like molar state, we computationally isolated clusters of mesenchymal cells and separately explored cells of Smart-seq2 and 10x Chromium platforms. Platform-specific mesenchymal cells were processed using routine *basicP2proc()* with default PAGODA2 batch correction across samples and dimensionality reduction to 10 principal components based on top 1000 overdispersed genes. t-SNE method with perplexity = 50 was used to make 2d embedding.

Differential gene expression between molar and distal incisor mesenchymal cells was estimated as fold change between cluster-specific expression levels, estimated as sum of gene reads to total reads in a cluster. Significance of expression changes was estimated as  $p$  value of  $t$ -test comparing group means between normalized expression levels of molar and distal incisor clusters.

**Joint analysis of human datasets.** Two growing apical papilla and five adult molar 10x Chromium datasets of human teeth, comprising totally 41673 cells, were analysed using single-cell variational inference (scVI) deep learning framework<sup>54</sup>. Gene space was subsampled to 3000 genes using *scVI subsample\_genes* routine following by setting up parameters of variational autoencoder using *VAE()* routine with parameters ( $n\_hidden = 128$ ,  $n\_latent = 30$ ,  $n\_layers = 2$  and  $dispersion = 'gene'$ ) and training it using *UnsupervisedTrainer()* routine with  $n\_epochs = 150$ . Batch effect correction was by default performed using harmonization approach<sup>55</sup>. The resulting 30-dimensional reduced scVI space was used to make 2d embedding of the datasets using *UMAP()* routine with parameter  $spread = 1$ . K-nearest neighbour cell graph ( $k = 30$ ) was constructed using cosine-based cell-cell distances estimated in scVI space and then used to make leiden clustering (resolution = 1).

To explore behaviour of apical and distal mouse-incisor gene modules across human mesenchyme populations, we chose apical-specific and distal-specific sets of genes and assessed their averaged expression in human mesenchyme clusters. In details, apical and distal-specific genes were defined as those having at least three-fold change between apical and distal incisor states and  $p$  value  $< 10^{-10}$  in both 10 Chromium and Smart-seq2 mouse-incisor datasets. We then calculated (1) average expression levels of each apical and distal-specific gene in human mesenchyme clusters and (2) cell-specific sum of expression levels of apical genes or distal genes.

Similarity of nondividing cells to a group of dividing mesenchymal cells was estimated as an average Pearson correlation with dividing cells in latent scVI space.

**Assignment of sub/clusters identities.** Cell clusters and subclusters were characterized on several levels. After the unbiased cell clustering based on the expression similarities we searched for the most specific and highly expressed genes for every main sub/cluster and performed manual literature search to define their identity. Every sub/cluster was characterized based on co-expression of several (5–10) genes known to be expressed in particular cell sub/type. For the small subclusters where the identity wasn't possible to determine by literature search because their identity was unknown we performed either immunostainings or in situ hybridizations to determine their histological location. Based on the position of these cells in the tissue and a specific expression patterns of the selected genes we could then assess their role in the tissue. No functional experiments to prove such a role was not performed.

**Reporting summary.** Further information on research design is available in the Nature Research Reporting Summary linked to this article.

### Data availability

All single-cell RNA-seq datasets have been deposited in the GEO under accession code GSE146123. Processed data and interactive views of datasets can be accessed on the authors' website: [<http://pklab.med.harvard.edu/ruslan/dental.atlas.html>].

### Code availability

Code is freely available on the authors' website: [<http://pklab.med.harvard.edu/ruslan/dental.atlas.html>].

Received: 9 May 2020; Accepted: 24 August 2020;

Published online: 23 September 2020

### References

- Jussila, M. & Thesleff, I. Signaling networks regulating tooth organogenesis and regeneration, and the specification of dental mesenchymal and epithelial cell lineages. *Cold Spring Harb. Perspect. Biol.* **4**, a008425 (2012).
- Balic, A. & Thesleff, I. Tissue interactions regulating tooth development and renewal. *Curr. Top. Dev. Biol.* **115**, 157–186 (2015).
- Krivanek, J., Adameyko, I. & Fried, K. Heterogeneity and developmental connections between cell types inhabiting teeth. *Front. Physiol.* **8**, 376 (2017).
- Zhang, Y. D., Chen, Z., Song, Y. Q., Liu, C. & Chen, Y. P. Making a tooth: growth factors, transcription factors, and stem cells. *Cell Res.* **15**, 301–316 (2005).
- Balic, A. Biology explaining tooth repair and regeneration: a mini-review. *Gerontology* **64**, 382–388 (2018).
- Monterubbianesi, R. et al. A comparative in vitro study of the osteogenic and adipogenic potential of human dental pulp stem cells, gingival fibroblasts and foreskin fibroblasts. *Sci. Rep.* **9**, 1761 (2019).
- Orsini, G., Pagella, P., Putignano, A. & Mitsiadis, T. A. Novel biological and technological platforms for dental clinical use. *Front. Physiol.* **9**, 1102 (2018).
- Shi, X., Mao, J. & Liu, Y. Concise review: pulp stem cells derived from human permanent and deciduous teeth: Biological characteristics and therapeutic applications. *Stem Cells Transl. Med.* **9**, 445–464 (2020).
- Hematti, P. Mesenchymal stromal cells and fibroblasts: a case of mistaken identity? *Cytotherapy* **14**, 516–521 (2012).
- Rahmani, W. et al. Macrophages promote wound-Induced hair follicle regeneration in a CX3CR1- and TGF-beta1-dependent manner. *J. Invest. Dermatol.* **138**, 2111–2122 (2018).
- Sehgal, A. et al. The role of CSF1R-dependent macrophages in control of the intestinal stem-cell niche. *Nat. Commun.* **9**, 1272 (2018).
- Picelli, S. et al. Smart-seq2 for sensitive full-length transcriptome profiling in single cells. *Nat. Methods* **10**, 1096–1098 (2013).
- Fan, J. et al. Characterizing transcriptional heterogeneity through pathway and gene set overdispersion analysis. *Nat. Methods* **13**, 241–244 (2016).
- Babajko, S., de La Dure-Molla, M., Jedeon, K. & Berdal, A. MSX2 in ameloblast cell fate and activity. *Front. Physiol.* **5**, 510 (2014).
- Moffatt, P., Wazen, R. M., Dos Santos Neves, J. & Nanci, A. Characterisation of secretory calcium-binding phosphoprotein-proline-glutamine-rich 1: a novel basal lamina component expressed at cell-tooth interfaces. *Cell Tissue Res.* **358**, 843–855 (2014).
- Smith, C. E. L. et al. Amelogenesis imperfecta: genes, proteins, and pathways. *Front. Physiol.* **8**, 435 (2017).
- Coste, B. et al. Piezo1 and Piezo2 are essential components of distinct mechanically activated cation channels. *Science* **330**, 55–60 (2010).
- Woo, S. H. et al. Piezo2 is required for Merkel-cell mechanotransduction. *Nature* **509**, 622–626 (2014).
- Lanner, J. T., Georgiou, D. K., Joshi, A. D. & Hamilton, S. L. Ryanodine receptors: structure, expression, molecular details, and function in calcium release. *Cold Spring Harb. Perspect. Biol.* **2**, a003996 (2010).
- Yoshizato, K., Thuy le, T. T., Shiota, G. & Kawada, N. Discovery of cytoglobin and its roles in physiology and pathology of hepatic stellate cells. *Proc. Jpn Acad. Ser. B Phys. Biol. Sci.* **92**, 77–97 (2016).
- Thuy le, T. T. et al. Absence of cytoglobin promotes multiple organ abnormalities in aged mice. *Sci. Rep.* **6**, 24990 (2016).
- Martin, C. E. & Jones, N. Nephron signaling in the podocyte: an updated view of signal regulation at the slit diaphragm and beyond. *Front. Endocrinol. (Lausanne)* **9**, 302 (2018).
- Mak, D. O., Dang, B., Weiner, I. D., Foskett, J. K. & Westhoff, C. M. Characterization of ammonia transport by the kidney Rh glycoproteins RhBG and RhCG. *Am. J. Physiol. Ren. Physiol.* **290**, F297–F305 (2006).
- Biehls, B. et al. BMI1 represses *Ink4a/Arf* and *Hox* genes to regulate stem cells in the rodent incisor. *Nat. Cell Biol.* **15**, 846–852 (2013).
- Juuri, E. et al. Sox2+ stem cells contribute to all epithelial lineages of the tooth via *Sfrp5+* progenitors. *Dev. Cell* **23**, 317–328 (2012).
- Seidel, K. et al. Hedgehog signaling regulates the generation of ameloblast progenitors in the continuously growing mouse incisor. *Development* **137**, 3753–3761 (2010).
- Seidel, K. et al. Resolving stem and progenitor cells in the adult mouse incisor through gene co-expression analysis. *elife* **6**, <https://elifesciences.org/articles/24712> (2017).
- Suomalainen, M. & Thesleff, I. Patterns of Wnt pathway activity in the mouse incisor indicate absence of Wnt/beta-catenin signaling in the epithelial stem cells. *Dev. Dyn.* **239**, 364–372 (2010).
- Gritli-Linde, A. et al. Shh signaling within the dental epithelium is necessary for cell proliferation, growth and polarization. *Development* **129**, 5323–5337 (2002).
- Balic, A. & Mina, M. Identification of secretory odontoblasts using DMP1-GFP transgenic mice. *Bone* **48**, 927–937 (2011).
- Vidovic, I. et al. alphaSMA-expressing perivascular cells represent dental pulp progenitors in vivo. *J. Dent. Res.* **96**, 323–330 (2017).
- Mark, M. P., Bloch-Zupan, A. & Ruch, J. V. Effects of retinoids on tooth morphogenesis and cytodifferentiations, in vitro. *Int. J. Dev. Biol.* **36**, 517–526 (1992).
- Rhinn, M. & Dolle, P. Retinoic acid signalling during development. *Development* **139**, 843–858 (2012).
- Zhao, H. et al. Secretion of shh by a neurovascular bundle niche supports mesenchymal stem cell homeostasis in the adult mouse incisor. *Cell Stem Cell* **14**, 160–173 (2014).
- Yu, T., Volponi, A. A., Babb, R., An, Z. & Sharpe, P. T. Stem cells in tooth development, growth, repair, and regeneration. *Curr. Top. Dev. Biol.* **115**, 187–212 (2015).
- La Manno, G. et al. RNA velocity of single cells. *Nature* **560**, 494–498 (2018).
- Hu, M. et al. Multilineage gene expression precedes commitment in the hemopoietic system. *Genes Dev.* **11**, 774–785 (1997).
- Vijaykumar, A. et al. Generation and characterization of DSPP-Cerulean/DMP1-Cherry reporter mice. *Genesis* **57**, e23324 (2019).
- Kaukua, N. et al. Glial origin of mesenchymal stem cells in a tooth model system. *Nature* **513**, 551–554 (2014).
- Barkas, N. et al. Joint analysis of heterogeneous single-cell RNA-seq dataset collections. *Nat. Methods* **16**, 695–698 (2019).
- Neves, V. C., Babb, R., Chandrasekaran, D. & Sharpe, P. T. Promotion of natural tooth repair by small molecule GSK3 antagonists. *Sci. Rep.* **7**, 39654 (2017).
- Nanci, A. *Ten Cate's Oral Histology-E-Book: Development, Structure, and Function* (Elsevier Health Sciences, 2017).
- Jontell, M., Okiji, T., Dahlgren, U. & Bergenholtz, G. Immune defense mechanisms of the dental pulp. *Crit. Rev. Oral Biol. Med.* **9**, 179–200 (1998).
- Pugach, M. K. & Gibson, C. W. Analysis of enamel development using murine model systems: approaches and limitations. *Front. Physiol.* **5**, 313 (2014).
- Vishwakarma, A., Sharpe, P., Shi, S. & Ramalingam, M. *Stem Cell Biology and Tissue Engineering In Dental Sciences* (Academic Press, 2014).
- Sharir, A. et al. A large pool of actively cycling progenitors orchestrates self-renewal and injury repair of an ectodermal appendage. *Nat. Cell Biol.* **21**, 1102–1112 (2019).
- An, Z. et al. A quiescent cell population replenishes mesenchymal stem cells to drive accelerated growth in mouse incisors. *Nat. Commun.* **9**, 378 (2018).
- Sharpe, P. T. Dental mesenchymal stem cells. *Development* **143**, 2273–2280 (2016).
- Maye, P. et al. A BAC-bacterial recombination method to generate physically linked multiple gene reporter DNA constructs. *BMC Biotechnol.* **9**, 20 (2009).
- Kobayashi, A. et al. Identification of a multipotent self-renewing stromal progenitor population during mammalian kidney organogenesis. *Stem Cell Rep.* **3**, 650–662 (2014).

51. Soldatov, R. et al. Spatiotemporal structure of cell fate decisions in murine neural crest. *Science* **364**, <https://science.sciencemag.org/content/364/6444/eaas9536> (2019).
52. Qi, M., Li, W., Tsang, I. W. & Yijun, S. Principal graph and structure learning based on reversed graph embedding. *IEEE Trans. Pattern Anal. Mach. Intell.* **39**, 2227–2241 (2017).
53. Wolock, S. L., Lopez, R. & Klein, A. M. Scrublet: computational identification of cell doublets in single-cell transcriptomic data. *Cell Syst.* **8**, 281–291.e289 (2019).
54. Lopez, R., Regier, J., Cole, M. B., Jordan, M. I. & Yosef, N. Deep generative modeling for single-cell transcriptomics. *Nat. Methods* **15**, 1053–1058 (2018).
55. Xu, C. et al. Harmonization and annotation of single-cell transcriptomics data with deep generative models. *bioRxiv*, 532895. Preprint at <https://www.biorxiv.org/content/10.1101/532895v1> (2019).

## Acknowledgements

I.A. was supported by an ERC consolidator grant (STEMMING-FROM-NERVE, 647844), EMBO young investigator program, Bertil Hallsten Research Foundation, Vetenskapsradet Project Grant and Ake Wiberg Foundation. J.K. was supported by the Grant Agency of Masaryk University, project MUNI/H/1615/201 and by funds from the Faculty of Medicine MU to junior researcher. T.H. was supported by an ERC consolidator grant (2015-AdG-695136). P.M. and O.D.K. were supported by NIH/NIDCR R35-DE026602. P.V.K. and R.A.S. were supported by NIH R01HL131768. We acknowledge the core facility CELLIM of CEITEC supported by the Czech-BioImaging large RI project (LM2018129 funded by MEYS CR) for their support with obtaining scientific data presented in this paper. We thank the BRC Flow Cytometry core at Guy's Hospital for their help and expertise. We would like to thank The Eukaryotic Single Cell Genomics facility of SciLifeLab and all members of Igor Adameyko's laboratory for technical help. Special thanks go to Andrew P. McMahon for providing *FoxD1<sup>CreERT2</sup>* mice and Thibault Gerald Boudier for assistance with sequencing. Finally, we would like to thank Vojtech Sobotka for his kind initial help with programming.

## Author contributions

J.K., R.A.S., P.V.K., and I.A. performed experiments, analysed the data and wrote the manuscript. M.E.K., A.N.H., J.P., B.S., M.L., V.K.M., L.L.H., U.K., I.V.Z., A.V., A.B., P.M., M.M., M.B., B.D.M., P.S., V.N., and V.Y. performed experiments and analysed data. T.C., O.D.K., T.H., and K.F. analysed data.

## Funding

Open Access funding provided by Karolinska Institute.

## Competing interests

P.V.K. serves on the Scientific Advisory Board to Celsius Therapeutics Inc. Other authors declare no competing interests.

## Additional information

Supplementary information is available for this paper at <https://doi.org/10.1038/s41467-020-18512-7>.

Correspondence and requests for materials should be addressed to P.V.K. or I.A.

Peer review information *Nature Communications* thanks Joy Richman and the other, anonymous, reviewer(s) for their contribution to the peer review of this work.

Reprints and permission information is available at <http://www.nature.com/reprints>

Publisher's note Springer Nature remains neutral with regard to jurisdictional claims in published maps and institutional affiliations.



**Open Access** This article is licensed under a Creative Commons Attribution 4.0 International License, which permits use, sharing, adaptation, distribution and reproduction in any medium or format, as long as you give appropriate credit to the original author(s) and the source, provide a link to the Creative Commons license, and indicate if changes were made. The images or other third party material in this article are included in the article's Creative Commons license, unless indicated otherwise in a credit line to the material. If material is not included in the article's Creative Commons license and your intended use is not permitted by statutory regulation or exceeds the permitted use, you will need to obtain permission directly from the copyright holder. To view a copy of this license, visit <http://creativecommons.org/licenses/by/4.0/>.

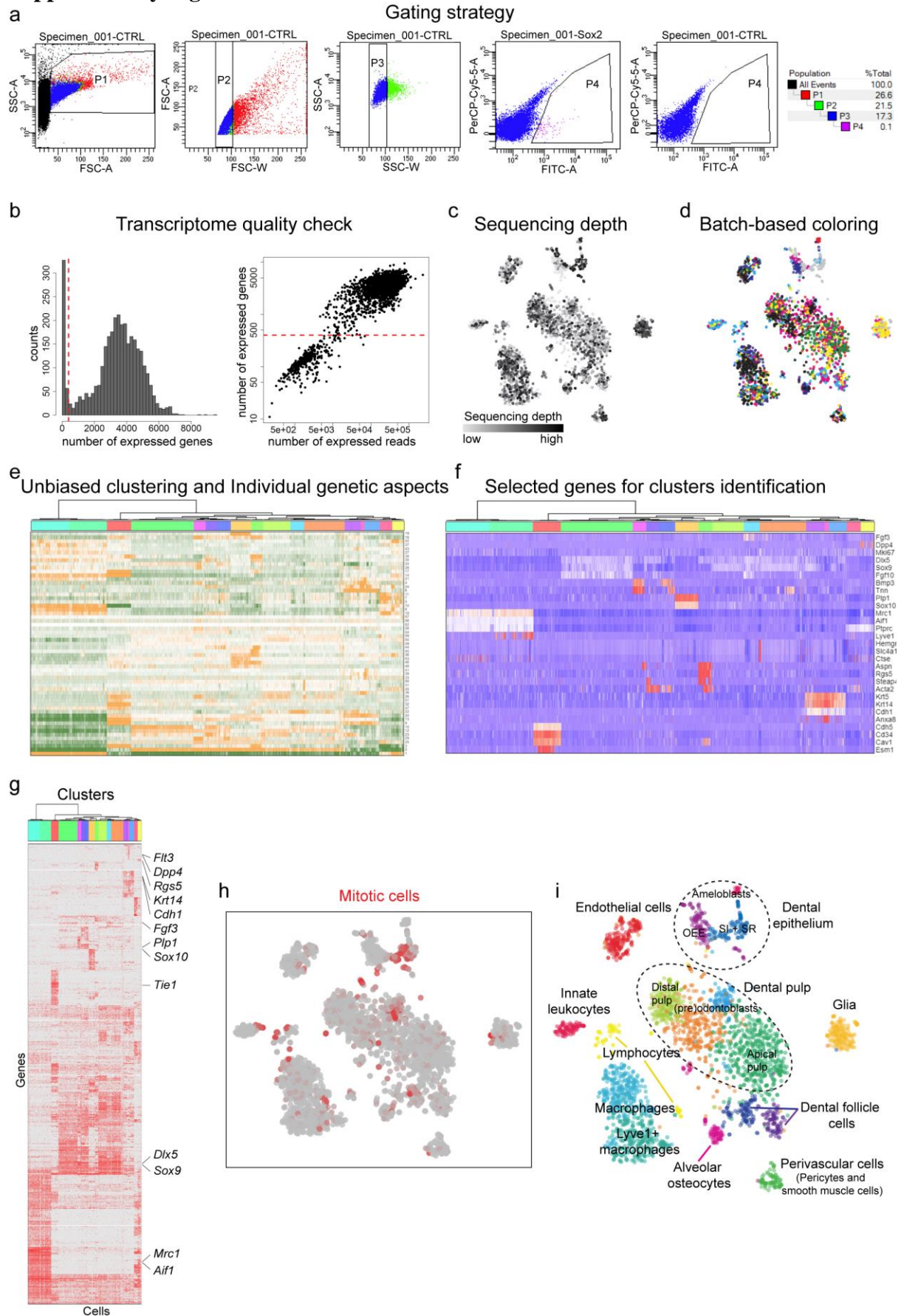
© The Author(s) 2020

# **Dental cell type atlas reveals stem and differentiated cell types in mouse and human teeth**

Krivanek et al.

# SUPPLEMENTARY FIGURES

## Supplementary Figure 1



**Supplementary Figure 1. Transcriptional patterns of major cell populations in the mouse incisor.**

**a)** Plots showing an example of gating strategy used for the single-cell sorting into 384-well plates for smart-seq2 protocol.

**b)** Number of reads and expressed genes per cell. Bimodal distribution of the number of expressed genes per cell (left) and high correspondence between number of reads and expressed genes per cell (right) allows to unambiguously identify and to exclude low quality cells.

**c)** Depth (number of reads) per cell and batches are only subtly associated with structure of clusters.

**d)** Batch effect. Plot shows the cell clustering based on different isolations (each color shows separate single-cell RNA-seq analysis).

**e)** Individual multigenic aspects of heterogeneity identified for the full dataset.

**f)** The selection of comprehensive and known markers outlining the clusters.

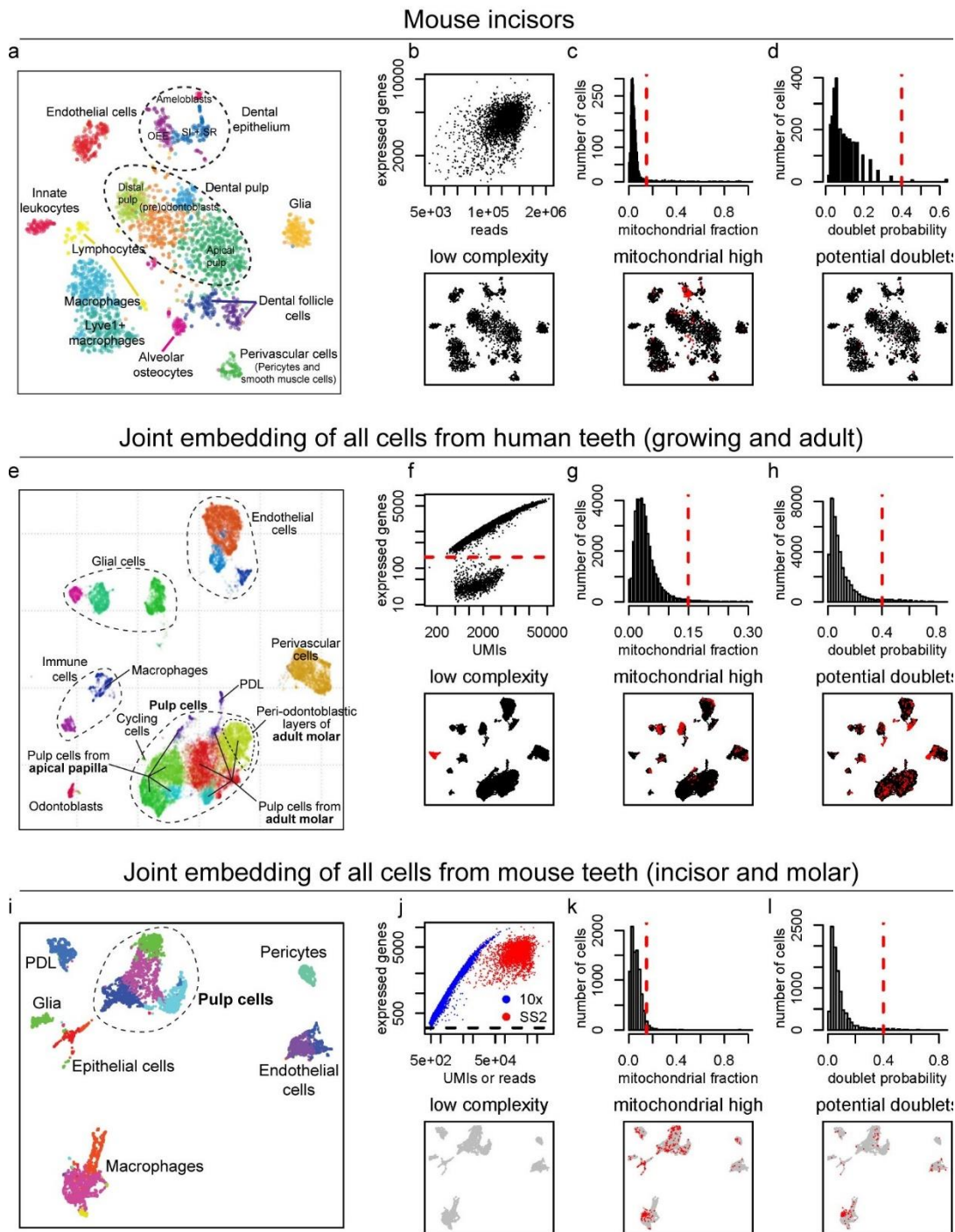
**g)** Heatmap showing combinatorial expression patterns of genes strongly associated with subpopulations used for cluster identification.

**h,i)** t-SNE dimensional reduction visualizes mitotic cells (**f**) among all major populations (**g**) identified in the whole dental cell type dataset.

(SI – stratum intermedium, SR – Stellate Reticulum, OEE – Outer Enamel Epithelium)

## Supplementary Figure 2

### Quality controls



**Supplementary Figure 2. Assessment of cell quality using three diagnostic metrics across four meta-datasets.**

**a,e,i)** Embeddings of four meta-datasets corresponding to Extended Data Figure 9, Figure 4, Figure 1, Extended Data Figure 13.

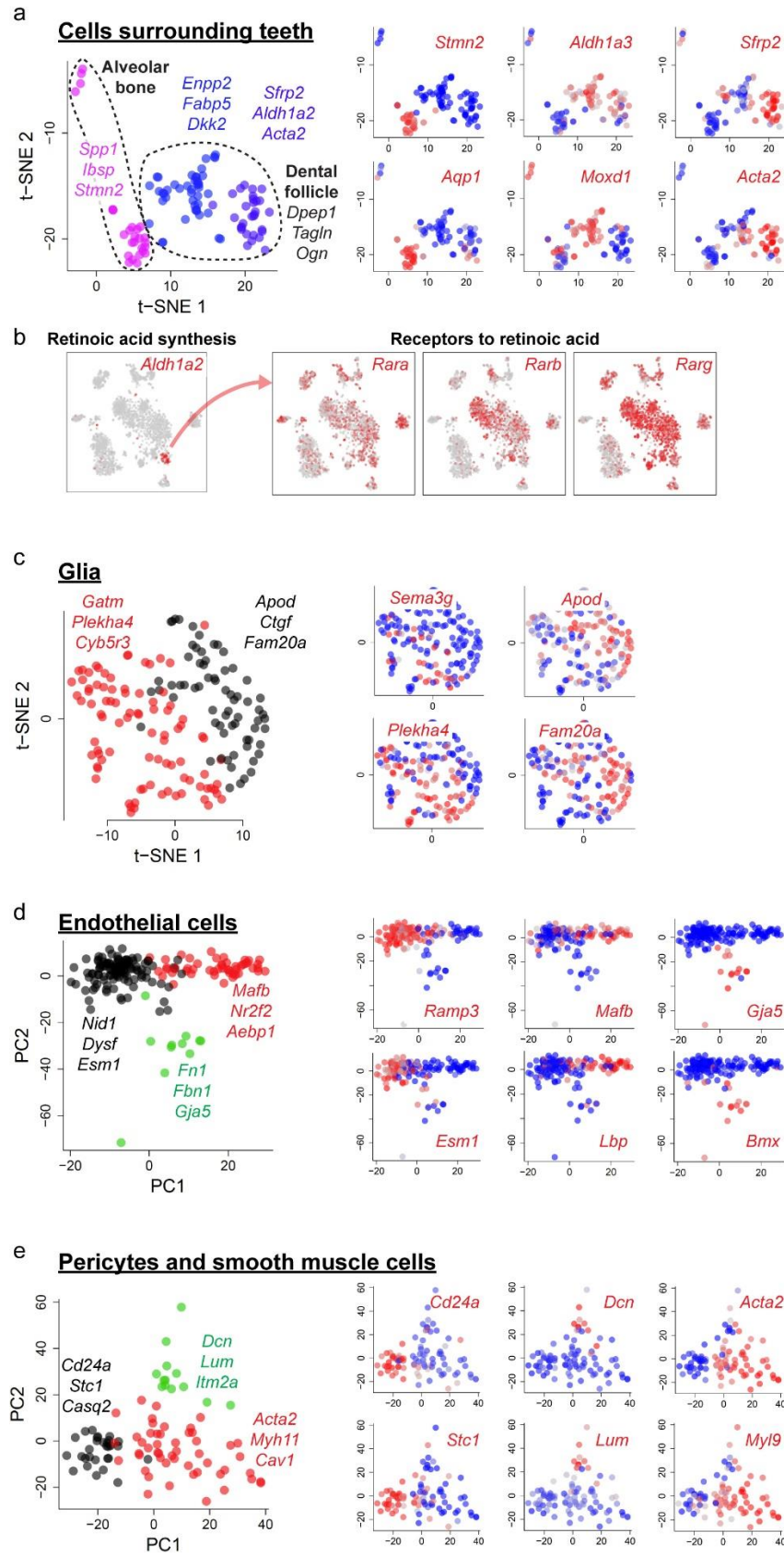
**b,f,j)** Relationship between number of UMIs (or reads for Smart-seq2) and number of expressed genes per cell (upper panel) reveals an outlier population with low complexity in

the human meta-dataset, panel f). Red cells in embeddings reflect cells with lower than 300 expressed genes (horizontal dotted line).

**c,g,k)** Distribution of fraction of mitochondrial reads per cells (upper panel) shows preferentially high-quality cells. Bottom plots show low-quality/suspicious cells onto embeddings (0.15 cutoff, see vertical red dotted line on the top plots).

**d,h,l)** Assessment of doublets in meta-datasets using Scrublet inferred doublet probabilities. Distribution of doublet probabilities (upper plots) reveals a number of cell groups in human meta-dataset likely composed of doublets, panel h). Cells with doublet probability of more than 0.4 are shown onto embeddings (bottom plots).

### Supplementary Figure 3

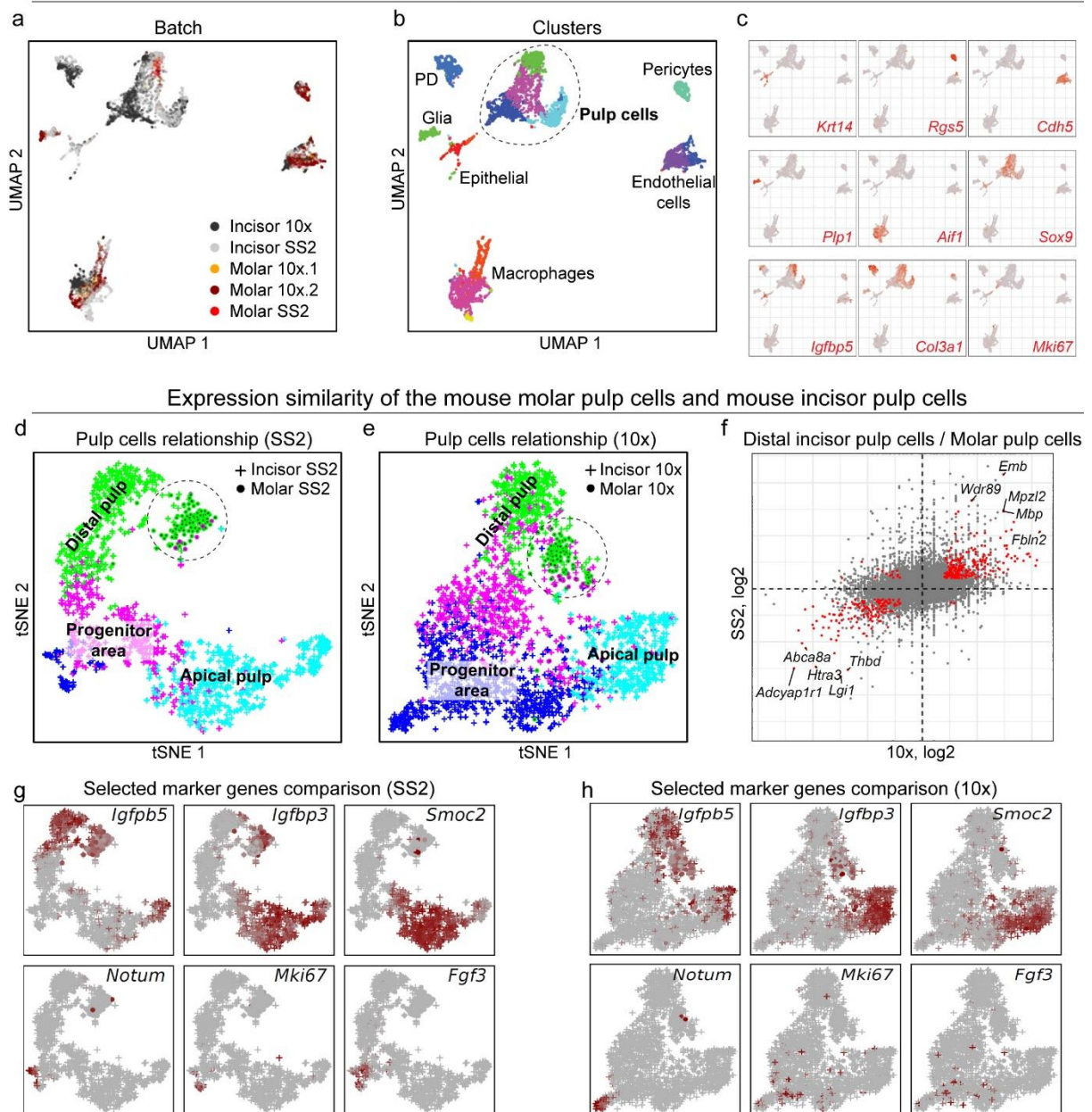


**Supplementary Figure 3. Heterogeneity of Cells surrounding teeth, Glial, Endothelial and Perivascular cells from the incisor tooth.**

- a)** Heterogeneity of cells surrounding the incisor. Two major cell populations can be distinguished: alveolar bone marked by *Ibsp*, *Bmp3*, *Dmp1*, *Spp1*, *Stmn2*, *Tnn* and *Ltbp2*, and the dental follicle marked by *Aldh1a2*, *Acta2*, *Tagln*, *Gdf10*, *Cldn2*, and *Igfbp5*.
- b)** The expression of *Aldh1a2* in the dental follicle suggests previously unanticipated roles of retinoic acid signalling in incisor maintenance. Correspondingly, complementary receptor genes *Rara*, *Rarb* and *Rarg* are expressed in some of the major populations of the tooth.
- c)** Internal heterogeneity of glial cluster.
- d)** Internal heterogeneity of endothelial cluster.
- e)** Internal heterogeneity of perivascular cells. Note: the red cluster outlined by expression of *Acta2*, *Myh11* and *Cav1* represents perivascular smooth muscle cells.

## Supplementary Figure 4

Joint embedding of all mice incisor and molar cells



### Supplementary Figure 4. Comparison of mouse incisor and molar teeth.

**a)** UMAP embedding of CONOS joint graph visualizes dental cell composition of 9164 cells across two incisor (4236 cells of 10x Chromium and 2889 cells of Smart-seq2) and three molar (1460 and 384 cells of 10x Chromium and 195 cells of Smart-seq2) mouse teeth datasets. Each dataset is composed of multiple teeth (for details please see materials and methods).

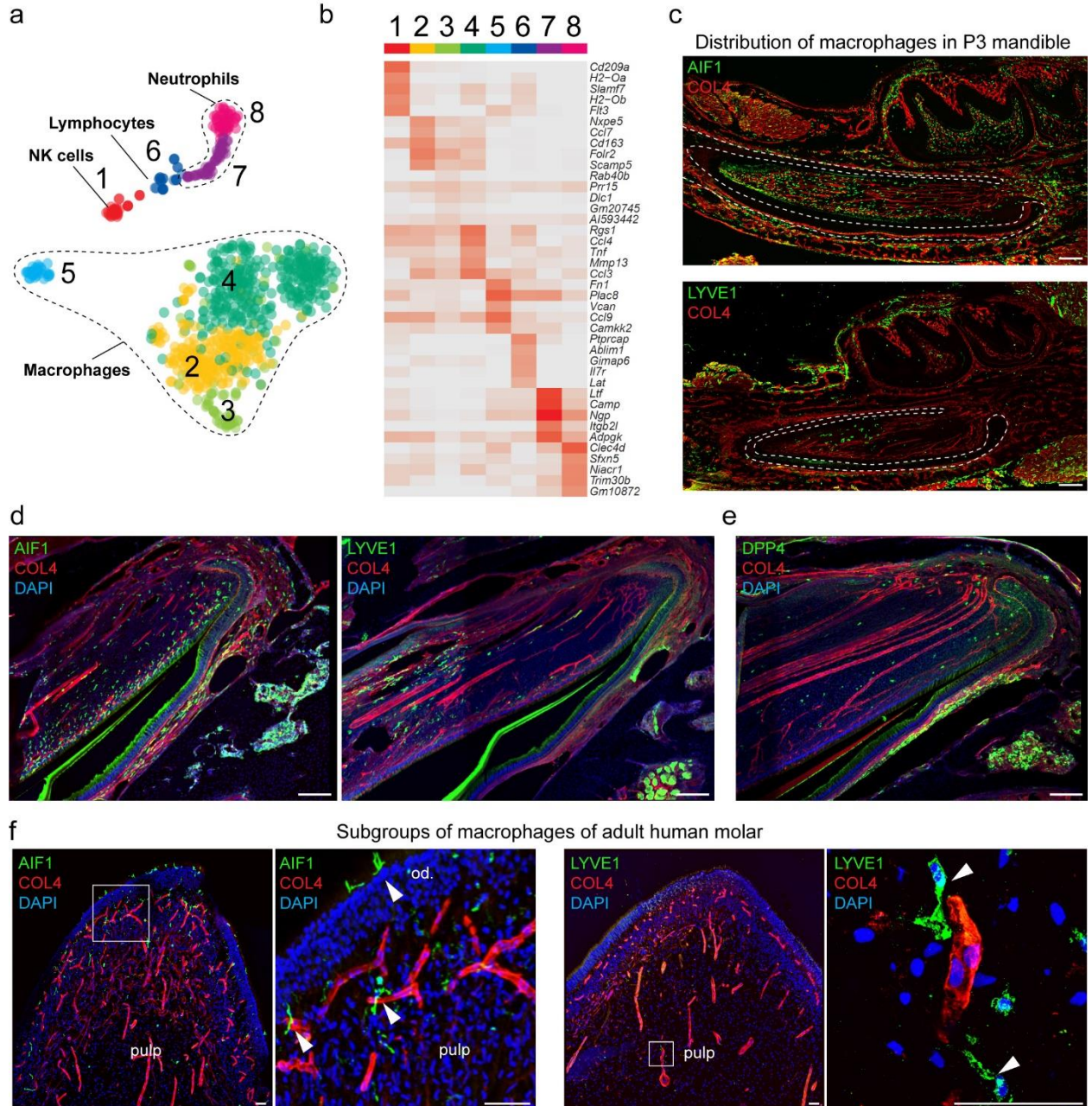
**b)** Leiden clustering (22 clusters) shows similarities and contrasts of dental cell states between incisor and molar. Colors of mesenchymal clusters match colors of incisor pulp subpopulations on Figure 3.

**c)** Expression of selected marker genes.

**d, e**) tSNE embedding of Smart-seq2 (**d**) or 10x Chromium (**e**) mesenchymal cells corroborates three-branch structure of mouse incisor mesenchyme and emphasize more homogeneous distal-like transcriptional state of mouse molar (dotted circle outline mouse molar pulp). Cell colors correspond to colors of clusters on panel b.

**f**) Differential expression analysis between distal incisor pulp and molar pulp is consistent between Smart-seq2 and 10x Chromium and reveals markers of molar pulp. X/Y axes show fold change of average gene expression levels between distal incisor and molar pulps, red color shows genes significantly differentially expressed in both platforms (at least two fold change and  $p < 10^{-2}$ , t-test).

## Supplementary Figure 5



### Supplementary Figure 5. Heterogeneity and signaling interactions in immune system of a tooth.

**a,b)** t-SNE dimensional reduction and corresponding heatmap with key differentially expressed genes visualizes 8 populations assigned as immune cells including lymphocytes, innate immune cells and macrophages. Markers of macrophage activation (*Nos1*, *Nos2*, *Nos3*, *Il4*, *Slc7a2*, *Arg1*, *Arg2*) were absent, suggesting that macrophages in non-damaged teeth remain inactive.

**c)** Cross-section through P3 mandible showing the differential spatial distribution of AIF1<sup>+</sup> and LYVE1<sup>+</sup> macrophages (immunohistochemistry). COL4 immunohistochemical staining visualize the blood vessels.

**d)** Immunohistochemistry-based validation of AIF1<sup>+</sup>, LYVE1<sup>+</sup> macrophages inside the mouse incisor. Together with the figure 5c these panels prove the different histological

positioning of two different kind of macrophages (LYVE1<sup>+</sup> and LYVE1<sup>-</sup>). AIF1<sup>+</sup> macrophages are located in the whole incisor including apical pulp, cervical loop, odontoblast layer and distal pulp in contrast to LYVE<sup>+</sup> macrophages which mostly resides in the middle part of the pulp, but not inside the odontoblast layer. COL4 immunohistochemical staining visualize the blood vessels.

**e)** Immunohistochemistry-based validation of the NK-cells cluster using DPP4 marker. Position of DPP4<sup>+</sup> cells outside the blood vessels in the tooth was proved in 5 independent animals. COL4 immunohistochemical staining visualize the blood vessels.

**f)** Two different types of macrophages (LYVE1<sup>+</sup> and LYVE1<sup>-</sup>) demonstrate spatially restricted distribution also in human molar (immunohistochemistry). Scale bars: 50  $\mu$ m.

## **Developmental mechanisms driving complex tooth shape in reptiles**

*Marie Landova Sulcova, Oldrich Zahradnicek, Jana Dumkova, Hana Dosedelova, **Jan Krivanek**, Marek Hampl, Michaela Kavkova, Tomas Zikmund, Martina Gregorovicova, David Sedmera, Jozef Kaiser, Abigail S Tucker, Marcela Buchtova*

# Developmental mechanisms driving complex tooth shape in reptiles

Marie Landova Sulcova<sup>1,2</sup> | Oldrich Zahradnicek<sup>3</sup> | Jana Dumkova<sup>4</sup> |  
 Hana Dosedelova<sup>1</sup> | Jan Krivanek<sup>4</sup> | Marek Hampel<sup>1,2</sup> | Michaela Kavkova<sup>5</sup>  |  
 Tomas Zikmund<sup>5</sup>  | Martina Gregorovicova<sup>6,7</sup>  | David Sedmera<sup>6,7</sup>  |  
 Jozef Kaiser<sup>5</sup>  | Abigail S. Tucker<sup>3,8</sup>  | Marcela Buchtova<sup>1,2</sup> 

<sup>1</sup>Laboratory of Molecular Morphogenesis, Institute of Animal Physiology and Genetics, Czech Academy of Science, Brno, Czech Republic

<sup>2</sup>Department of Experimental Biology, Faculty of Science, Masaryk University, Brno, Czech Republic

<sup>3</sup>Institute of Experimental Medicine, Czech Academy of Science, Prague, Czech Republic

<sup>4</sup>Department of Histology and Embryology, Faculty of Medicine, Masaryk University, Brno, Czech Republic

<sup>5</sup>CEITEC-Central European Institute of Technology, University of Technology, Brno, Czech Republic

<sup>6</sup>Institute of Anatomy, Medical Faculty, Charles University, Prague, Czech Republic

<sup>7</sup>Institute of Physiology, Czech Academy of Sciences, Prague, Czech Republic

<sup>8</sup>Centre for Craniofacial and Regenerative Biology, Faculty of Dentistry, Oral and Craniofacial Sciences, King's College London, London, UK

## Correspondence

Marcela Buchtova, Laboratory of Molecular Morphogenesis, Institute of Animal Physiology and Genetics, v.v.i., Czech Academy of Sciences, Veveri 97, Brno 602 00, Czech Republic.  
 Email: buchtova@iach.cz

## Funding information

Czech Science Foundation, Grant/Award Number: 17-14886S; Ministry of Education, Youth and Sports of the Czech Republic, Grant/Award Numbers: CZ.02.1.01/0.0/0.0/15\_003/0000460, LM2015062, LQ1601

## Abstract

**Background:** In mammals, odontogenesis is regulated by transient signaling centers known as enamel knots (EKs), which drive the dental epithelium shaping. However, the developmental mechanisms contributing to formation of complex tooth shape in reptiles are not fully understood. Here, we aim to elucidate whether signaling organizers similar to EKs appear during reptilian odontogenesis and how enamel ridges are formed.

**Results:** Morphological structures resembling the mammalian EK were found during reptile odontogenesis. Similar to mammalian primary EKs, they exhibit the presence of apoptotic cells and no proliferating cells. Moreover, expression of mammalian EK-specific molecules (SHH, FGF4, and ST14) and GLI2-negative cells were found in reptilian EK-like areas. 3D analysis of the nucleus shape revealed distinct rearrangement of the cells associated with enamel groove formation. This process was associated with ultrastructural changes and lipid droplet accumulation in the cells directly above the forming ridge, accompanied by alteration of membranous molecule expression (Na/K-ATPase) and cytoskeletal rearrangement (F-actin).

**Conclusions:** The final complex shape of reptilian teeth is orchestrated by a combination of changes in cell signaling, cell shape, and cell rearrangement. All these factors contribute to asymmetry in the inner enamel epithelium development, enamel deposition, ultimately leading to the formation of characteristic enamel ridges.

## KEYWORDS

chameleon, crocodile, enamel ridge, gecko, matriptase, Na,K-ATPase, nuclei shape, SHH, tooth shape

## 1 | BACKGROUND

Toothed vertebrates have evolved many types of dentition with different tooth complexity level as an adaptation to distinct food requirements. The shape of teeth in vertebrates varies from simple conical to multicuspid, and their surface morphology can include tooth cusps, enamel ridges, or tubercles with serrated edges.<sup>1</sup> Such heterogeneity brought us to the question of whether there is any conserved mechanism driving the process of tooth shaping.

Formation of complex tooth shape during mammalian embryogenesis is well known from the intensive study of mouse odontogenesis. The enamel knot (EK) is one of the key players contributing to the regulation of enamel organ development and shaping of the inner enamel epithelium.<sup>2-6</sup> An EK is formed from cluster of cells within the dental epithelium.<sup>4</sup> EK cells serve as a source of numerous signaling molecules such as SHH or members of the WNT, BMP, and FGF families.<sup>4,7-13</sup> All these proteins and their mutual cooperation help to drive numerous cellular processes contributing to final tooth shape, including proliferation (stratification), cell rearrangements (invagination), and localized apoptosis. Moreover, changes in individual cell morphology are necessary for final tooth crown shaping. These processes depend on precise local regulation of cellular geometry with the involvement of actin filaments and adherent junction rearrangement.<sup>14</sup>

It is still unclear whether signaling centers are apomorphies of mammals and drive the bud-cap transition or participate in tooth shape formation in non-mammalian species. In the shark *Scyliorhinus canicula*, a chondrychthian, cytologically distinct structures reminiscent of mammalian EKs have been observed.<sup>15</sup> The folded tip of the epithelial bud is formed by slowly proliferating cells, but apoptosis has not been detected. However, co-expression of *Shh* and *Fgf8* orthologs is present in this area.<sup>15,16</sup> In reptiles, structures resembling primary EKs have been indicated in the alligator, which has single cuspid teeth,<sup>17,18</sup> and also in several squamate species with both single and multicuspid teeth.<sup>1,19-21</sup> On the other hand, an evaluation of *Shh* and *Fgf4* expression in crocodylians did not confirm the presence of an EK.<sup>22</sup> Similarly, in squamates with single cuspid teeth, localized expression of key mammalian EK markers (eg,

*Bmp2*, *Bmp4*, *Axin2*, and *Wnt10b*) was not observed.<sup>20,23</sup> Interestingly, *Bmp2* was found to be expressed in the enamel epithelial bulge cells in *Eublepharis macularius*, which exhibits two enamel ridges on the tooth surface.<sup>20</sup> This indicated the possibility that an EK-like structure might exist in squamate reptiles with complex tooth morphology.

Therefore, we focused on the development of complex reptilian teeth with labial and lingual enamel ridges, using the veiled chameleon (*Chamaeleo calypttratus*) as a model species. For comparison, we used the ocelot gecko (*Paroedura picta*) with cylindro-conical teeth divided by enamel ridges on its tips, and the Siamese crocodile (*Crocodylus siamensis*), which has more simplified conical tooth morphology.

Here, we evaluated the presence of an EK-like structure in complex reptilian teeth at the cellular and ultrastructural level during odontogenesis. According to our results, molecular signaling in the reptilian EK-like structure strongly resembles that in the mammalian EK. Moreover, we describe the mechanism of cell shape changes, which lead to the formation of enamel ridges on both unicuspid and more complex multicuspid teeth.

## 2 | RESULTS

### 2.1 | Tooth morphology across diverse reptile species

To analyze the development of tooth complexity in reptiles, we selected the veiled chameleon (*C. calypttratus*) as a species from Acrodonta lineage of squamates and ocelot gecko (*P. picta*) as a representative of the basal squamates of Gekkota lineage, which both exhibit distinct structures (ridges/crests) on their tooth surface. These ridges in the gecko have been shown to arise due to asymmetrical enamel deposition leading to thick enamel production at the crests and reduced enamel in the grooves.<sup>1,21</sup> Tooth morphology during development was compared to that in the Siamese crocodile (*C. siamensis*), member of Archosauria lineage of reptiles, which exhibits a simpler conical tooth shape.

To highlight the differences in morphology of adult dentition in the different species used in this study, we

have taken advantage of microCT and SEM imaging techniques to obtain a detailed structural information. The veiled chameleon possesses heterodont teeth with tooth shape complexity increasing in a caudal direction along the jaw (Figure 1A). The most rostral teeth were nearly conical with one rounded tip. The more caudal teeth possessed a dominant central cusp flanked by accessory cusps (Figure 1A'). The central cusp was divided into the labial and lingual enamel crests, separated by a shallow groove (Figure 1A'').

The ocelot gecko dentition displayed small peg-shaped teeth (Figure 1B,B'). However, as in the chameleon, their tip was divided into labial and lingual enamel crests, which were directed lingually and separated by a groove. The labial crest extended from the tooth tip along the whole mesial and distal side of the tooth crown (Figure 1B'').

Crocodile teeth were selected as an example of simply shaped unicuspid teeth without the presence of additional enamel crest or ridge ornaments. These teeth are found spaced out over the jaw (Figure 1C,C').

## 2.2 | EK-resembling cluster of cells is formed in the center of the enamel organ during chameleon tooth development

To identify whether the complex teeth of chameleons are regulated by EK-like clusters of cells during development, we assessed the morphology of the dental epithelium during the cap and early bell stages of tooth development. Interestingly, morphologically distinct clusters of cells were observed in the inner enamel epithelium from the cap to the bell stage (Figure 2A-F').

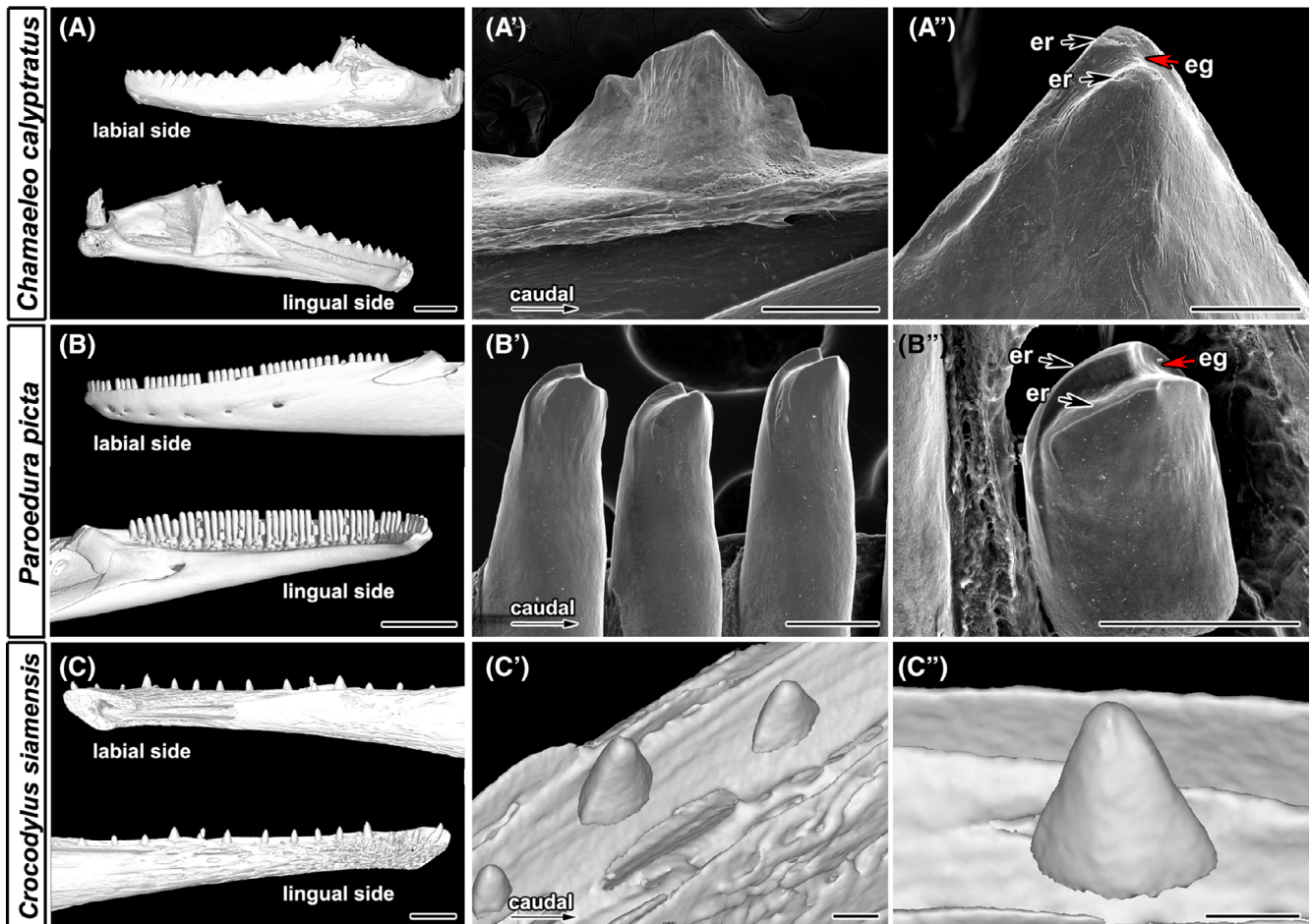


**FIGURE 1** Teeth morphology varies across reptile species. A-A'', Chameleon dentition possesses both monocuspid teeth in the rostral part of the jaw and tricuspid teeth with one large central cusp and two smaller lateral cusps in the caudal part of the jaw (A'). Along the tip of the central cusp, there is groove-shaped socket (eg) surrounded by two enamel ridges (er) (A''). B,B'', In contrast to chameleon, ocelot gecko's dentition is uniformly shaped (B'). Teeth are strictly monocuspid with two sharp enamel ridges (er) and deep groove (eg) at the tip between ridges (B''). C,C'', Siamese crocodile possesses simple monocuspid cylindroconical teeth with sharp and pointed tips along the whole jaw (C''). Scale bars (A,B,C) = 2 mm, (A',A'',B',B'') = 100  $\mu$ m, (C',C'') = 300  $\mu$ m

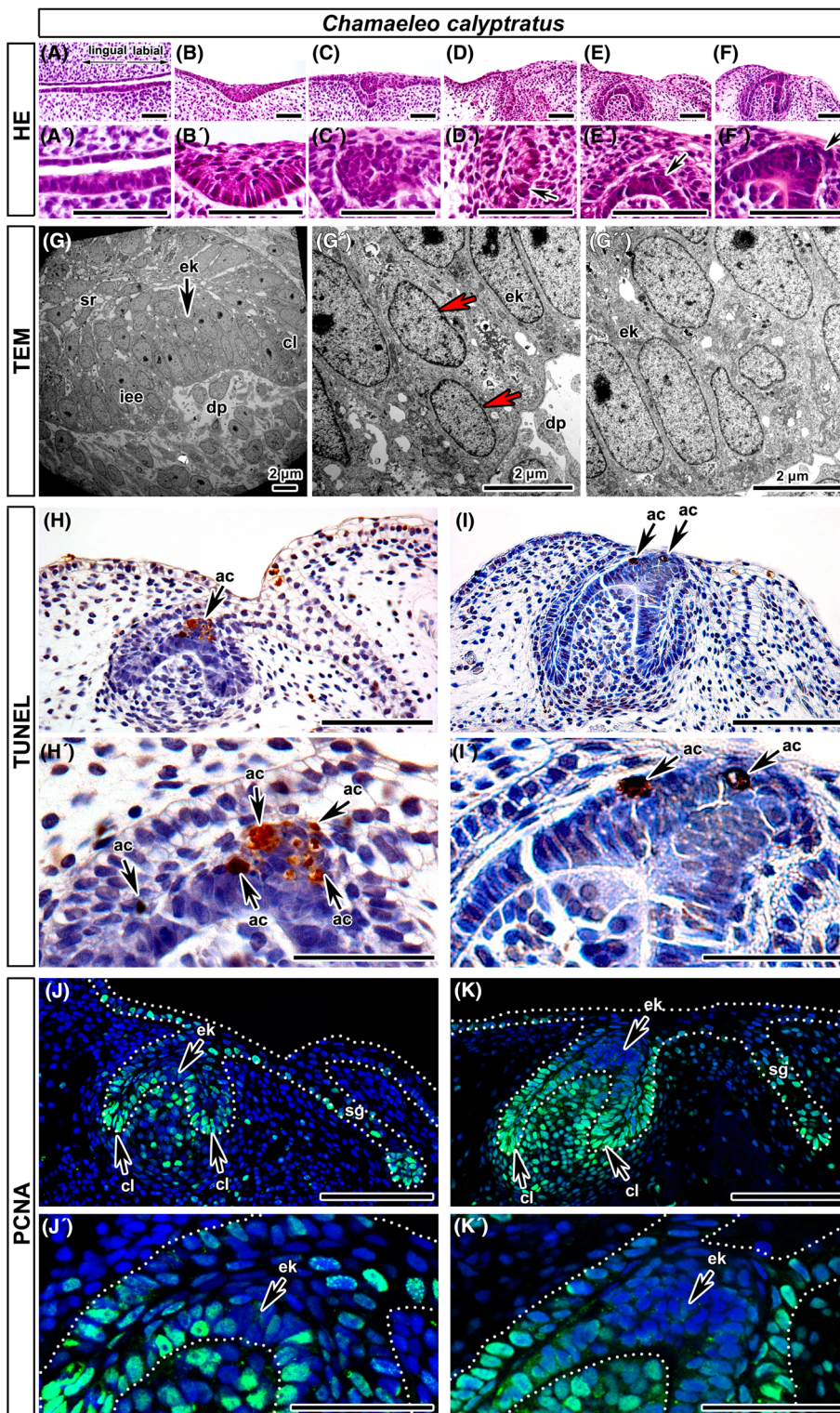


**FIGURE 2** Bulge cells resemble mammalian enamel knot cells in veiled chameleon. A-F', Morphology of individual tooth germ stages during odontogenesis in chameleon. A,A', Epithelial thickening; B,B', early epithelial invagination; C,C', late epithelial invagination; D,D', bud stage; E,E', late cap stage; F,F', bell stage. D', At the bud stage, EK-like cells (arrow) form the cluster of cells in the inner enamel epithelium with distinct shape and arrangement. E',F', Later in development, EK-like cells (arrows) are protruding toward oral epithelium and cell rearrangement occurs. Scale bar (A-F') = 50  $\mu\text{m}$ . (G-G'') Ultrastructure of enamel knot area in transmission electron microscope. G, Enamel knot area (ek) is surrounded by stellate reticulum (sr) at early cap stage. G', Distinct population of border cells (red arrows) outline enamel knot area. G'', Detail of enamel knot area with few small cells close to the basal membrane. Inner enamel epithelium (iee), cervical loop (cl) area and dental papilla (dp) are visible on lower power image (G). H-I', TUNEL analysis revealed few apoptotic cells (ac) located in presumptive EK cells or adjacent cells at late cap stage (H'). At bell stage (I'), few apoptotic cells are again situated in the cluster of EK-like area or the adjacent cells in the stratum intermedium. TUNEL-positive cells (brown, DAB), TUNEL-negative cells (blue, Hematoxylin). (J-K') The enamel knot area (ek) contains mostly PCNA-negative cells. Higher power image of the enamel knot area at late cap stage (J') and the bell stage (K'). The cervical loops (cl) exhibit high PCNA-positivity at all analyzed stages. sg-salivary gland. PCNA-positive cells (green, AlexaFluor 488), PCNA-negative cells (blue, DAPI). Scale bars (H-K) = 100  $\mu\text{m}$ , (H'-K') = 25  $\mu\text{m}$

Ultrastructural analysis using transmission electron microscopy revealed that this cluster consists of stratified cells with rounded nuclei and a very low glycogen content (Figure 2G,G''). Cells within the cluster were compact with very small intercellular spaces compared to the cells located at the periphery of the cellular cluster (Figure 2G',G'').

The mammalian EK is characterized by high levels of apoptosis and low proliferation, in contrast to the rest of the dental epithelium.<sup>5</sup> Therefore, we analyzed the distribution of proliferation and apoptosis in cap-stage tooth germs in the chameleon. TUNEL analysis uncovered a group of apoptotic cells associated with the epithelial cluster, located at the tip of tooth germ

(Figure 2H,H'). At the early bell stage, TUNEL-positive cells were observed in the area of the future central cusp (Figure 2I,I'). Interestingly, the epithelial cluster contained only PCNA-negative cells while numerous PCNA-positive cells were located in the surrounding epithelial areas of the tooth from the early cap stage up to the bell stage (Figure 2J-K'). This cluster, therefore, has similar general features of a mammalian EK.

### 2.3 | An EK-like cluster of cells is conserved in other unrelated reptile species

Next, we wanted to determine if an EK-like structure is also found in other reptile species with simpler tooth shape. The ocelot gecko displayed a recognizable EK-like cluster of cells from the cap to the mineralization stage (Figure 3A-D). In the inner enamel epithelium, long nexuses were found between the compacted rounded EK-like cells and elongated cells located on the cluster margin (Figure 3E-H'). The edges of the EK were very clear because of the distinct shape differences of the cells outlining the EK cluster (Figure 3G,H).

The pattern of apoptotic cells within enamel organ was similar in the gecko to that in chameleon embryos, with TUNEL-positive cells located closely associated with the inner enamel epithelium at the early bell stage and above the developing enamel ridges at the mineralization stage (Figure 3I,J'). Analysis of proliferating cells revealed PCNA-positive cells in the cervical loop and negative cells in the EK-like area (Figure 3K-L').

An EK-like cluster of cells was also observed at the early cap stage in the monocuspid teeth of crocodile (Figure 4A,A''), but this structure was less distinct when compared to the chameleon or gecko. However, while the EK cluster of cells persisted until the late mineralization stage in the chameleon and gecko, the cluster disappeared at the mineralization stage in the crocodile (Figure 4A''). Retention of the cluster, therefore, correlates to the delayed development of crests on the top of the more complex tooth. In contrast to the chameleon and gecko, only a few apoptotic cells were observed in crocodile teeth, raising the question of whether such monocuspid teeth have a robust EK-like structure (Figure 4B,B''). The distribution of PCNA-positive cells at the cap stage resembled that of other reptilian teeth, with PCNA-negative cells located in the area of the future cusp, and positive cells in the extending cervical loops (Figure 4C,C'').

### 2.4 | SHH expression is localized to the EK regions during chameleon odontogenesis

In addition to being morphologically distinct, the mammalian EK acts as a signaling center directing the development of the tooth.<sup>4</sup> Therefore, we analyzed the presence of mammalian EK markers at the cap and early bell stages. Since SHH is one of the most common markers of EK cells and this molecule is thought to be key for tooth shaping in mammals,<sup>10</sup> we first analyzed its expression in chameleon embryos. SHH expression was observed in the chameleon in the thickening of the oral epithelium (Figure 5A,A'). During epithelial invagination, there was a clear expression in a bulge of cells at the interface of the developing dental lamina and the oral epithelium (Figure 5B,B'). The cluster of SHH-positive cells was located asymmetrically in the epithelial thickening. At the bud stage, we detected SHH-positive cells in the area of the future inner enamel epithelium (Figure 5C,C'). Later, a cluster of SHH expression was present in the EK area at the cap and early bell stages (Figure 5D-F'). Interestingly, the SHH expression domain was not confined just to the inner enamel epithelium but was also observed in the epithelial cells above this area, similarly to TUNEL-positive cell distribution (Figure 5D, see Figure 2I'). At the bell stage, SHH was expressed in a large cluster of rounded stacked cells in the area of tooth cusp formation (Figure 5E,E'). During the mineralization stage, SHH expression was shifted toward the cervical loops (Figure 5F,F'). This phenomenon has been previously described in the python as well as in the mouse, where this protein was found to be important in the process of odontoblast and ameloblast differentiation.<sup>24,25</sup>

### 2.5 | Interspecies comparison of SHH expression during reptile odontogenesis

In the ocelot gecko, the expression of SHH followed a similar pattern to that in the chameleon, with a positive signal in the inner enamel epithelium and overlying epithelial cells (Figure 6A,B,E,E'). As for the chameleon, SHH expression shifted apically toward the cervical loops at the bell stage in the gecko (Figure 6C,D,F,F'). A similar dynamic pattern was observed in the Siamese crocodile, but with a few differences. At the early cap stage, SHH-positive cells formed a less distinct cluster of cells, which is consistent with the presence of a

less obvious EK-like structure in this species (Figure 6G,G'). Later in development, SHH was expressed in the differentiating inner enamel epithelium and was absent in the crown of the mineralizing tooth (Figure 6G,G'), similar to observations in the chameleon.

## 2.6 | Matriptase ST14 and other EK markers expression in reptiles

To further analyze expression pattern in the EK area, we selected several EK markers including FGF4 and ST14. While FGF4 is well known molecule expressed in the EK

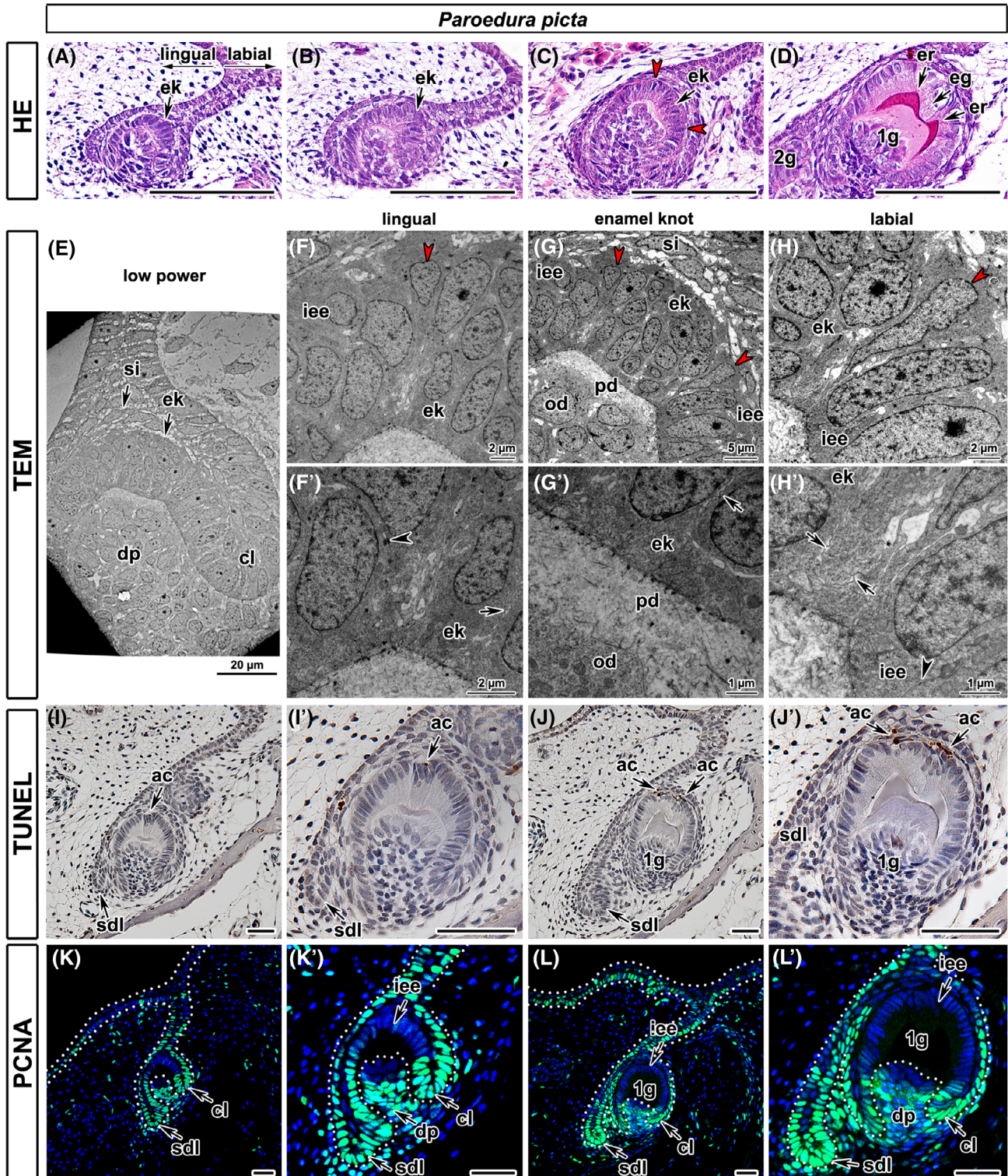


FIGURE 3 Legend on next page.

area,<sup>4</sup> we revealed new molecule, matriptase (also known as ST14, TADG15, or epithin), to be expressed in this region. Matriptase is a membrane-associated protease, which regulates cell motility and tight junction assembly.<sup>26</sup> In mouse embryos, ST14 expression overlaps with the expression domains of SHH and FGF4 in the EK as visualized by RNAscope (Figure 7A-C).

In chameleon, FGF4-positive cells (Figure 7D) were distributed in the EK area of cap stage tooth. Later, FGF4 protein expression became weaker and obtained dispersed pattern mostly associated with the inner enamel epithelium (Figure 7E). ST14 was expressed in the EK-like cluster of cells at the cap stages (Figure 7F, G), with the highest levels in the cells above the inner enamel epithelium. In addition to its expression in the EK area, ST14 was detected in the oral epithelium and outer enamel epithelium on the lingual side of the developing tooth germ (Figure 7F-I). At the early bell stage, the expression persisted in the EK-like cell cluster (Figure 7H). At the late bell stage, expression of ST14 spread toward the cervical loops, similar to SHH expression (Figure 7I). Moreover, chameleon EK area was GLI2-negative (Figure 7J,K) similar to mice.<sup>27</sup>

## 2.7 | Cell rearrangement is associated with enamel ridge and groove formation

In complex reptilian teeth, after formation of the central cusp, the developing tooth undergoes further changes to drive formation of the enamel ridges at the top of the central cusp. To understand the cellular processes associated with formation of these structures, we analyzed sections of chameleon teeth by confocal microscopy with nuclei stained for DRAQ5 (Figure 8). Here, we

compared areas at the tip of the main cusp with two ridges to those through the accessory cusps that do not possess this enamel groove (Figure 8A-C). Cells were automatically grouped based on the shape of their nuclei in IMARIS (Figure 8E,E'',G,G''). This analysis revealed distinct cellular populations within the developing tooth. Nuclei of cells in the cervical loop were strictly columnar in shape (Figure 8D'',E'',F'',G'') in comparison to the rounded nuclei of cells located in the tip area (Figure 8F',G'). In the mesial areas with the formation of only one sharp ridge, there were only small clusters of cells with spherical nuclei (Figure 8D',E'). In contrast, in the central part of the tooth where an enamel groove forms, there was a large cluster of round-nuclei cells (Figure 8F',F',G,G'). These differences in shape of the epithelial cells preceded the deposition of enamel to create the ridges and may, therefore, drive the process of ridge formation.

As 2D analysis revealed a distinct cellular population in the EK-like clusters, we next focused on uncovering whether possible differences in cell arrangement were responsible for the later asymmetrical enamel deposition (as previously described in the gecko by Reference 21). We visualized cell nuclei in 3D and this analysis revealed continuous mesio-distal ridge formation along the tooth (Figure 9A,C,D). From a superficial view, there were distinct enlarged areas corresponding to the future enamel ridges (Figure 9B). On top of the enamel ridge-forming area, there were distinct clusters of small concave cells heading into the groove-forming area (Figure 9B,D,E', arrowheads). Cells of the groove area were elongated in the horizontal direction (Figure 9A,C,D,E,E',arrows). These findings are suggestive of cell rearrangements such as those involving cell intercalation, but live cell imaging will be necessary in future to provide deeper insight into this process.

**FIGURE 3** Tooth germ development in ocelot gecko. A-D, Morphology of individual tooth germ across stages during odontogenesis in gecko. A, Cap stage, B, bell stage, C, predentin production, D, mineralization stage with dentin and enamel production. Enamel groove (eg) is surrounded by two enamel ridges (er). The first (1g) and the second (2g) tooth generations are visible. Distinct cluster of cells forming enamel knot area (ek) is visible at the cap and bell stage. Red arrowheads label narrow and triangular border cells surrounding enamel knot, white arrowhead labels stratum intermedium. Scale bars (A-D) = 50  $\mu$ m. E-H', Ultrastructure of gecko's enamel knot area in transmission electron microscope. Enamel knot area (ek) is surrounded by flat cells of stratum intermedium (si) at the early bell stage (E). Cervical loop (cl) and dental papilla (dp) are visible on lower power image (E). F-H, Distinct population of border cells (red arrowheads) outline enamel knot area. F'-H', Long nexuses (black arrows) are located between enamel knot cells and elongated cells on their edge. F',H', Short desmosome (black arrowheads) can be found between cells of inner enamel epithelium (iee). Odontoblasts (od) are already differentiated in the tip of the dental papilla and produce a thin layer of predentin (pd). I-J', Apoptotic cells (ac) are located close to the inner enamel epithelium at the early bell stage (I,I') and above developing enamel ridges at mineralization stages (J,J'). sdl - successional dental lamina, 1g-the first tooth generation. TUNEL-positive cells (brown, DAB), TUNEL-negative cells (blue, Hematoxylin). Scale bars (I-J') = 50  $\mu$ m. (K-L') PCNA-positive cells are located in the cervical loop area (cl), in the successional dental lamina (sdl) and dental papilla (dp) of gecko embryos. Inner enamel epithelium (iee) in the EK-like area is free of proliferating cells (black arrows). 1g-the first tooth generation. PCNA-positive cells (green, AlexaFluor 488), PCNA-negative cells (blue, DRAQ5). Scale bars (K-L') = 40  $\mu$ m

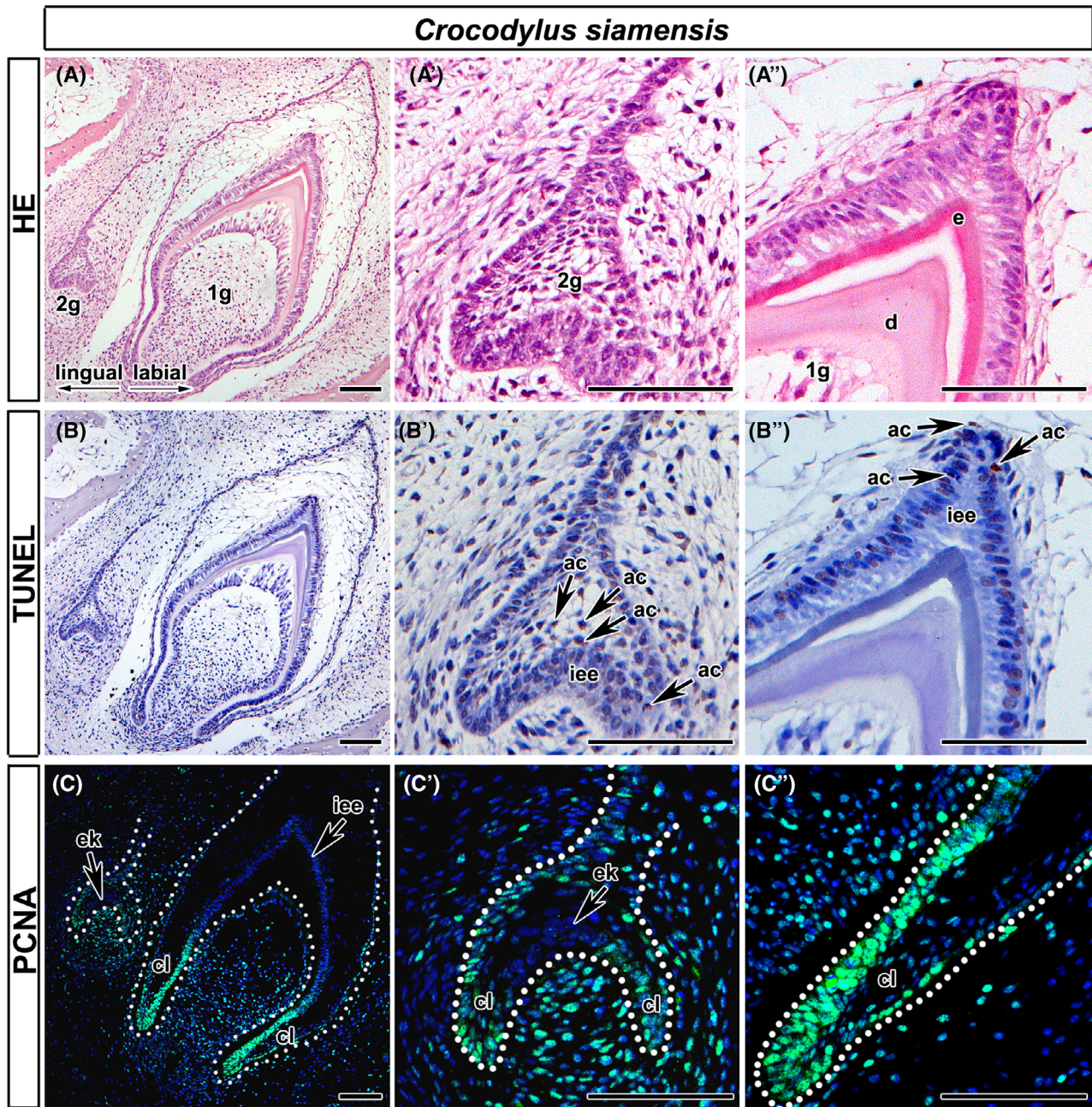


**FIGURE 4** Snap shoot to tooth development in Siamese crocodile. A-A', Early cap and late bell stage with visible mineralization, including dentin (d) and enamel (e) production. 1g-the first tooth generation, 2 g-the second tooth generation. B-B'', TUNEL-positive cells (apoptotic -ac) are situated in the external surface of the inner enamel epithelium (iee) close to EK cells (B') of early cap stage tooth. B'', Later in development, few TUNEL-positive cells are located above the tooth tip within the enamel organ. TUNEL-positive cells (brown, DAB), TUNEL-negative cells (blue, Hematoxylin). C, C'', PCNA-negative cells are visible in the enamel knot (ek) area (C') and the inner enamel epithelium (iee) of monocuspid tooth tip (C''). C', C'', Cervical loops (cl) of both displayed stages exhibit high PCNA positivity. PCNA-positive cells (green, AlexaFluor 488), PCNA-negative cells (blue, DRAQ5). Scale bars (A-C'') = 50  $\mu$ m

## 2.8 | Ultrastructural analysis reveals lipid accumulation above enamel ridges in chameleons

To follow formation of the enamel crests on the central cusp in more detail, we used transmission electron

microscopy (TEM). The enamel organ at the bell stage consists of the outer enamel epithelium, composed of simple cuboidal cells containing a large amount of glycogen, typical stellate reticulum, and inner enamel epithelium with large columnar cells with basally located oval nuclei (Figure 10A). Nuclei in the groove area had round

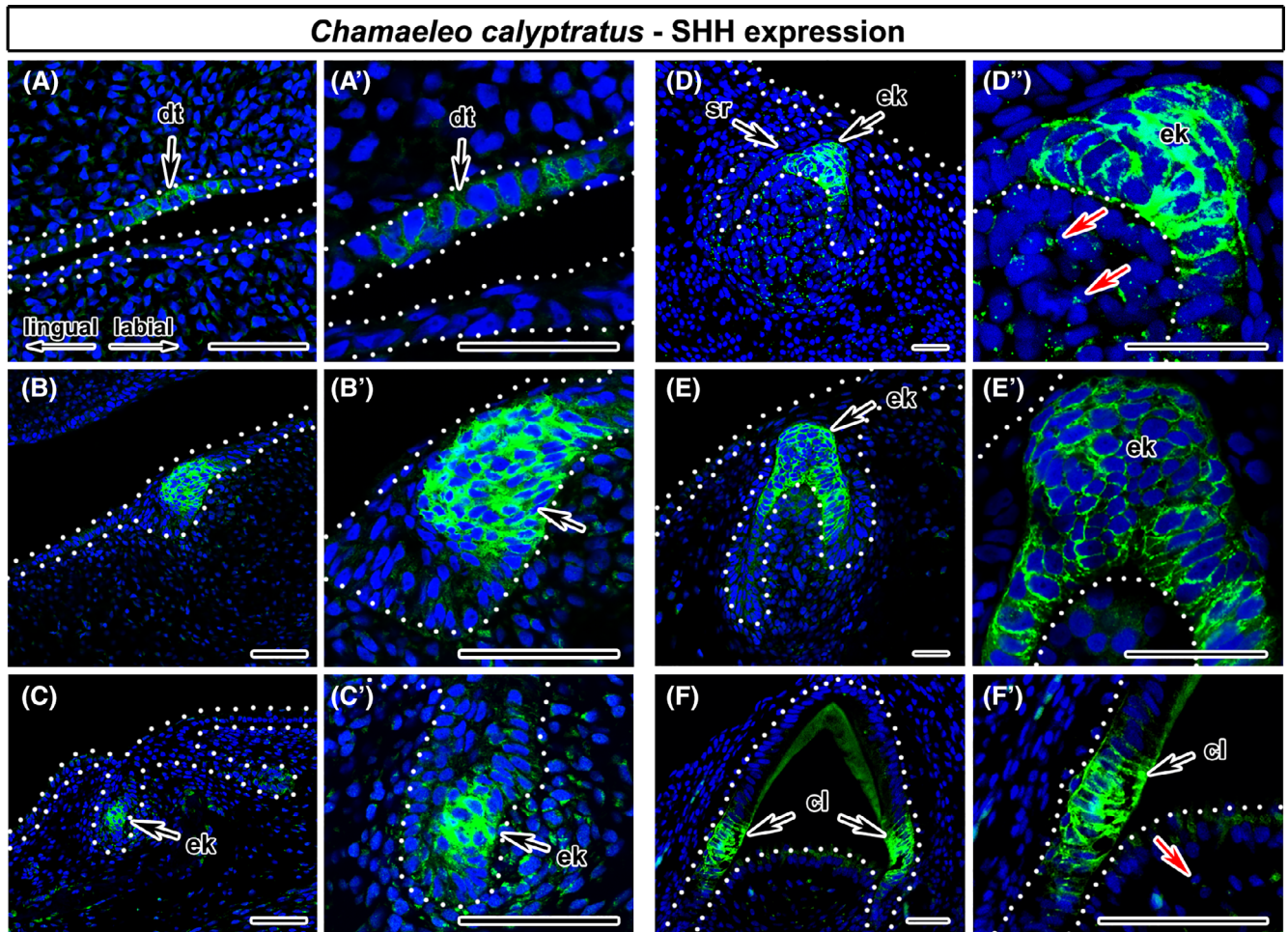


**FIGURE 5** SHH expression during early tooth germ development in veiled chameleon. A,A', SHH expression is located in the epithelial dental thickening (dt) during early odontogenesis. B,B', SHH appearance persists during epithelial invagination predominantly in the cluster of cells localized labially (arrow). C,C', At the bud stage, SHH-positive cells are located asymmetrically in labial part in the enamel knot area (ek). D,D', At late cap stage, strong expression of SHH is located in enamel knot cells (ek) as well as adjacent cells of stellate reticulum (sr) and continues up to early bell stage. Asymmetrical SHH expression is visible in the mesenchymal cells of the dental papilla (red arrows). E,E', Later, SHH expression persists in the bulge cells resembling EK (ek). F,F', During mineralization stage, SHH expression is no longer visible at the tip of developing tooth, however, it is allocated to the cervical loop area (cl). F', Few SHH-positive cells is again visible in surrounding mesenchyme (red arrow). SHH-positive cells (green, Alexa488), SHH-negative cells (blue, DRAQ5). Scale bars (A-C') = 50  $\mu$ m, (D-F') = 25  $\mu$ m

shape on transversal section through the tooth, with cytoplasm visible in areas closest to the already produced layer of enamel (Figure 10B,B').

Above the presumptive enamel ridge, the inner enamel epithelial cells were heading toward each other, and their basal poles were enclosed together (Figure 10B-E). Long nexuses and expanded intercellular spaces were observed in the areas above the enamel ridge (Figure 10C-E). Bundles of intermediate filaments were directed perpendicularly, toward the basal membrane (Figure 10E).

The most superficial cells exhibited a triangular or cuneiform shape and filled the space above the forming ridge (Figure 10F-H). Apoptotic bodies were observed in the stellate reticulum cells directly above the enamel

ridge area (Figure 10H). A large amount of lipid droplets had accumulated in the basal part of the cytoplasm of superficially located cells (Figure 10F-H).

## 2.9 | Apoptotic cells are located only in distinct areas above the future enamel crest formation

As ultrastructural analysis also uncovered a few apoptotic cells in the future enamel ridge area, we wanted to analyze in detail if this pattern is typical just for the central ridge area or whether it can also be observed in the mesial region of the tooth. During mineralization, TUNEL-positive cells

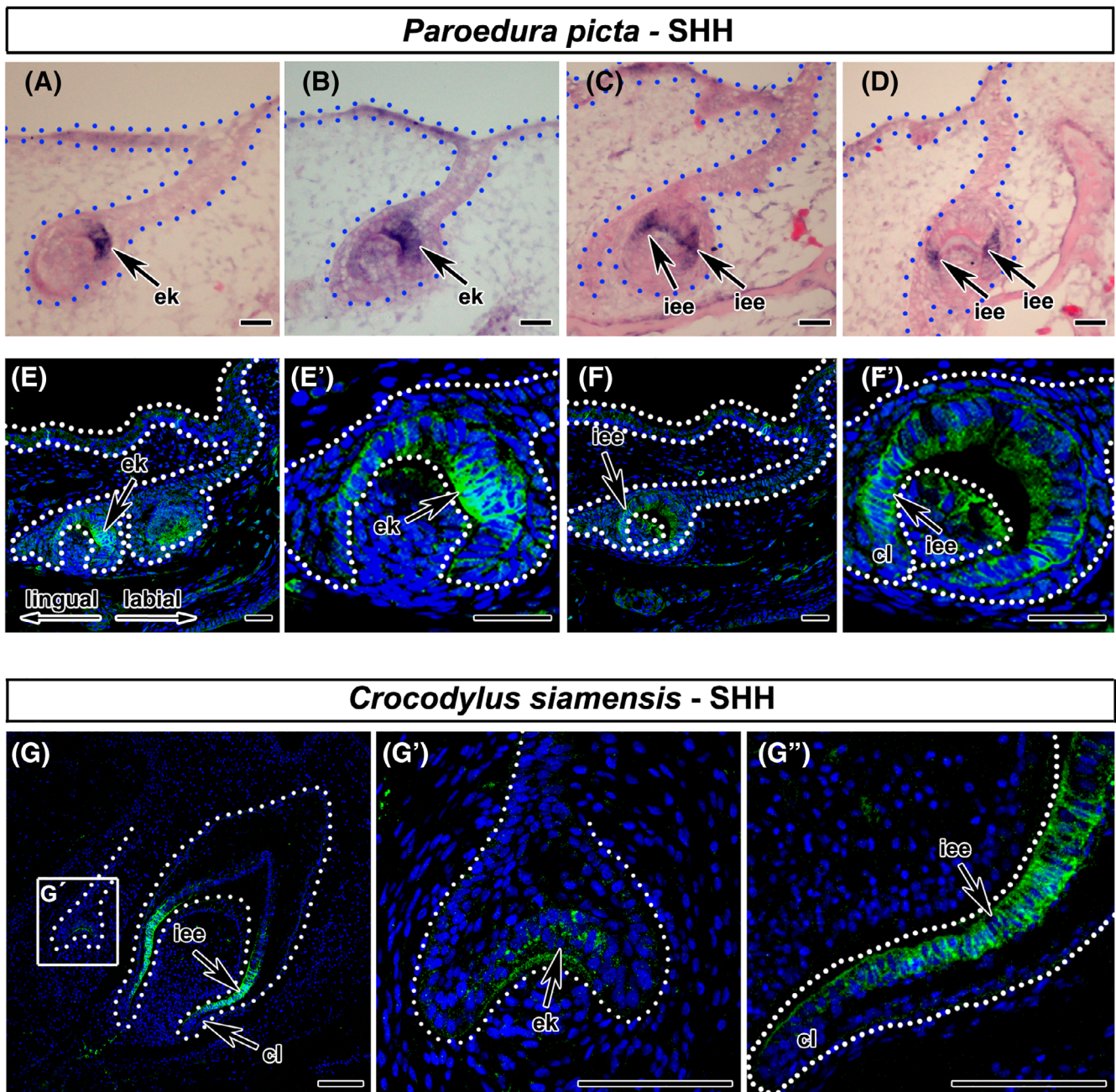


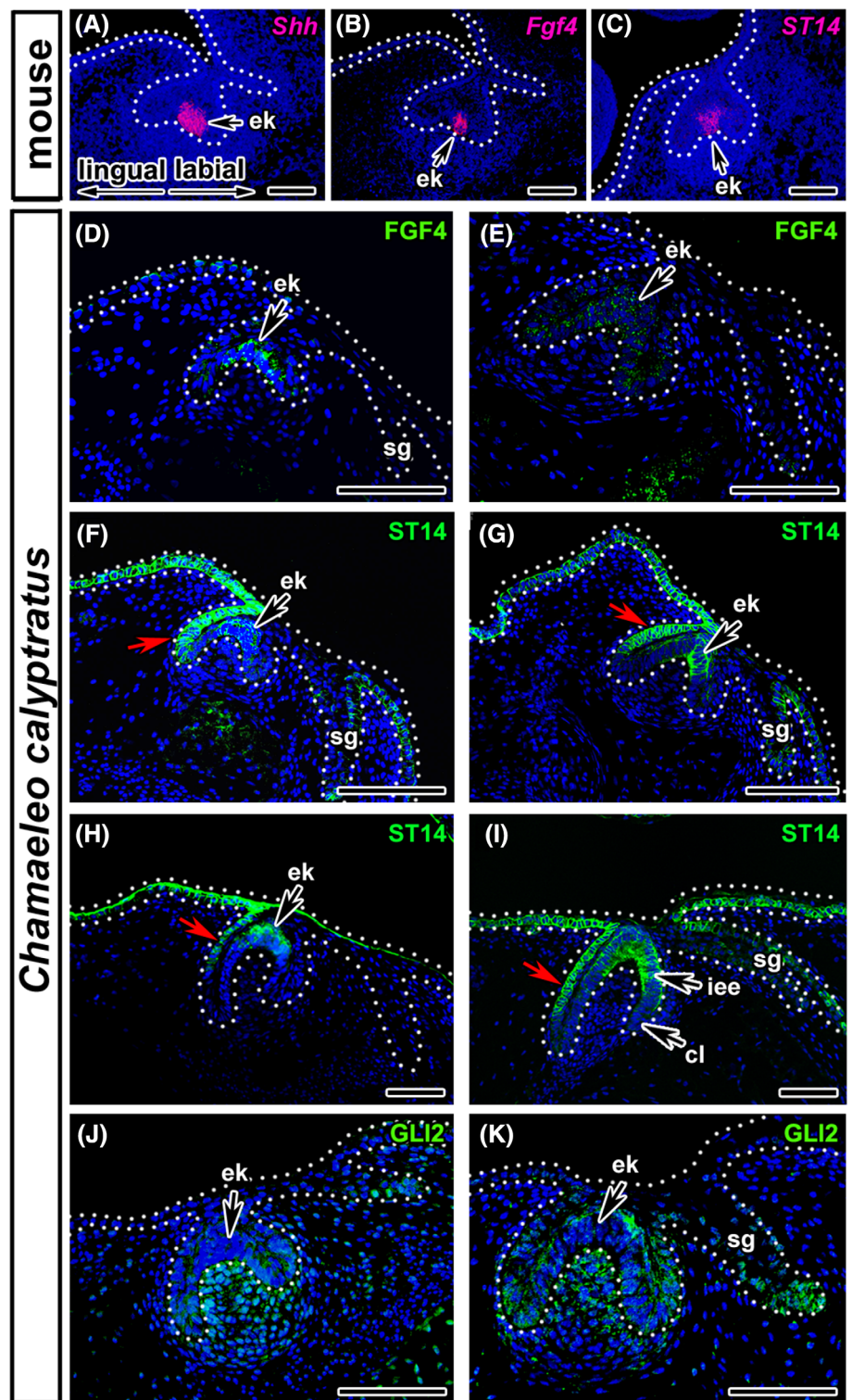
**FIGURE 6** SHH expression during tooth germ development in ocelot gecko and Siamese crocodile. A-D, *Shh* gene expression analyzed by in situ hybridization. E-F' SHH protein expression detected by immunohistochemical labelling. *Shh*-positive signal purple, background - Eosin. A,B,E,E', SHH signal is visible in the enamel knot cells (ek) in gecko. C,D,F,F', Later in development, SHH expression is located in the inner enamel epithelium (iee) and expands into the cervical loop (cl) cells of gecko teeth. G-G'', In Siamese crocodile, SHH expression is located in the enamel knot area (ek) at the cap stage. Later at the bell stage, it is allocated into the inner enamel epithelium (iee) of the cervical loop (cl) area (G''). SHH-positive cells (green, Alexa488), SHH-negative cells (blue, DRAQ5). Scale bars (A-F') = 25  $\mu$ m, (G-G'') = 50  $\mu$ m

were located in the area where cell rearrangement occurred (Figure 11). In the more mesial part of the tooth, TUNEL-positive cells were situated in one spot within enamel organ just above the membrane junction in the enamel crest-forming area (Figure 11A,A',B,B'). In the central area where the enamel ridge/groove is formed, two TUNEL-positive zones were determined just above

individual crests (Figure 11C,C',D,D'). TUNEL-negative cells were located in the area between them and they were adjacent to the enamel groove zone (Figure 11C',D').

Based on these observations, we propose a model where the cluster of nonapoptotic and nonproliferating cells (large black spot) represents an area with the ability to form an enamel groove in future (Figure 11E,E').

**FIGURE 7** ST14 and other EK markers in chameleon embryos. A-C, Expression of enamel knot specific molecules (arrows) at cap stage in mouse embryos detected by RNAScope-*Shh* (A), *Fgf4* (B), and *ST14* (C). Gene expression in mouse teeth is visualized by red signal (Cy3), cell nuclei are stained by DAPI (blue). Scale bar (A-C) = 100  $\mu$ m. (D,E) FGF4 positive signal is located in the enamel knot (ek) of chameleon cap stage tooth and weak signal was still visible at bell stage with some dispersion of signal to the other areas of the enamel organ. F-I, In chameleon embryos, ST14 is expressed in the enamel knot areas (ek) at the late cap and bell stages. Later, signal expands to the inner enamel epithelium (iee) of the cervical loop (cl). In monophyodont dentition of chameleon, ST14-positive cells were also located in the lingual side of the tooth germ where successional dental lamina is initiated (red arrow). J,K, The enamel knot in chameleon is GLI2-negative. sg - salivary gland. FGF4, ST14, and GLI2-positive cells (green, Alexa488), FGF4, ST14, and GLI2-negative cells (blue, DRAQ5). Scale bar (D-F') = 50  $\mu$ m



These cells elongate in a horizontal direction and thus constitute the steady region which is surrounded by more active differentiating cells (Figure 10). This is in contrast to the mesial areas with a simple enamel ridge where only rare apoptotic cells are located in a distinct small zone in the junctional area and cellular reorganization occurs around them (Figure 11F,F').

## 2.10 | Cytoskeleton rearrangement is associated with ridge formation

Numerous intercellular junctions were observed by TEM in the area above the enamel ridge where two opposite cells of the inner enamel epithelium were heading toward each other (Figure 10C-E). Moreover,

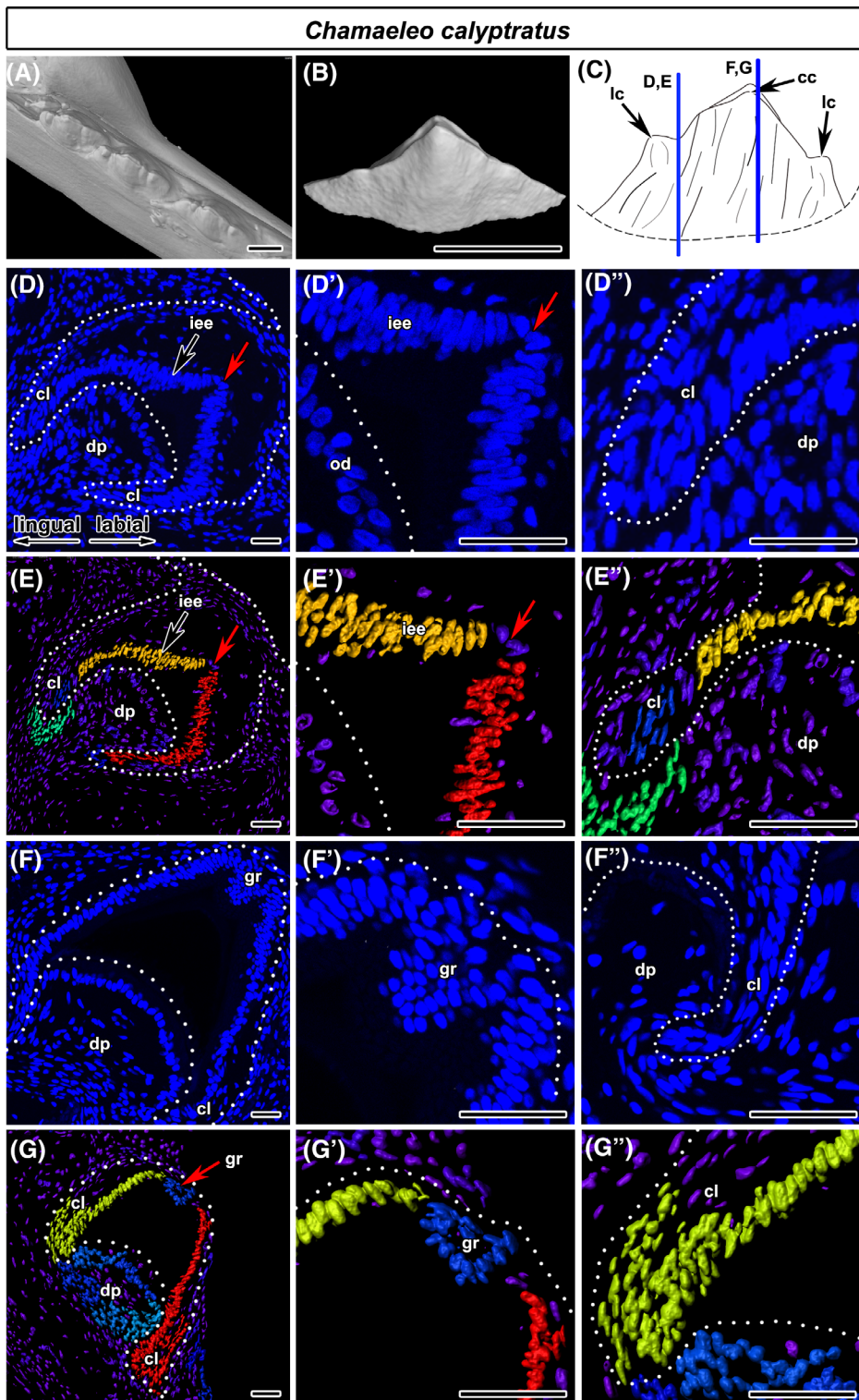


**FIGURE 8** Cells located in the future groove area are morphologically distinct from the rest of inner enamel epithelial cells in chameleon. A,B, For cell shape analysis, we selected tricuspid caudal teeth with distinct enamel groove in the central cusp (cc) and two smaller lateral cusps (lc). C, Two transversal areas were chosen: mesial area (D,E) with one sharp ridge, and more central area (F,G) with deep groove located in the largest central cusp. D-G, 2D analysis of transversal sections reveals variability in cell nuclei shape in different areas of chameleon tooth. D,E, In the mesial area, cells of the inner enamel epithelium (iee) contain ellipsoid nuclei (D'). Only a few cells on the tip of tooth exhibit distinct morphology (E', red arrow). D',E' Cells of the cervical loop (cl) area are thinner and elongated. F,G, In the central tooth area, there is a large cell cluster with round nuclei, which will later form groove (gr) at the main cone of the tooth (F',G'). G', Cells were more tightly packed in the cervical loop (cl) in this area. Nuclei are counterstained with DRAQ5 (blue). E-E'',G-G'', Artificial colors of nuclei were produced in software IMARIS followed by segmentation and analysis for cell nuclei shape differences. dp, dental papilla; od, odontoblasts. Scale bars (A,B) = 500  $\mu\text{m}$ , (D-G'') = 25  $\mu\text{m}$

bundles of intermediate filaments were located in the inner enamel epithelium facing toward the common basal membrane (Figure 10E). Therefore, we analyzed possible changes in cytoskeleton rearrangement during cell cluster formation in chameleon (Figure 12A-D') and gecko (Figure 12E-H'). For this purpose, we used a phalloidin to label F-actin expression. Cytoskeletal

rearrangement was detected during cell cluster formation in both analyzed species, with asymmetrical and strong F-actin expression localized in EK-like cells (Figure 12A',B',E',F',G'). At the mineralization stage of chameleon odontogenesis, there was distinct variability in F-actin expression in different tooth areas (Figure 12C-D'). In the mesial area, future ameloblasts

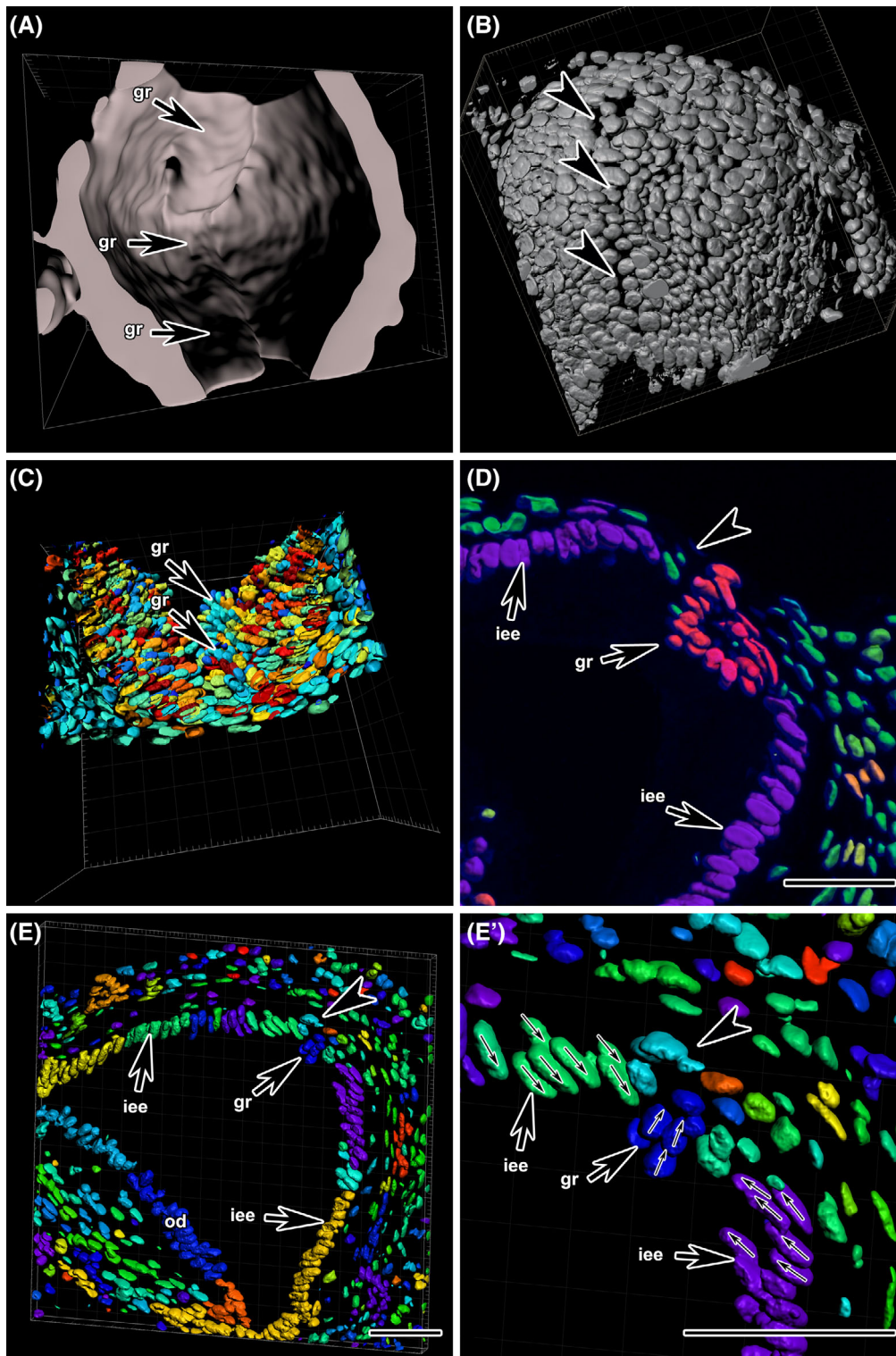


**FIGURE 9** Three dimensional analysis of cells in the enamel groove area in chameleon. A, 3D analysis of 300 µm thick transversal slice through caudal tooth germ at mineralization stage. Stripe of invaginating epithelial cells is visualized from the internal view of future enamel groove (gr). B, Superficial view from the side of inner enamel epithelium displays suture-like pattern in the area where a cluster of groove forming cells (arrowheads) are detaching and future sharp ridge will form. C, Inner view on the cell cluster forming enamel groove (gr) in 3D with artificially stained nuclei. D, Detail of groove area (gr) with conical cells (arrowhead) heading toward groove zone. E, E', 3D analysis on 5 µm transversal slice through the caudal tooth germ to uncover direction of elongated cells. Cells in the groove area (gr) are elongated in the horizontal direction in contrast to the rest of the inner enamel cells (iee) elongated centrifugally to the dentin producing area. Arrowhead points to the conical cells moving to the groove zone. Small arrows visualize the direction of the elongated axis of cell nuclei. Nuclei were counterstained by DRAQ5. Nuclei were automatically colored by software IMARIS following analysis of differences in ellipsoid shape of nuclei. Iee, inner enamel epithelium; od, odontoblasts. Scale bars (D-E') = 25 µm

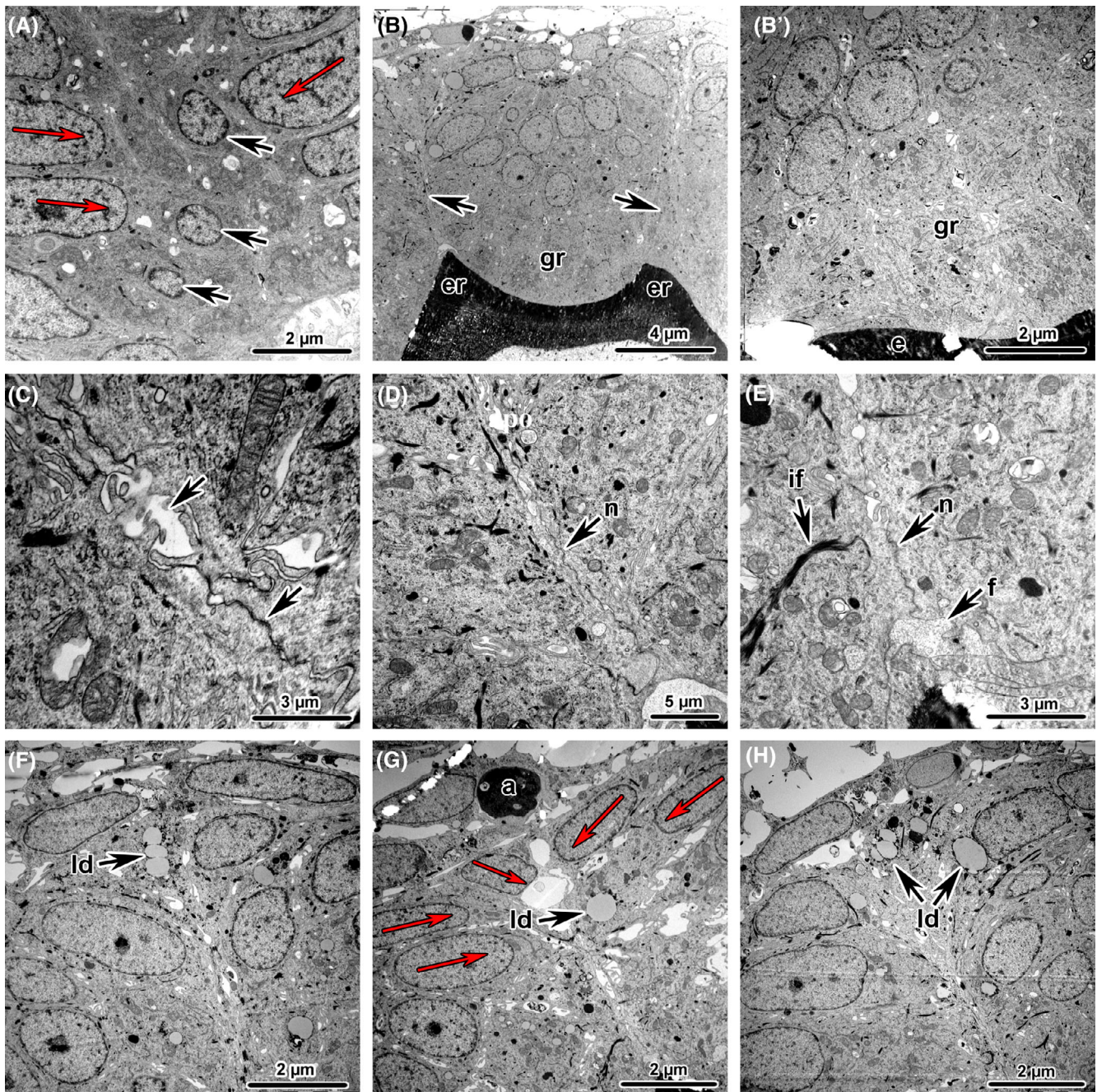


**FIGURE 10** Ultrastructure of epithelial cells above enamel crest in chameleon embryos. A, Inner enamel epithelium of early cap stage tooth with cell arrangement at the future ridge area (red arrow) and small round cells just above this zone (black arrow). B, B', Enamel groove area (gr) during mineralization stage and its detail with the typical cellular junctions (arrows) above enamel ridges (er). C-E, Detail of area above enamel ridge with bundles of intermediate filaments (if) directing toward the basal membrane, long nexuses (n) and expanded intercellular spaces (arrow). F-H, Apoptotic bodies (a) were observed in the area directly above enamel crest. Lipid droplets (ld) accumulate in the basal parts of enamel ridge associated cells. G, Above the enamel crest, cells of the inner enamel epithelium lead centrifugally toward the dentin surface (red arrow). These cells join apically with each other in the central area. The most superficial cells are small "cuneiform" cells. e, enamel

were strictly outlined by an F-actin border (Figure 12C, C'). In the central area, F-actin aligned the emerging groove zone (Figure 12D, D'). In the gecko, the

expression pattern of F-actin closely resembled that in the chameleon (Figure 12E-H'), with a strong positive signal around future groove cells (Figure 12E', F', G', H').

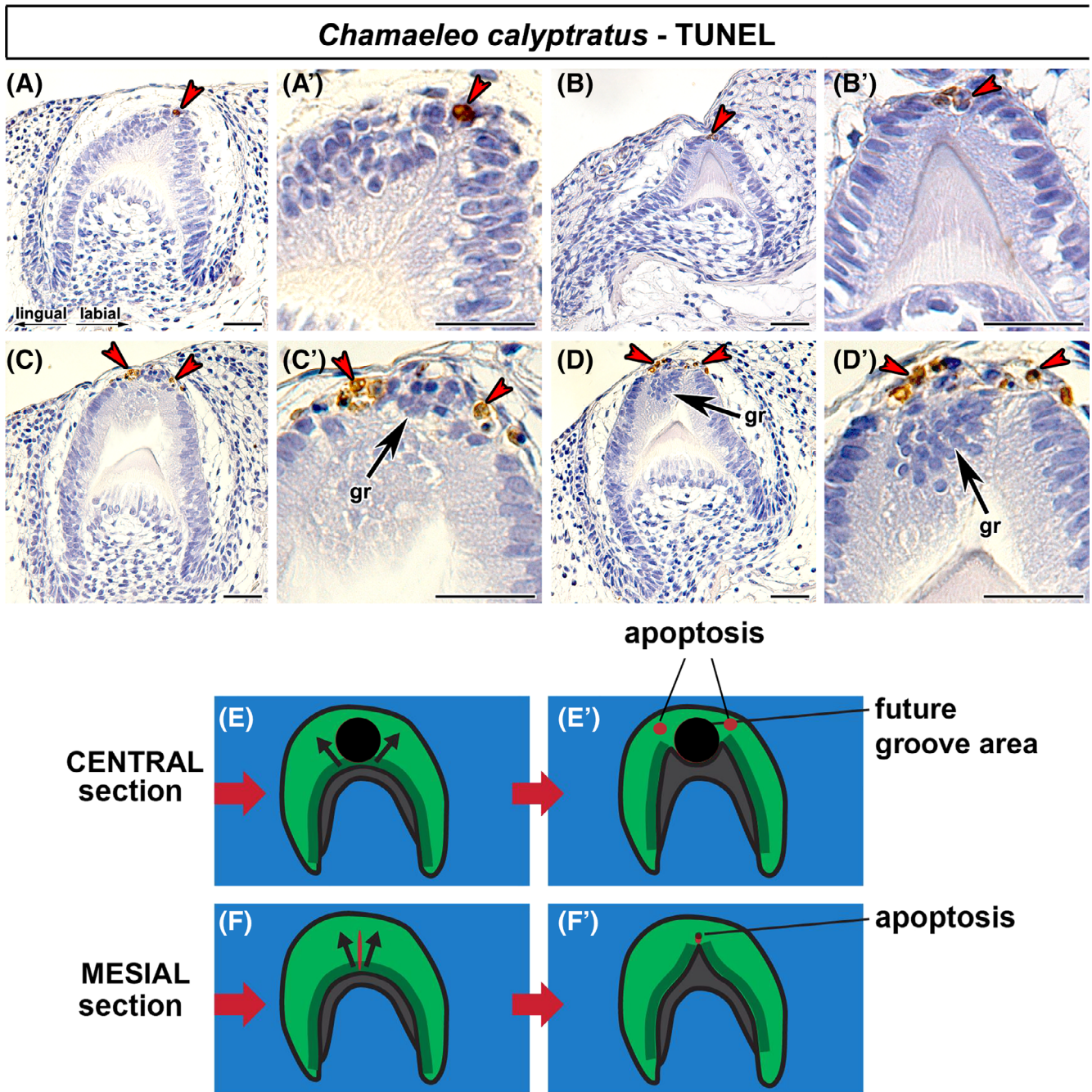


**FIGURE 11** Distribution of TUNEL-positive cells during enamel ridge and groove formation in chameleon embryos. A-B', In more mesial part of the tooth, TUNEL-positive cells are located just above membrane junction in the enamel crest forming area (red arrowheads). C-D', In the most central area where two enamel ridges with the separating groove are formed, two TUNEL-positive zones can be seen. C',D', Each TUNEL-positive domain is located above individual crest (red arrowheads) while TUNEL-negative cells are situated between them in the future groove area (gr). TUNEL-positive cells (brown, DAB), TUNEL-negative cells (blue, Hematoxylin). Scale bars (A-D') = 25  $\mu$ m. E, Scheme of proposed model display two areas of tooth: more central area with two ridges and future groove (the first row-E, E') and more mesial area where only one enamel ridge will be formed (the second row-F, F'). The first column (E,F) represent the early developmental stage and the second column (E',F') mineralization stage with massive hard tissue production. E',F', Apoptosis (red spots) is located in two or one zone with negative area (black circle between them). E,F, Arrows indicate direction of tissue growth and cell rearrangement with just small junctional area (red line) formed in the mesial section (F). Main cellular axes of a central cluster of cells (large black circle) are reoriented in the horizontal direction, which later during development become a cluster of cells inside the enamel groove (E)

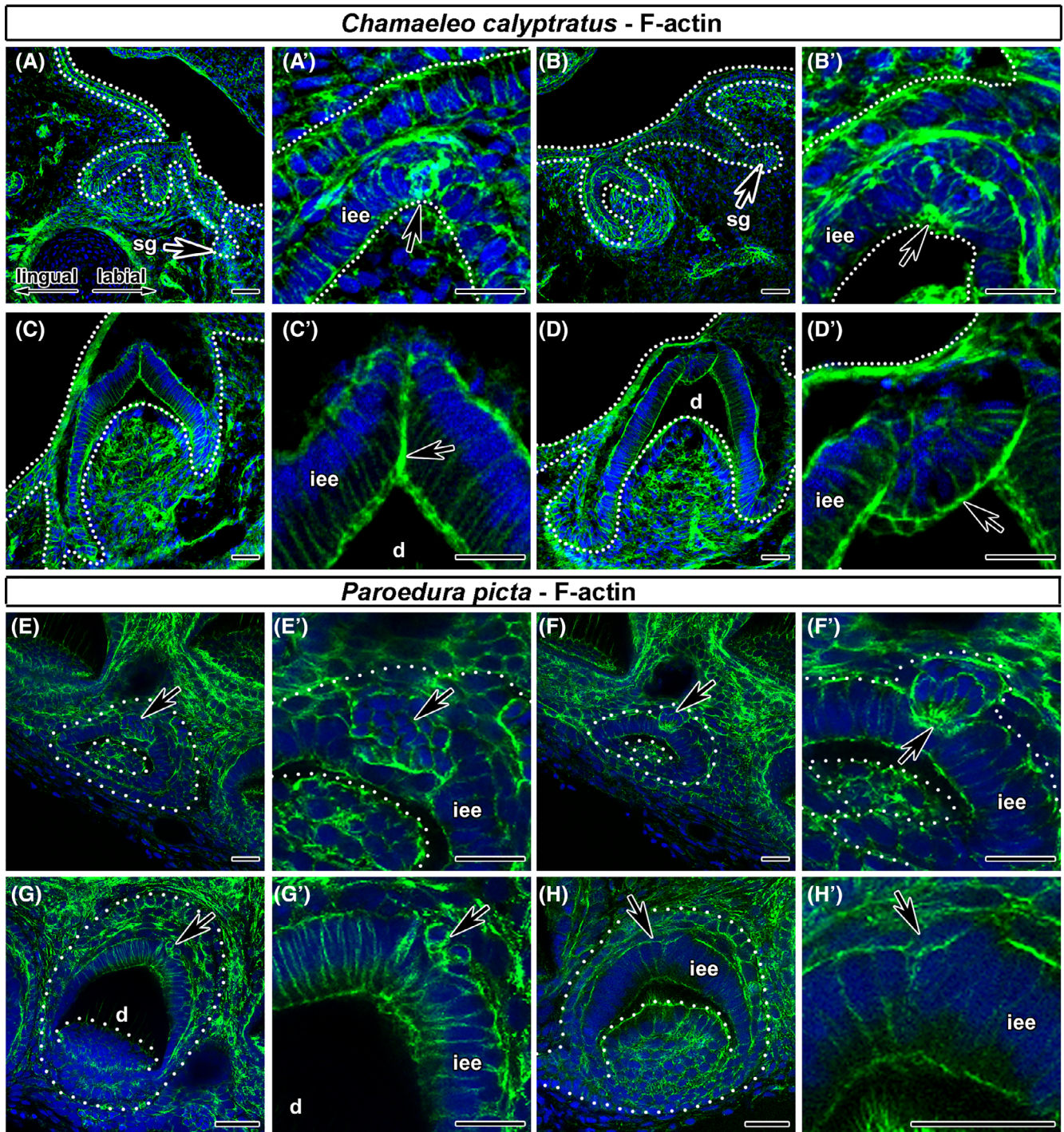


**FIGURE 12** F-actin expression during ridge formation in chameleon and gecko embryos. A,A', At early bell stage, cluster of cells resembling EK exhibited strong actin expression especially in the area surrounding enamel knot (arrows) in chameleon. B,B', Strong expression of F-actin is located in the central area on the tooth tip (arrow) and also asymmetrically on several cells located more superficially in this area. C,C', Later in development, F-actin is concentrated in the junctional zone of mesial section. D,D', In the central section, F-actin is concentrated around the cluster of cells forming enamel groove (arrow). E,E',F,F', At early bell stage, cluster of cells resembling enamel knot exhibits strong actin expression especially in the area surrounding enamel knot (arrows) in gecko. G,G', At the mineralization stage in gecko, phalloidin labelling revealed distinct rearrangement of actin in the cluster of cells (arrows) contributing to groove formation. H,H', More mesial section, where only one enamel ridge is formed, exhibits less F-actin positivity. F-actin-positive cells (green, AlexaFluor488), F-actin-negative cells (blue, DRAQ5). d, dentin; iee, inner enamel epithelium; sg, salivary gland. Scale bars (A-H') = 25  $\mu$ m

## 2.11 | Na<sup>+</sup>/K<sup>+</sup>-ATPase expression is downregulated during cell rearrangement in the enamel ridge area

As we observed significant changes at the ultrastructural level of cellular membranes, we wanted to further analyze possible differences in membrane activity, which could be behind the process of cell rearrangement contributing to ridge formation. Na<sup>+</sup>/K<sup>+</sup>-ATPase is a transmembrane enzyme contributing to ion exchange and which may act as a signal transducer.<sup>28</sup> We observed strong Na<sup>+</sup>/K<sup>+</sup>-ATPase expression in large cells located on the sides of the forming enamel ridge in chameleon (Figure 13A,B), especially in the mesial area (Figure 13A,A'). In the tip of the tooth, expression of Na<sup>+</sup>/K<sup>+</sup>-ATPase was downregulated from the first sign of cell rearrangement (Figure 13B,B',C,C'). In contrast, the enamel groove area was almost negative for the expression of this protein (Figure 13D,D'). In gecko, there was strong expression on the sides of forming ridges (Figure 13E,F'). In crocodile, stronger expression was located on the outer and inner surface of the inner enamel epithelium while only a weak signal was observed on the tooth tip (Figure 13G-G''').

## 2.12 | Gain-of-function or loss-of-function of SHH signaling leads to changes in inner enamel cell morphology

Finally, we wanted to prove if activity of the SHH pathway is directly related to the shape of the cell cluster in the enamel ridge-forming area. We established organ cultures from embryonic chameleon mandibles, which were cultured for 3 weeks. Cyclopamine treatment was used to inhibit the SHH signaling pathway, and SHH ligand was used to activate the SHH signaling pathway.

Cyclopamine treatment resulted in a simpler teeth morphology (Figure 14C,D) and the presence of smaller cells in the inner enamel epithelium on the tip of teeth (Figure 14D) in comparison to the control (Figure 14B). Also, the whole size of teeth was smaller in comparison to control jaws cultured just in media with DMSO (vehicle control; Figure 14C compared to A).

This result was in strong contrast to SHH-treated mandibles (Figure 14G,H), where teeth were larger (Figure 14G compared to E). Moreover, a cell cluster of the future enamel ridge area expanded to form a cauliflower-like epithelial structure with branching morphology (Figure 14H compared to F).

## 3 | DISCUSSION

Reptilian tooth shape can be very heterogeneous ranging from the simple monocuspid up to complex multicuspoid teeth. However, the developmental mechanisms involved in the formation of reptilian enamel ridges in unicuspid and also multicuspoid teeth have not previously been studied in detail. In this study, therefore, we describe the developmental processes of tooth shape establishment in chameleons and compare them with those of two other reptile species with different tooth morphology. Here, we revealed an EK-like structure in all reptile species analyzed, which exhibits cell dynamics and signaling resembling those in mammalian EK. Moreover, we described how the ridge-shaped socket at the tip of the central cusp is formed and that this developmental mechanism is conserved across reptilian species.

The developmental processes driving the invagination of dental epithelium are strictly controlled by signaling molecules originating from EKs in mammals.<sup>29</sup> However, the question is if a similar signaling center such as mammalian EK is present in reptiles. Our analysis of the main characteristics, which are typical for mammalian EK, confirmed its presence at least in species with a complex tooth shape such as chameleon and gecko. The proliferation pattern at the cap stage closely resembles the state in mouse EK, with no dividing cells in this area.<sup>6</sup> Also, a small cluster of apoptotic cells is located adjacent to the bulge in the inner enamel epithelium, resembling their location in mouse.<sup>30</sup>

In addition to proliferation and apoptosis, SHH is a protein routinely known to be a marker of EK cells.<sup>27,31</sup> In all studied species, SHH was expressed in an area resembling mouse EK, which confirms the presumption about the existence of EK in reptiles. Moreover, loss of SHH signaling due to cyclopamine treatment caused the development of smaller preameloblast cells in the inner enamel epithelium, with loss of the typical arrangement of enamel bulge cells. Similarly, a loss of elongated cells in both basal and suprabasal layers caused by cyclopamine treatment has previously been observed in the dental placodes as a key event contributing to cell elongation.<sup>14</sup> Furthermore, the expression of FGF4 and ST14 was detected in the EK area, similar to that observed in mouse.<sup>4</sup> All these data indicate that an EK-like structure exists also during odontogenesis in reptiles.

We also observed differences in cytoskeletal organization and the alteration of ion channel expression during rearrangement of epithelial cells in the area contributing to the formation of superficial enamel structures. This alteration of Na/K-ATPase activity indicates modifications in membrane function as a possible developmental

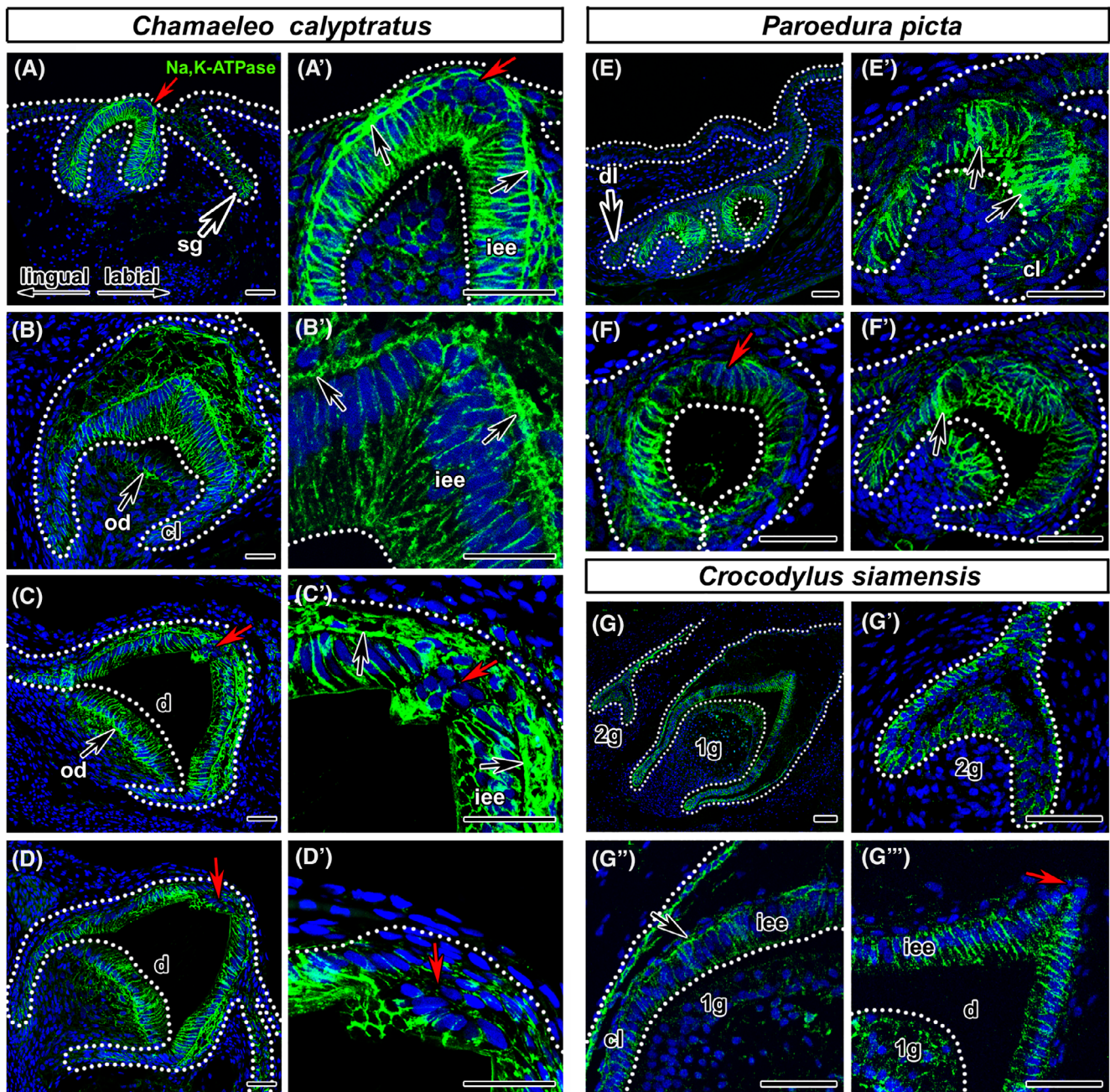


**FIGURE 13** Na,K-ATPase expression in the cell membrane of tooth germ. A,A', In the mesial tooth area, the strong expression of Na,K-ATPase is located in the membranes along the inner enamel epithelium toward stellate reticulum in chameleon. B,B',C,C',D,D', In the bulge of the groove forming cells, few cells with no Na,K-ATPase expression are visible (red arrows) in contrast to surrounding ameloblasts (black arrows) with high Na,K-ATPase-positivity. E-F', In gecko, cells surrounding future enamel groove (black arrows) exhibit high Na,K-ATPase-positivity while more centrally located cells (red arrow) are less positive. G-G''', In crocodile, strong Na,K-ATPase expression is located in the outer and inner membranes of differentiating ameloblasts (black arrow). Few cells on the tooth tip are Na,K-ATPase-negative (red arrow). Na,K-ATPase-positive cells (green, AlexaFluor488), Na,K-ATPase-negative cells (blue, DRAQ5). 1g, first generation of teeth; 2g, second generation of teeth; cl, cervical loop; d, dentin; dl, dental lamina; iee, inner enamel epithelium; od, odontoblast; sg, salivary gland. Scale bars (A-F') = 25  $\mu$ m, (G-G''') = 50  $\mu$ m

process responsible for the cell shape changes during enamel ridge formation. Similarly, disruption of the main components of the cytoskeleton-associated proteins has been found to contribute to the misshaping of the final

cuspid pattern in mammals.<sup>32</sup> Also, the disturbance of fibronectin, E-cadherin, or F-actin distribution in lop-dont gerbils has been previously described to contribute to ectopic invagination of inner enamel epithelium.<sup>32</sup>

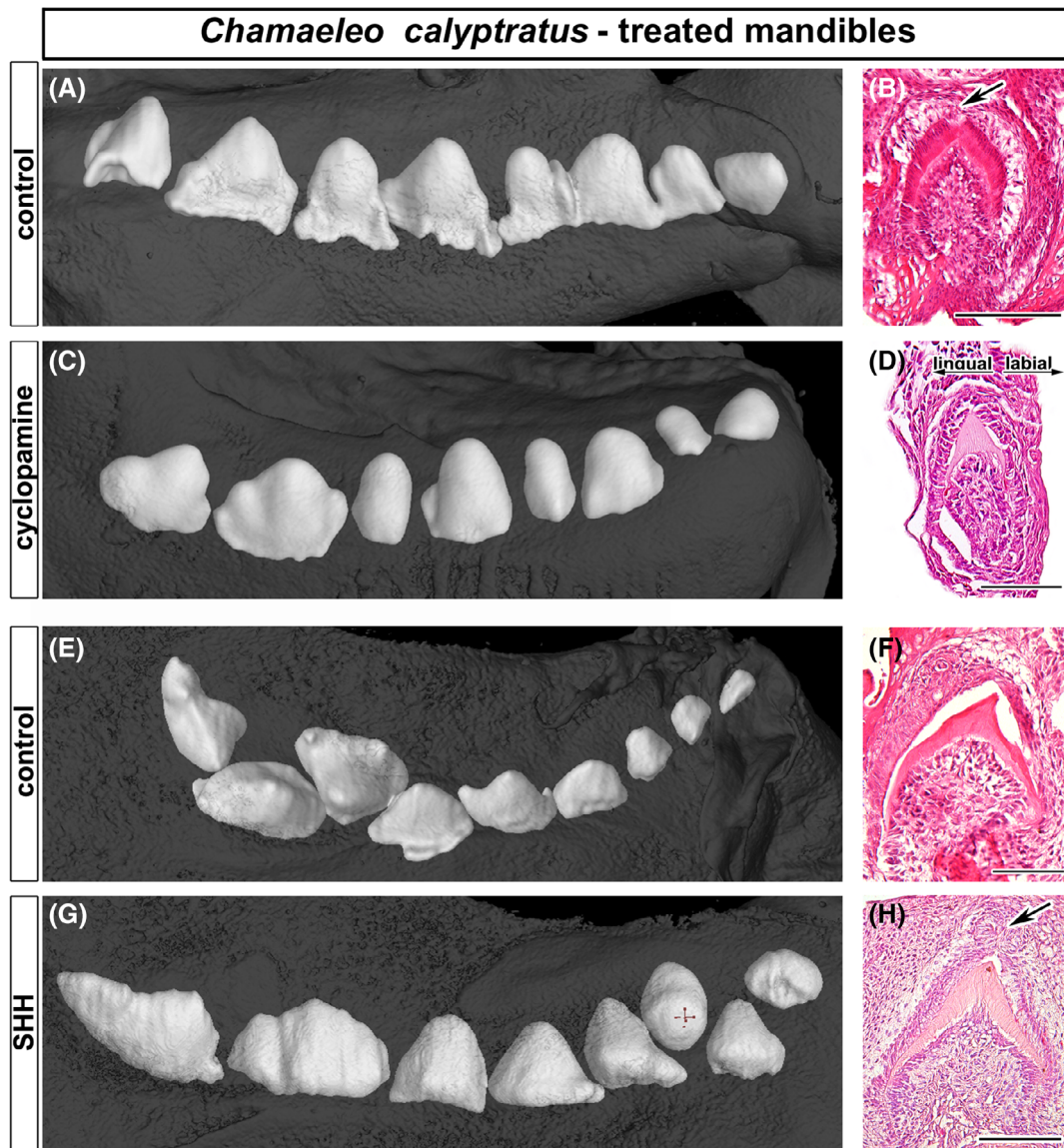


**FIGURE 14** Mandibular cultures of chameleon treated by cyclopamine and SHH. A,B, Tooth morphology of control teeth germs corresponded to physiological tooth development with epithelial cluster (arrow) formation located in future groove area above the tip of the central cusp. C,D, In contrast, mandibular cultures treated with cyclopamine for 3 weeks exhibited growth retardation compared to control samples. D, Cyclopamine treatment leads to the formation of more simple tooth germs. Cluster of cells at the tip of the central cusp was not observed. E-H, Mandibular cultures treated with SHH for 3 weeks exhibited progressed growth in contrast to control samples. G,H, SHH treatment leads to the formation of more complex tooth shape. Cluster of cells at the tip of the central cusp was expanded and exhibits round or branching morphology (arrow). Scale bars (B,D,F,H) = 100  $\mu\text{m}$

Moreover, the expression of matriptase (ST14), which mediates assembly of adherent junctions,<sup>26,33,34</sup> is lost in these epithelial cells, confirming specific changes in cell membranes during cluster cell formation. In agreement, our study revealed that the ridge-shaped socket at the tip of the central cusp is also formed by the combination of cells' rearrangement, changes in their orientation and alteration of the cytoskeleton. By such cell shape rearrangement, the central inner enamel cells protrude deeper toward the dental papilla to form an enamel groove area.

In the ridge area, cells exhibited increased production of lipid droplets, which are deposited in the direction toward joint membranes. Lipids were accumulated especially in cells surrounding apoptotic bodies in the area just above crest formation. PI3K/Akt/mTOR signaling has previously been shown to be responsible for the accumulation of intracellular lipids by regulating fatty acid synthesis, which in turn controls cell senescence.<sup>35</sup> Moreover, it is known that apicobasal actinomyosin cables detected in apoptotic cells can contribute to the process of cell sheet bending by local deformation of the surrounding epithelial

surface, resulting in fold formation.<sup>36</sup> In the future enamel ridge area of chameleon, the membrane activity is lower as shown by Na/K-ATPase; therefore, we suggest that asymmetrical lipid accumulation leads to cellular senescence in the cells located above the tip of the forming ridge, resulting in the delay of ameloblast differentiation. Based on the abovementioned cellular processes together with cell rearrangement, which could be caused by the presence of apoptotic cells, we propose a model with the existence of an inhibition zone in the dental epithelium, which is closely attached to the inner enamel epithelium and located just above future enamel ridge areas. However, it will be necessary to examine the actual involvement of mTOR signaling and apoptosis in these processes during complex tooth shape formation in future.

## 4 | EXPERIMENTAL PROCEDURES

### 4.1 | Animals

Specimens of *C. calyptatus*, *P. picta*, and *C. siamensis* were obtained from private and commercial breeders. Embryos and fetuses at different stages of development were collected to analyze the progress of development. Eggs were incubated at a temperature of 27 to 29°C. At selected time points, eggs were opened, and embryos were euthanized by decapitation and fixed in 4% PFA at least overnight. The juveniles and adults used were naturally deceased specimens.

All procedures were carried out according to the experimental protocols and rules run by the Laboratory Animal Science Committee of the IAPG, v.v.i. (Liběchov, Czech Republic).

### 4.2 | Histology and immunohistochemical labelling

Specimens for histological and immunohistochemical analysis were decalcified in 12.5% EDTA in 4% PFA at

room temperature and then embedded in paraffin. Paraffin-embedded tissues were cut in the transverse plane to get serial transversal histological sections. These sections were stained with hematoxylin-eosin and alternate slides were used for immunohistochemical analysis. Alternate slides were deparaffinized and rehydrated through an ethanol series. A water bath (97°C) in citrate buffer (0.1 M; pH = 6) for 20 minutes was used for antigen retrieval. To prevent nonspecific binding of antibodies, blocking serum (goat serum, Vectastain ABC kit, PK-6101, Vector Laboratories, Burlingame, California) was applied on the samples for 20 minutes. Next, slides were incubated with primary antibodies (Table 1) for 1 hour or overnight, alternately. The secondary antibodies (goat anti-rabbit Alexa Fluor 488, cat. No. A11008; donkey anti-rabbit Alexa Fluor 555, cat. No. A31572; goat anti-mouse Alexa Fluor 488, cat. No. A-11001, all Thermo Fisher, Waltham, Massachusetts) were applied for 30 minutes, and DAPI (cat. No. P36935, Invitrogen, Carlsbad, California) or DRAQ5 Fluorescent Probe Solution (cat. No. 62251, Thermo Fisher) was used for the counterstaining. Photographs were taken under a Leica DM LB2 fluorescence microscope (Leica Microsystems, Wetzlar, Germany) and merged together in Adobe Photoshop 7.0 (Adobe Systems Incorporated, San Jose, California). High-power images were taken on a Leica SP8 confocal microscope using ×20 and ×40 (water immersion) objectives (Leica Microsystems, Wetzlar, Germany) with Leica Application Suite software (Leica Microsystems, Wetzlar, Germany); pictures were processed using IMARIS software (Bitplane, Zürich, Switzerland).

### 4.3 | Cryo-sectioning and immunohistochemistry for Phalloidin labelling

Tissue samples were fixed in 4% PFA and then emerged in the 30% Sucrose (cat. No. S0389, Sigma Aldrich, St. Louis, Missouri) O/N on 4°C followed by

**TABLE 1** List of used primary antibodies

Antibody	Clonality	Dilution	Cat. No.	Company
SHH (rabbit)	polyclonal	1:100	sc-9024	Santa Cruz, Santa Cruz, California
ST14 (rabbit)	polyclonal	1:50	ABIN2773910	Antibodies online, Aachen, Germany
Na,K-ATPase (rabbit)	monoclonal	1:50	ab76020	Abcam, Cambridge, UK
PCNA (mouse)	monoclonal	1:50	M0879	Agilent Dako, Santa Clara, California
Phalloidin	-	1:50	A12379	Thermo Fisher Scientific, Waltham, Massachusetts
FGF4 (rabbit)	polyclonal	1:50	ab65974	Abcam, Cambridge, UK
GLI2 (rabbit)	polyclonal	1:50	18 989-1-AP	ProteinTech, Rosemont, Illinois

embedding in OCT (FSC 22 Clear, cat. No. 3801480, Leica Biosystems) and frozen at  $-20^{\circ}\text{C}$ . Tissue sections were obtained on cryostat Leica CM1850 (Leica Biosystems, Wetzlar, Germany) in the transversal plane at 10 to 16  $\mu\text{m}$  thickness. For immunohistochemistry, sections were washed in PBS-T (1x PBS with 1% Tween20, cat. No. P1379, Sigma Aldrich), then Phalloidin conjugate was applied and incubated for 1 hour. After washing in PBS-T, DRAQ5 Fluorescent Probe Solution (cat. No. 62251, Thermo Fisher) was applied for nuclei counterstaining. Finally, after a quick wash, sections were mounted and processed for the visualization.

The photos were taken on confocal microscope Leica SP8 using  $\times 20$  and  $\times 40$  (water immersion) objectives (Leica Microsystems) with Leica Application Suite software (Leica Microsystems). Pictures were processed by software IMARIS (Bitplane, Zürich, Switzerland).

#### 4.4 | 3D analysis of nucleus shape

Thick transversal slices (300  $\mu\text{m}$ ) of the mandible of chameleon embryos at the mineralization stage were decalcified in 10% EDTA, cleared in CUBIC I solution (25% urea, cat. No. U5378; 25%  $N,N,N,N'$ -tetrakis[2-hydroxypropyl]ethylenediamine, cat. No. 122262-1L; 15% Triton X-100, cat. No. T8787; all Sigma Aldrich; diluted in distilled water), stained with DAPI (D9542, Sigma Aldrich) and again cleared in CUBIC II solution (50% sucrose, cat. No. S0389; 25% urea, cat. No. U5378; 10% 2,2',2''-nitrioltriethanol, cat. No. 90279; 0.1% Triton X-100, cat. No. T8787; all Sigma Aldrich; diluted in distilled water). Finally, pictures were acquired using a Zeiss LSM 880 confocal microscope (Carl Zeiss Microscopy, Jena, Germany) using  $\times 40$  (water immersion) or  $\times 63$  (oil immersion) objectives. Pictures were automatically processed using IMARIS software (Bitplane, Zürich, Switzerland) for the purpose of visualization by different colors according to cell nucleus shape.

#### 4.5 | TUNEL assay

Localization of apoptotic cells was analyzed by the detection of DNA fragments in situ by the TUNEL method (ApopTag Peroxidase In Situ Apoptosis Detection Kit-S7101, Chemicon, Temecula, USA). Counterstaining with hematoxylin was performed. Sections were photographed under bright field illumination with a Leica DMLB2 compound microscope (Leica Microsystems, Wetzlar, Germany).

#### 4.6 | Transmission electron microscopy

Samples were fixed in 3% glutaraldehyde for 24 hours, washed three times in 0.1 M cacodylate buffer and post-fixed in 1%  $\text{OsO}_4$  (cat. No. 02601-AB, SPI-Chem, West Chester, Pennsylvania) solution for 1 hour. Samples were then dehydrated in an ethanol series, followed by acetone, and embedded in Durcupan epoxy resin (cat. No. 44610, Sigma Aldrich). Semithin sections were stained with Toluidine Blue (cat. No. 02576-AB, SPI-Chem, West Chester) and examined by light microscopy. Ultrathin sections (60 nm thick) were cut using a Leica EM UC6 ultramicrotome (Leica Microsystems GmbH, Vienna, Austria) and placed on formvar-coated nickel grids.

Sections contrasted with lead citrate and uranyl acetate were observed using a Morgagni 268 TEM (FEI Company, Eindhoven, Netherlands) and JEOL JEM-1011 (JEOL, Peabody, Massachusetts). Photographs were taken using a Veleta CCD camera (Olympus, Münster, Germany).

#### 4.7 | Scanning electron microscopy

Lower jaws were dissected from collected animals and then fixed in 70% ethanol. The samples were dehydrated in a graded ethanol series and placed in 100% ethanol. Just before scanning, they were air-dried, glued onto an aluminum support, coated with a thin layer of gold and analyzed in a JEOL SEM 6380 LV (JEOL).

#### 4.8 | Mandibular organ cultures

We prepared organ cultures from the mandible by dissecting them out of embryos and placing them on Millipore filters and a metal mesh. They were cultured for three weeks at 29 to  $30^{\circ}\text{C}$  in Advanced media (Gibco Advanced DMEM/F12 1:1, cat. No. 12634-010, Thermo Fisher Scientific; 1% penicillin/streptomycin, cat. No. P0781, Sigma Aldrich; 1% L-glutamine, cat. No. G7513, Sigma Aldrich; 0.25 mg/mL ascorbic acid, A4544, Sigma Aldrich) supplemented with SHH growth factor (high-activity recombinant human SHH, 100 ng/mL, cat. No. 8908-SH-005, R&D Systems, Minneapolis, Minnesota) or SHH inhibitor (cyclopamine, 100 nM, cat. No. GR-334, Biomol International, Plymouth, Pennsylvania). The right jaw was treated with SHH protein or SHH inhibitor, and the left jaw was cultured just in plain media and used as a control. The experiment was repeated on four animals for each treatment.

**TABLE 2** Parameters of microCT scan

Sample	Acceleration voltage (kV)	X-ray tube current ( $\mu$ A)	Exposure time (ms)	Number of projections	Voxel resolution ( $\mu$ m)
Gecko skull	60	200	750	2500	12.5
Chameleon skull	60	250	400	2500	18
Chameleon embryos - mandibular organ cultures	60	200	400	2400	6

Cultures were fixed in 4% PFA and processed for histological analyses. For the clear determination of changes in cusp formation under the influence of growth factors, jaws were stained with 1% PTA in 90% MeOH for 3 days and analyzed by microCT (GE Phoenix v|tomelx L 240, GE Sensing & Inspection Technologies GmbH, Hürth, Germany).

#### 4.9 | X-ray micro computed tomography

For the purpose of motion stabilization during the micro CT scan, gecko skull was embedded in 1% agarose gel in a Falcon conical centrifuge tube, and chameleon embryonal mandibular organ cultures were embedded in 1% agarose gel in Kapton tubes. Chameleon skull was attached to polystyrene with parafilm.

Micro CT scanning was performed using a GE Phoenix v|tomelx L 240 laboratory system (GE Sensing & Inspection Technologies GmbH, Hürth, Germany) equipped with a 180 kV/15 W maximum power nanofocus X-ray tube and DXR250 high-contrast flat panel detector (2048  $\times$  2048 px with 200  $\times$  200  $\mu$ m pixel size).

Measurements were carried out in an air-conditioned cabinet (21°C). The parameters of each scan were set individually (Table 2) considering the size of the sample.

The tomographic reconstruction was realized with GE Phoenix datosix 2.0 software (GE Sensing & Inspection Technologies GmbH, Hürth, Germany). Images of 3D renders were created in VG Studio MAX 3.1 software (Volume Graphics GmbH, Heidelberg, Germany). Developing chameleon teeth in mandibular organ cultures were manually segmented in Avizo 9.5.0 (Thermo Fisher Scientific).

#### 4.10 | RNAScope

Gene expression analysis was performed on mouse embryos which were collected at embryonic day 14. Embryos were euthanized by decapitation and fixed in 10% PFA for a maximum of 36 hours. Next, samples were

dehydrated by standard ethanol series followed by xylene and embedded in paraffin. Five micrometer-thick alternate sections were prepared to be used with several probes.

Transcripts were detected using an RNAScope Multiplex Fluorescent v2 assay for formalin-fixed paraffin-embedded tissue (323 110, Advanced Cell Diagnostics, Newark, California, USA). *Fgf4* (514 311, Advanced Cell Diagnostics), *Shh* (314361-C2, Advanced Cell diagnostics), and *ST14* (422 941, Advanced Cell Diagnostics) probes were used. Before hybridization, samples were pretreated with hydrogen peroxidase (322 335, Advanced Cell Diagnostics) and Protease Plus (322 331, Advanced Cell Diagnostics) reagents. Visualization of hybridized probes was done using a TSA-Plus Cyanine 3 system (NEL744001KT, Perkin-Elmer, Waltham, Massachusetts) according to the manufacturer's protocol. DAPI (323 108, Advanced Cell Diagnostics) was used for cell nucleus staining. Photographs were taken under a Leica DM LB2 fluorescence microscope (Leica Microsystems, Wetzlar, Germany) and merged together in Adobe Photoshop 7.0 (Adobe Systems Incorporated).

#### 4.11 | In situ hybridization on gecko sections

Nonradioactive in situ hybridization was performed, and the UTP were labelled with digoxigenin (cat. No. 11209256910, Roche, Mannheim, Germany). The *Shh* probe against the *Python saebe* gene was used as previously published.<sup>24</sup> This was linearized with HindIII (R6041, Promega, Madison, Wisconsin) and transcribed with T7 (cat. No. 10881767001, Roche). Frontal paraffin sections through gecko head were treated with 10  $\mu$ g/mL proteinase K (P2308, Sigma Aldrich) for 15 minutes, and the hybridization was carried out at 60°C. Eosin (cat. No. 102439, Sigma Aldrich) was used for counterstaining.

#### ACKNOWLEDGMENT

This work was supported by the Czech Science Foundation (17-14886S) and by the Ministry of Education, Youth

and Sports of the Czech Republic (CZ.02.1.01/0.0/0.0/15\_003/0000460) to MB lab. We acknowledge the core facility CELLIM of CEITEC supported by the Czech-BioImaging large RI project (LM2015062 funded by MEYS CR) for their technical support with obtaining scientific data presented in this article. JK lab is supported by the project CEITEC 2020 (LQ1601) with financial support from the Ministry of Education, Youth and Sports of the Czech Republic under the National Sustainability Programme II. We acknowledge prof. Jiri Kratochvil from the Department of Ecology, Faculty of Science, Charles University in Prague for providing embryonic material of gecko *Paroedura picta*. The authors wish to thank the Crocodile Zoo Protivin, namely Miroslav Prochazka, for permission to obtain the fertilized Siamese Crocodile eggs.

### CONFLICT OF INTEREST

The authors declared that there is no conflict of interest.

### ORCID

Michaela Kavkova  <https://orcid.org/0000-0001-7435-9292>

Tomas Zikmund  <https://orcid.org/0000-0003-2948-5198>

Martina Gregorovicova  <https://orcid.org/0000-0002-4982-4524>

David Sedmera  <https://orcid.org/0000-0002-6828-3671>

Jozef Kaiser  <https://orcid.org/0000-0002-7397-125X>

Abigail S. Tucker  <https://orcid.org/0000-0001-8871-6094>

Marcela Buchtova  <https://orcid.org/0000-0002-0262-6774>

### REFERENCES

- Zahradnicek O, Buchtova M, Dosedelova H, Tucker AS. The development of complex tooth shape in reptiles. *Front Physiol.* 2014;5:7.
- Butler PM. The ontogeny of molar pattern. *Biol Rev Camb Philos Soc.* 1956;31:30-70.
- Coin R, Lesot H, Vonesch JL, Haikel Y, Ruch JV. Aspects of cell proliferation kinetics of the inner dental epithelium during mouse molar and incisor morphogenesis: a reappraisal of the role of the enamel knot area. *Int J Dev Biol.* 1999;43:261-267.
- Jernvall J, Kettunen P, Karavanova I, Martin LB, Thesleff I. Evidence for the role of the enamel knot as a control center in mammalian tooth cusp formation - nondividing cells express growth-stimulating Fgf-4 gene. *Int J Dev Biol.* 1994;38:463-469.
- Lesot H, Vonesch JL, Peterka M, Tureckova J, Peterkova R, Ruch JV. Mouse molar morphogenesis revisited by three-dimensional reconstruction .2. Spatial distribution of mitoses and apoptosis in cap to bell staged first and second upper molar teeth. *Int J Dev Biol.* 1996;40:1017-1031.
- Vahtokari A, Aberg T, Jernvall J, Keranen S, Thesleff I. The enamel knot as a signaling center in the developing mouse tooth. *Mech Dev.* 1996;54:39-43.
- Aberg T, Wozney J, Thesleff I. Expression patterns of bone morphogenetic proteins (Bmps) in the developing mouse tooth suggest poles in morphogenesis and cell differentiation. *Dev Dyn.* 1997;210:383-396.
- Bei M, Maas R. FGFs and BMP4 induce both Msx1-independent and Msx1-dependent signaling pathways in early tooth development. *Development.* 1998;125:4325-4333.
- Chen YP, Bei M, Woo I, Satokata I, Maas R. Msx1 controls inductive signaling in mammalian tooth morphogenesis. *Development.* 1996;122:3035-3044.
- Dassule HR, Lewis P, Bei M, Maas R, McMahon AP. Sonic hedgehog regulates growth and morphogenesis of the tooth. *Development.* 2000;127:4775-4785.
- Sarkar L, Sharpe PT. Expression of Wnt signalling pathway genes during tooth development. *Mech Dev.* 1999;85:197-200.
- Sharpe PT. Homeobox genes and orofacial development. *Connect Tissue Res.* 1995;32:17-25.
- Thesleff I, Sharpe P. Signalling networks regulating dental development. *Mech Dev.* 1997;67:111-123.
- Li JJ, Chatzeli L, Panousopoulou E, Tucker AS, Green JBA. Epithelial stratification and placode invagination are separable functions in early morphogenesis of the molar tooth. *Development.* 2016;143:670-681.
- Debiais-Thibaud M, Chiori R, Enault S, et al. Tooth and scale morphogenesis in shark: an alternative process to the mammalian enamel knot system. *BMC Evol Biol.* 2015;15:17.
- Rasch LJ, Martin KJ, Cooper RL, Metscher BD, Underwood CJ, Fraser GJ. An ancient dental gene set governs development and continuous regeneration of teeth in sharks. *Dev Biol.* 2016; 415:347-370.
- Westergaard B, Ferguson MWJ. Development of the dentition in Alligator-Mississippiensis - early embryonic-development in the lower jaw. *J Zool.* 1986;210:575-597.
- Westergaard B, Ferguson MWJ. Development of the dentition in Alligator-Mississippiensis. Later development in the lower jaws of embryos, hatchlings and young juvenils. *J Zool.* 1987;212:191-222.
- Buchtova M, Zahradnicek O, Balkova S, Tucker AS. Odontogenesis in the Veiled Chameleon (*Chamaeleo calytratus*). *Arch Oral Biol.* 2013;58:118-133.
- Handrigan GR, Richman JM. Unicuspid and Bicuspid Tooth Crown Formation in Squamates. *J Exp Zool Part B-Mol Dev Evol.* 2011;316B:598-608.
- Zahradnicek O, Horacek I, Tucker AS. Tooth development in a model reptile: functional and null generation teeth in the gecko *Paroedura picta*. *J Anat.* 2012;221:195-208.
- Weeks O. Molecular characterization of dental development in a toothed archosaur, the American alligator *Alligator mississippiensis* (vol 15, pg 393, 2013). *Evol Dev.* 2014;16:121-121.
- Handrigan GR, Richman JM. A network of Wnt, hedgehog and BMP signaling pathways regulates tooth replacement in snakes. *Dev Biol.* 2010;348:130-141.
- Buchtova M, Handrigan GR, Tucker AS, et al. Initiation and patterning of the snake dentition are dependent on Sonic Hedgehog signaling. *Dev Biol.* 2008;319:132-145.
- Nakatomi M, Morita I, Eto K, Ota MS. Sonic hedgehog signaling is important in tooth root development. *J Dent Res.* 2006; 85:427-431.
- Oberst MD, Singh B, Ozdemirli M, Dickson RB, Johnson MD, Lin CY. Characterization of matriptase expression in normal human tissues. *J Histochem Cytochem.* 2003;51:1017-1025.

27. Hardcastle Z, Mo R, Hui CC, Sharpe PT. The Shh signalling pathway in tooth development: Defects in Gli2 and Gli3 mutants. *Development*. 1998;125:2803-2811.
28. Garcia MA, Nelson WJ, Chavez N. Cell-Cell Junctions Organize Structural and Signaling Networks. *Cold Spring Harb Perspect Biol*. 2018;10:27.
29. Zhang YD, Chen Z, Song YQ, Liu C, Chen YP. Making a tooth: growth factors, transcription factors, and stem cells. *Cell Res*. 2005;15:301-316.
30. Jernvall J, Aberg T, Kettunen P, Keranen S, Thesleff I. The life history of an embryonic signaling center: BMP-4 induces p21 and is associated with apoptosis in the mouse tooth enamel knot. *Development*. 1998;125:161-169.
31. Zhang L, Hua F, Yuan GH, Zhang YD, Chen Z. Sonic hedgehog signaling is critical for cytodifferentiation and cusp formation in developing mouse molars. *J Mol Histol*. 2008;39: 87-94.
32. Li LW, Tang QH, Nakamura T, Suh JG, Ohshima H, Jung HS. Fine tuning of Rac1 and RhoA alters cuspal shapes by remodeling the cellular geometry. *Sci Rep*. 2016;6:12.
33. Hung RJ, Hsu IWJ, Dreiling JL, et al. Assembly of adherens junctions is required for sphingosine 1-phosphate-induced matriptase accumulation and activation at mammary epithelial cell-cell contacts. *Am J Physiol Cell Physiol*. 2004;286:C1159-C1169.
34. List K, Haudenschild CC, Szabo R, et al. Matriptase/MT-SP1 is required for postnatal survival, epidermal barrier function, hair follicle development, and thymic homeostasis. *Oncogene*. 2002; 21:3765-3779.
35. Flor AC, Wolfgeher D, Wu D, Kron SJ. A signature of enhanced lipid metabolism, lipid peroxidation and aldehyde stress in therapy-induced senescence. *Cell Death Discov*. 2017;3:17075.
36. Monier B, Gettings M, Gay G, et al. Apico-basal forces exerted by apoptotic cells drive epithelium folding. *Nature*. 2015;518: 245-U252.

**How to cite this article:** Landova Sulcova M, Zahradnicek O, Dumkova J, et al. Developmental mechanisms driving complex tooth shape in reptiles. *Developmental Dynamics*. 2020;249: 441–464. <https://doi.org/10.1002/dvdy.138>

## **Dental stem cells: Developmental aspects**

kapitola publikované v knize

## **Cell-to-cell communication: Cell-atlas – visual biology in oral medicine**

*Jan Krivanek, Kaj Fried*

# Dental Stem Cells: Developmental Aspects

[Dental Stem Cells: Latin *dens* (tooth) and German *Stammzellen* (stem cells)]

*Jan Krivanek and Kaj Fried*

Late cap stage of developing molar in a 16.5-day-old mouse embryo (original magnification  $\times 300$ ).

## Definition, Etymology and Histologic Appearance

Teeth in mammals develop through an interaction between cells of the ectoderm of the first pharyngeal arch in the fetus and neural crest-derived ectomesenchyme (see, eg, Balic and Thesleff 2015 for review). After initiation, this process continues throughout human fetal life and is eventually finalized before adulthood, when progenitor cells vanish. The major types of basic cells involved have been identified for

quite some time. However, not until recently has some light been shed on the stem cell heterogeneity in these populations. This heterogeneity reflects the mechanisms of tooth growth and pertains, among other things, to clonal development and to the identities of rare and transient cell types. Histologic identification cannot be made using pure morphologic criteria but requires specific molecular in situ protein or messenger RNA (mRNA) detection. Much of what we know regarding dental stem cells (first mentioned by E. Haeckel, 1868) derives from experimental

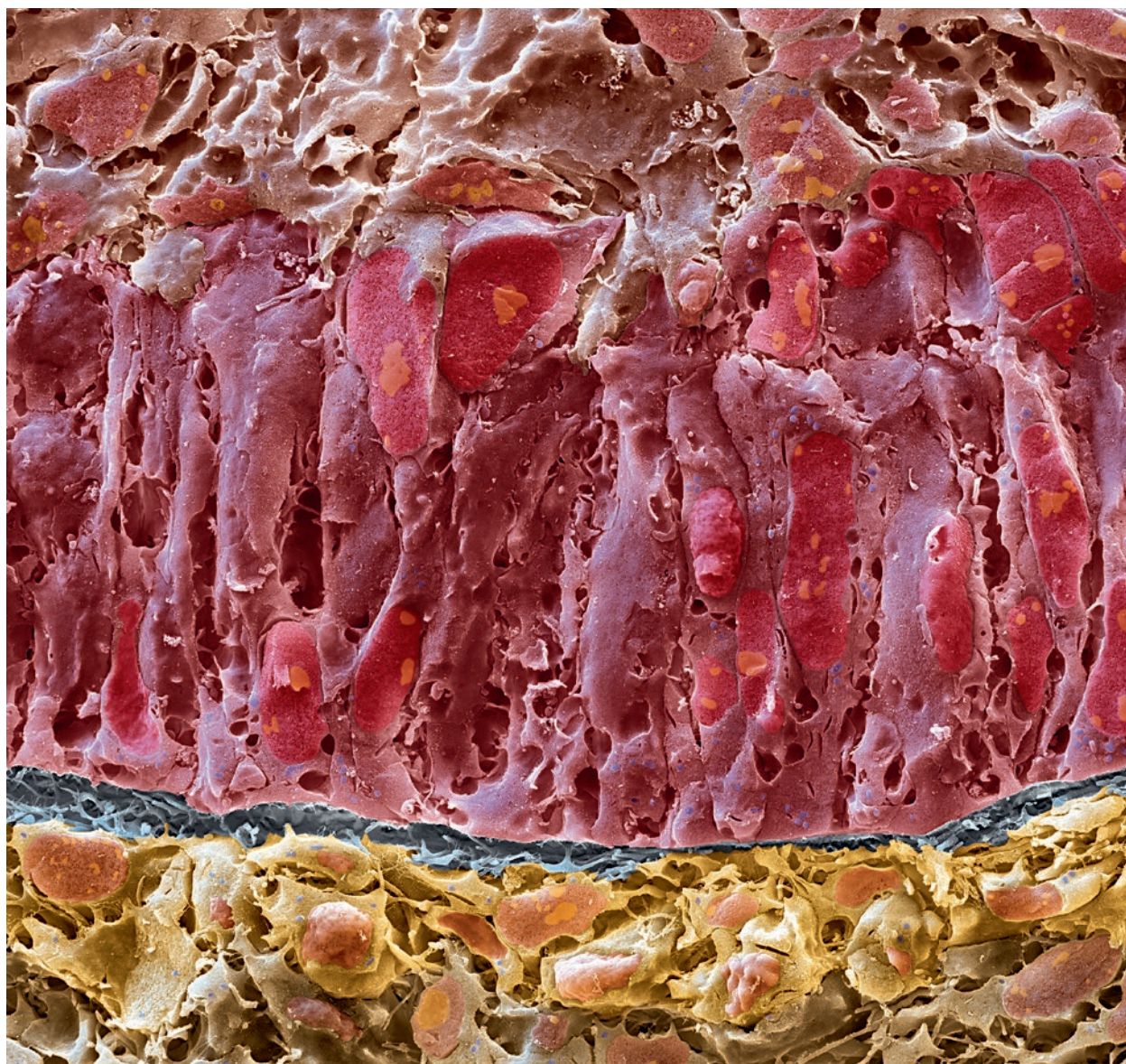


**Fig 1** Interaction interphase between preameloblasts and preodontoblasts with other adjacent epithelial and mesenchymal layers during molar development in a 16.5-day-old mouse embryo (original magnification  $\times 2500$ ). (Courtesy of eye of science.)

studies with a focus on the self-renewing rodent incisor (see, eg, Krivanek et al 2017, Sharpe 2016, or Yu and Klein 2020 for review). Ample evidence indicates that this is a reasonable model for studies of tooth development in humans. However, human-specific patterns of cellular organization are clearly discernible, with subpopulations that probably contribute to human tooth development, homeostasis, and progression of disease in unique ways (Krivanek et al 2020).

## Cell Types in Interaction with Their Environment

As mentioned above, teeth and adjacent periodontium develop through mutual interaction between ectoderm (dental epithelium) and surrounding ectomesenchyme (neural crest-derived; Balic and Thesloff 2015, Thesloff and Hurmerinta K). During embryogenesis and later, these two cell populations proliferate and differentiate to form the fully functional dental organ (Figs 1 and 2). Based on the different origins,

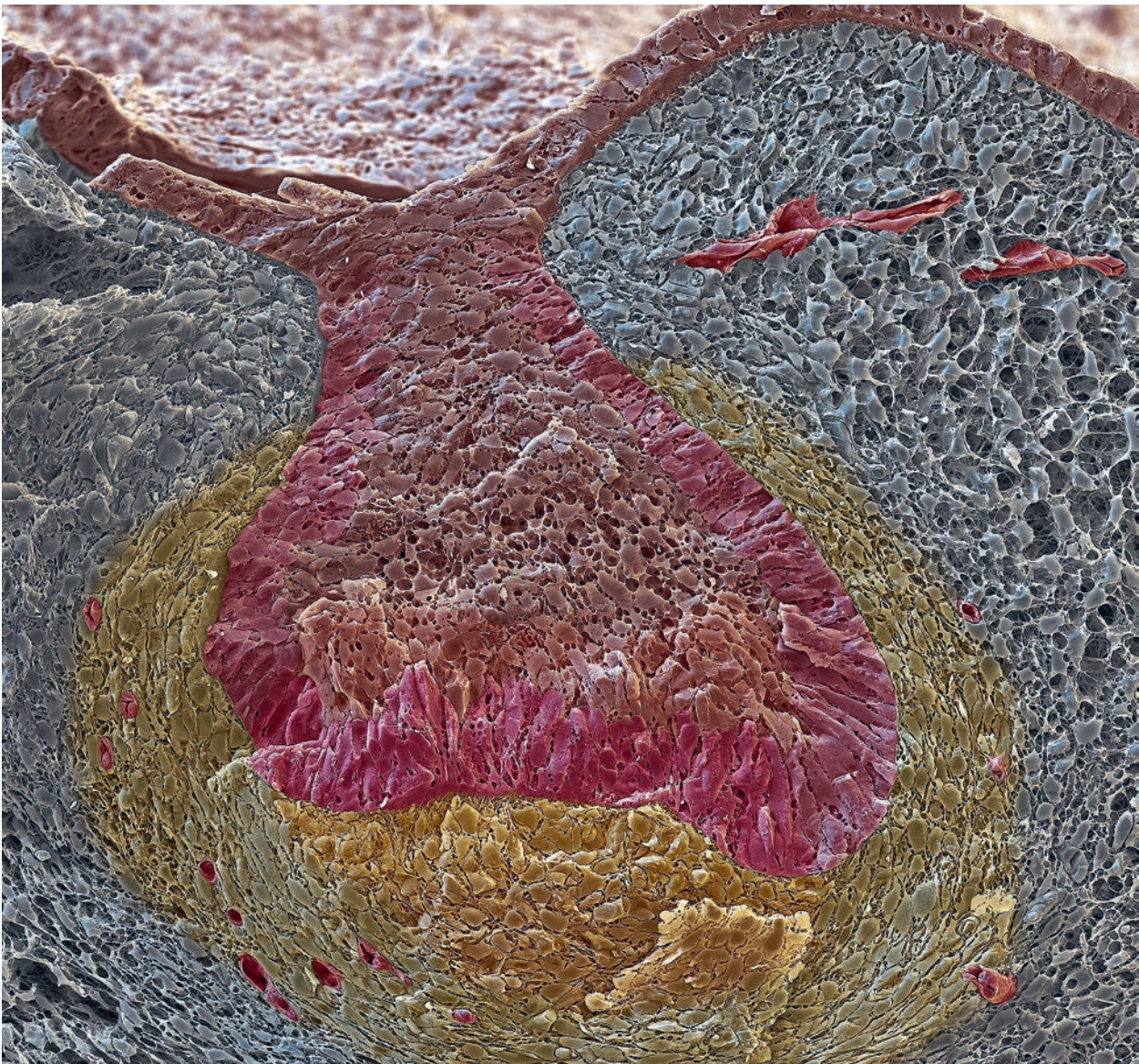


**Fig 2** Early cap stage of mouse molar (original magnification  $\times 450$ ). (Courtesy of eye of science.)

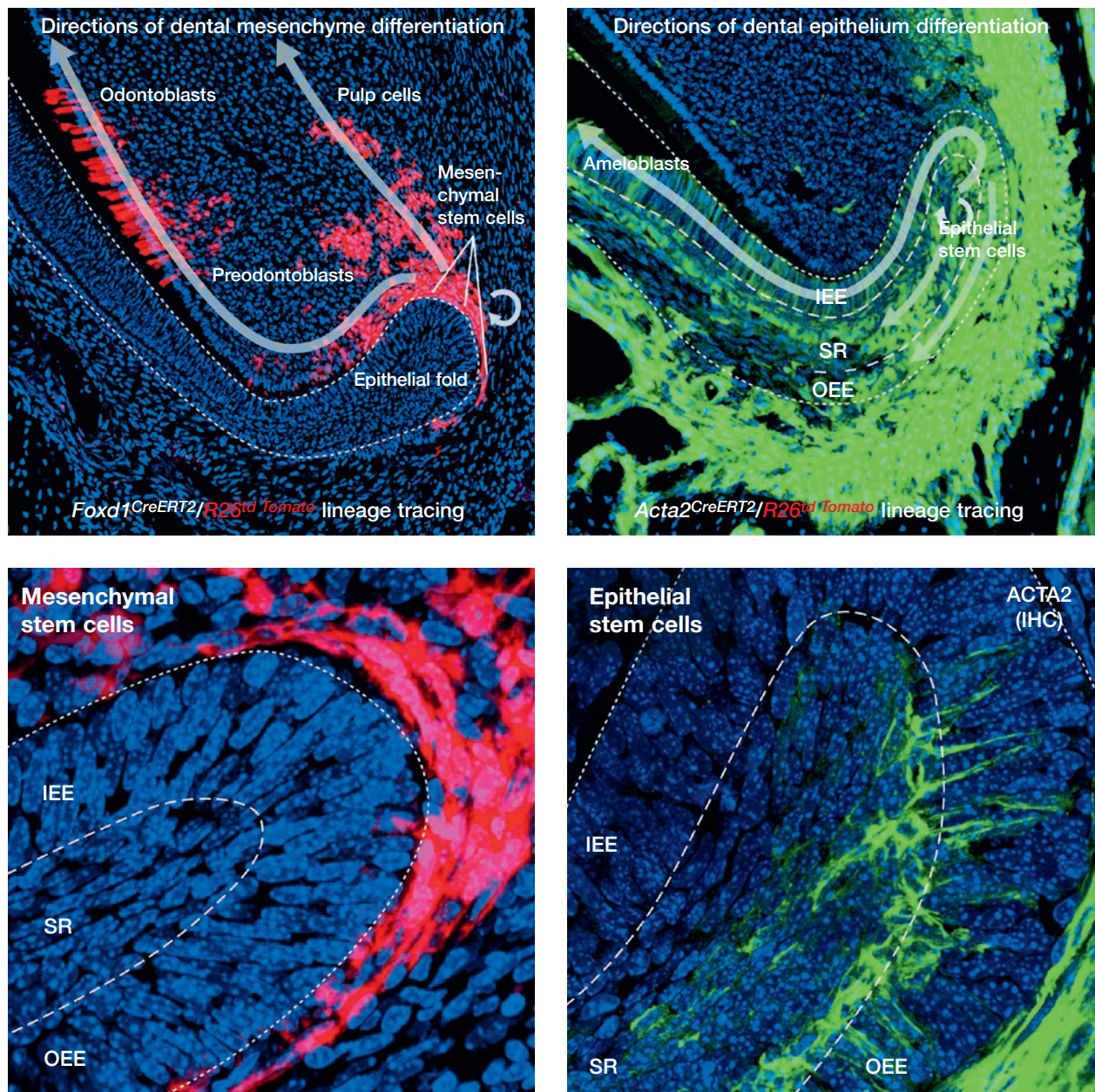


**Fig 3** Dynamics and shapes of dental mesenchymal (*right panel*) and epithelial stem cells (*left panel*) in a continuously growing mouse incisor visualized by lineage tracing and immunohistochemistry. IEE, inner enamel epithelium; SR, stellate reticulum; OEE, outer enamel epithelium.

two main types of dental stem cells can be distinguished (Fig 3): dental epithelial stem cells (DESCs) and dental mesenchymal stem cells (DMSCs).

### Dental epithelial stem cells

DESCs are quiescent (slowly dividing) multipotent cells that originate from an embryonic oral epithelium

invagination known as the dental lamina. They can be divided into primordial cells necessary for initial organogenesis (odontogenesis) and adult stem cells responsible for tissue homeostasis and repair after the dentition is fully formed. They are of various shapes, and their location is limited to epithelial structures only. During tooth development, primordial stem cells drive the growth of the dental epithelium, which in

turn interacts with the surrounding ectomesenchyme to give rise to the teeth of the primary dentition. Some epithelial cells retain multipotent characteristics and persist as DESCs within the dental lamina (Priya et al 2015). They will generate a successional dental lamina, from which tooth buds of the permanent dentition later develop. Of note, permanent molars develop from distal extensions of the primary dental lamina, which means that from a developmental perspective they belong to the primary dentition. After completion of the permanent dentition, the dental lamina ultimately disappears, and the ability to renew the teeth is forever lost (Dosedělová et al 2015, Kim et al 2020). It has been shown that slow-cycling DESCs are located in the stellate reticulum, a mesenchyme-like part of the dental epithelial fold that is located between the inner and the outer enamel epithelium (Harada et al 1999). From here, stem cells give rise to transit-amplifying cells, a fast-cycling cell population that sits on the edges of the inner and outer enamel epithelia. This population further differentiates into ameloblasts and the adjacent stratum intermedium to build the crown of the tooth. In addition, it also provides cells for the Hertwig epithelial root sheath (HERS), which interacts with developing odontoblasts and cementoblasts to form the tooth root (Harada et al 2006). In contrast to the crown of the tooth, no functional tissue in the root is formed by epithelium. However, root development is entirely dependent on the HERS. This structure serves as an interactive partner to the surrounding ectomesenchyme and controls root patterning and growth. After root formation, the HERS partly undergoes apoptosis and is partly retained as the epithelial rests of Malassez (ERM), a thin mesh-like structure covering the roots. ERM is the only persisting epithelial structure of dental lamina origin in the fully developed adult dentition. There is still no general consensus about the role of this structure. However, ERM can undergo epithelial-to-mesenchymal transition and may contribute to periodontal ligament homeostasis and prevent ankylosis or bone resorption. Tentatively, this structure may serve as a reservoir of stem cells in the periodontal space (Rincon et al 2006, Xiong et al 2013).

## Dental mesenchymal stem cells

The dental pulp (including odontoblasts) is formed by ectomesenchymal cells, most of which reach the future jaws through direct migration from the neural crest (Etchevers et al 2019). However, a substantial number is recruited from glial precursors (immature Schwann cells) that sit on basket-like nerve arborizations that contact the tooth bud (Kaukua et al 2014). The dental mesenchymal stem cells are located in a niche between folds of the dental epithelium at the apical end of the tooth anlage. The cell subtypes in this region gradually include different pools of quiescent stem cells and stromal cells, which probably support the stem cell niche. Other cells destined to become pulp cells continue along trajectories of differentiation. Clonal genetic tracing has shown that the mesenchymal stem cells of the dental papilla are bipotent, ie, they can produce both odontoblasts and pulpal cells (An et al 2018, Kaukua et al 2014, Zhao et al 2014). The fate and amount of the progeny is determined by signals from the dental epithelium. In fact, proximity of a stem cell to the epithelial fold (cervical loop) will bias the stem cell progeny to an odontoblast fate. Hence, the initial site of a dental mesenchymal stem cell along the central longitudinal axis of the forming tooth will determine transcriptional state, migratory trajectory, and fate progeny (Krivanek et al 2020). Overall, the mesenchymal stem cell population of the growing apical dental papilla seems to display a high degree of differentiation plasticity, spatial heterogeneity, and hierarchical potential. Mature human dental pulps contain a number of cellular subpopulations, which are distinguished by, eg, specialized matrix production and other parameters. However, it is unclear whether mesenchymal stem cells exist in the pulp of fully formed human teeth.

## Molecular Aspects of Tissue Growth and Cell Communication

Multiple signaling pathways are active during dental development, including Wingless/int-1 (WNT), fibro-

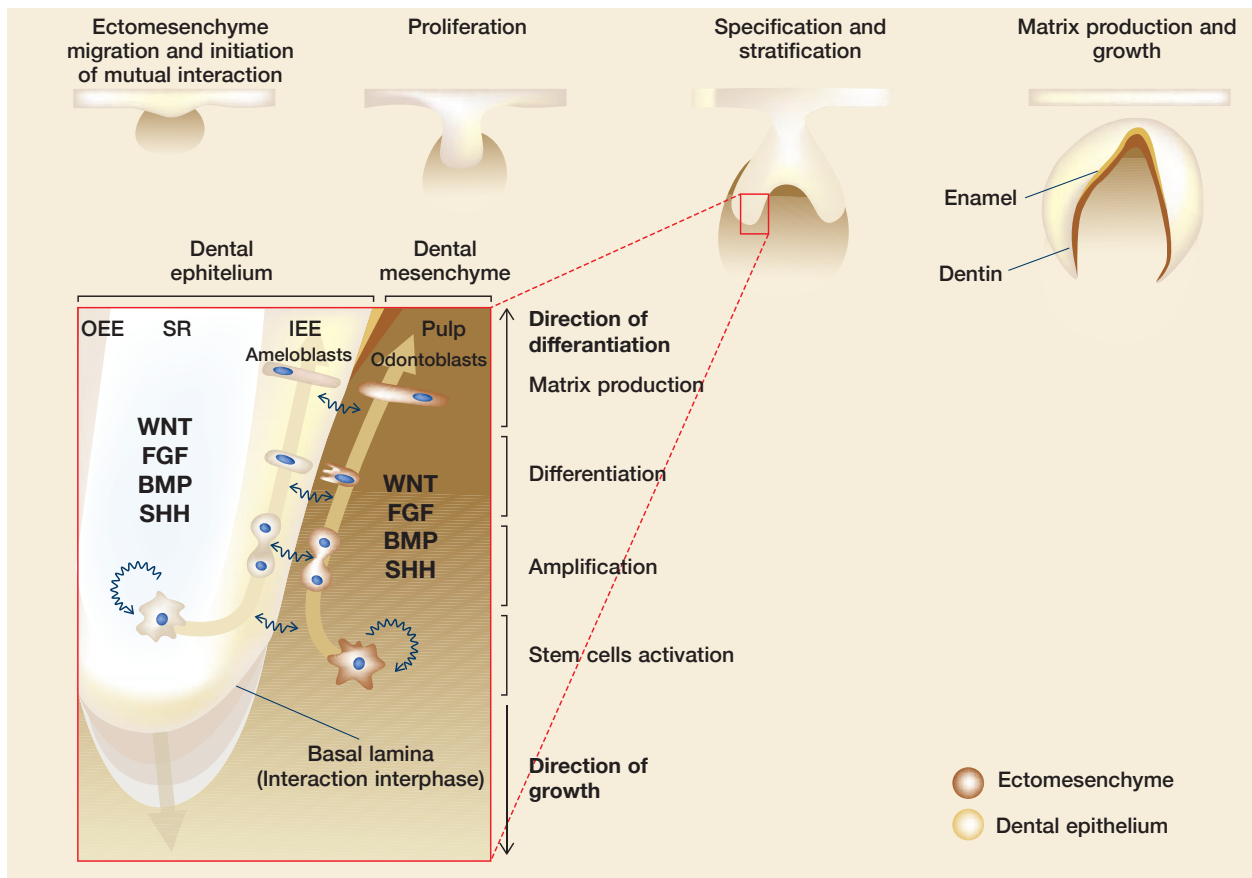


**Fig 4** Schematic illustration of development and interactions of dental epithelium and mesenchyme. IEE, inner enamel epithelium; SR, stellate reticulum; OEE, outer enamel epithelium.

blast growth factor (FGF), BMP (bone morphogenetic protein), and Sonic hedgehog (SHH), as depicted in Fig 4 (Balic and Thesleff 2015). This precisely controlled molecular interaction is responsible for proper development of teeth and a complete dentition. Several molecular markers characterize DESCs. Among those are Sox2, Bmi1, Lrig1, Gli1, Igfbp5, and Acta2 (Biehs et al 2013; Juuri et al 2012; Krivanek et al 2020; Seidel et al 2010, 2017; Zhao et al 2014). One of the first and most generally accepted markers used for identification of DESCs is Sox2 (Juuri et al 2012). Although expression of Sox2 by DESCs was initially described in the mouse incisor, further studies showed that expression of Sox2 is characteristic for DESCs across species. Sox2+ DESCs do not only play roles in maintenance of the continuous tooth growth in rodents; they are also important for diphyodont tooth replacement (ie, two successive

sets of teeth as in humans; Juuri et al 2012, 2013). As for the heterogeneous DMSCs that engage in dental pulp formation, they may express molecular markers such as Foxd1, Thy1, Gli1, and Plp1 (An et al 2018, Kaukua et al 2014, Zhao et al 2014). In addition, pulpal stem cells possess the Shh receptor Gli1 and are in this way influenced by Shh secreted by local neurovascular bundles (Zhao et al 2014). This shows the importance of functional innervation for tooth growth and perhaps also for homeostasis and regeneration. During recent years, a large number of studies have reported on the gene expression signature of human dental mesenchymal stem cells cultivated in vitro. However, comparisons between dental stem cells in situ and in vitro suggest that many previously reported in vitro markers likely emerge during ex vivo manipulations with dental mesenchymal cells.

## Preclinical Research and Pathologic Aspects

The patterning and final formation of the dentition is in general very precisely controlled. Despite this, different kinds of dental congenital malformations are relatively common defects. Unraveling the processes that guide normal dental development can help us to understand the etiology of different kinds of hereditary and/or acquired abnormalities. Importantly, it may also lead to new therapeutic methods to regrow, repair, or replace damaged or diseased dental cells, tissues, or organs.

Dental malformations appear in a wide variety of forms; almost any conceivable defect may arise. At one end is anodontia, ie, when teeth are missing. On the other end are rare odontogenic tumors. Among the most frequent human dental malformations are numeric aberrations (generally described as hyper-

dontia or hypodontia). The cause of this is usually genetic malfunction in initial tooth patterning. In the case of hyperdontia, the successional dental lamina fails to dissipate after the permanent dentition is formed, and one or more extra tooth buds develop and ultimately produce supernumerary teeth. Of note is the birth defect cleidocranial dysplasia, in which successional dental laminae do not regress (Jensen and Kreiborg 1990, Kreiborg and Jensen 2018). This syndrome (which coexists with other serious non-dental congenital defects) is characterized by various numbers of supernumerary teeth. Selected examples of clinical manifestations are shown in Figs 5 to 8.

Turning to the main hard dental tissues, dentin, as opposed to enamel, is a living material that can perceive outer environment and react to damage or increased wear. This perception and eventual changes in dentin microstructure or increase in dentin width are ensured by long-lived odontoblasts during

**Fig 5** Cleidocranial dysplasia in a 17-year-old male patient. Example of congenital malformation when dental lamina fails to dissipate and multiple additional teeth develop, causing a characteristic form of hyperdontia. (Courtesy of P. Cernochova and L. Izakovicova Holla.)



**Fig 6** Hypodontia in a 17-year-old male patient. Condition when incomplete dentition is developed and single teeth are absent. (Courtesy of V. Kovar Matejova and L. Izakovicova Holla.)





**Fig 7** Oligodontia in a 4.5-year-old male patient. Developmental anomaly of different etiology resulting in partial tooth loss. (Courtesy of P. Cernochova and L. Izakovicova Holla.)

secondary and reparative dentinogenesis (see Fig 8a). However, if a lesion on a tooth is more widespread, there is an urgent need to seal the lesion with newly generated dentin to safeguard the vitality of the tooth. New dentin-forming odontoblasts are then differentiated from so-called dental pulp (mesenchymal) stem cells (DPSCs). Further, small alterations in the activity of these cells may lead to the formation of pulp stones (denticles, pulpal calcifications), which often occur with increasing age (see Figs 8b and 8c). This condition may not be classified as pathologic but can cause severe complications in endodontics. Among researchers there is considerable interest in DPSCs because of their high clinical potential and easy access (Gan et al 2020, Sharpe 2016). However, their origin and dynamics in vivo remain elusive. Further in-depth studies of processes such as tooth tissue regeneration after damage or formation of pulp stones will be necessary to understand the detailed behavior of these cells.

As discussed above, although the adult human dentition has lost the ability to restore enamel or roots, small islands of their original tissue, the dental epithelium, remain as ERM on the surface of roots. Clinically, ERM malfunctions may manifest themselves as apical cysts or tumor formations (Lin et al 2007, Priya et al 2015, Rincon et al 2006). Considering the stemness properties of the ERM, this structure may also have a potential role in regenerative medicine.

## Summary and Future Perspectives

A profound insight into the complex cellular machinery that is responsible for tooth growth is necessary for reconstruction and engineering of teeth. The detailed cellular organization in this process has only recently started to become identified in a more systematic way.

An obvious approach in regenerative dentistry is to exploit the properties of stem cells to build new tissue. Several studies have focused on the differentiation and use of cultured stem cells in regeneration of enamel, dentin, or periodontal tissue (Han et al 2014, Hu et al 2018, Pandya and Diekwisch 2019; Sismanoglu and Ercal 2020). However, treatment with cells that have been differentiated in vitro does not appear to be the only possible way. For example, interventions in the WNT-signaling pathway in resident cells with stem properties in damaged teeth can lead to an acceleration of regenerative dentin formation (Neves et al 2017, Zaugg et al 2020).

To conclude, much greater and deeper knowledge is needed in order to be able to characterize how various stem cell subpopulations interact and contribute to the development of human teeth. Furthermore, additional investigations should clarify in what way dental cell subpopulations are engaged in tooth homeostasis. Finally, progression of disease might potentially induce drastic changes in the cellular composition of teeth. An understanding of such events is obviously needed for new clinical approaches to regenerating damaged or lost dental tissue.

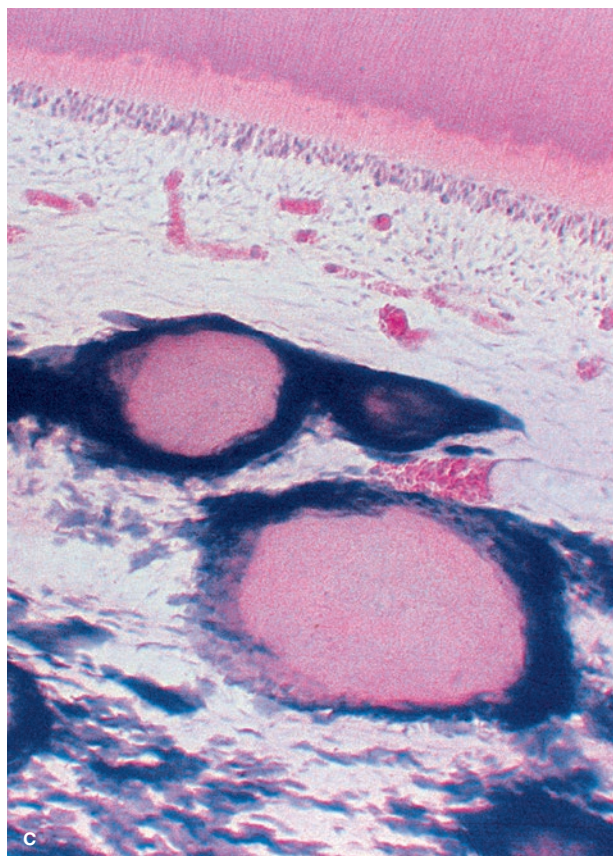
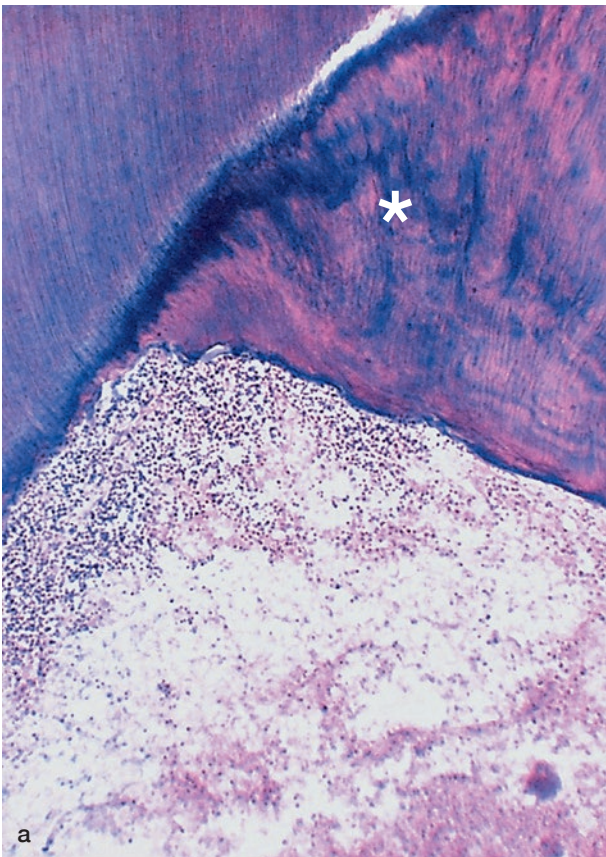


**Fig 8** (a) Tertiary dentin (\*). (b and c) Pulp stones (hematoxylin & eosin, original magnification x40). (Courtesy of M. Kukletova and L. Izakovicova Holla.)

## References

- An Z, Sabalic M, Bloomquist RF, Fowler TE, Strelman T, Sharpe PT. A quiescent cell population replenishes mesenchymal stem cells to drive accelerated growth in mouse incisors. *Nat Commun* 2018;9:378.
- Balic A, Thesleff I. Tissue interactions regulating tooth development and renewal. *Curr Top Dev Biol* 2015;115:157–186.
- Biehs B, Hu JKH, Strauli NB, et al. BMI1 represses *Ink4a/Arf* and *Hox* genes to regulate stem cells in the rodent incisor. *Nat Cell Biol* 2013;15:846–852.
- Dosedělová H, Dumková J, Lesot H, et al. Fate of the molar dental lamina in the monophyodont mouse. *PLoS One* 2015;10(5):e0127543.
- Etchevers HC, Dupin E, Le Douarin NM. The diverse neural crest: From embryology to human pathology. *Development* 2019;146(5):dev169821.
- Gan L, Liu Y, Cui DX, Pan Y, Wan M. New insight into dental epithelial stem cells: Identification, regulation, and function in tooth homeostasis and repair. *World J Stem Cells* 2020;12:1327–1340.
- Haeckel E. *Natural History of Creation: Commonly Understood Scientific Lectures on the Theory of Evolution in General and That of Darwin, Göthe and Lamarck in Particular, on the Application of the Same to the Origin of Man and Other Related Fundamental Questions of Natural Science. With Boards, Woodcuts, Systematic and Genealogical Tables [in German].* Berlin: Reimer, 1868.
- Han J, Menicanin D, Gronthos S, Bartold PM. Stem cells, tissue engineering and periodontal regeneration. *Aust Dent J* 2014;59(Suppl 1):117–130.
- Harada H, Ichimori Y, Yokohama-Tamaki T, et al. Stratum intermedium lineage diverges from ameloblast lineage via Notch signaling. *Biochem Biophys Res Commun* 2006;340:611–616.
- Harada H, Kettunen P, Jung HS, Mustonen T, Wang YA, Thesleff I. Localization of putative stem cells in dental epithelium and their association with Notch and FGF signaling. *J Cell Biol* 1999;147:105–120.
- Hu L, Liu Y, Wang S. Stem cell-based tooth and periodontal regeneration. *Oral Dis* 2018;24:696–705.
- Jensen BL, Kreiborg S. Development of the dentition in cleidocranial dysplasia. *J Oral Pathol Med* 1990;19(2):89–93.
- Juuri E, Jussila M, Seidel K, et al. Sox2 marks epithelial competence to generate teeth in mammals and reptiles. *Development* 2013;140:1424–1432.
- Juuri E, Saito K, Ahtiainen L, et al. Sox2+ stem cells contribute to all epithelial lineages of the tooth via *Sfrp5+* progenitors. *Dev Cell* 2012;23:317–328.
- Kaukua N, Shahidi MK, Konstantinidou C, et al. Glial origin of mesenchymal stem cells in a tooth model system. *Nature* 2014;513(7519):551–554.
- Kim EJ, Jung SY, Wu Z, Zhang S, Jung HS. Sox2 maintains epithelial cell proliferation in the successional dental lamina. *Cell Prolif* 2020;53(1):e12729.
- Kreiborg S, Jensen BL. Tooth formation and eruption—Lessons learnt from cleidocranial dysplasia. *Eur J Oral Sci* 2018;126(Suppl 1):72–80.
- Krivanek J, Adameyko I, Fried K. Heterogeneity and developmental connections between cell types inhabiting teeth. *Front Physiol* 2017;8:376.
- Krivanek J, Soldatov RA, Kastrić ME, et al. Dental cell type atlas reveals stem and differentiated cell types in mouse and human teeth. *Nat Commun* 2020;11:4816.
- Lin LM, Huang GTJ, Rosenberg PA. Proliferation of epithelial cell rests, formation of apical cysts, and regression of apical cysts after periapical wound healing. *J Endod* 2007;33:908–916.
- Neves VCM, Babb R, Chandrasekaran D, Sharpe PT. Promotion of natural tooth repair by small molecule GSK3 antagonists. *Sci Rep* 2017;7:39654.
- Pandya M, Diekwisch TGH. Enamel biomimetics—Fiction or future of dentistry. *Int J Oral Sci* 2019;11(1):8.
- Priya SP, Higuchi A, Fanas SA, et al. Odontogenic epithelial stem cells: Hidden sources. *Lab Invest* 2015;95:1344–1352.
- Rincon JC, Young WG, Bartold PM. The epithelial cell rests of Malassez—A role in periodontal regeneration? *J Periodontol Res* 2006;41(4):245–252.
- Seidel K, Ahn CP, Lyons D, et al. Hedgehog signaling regulates the generation of ameloblast progenitors in the continuously growing mouse incisor. *Development* 2010;137:3753–3761.
- Seidel K, Marangoni P, Tang C, et al. Resolving stem and progenitor cells in the adult mouse incisor through gene co-expression analysis. *Elife* 2017;6:e24712.
- Sharpe PT. Dental mesenchymal stem cells. *Development* 2016;143:2273–2280.
- Sismanoglu S, Ercal P. Dentin-pulp tissue regeneration approaches in dentistry: an overview and current trends. *Adv Exp Med Biol* 2020;1298:79–103.
- Thesleff I, Hurmerinta K. Tissue interactions in tooth development. *Differentiation* 1981;18(2):75–88.
- Xiong J, Gronthos S, Bartold PM. Role of the epithelial cell rests of Malassez in the development, maintenance and regeneration of periodontal ligament tissues. *Periodontol* 2000 2013;63:217–233.
- Yu T, Klein OD. Molecular and cellular mechanisms of tooth development, homeostasis and repair. *Development* 2020;147:dev184754.
- Zaugg LK, Banu A, Walther AR, et al. Translation approach for dentine regeneration using GSK-3 antagonists. *J Dent Res* 2020;99:544–551.
- Zhao H, Feng J, Seidel K, et al. Secretion of *shh* by a neurovascular bundle niche supports mesenchymal stem cell homeostasis in the adult mouse incisor. *Cell Stem Cell* 2014;14(2):160–173.

## **Heterogeneity and developmental connections between cell types inhabiting teeth**

*Jan Krivanek, Igor Adameyko, Kaj Fried*



# Heterogeneity and Developmental Connections between Cell Types Inhabiting Teeth

Jan Krivanek<sup>1</sup>, Igor Adameyko<sup>1,2\*</sup> and Kaj Fried<sup>3\*</sup>

<sup>1</sup> Department of Molecular Neurosciences, Center for Brain Research, Medical University Vienna, Vienna, Austria,

<sup>2</sup> Department of Physiology and Pharmacology, Karolinska Institutet, Stockholm, Sweden, <sup>3</sup> Department of Neuroscience, Karolinska Institutet, Stockholm, Sweden

## OPEN ACCESS

### Edited by:

Thimios Mitsiadis,  
University of Zurich, Switzerland

### Reviewed by:

Pierfrancesco Pagella,  
University of Zurich, Switzerland  
Hidemitsu Harada,  
Iwate Medical University, Japan

### \*Correspondence:

Igor Adameyko  
igor.adameyko@ki.se  
Kaj Fried  
kaj.fried@ki.se

### Specialty section:

This article was submitted to  
Craniofacial Biology and Dental  
Research,  
a section of the journal  
Frontiers in Physiology

**Received:** 25 April 2017

**Accepted:** 19 May 2017

**Published:** 07 June 2017

### Citation:

Krivanek J, Adameyko I and Fried K  
(2017) Heterogeneity and  
Developmental Connections between  
Cell Types Inhabiting Teeth.  
*Front. Physiol.* 8:376.  
doi: 10.3389/fphys.2017.00376

Every tissue is composed of multiple cell types that are developmentally, evolutionary and functionally integrated into the unit we call an organ. Teeth, our organs for biting and mastication, are complex and made of many different cell types connected or disconnected in terms of their ontogeny. In general, epithelial and mesenchymal compartments represent the major framework of tooth formation. Thus, they give rise to the two most important matrix-producing populations: ameloblasts generating enamel and odontoblasts producing dentin. However, the real picture is far from this quite simplified view. Diverse pulp cells, the immune system, the vascular system, the innervation and cells organizing the dental follicle all interact, and jointly participate in transforming lifeless matrix into a functional organ that can sense and protect itself. Here we outline the heterogeneity of cell types that inhabit the tooth, and also provide a life history of the major populations. The mouse model system has been indispensable not only for the studies of cell lineages and heterogeneity, but also for the investigation of dental stem cells and tooth patterning during development. Finally, we briefly discuss the evolutionary aspects of cell type diversity and dental tissue integration.

**Keywords:** odontogenesis, tooth, dental development, stem cells, cell heterogeneity, dental pulp, odontoblast, ameloblast

## HETEROGENEITY OF THE DENTAL EPITHELIAL COMPARTMENT

Epithelia are reasonably simple tissues, and yet they are very powerful. Controlled heterogeneity of the epithelial cell populations enables multiple variations of reasonably similar structures, and is necessary for the general composition of the tooth. Epithelium-based morphogenesis generates remarkable examples of complexity, found in e.g., feathers, hair follicles, multiple glands, and finally, teeth. Indeed, epithelia are dominant guides not only for themselves, but also for underlying cell types, for example dental mesenchyme. In teeth, multiple epithelial cell subtypes are interacting with other tissues, maintaining stem cell properties, producing the tissue bends, and generating ameloblasts—the key enamel-producing cell type.

Beginning at the very onset of tooth development, a rather uniform dental epithelium gives rise to a folded structure known as a dental lamina, which in turn yields a complex structure of quite different epithelial-derived cells. These include the cells of the inner (IEE) and the outer (OEE) enamel epithelium, which meet at the folded cervical loops. The IEE is a necessary interaction partner for underlying mesenchymal cells. Under the influence of IEE, the mesenchyme differentiates toward the odontoblast lineage, and conversely, the mesenchyme directs the IEE into

ameloblast differentiation (Balic and Thesleff, 2015). Between the IEE and the OEE is a loosely composed cell assembly, the stellate reticulum, where stem cells that give rise to all mentioned epithelial compartments are located. The cells of the stellate reticulum are separated from the IEE by a very thin cell layer at the inner rim of the IEE, the stratum intermedium. The stem cells between the IEE and the OEE enable growth of the epithelium, and in continuously growing teeth they contribute to the regeneration of epithelium and stratum intermedium, respectively (Juuri et al., 2012).

Specification of the dental epithelium is initiated by mutual interactions with ectomesenchyme. The ectomesenchyme is derived from migrating cranial neural crest in places where teeth are going to develop (Koussoulakou et al., 2009). In this way, dental placodes arising from epithelial thickenings are formed. Further cell divisions of the dental epithelium give rise to tooth buds, which as yet consist of uniform cells (Koussoulakou et al., 2009). Differentiation and early shaping of the future tooth is initiated by the formation of the primary enamel knot, a signaling cell complex which arrests cell division in the most apical part of the bud, leading to proliferation in lateral parts only (Vaahotkari et al., 1996; Jernvall and Thesleff, 2000; Thesleff et al., 2001; Harada and Ohshima, 2004). With subsequent development, the tooth bud will advance into the cap stage, where the first differentiation of cells gives rise to the cervical loops with IEE/OEE as well as the stellate reticulum possessing stemness activity. Depending on future tooth type, other enamel knots are later formed which provide for the vast heterogeneity of all different tooth shapes that have evolved within different species (Jernvall and Thesleff, 2012).

In the continuously growing mouse incisor, the entire spectrum of developmental and adult stages of epithelial cells are seen throughout life. This includes SC's (stem cells) maintaining their niche and producing a highly mitotically active population of TAC's (transit amplifying cells). These non-differentiated cells are pushed into differentiation pathways by numerous molecular factors from the environment (mainly FGF, WNT, BMP, and Shh pathways), but also by influences from cell movements and physical forces in surrounding tissues. In spite of the fact that the initial phases of cell specification are more or less similar for both mesenchymal and epithelial compartments, the molecular mechanisms maintaining these niches are substantially different (Thesleff and Tummers, 2008; Koussoulakou et al., 2009).

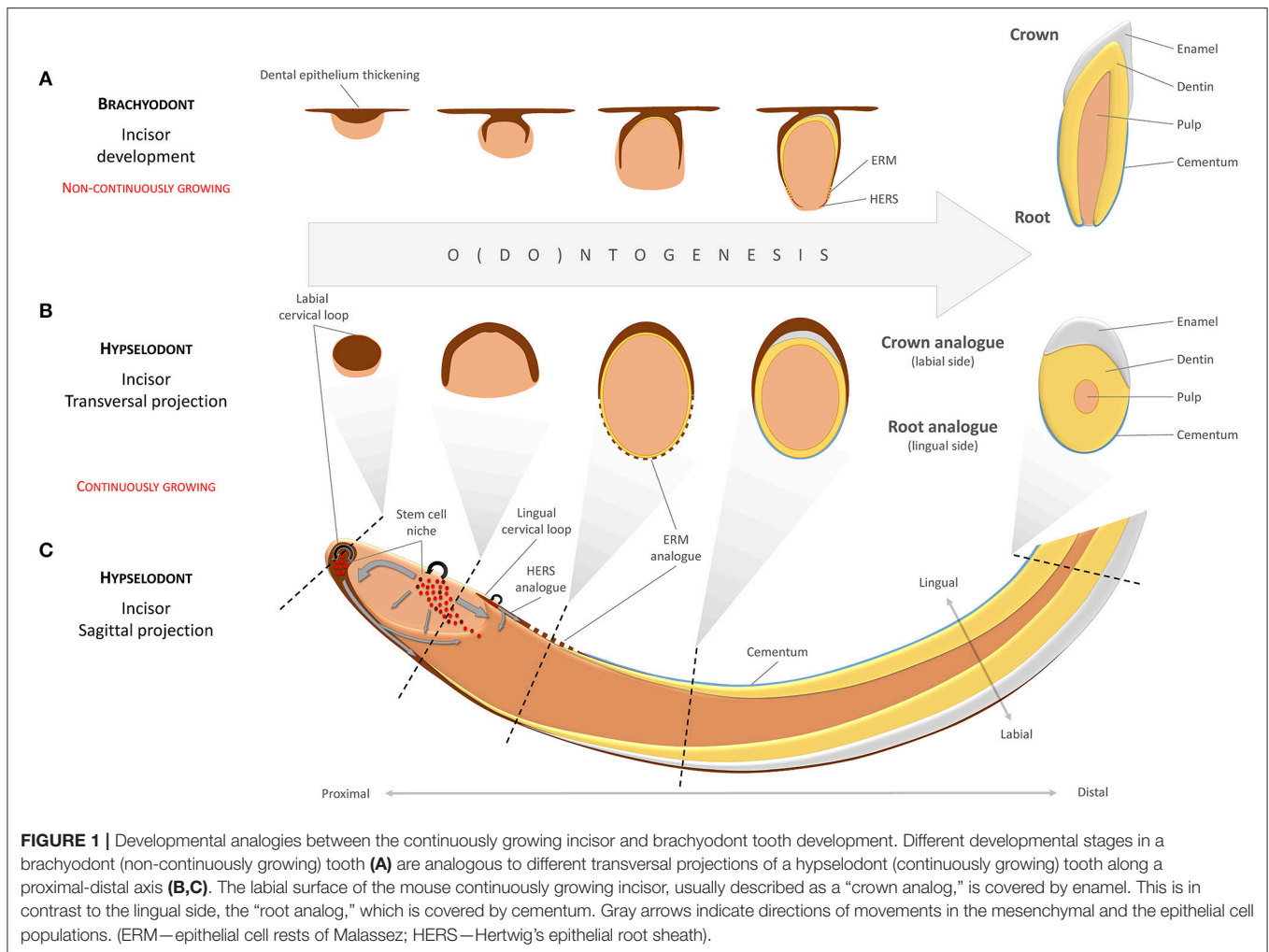
Incisor-renewing epithelial stem cells are located in the most apical part of the tooth at the cervical loop, which consists of folded epithelium (the morphologically and functionally distinct OEE and IEE). The SC niche is lodged between the OEE and IEE, respectively (Harada et al., 1999; Juuri et al., 2012). There are obvious functional differences between the labial and the lingual surfaces of the incisor. In spite of the fact that both the labial (LaCL) and the lingual (LiCL) cervical loop possess the capacity to regenerate, only the LaCL is capable of forming functional enamel-producing ameloblasts on the side of the IEE (**Figure 1**). Consequently, since it generates enamel, the labial aspect is often called "crown analog." In parallel to this, the LiCL, is referred to as "root analog" since it resembles developing roots that lack ameloblasts but possess cementoblasts and cementum (Stern,

1964; Warshawsky, 1968; Beertsen and Niehof, 1986; Balic and Thesleff, 2015). Using Sox2-traced mice, it has been shown that the slow-cycling stem cells located in the LaCL remain in their locus for long periods, and have the potential to continuously produce cells for both OEE, IEE, and functional ameloblasts (Juuri et al., 2012).

SC's are maintained through a highly complex process that depends on interactive signaling between dental papilla/pulp and epithelium. Distinct pathways and feedback loops are used for keeping SC's in the stellate reticulum active. FGF3 and FGF10 are major molecular factors in this process. They are produced by the mesenchyme near the cervical loop and subsequently interact with FGFR1b and FGFR2b receptors in the cervical loop (Harada et al., 1999, 2002, reviewed in Balic and Thesleff, 2015). Different knockout experiments have shown that LaCL renewal becomes impaired after targeting of FGF ligands or receptors (Wang et al., 2007; Klein et al., 2008; Lin et al., 2009). However, if negative FGF feedback loops controlled by Sprouty genes are disrupted in the pulp, enamel is produced also by LiCL (Klein et al., 2008). Other pathways that are important for maintaining the epithelial SC niche include Notch, BMP, and Wnt (reviewed by Tummers and Thesleff, 2003; Li et al., 2017).

During the past few years, a number of studies have appeared which have increased the understanding of the complex 3-dimensional aspects of the LaCL/LiCL and associated movements of cells that generate hard matrices (Charles et al., 2011; Juuri et al., 2012; Cox, 2013; Lesot et al., 2014). Sox2+ stem cells produce progeny that migrate to the enamel epithelium, but also cells that maintain the stellate reticulum itself. Cells are moving further in the labial-distal direction and differentiate into ameloblasts. This process is regulated by an Shh positive feedback loop. Cells are also migrating medio/latero-distally to the IEE/OEE ridge, a process which is marked by Wnt inhibitor SFRP5 expression (Seidel et al., 2010; Juuri et al., 2012). Populations of Sox2+, Sfrp5+, and Shh+ cells are subsequently located in different, non-overlapping positions (Seidel et al., 2010; Juuri et al., 2012).

The entire developmental history of ameloblasts (and also odontoblasts) is literally sealed in the inner structure of enamel (dentin respectively). Ameloblasts are moving during matrix secretion, but so far only little is known about the exact mechanism of this movement (**Figure 2**). Enamel is created by walled matrix blocks which form enamel rods during the ameloblast secretory stage. The rods become fully mineralized within the maturation phase (Smith, 1998; Zheng et al., 2014). The formation of enamel is characterized by a complex microstructure, making it the hardest tissue of the body. Hardness itself is dependent not only on a high content of hydroxyapatite crystals, but importantly, also on the micro-patterning of the enamel. Enamel decussation, where bundles of rods cross each other throughout the distance from the enamel-dentine junction to the outer enamel surface, is highly variable in different species. It is adapted to animal life conditions in order to provide specific hardness and ability to absorb mechanical energy. The extremely organized rod decussation in mouse enamel explains how it can be so hard in spite of its relative small size in comparison to e.g., human teeth. Human



enamel, in turn, have different decussation patterns as compared to mouse enamel. There is a wavy structure in inner human enamel which is able to stop inward spreading of cracks from the straight rod structure of the outer enamel (Skobe and Stern, 1980; Bajaj and Arola, 2009). Interestingly, enamel protein secretion is under control of circadian “clock” genes which controls enamel production differently during day and night (reviewed in Zheng et al., 2014). During the entire secretory phase, each ameloblast produces one enamel rod to form organized matrix with desired mechanical abilities. When the secretory stage is over, one quarter of ameloblasts undergo apoptosis and after the maturation phase only half of the ameloblasts remain to form a protective layer, which disappears completely in human teeth during eruption (Smith, 1998). Some evidence suggests that TGF- $\beta$ 1 with the Smad2/3 signaling pathway are involved in the induction of apoptosis in the maturation phase (Tsuchiya et al., 2009).

Thus, the heterogeneity and functional division between epithelial subtypes in the embryonic and mature teeth provides for tissue-tissue interaction and production of hard matrix at the correct time and location. It enables shaping and morphogenesis, self-renewal, growth and many other functions. Generation of

epithelial subtypes in the tooth is not well understood and requires extensive further investigations.

#### Key papers:

- Balic and Thesleff (2015).
- Cox (2013).
- Yu et al. (2015).
- Koussoulakou et al. (2009).

## HETEROGENEITY OF THE MESENCHYMAL COMPARTMENT

The mesenchymal compartment of the fully formed tooth includes various cell types and subtypes that are largely represented by odontoblasts, diverse pulp cells and dental mesenchymal stem cells together with transiently amplifying cells (if retained). Hence, the pulpal cells have multifarious identities, originating in an intricate developmental history.

Mouse tooth development is based on dynamic interactions between epithelial and mesenchymal compartments. The

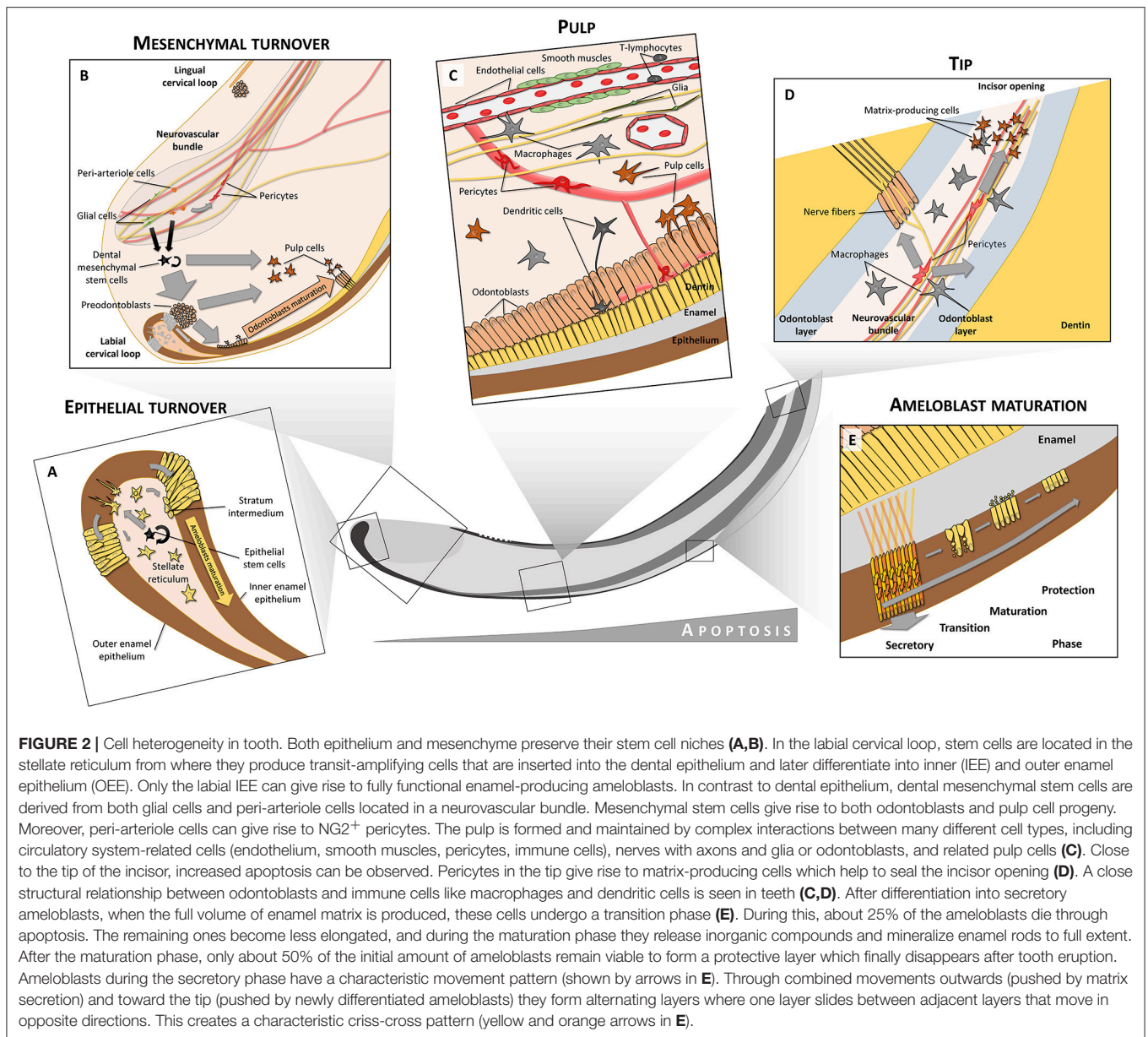


**FIGURE 2 |** Cell heterogeneity in tooth. Both epithelium and mesenchyme preserve their stem cell niches (A,B). In the labial cervical loop, stem cells are located in the stellate reticulum from where they produce transit-amplifying cells that are inserted into the dental epithelium and later differentiate into inner (IEE) and outer enamel epithelium (OEE). Only the labial IEE can give rise to fully functional enamel-producing ameloblasts. In contrast to dental epithelium, dental mesenchymal stem cells are derived from both glial cells and peri-arteriole cells located in a neurovascular bundle. Mesenchymal stem cells give rise to both odontoblasts and pulp cell progeny. Moreover, peri-arteriole cells can give rise to NG2<sup>+</sup> pericytes. The pulp is formed and maintained by complex interactions between many different cell types, including circulatory system-related cells (endothelium, smooth muscles, pericytes, immune cells), nerves with axons and glia or odontoblasts, and related pulp cells (C). Close to the tip of the incisor, increased apoptosis can be observed. Pericytes in the tip give rise to matrix-producing cells which help to seal the incisor opening (D). A close structural relationship between odontoblasts and immune cells like macrophages and dendritic cells is seen in teeth (C,D). After differentiation into secretory ameloblasts, when the full volume of enamel matrix is produced, these cells undergo a transition phase (E). During this, about 25% of the ameloblasts die through apoptosis. The remaining ones become less elongated, and during the maturation phase they release inorganic compounds and mineralize enamel rods to full extent. After the maturation phase, only about 50% of the initial amount of ameloblasts remain viable to form a protective layer which finally disappears after tooth eruption. Ameloblasts during the secretory phase have a characteristic movement pattern (shown by arrows in E). Through combined movements outwards (pushed by matrix secretion) and toward the tip (pushed by newly differentiated ameloblasts) they form alternating layers where one layer slides between adjacent layers that move in opposite directions. This creates a characteristic criss-cross pattern (yellow and orange arrows in E).

mesenchymal compartment consists of the condensed mesenchyme during early embryonic development. This mesenchyme will eventually differentiate into pulp tissue and dentin-producing odontoblasts.

Mouse molars are stationary during adult life in terms of cell dynamics, while the incisors keep growing throughout the entire life. During this growth, pulp cells and odontoblasts are renewed by dental mesenchymal stem cells that reside in the area between the cervical loops at the tooth apex. Recently it was discovered that these mesenchymal stem cells are heterogeneous and demonstrate differences in terms of markers that are expressed and in the amount of progeny. For instance, slow cycling cells in the dental pulp of mouse incisor express Thy1 (CD90). In line with this, genetic tracing with Thy1-Cre has

demonstrated a long-term presence of the Thy1<sup>+</sup> progeny in the tooth (Kaukua et al., 2014). This progeny consisted of 10–20% of all odontoblasts and pulp cells, corresponding to the actual proportion of Thy1<sup>+</sup>/slow cycling cells among all slow cycling cells at the tooth apex (Sharpe, 2016).

Another marker that co-localizes with slow cycling cells is Gli1 (Zhao et al., 2014). In line with the results obtained with Thy1<sup>+</sup> cells, lineage tracing in the Gli1-CreERT2 mouse line demonstrated the presence of a long-lasting population consisting of pulp cells and odontoblasts. The proportion of Gli1-traced cells appeared to be very high, close to 100%. Dental mesenchymal stem cells expressing Gli1 are located around and inside the neuro-vascular bundle, and are Shh-dependent. One of the key sources of Shh inside of the tooth has turned out

to be pulpal sensory nerves (Zhao et al., 2014). Accordingly, experimental denervations of mouse incisors result in tooth growth arrest, confirming that the nerve is important for tooth growth and self-renewal (Kaukua et al., 2014; Zhao et al., 2014).

The actual developmental origin of dental mesenchymal stem cells is still unclear. It is obvious that they are progenies of the neural crest. However, it is not yet established whether most of the dental mesenchymal stem cells form at the end of embryonic development, when general proliferation decreases inside of the tooth, or if these stem cells segregate much earlier and then carry out their key role postnatally. Some of the dental mesenchymal stem cells are supplied by the innervation (see below). Peripheral glial cells can be recruited into the mesenchymal stem cell niche postnatally in low numbers. During early age the contribution of these glia-derived mesenchymal cells to odontoblasts and pulp cells is relatively low, but it tends to increase toward the end of the animal's life (Kaukua et al., 2014).

Much attention has been focused on the identification of dental mesenchymal stem cells *in vitro* and *in vivo* after damage. However, these studies often do not relate directly to the physiological *in vivo* tooth self-renewal situation (Sloan and Waddington, 2009). At present, it seems that further long-term lineage tracing experiments are needed in order to resolve this issue.

Clonal genetic tracing experiments involving color multiplexing with Confetti reporters demonstrated that an individual mesenchymal stem cell is bipotent, and can give rise to both pulp and odontoblast fates. Recent data suggests that this fate selection depends on the extrinsic signals potentially provided by the epithelial compartment. Thus, odontoblasts are induced only in association with the epithelial layer at the tooth apex (Kaukua et al., 2014). Further studies of the regulation of the apical stem cell compartment that produces spatially defined population of transiently amplifying progenitors will hopefully elucidate at which level of cellular hierarchy the fate split occurs.

Odontoblasts undergo further maturation and reorganize their branched processes simultaneously with intense matrix production. In the mature phase, odontoblast express certain ion channels and other markers, which suggest that they may subserve a sensory function (reviewed in Chung et al., 2013). This could be achieved through communications with associated nerve fibers and/or through interactions with immune cells.

Mature odontoblasts from mouse incisors demonstrate heterogeneity in terms of cell configuration: a fraction of odontoblasts appear pyramidal in shape with their nuclei in a position next to the matrix and without any process entering into the dentinal tubule (Khatibi Shahidi et al., 2015). The heterogeneity of other mesenchymal cells in the mature dental pulp is not well understood. Among those with a hitherto unknown identity are perivascular pulp cells that contact pericytes, and morphologically aberrant cells in the layer immediately below the odontoblasts. These latter cells project fine processes deep into the odontoblast layer toward the hard matrix (Khatibi Shahidi et al., 2015). The function of these projections is unclear.

Thus, the heterogeneity of the mesenchymal compartment is much higher than is commonly thought, starting from

different subtypes of stem cells and extending all the way to morphologically diverse populations of odontoblasts.

#### Key papers:

- Sharpe (2016).
- Sloan and Waddington (2009).

## CELL TYPES OF THE DENTAL FOLLICLE AND ROOT FORMATION

The root system anchors the tooth to the alveolar bone of the maxilla or mandible. It transfers occlusal forces to the jaw bones, and monitors these forces through an elaborate periodontal proprioceptive innervation (Trulsson and Johansson, 2002). The cells that give rise to root tissue are of both epithelial and mesenchymal origin, but the epithelium has mainly signaling functions. The mesenchymal cells differentiate along distinctly dissimilar paths and form pulp, dentin, cementum and the periodontal ligament. The diversity and putative varying functions among the cell types that create these different tissues are largely unknown. Likewise, it is not known in detail how they differ from similar cell types in other locations, e.g. cementoblasts vs. odontoblasts or osteocytes.

During early odontogenesis, cells at the periphery of the condensed dental mesenchyme form the dental follicle. In teeth that do not grow continuously, these cells will differentiate into cementoblasts and periodontium and produce the root segments of the tooth. In this process, the cervical loop will lose its central cellular content so that only a double layer of basal epithelium remains (the epithelial diaphragm). This double layer constitutes Hertwig's epithelial root sheet (HERS), an important structure in root development, responsible for shaping and scaling of roots by physical division of the dental papilla and the dental follicle (Xiong et al., 2013). After matrix production by odontoblasts has been commenced, HERS is fenestrated into small fragments and remains in the periodontal connective tissue as the epithelial cell rests of Malassez (ERM) (Figure 1). The ERM seems to play an important role in periodontal ligament homeostasis, and contributes to alveolar bone remodeling (Diekwisch, 2001; Luan et al., 2006).

Neither HERS nor ERM seem to have much potential for further growth, but HERS plays an important role in root elongation by secreting Shh. This secretion, which is under the control of BMP/TGFbeta/SMAD signaling, probably safeguards appropriate levels of Shh in the dental mesenchyme that forms the root (Nakatomi et al., 2006; Huang et al., 2010). Thus, experimental manipulations of Shh in this region results in shortening of the root (Liu et al., 2015). Furthermore, Wnt/beta-catenin and BMP/TGFbeta activity in odontoblasts and dental mesenchyme influence root growth, although the precise mechanisms involved are still unclear (Kim et al., 2013; Rakian et al., 2013; Wang et al., 2013).

The properties of the mesenchymal progenitors from the dental follicle that eventually will give rise to the tissues of the root have not been fully understood. There seem to be clearcut similarities between osteoblast and cementoblast differentiation, since both Runx2 and Osterix (Osx) have vital functions in these

two processes (Nakashima et al., 2002). Conditional deletion of *Osx* in dental mesenchymal cells leads to a reduced cellular cementum formation and lowered dentin matrix protein (DMP1) gene expression in cementocytes (Cao et al., 2012).

Recently, in a series of lineage tracing and genetic labeling/mutation studies, it was shown that *Osx*-expressing mesenchymal dental follicle progenitors contribute to all root tissues: odontoblasts, pulp cells, cementoblasts and some periodontal ligament (PDL) cells (Ono et al., 2016). Furthermore, cementoblast differentiation and tooth root formation requires the parathyroid hormone/parathyroid hormone-related protein (PTHrP) receptor PPR in these progenitors. PTHrP is expressed in the dental follicle as well, and it was suggested that its primary target is *Osx*-lineage progenitors involved in PPR signaling. PTHrP can in this way influence root formation, tooth eruption and PDL attachment (Ono et al., 2016), which is underlined by the fact that an autosomal dominant mutation of the PPR causes a primary failure of tooth eruption in human (Frazier-Bowers et al., 2014). However, detailed information concerning the time-related activities of the PTHrP-PPR signaling system in cementogenesis, general root formation and tooth eruption is still lacking.

Membrane-type matrix metalloproteinase 1 (MT1-MMP) is also indispensable in the organization of the dental follicle/PDL region and dental root development. Thus, a selective knock-out of MT1-MMP in *Osx*-expressing mesenchymal cells yielded multiple defects: short roots, defective dentin formation and mineralization, and reduced alveolar bone formation. This suggests that MT1-MMP activity in the dental mesenchyme is vital for tooth root formation and eruption, e.g. by processing signaling molecules that affect Wnt and Notch signaling pathways during dental development (Xu et al., 2016).

To summarize, spatiotemporal interactions between epithelium and mesenchyme will in due course form the dental follicle and subsequently advance the establishment of root dentin, cementum and periodontal tissues. Complex molecular networks that involve a multiplicity of cell types will determine features necessary for adequate function at specific sites, such as root number, shape and trajectory.

#### Key papers:

- Diekwisch (2001).
- Huang et al. (2009).
- Li et al. (2017).

## CELL TYPES RELATED TO INNERVATION AND VASCULAR SYSTEM

Teeth are complex organs that require a vascular system to transport gases, nutrients and metabolites as well as a sensory system to, among other things, control biting strength. Indeed, the abundant pulpal innervation is a hallmark of the mammalian tooth. This is perhaps not surprising, if one considers the proposal that the tooth is a modified pre-historic primary mechanosensory organ (Northcutt and Gans, 1983). Throughout millions of years, its pulpal nerve fibers may gradually have

evolved into transducers of signals that evoke pain sensations only (see Fried et al., 2011).

The innervation of the mouse tooth provides a very useful prototype system for studies of mammalian nerve-target interactions during development, in adult life homeostasis, after injury and in senescence. The mouse possesses two types of teeth with different innervation patterns. The three molars develop, function and are innervated much as other mammalian molars, including human. The continuously growing rodent incisor renews its tissue on a monthly basis, thus offering a model structure that includes highly active stem cell regions throughout adulthood. Its innervation can best be described as permanently immature.

During fetal life, pioneer trigeminal axons are present in the branchial/pharyngeal arches at the earliest stages of mouse development, well before the initial signs of tooth development are evident. These axons branch and innervate the developing jaw processes, but avoid the areas of mesenchymal condensations that mark the sites of tooth formation (reviewed by Fried and Gibbs, 2014). The issue of whether nerve fibers actually may have an inductive role in tooth initiation, as is the case in e.g. salivary glands (Nedvetsky et al., 2014) is still unresolved. Tooth explants that are removed grow without nerve fibers *in vitro* (Lumsden and Buchanan, 1986; Sun et al., 2014), but it cannot be excluded that nerves influence the ectomesenchyme or dental epithelium earlier, when teeth actually are induced. To experimentally address this in the mouse, however, would require sophisticated nerve ablation experiments that as yet have not been performed.

Throughout fetal development, mandibular and maxillary sensory innervation proceeds. Basket-like axonal arborizations form around the incisor and molar tooth buds. However, although surrounding submucosa and other soft tissues become highly innervated, no axons enter the condensed dental mesenchyme/dental papilla until several days postnatally. This is in spite of the fact that the future dental pulp is among the most densely innervated tissue in the body. Unexpectedly and perhaps explaining the delay in tooth sensory innervation, these nerve networks have been shown to serve as stem cell niches for the developing tooth.

Textbooks have for decades taught that dental mesenchyme and odontoblasts are derived directly from migrating cranial neural crest cells. However, recent data have established an additional important glial source. Using genetic tools in mouse model systems, it was shown that multipotent Schwann Cell Precursors (SCP) of the axonal networks that are associated with the tooth anlagen leave their nerve branches and contribute with pulp cells as well as odontoblasts in clonal configurations.

For experiments, advantage was taken of the fact that PLP1 and Sox10 are expressed in cranial neural crest, but after migration around embryonic days (E)9–10, they are retained in SCPs and not in mesenchyme. Lineage tracing studies with PLP-CreERT2 and Sox10-CreERT2 mice where recombination was induced at E12.5 and/or later showed traced SCP in peripheral nerves close to tooth placodes. Around early and late bell stage, traced SCP-derived progeny formed streams of cells consisting of dental mesenchymal stem cells, pulp cells and odontoblasts in

the developing tooth. A similar mechanisms whereby trigeminal nerve glia contributes with pulpal cells continues to operate during adult renewal of the continuously growing mouse incisor (Kaukua et al., 2014).

A complex interplay between deployed incisor pulpal stem cells and nerves is indicated by the fact that Shh secreted from nerve endings within the neuro-vascular bundle seems to warrant continuous tooth growth. This is probably by acting on associated Gli1<sup>+</sup> dental mesenchymal stem cells (including SCP), see **Figure 2B** (Zhao et al., 2014). Presumably, such a mechanism is at hand during embryonic odontogenesis as well.

In contrast to nerve fibers, blood vessels, as detected by endothelial markers, are present in mouse molars as early as at E16 (early bell stage; Nait Lechguer et al., 2008). These blood vessels are composed of mesoderm-derived endothelial cells, which invade the dental papilla at the late cap stage, and form the vascular network *in situ*. Thus, the blood supply is created through vasculogenesis (newly formed vessels) rather than angiogenesis (ingrowth of vessels from surrounding pre-existing vessels; Rothová et al., 2011). It is unclear whether these early blood vessels serve as guiding cues for the axons that arrive later. However, it seems likely that true pulpal neurovascular bundles that carry arteries form only later. Thus, in limb skin, the pattern of peripheral nerve branching provides a template for branching of the emerging arterial vascular network. The specification is performed through a loop between nerve-derived VEGF and the endothelial VEGF-coreceptor NRP1 (Mukouyama et al., 2005). The same process may occur in the dental papilla/pulp once axons have entered.

In adult tissue, dental pericytes have attracted specific interest as a potential source of mesenchymal stem cells. They dwell on the abluminal surface of endothelial cells in the microvasculature of the pulpal tissue. These cells in mouse incisor have the capacity to transform into odontoblasts in response to injury, but also it has been recently shown that in non-continuously growing molars perivascular  $\alpha$ SMA<sup>+</sup> cells are able to differentiate into odontoblast to seal the injury site (Feng et al., 2011; Vidovic et al., 2017). Mouse incisors are continuously abraded during the lifespan, and undergo constant damage at the tip leaving exposed pulp underneath. It was recently shown that the opening of the tip of the incisor is continuously sealed with dentin-like matrix which is produced by cells that differentiate from perivascular pericytes (Pang et al., 2016). NG2-CreERT2 and Nestin-Cre genetic tracing showed that large numbers of pericyte-derived cells are produced within the tip, and some of them have odontoblast-like shapes. Thus, pericytes at this site serve as a reservoir for reparative cells, and help to maintain tissue homeostasis.

The spatial and temporal patterns of dental papilla pericyte development is not known, and consequently it is not known if pericytes have any specific roles in the organogenesis (aside from vasculogenesis) of the tooth.

Taken together, in addition to a number of classical functions performed by the vascular and nervous systems, the heterogeneity of nerves, glial cells and vessel-associated cell types accommodates for advanced reparative capacities and self-renewal of teeth.

### Key papers:

- Kaukua et al. (2014).
- Pang et al. (2016).
- Zhao et al. (2014).
- Vidovic et al. (2017).

## DIVERSITY OF IMMUNE CELLS DWELLING IN THE PULP

As mentioned above, the dental pulp is far from being a homogeneous tissue. Although most of the pulp is composed of mildly diverse cells of the mesenchymal compartment, it also hosts the immune system which has an as yet uncertain degree of cellular heterogeneity. The fact that the pulp is encased in a mineralized cavity makes it demarcated and suitable for both general and pulp-specific studies of the immune system during development, self-renewal, infection and homeostasis.

The environment within the tooth must be accurately surveyed for signs of infectious invasion. Knowledge of the immune cell signature of the pulp is vital in efforts to find new ways to protect teeth from infections. Additionally, immune cells may potentially influence hard matrix repair. The innate immunity response to bacteria invading the teeth includes the arrival of phagocytic cells and the generation of various inflammatory cytokines. When a dental infection becomes chronic, the adaptive immunity response kicks in: different subtypes of T-cells infiltrate the inflamed teeth (AlShwaimi et al., 2009). The most abundant T-cell type in the dental pulp is CD8<sup>+</sup> cells (Hahn et al., 1989; Izumi et al., 1995; Sakurai et al., 1999). Their functions in non-inflamed tooth are currently unclear, although it is known that these cells are potent protectors against viral infections and are capable of augmenting phagocytosis. CD8<sup>+</sup> T-lymphocytes are migratory, and can travel long distances from the site where they initially encountered an antigen (Marshall et al., 2001; Masopust et al., 2004). Some studies suggest that their main function in the pulp is immunosurveillance (extensively reviewed in Hahn and Liewehr, 2007).

Treg lymphocytes, a population known to prevent autoimmunity, are also found in low numbers around the roots of mouse molar teeth. However, in the case of tooth damage with periapical lesions, Foxp3-expressing cells (Foxp3 is a master gene for Treg) infiltrate the region around the lesion and dramatically increase in numbers in a time-dependent fashion. Additionally, these cells appear in large quantities in cervical lymph nodes after initiation of tooth pulp infection. This strongly suggests that Treg lymphocytes might play some role in the local immune response and the general regenerative capacity in teeth (AlShwaimi et al., 2009).

Macrophages and dendritic cells together represent one of the major immunocompetent cell types that are protective against dental infection and are necessary to remove senescent cells. These phagocytic cells are widely spread throughout the pulp cavity and can also project into dentinal tubules. During late embryonic development, around embryonic day 16, F4/80<sup>+</sup> and CD68<sup>+</sup> macrophages invade mouse molars and then continue

to increase their numbers. M-CSF secreted by pulp cells plays a significant role in maintenance and proliferation of resident macrophages. It has been shown that a majority of the mouse pulpal macrophages proliferate locally and maintain their pool without additional recruitment from the blood supply (Iwasaki et al., 2011). Furthermore, secretion of OPN (Osteopontin) and M-CSF by immune cells correlates with the deployment of macrophages along the pulp-dentin border exactly when reparative matrix allocation commences in a mouse model of tooth transplantation. It was suggested that secretion of these soluble ligands that influence macrophages can stimulate differentiation of odontoblasts and production of reparative dentin (Saito et al., 2011). Other studies also highlighted the possibility that macrophages and dendritic cells might regulate the function and differentiation of odontoblasts (Ohshima et al., 1995; Tsuruga et al., 1999; Nakakura-Ohshima et al., 2003).

Dendritic cells demonstrate an exceptional capacity to capture antigens with their long filaments, and to process them. Two types of dendritic cells seem to be present in the dental pulp: CD11c<sup>+</sup> sentinel and F4/80<sup>+</sup> interstitial cells (Zhang et al., 2006). The CD11c<sup>+</sup> dendritic cells express toll-like receptors two and four, they are highly migratory and can move around the pulp in case of infection or even travel to the lymph nodes. Quite on the opposite, F4/80<sup>+</sup> cells show low migratory activity and are rather residential. Also, these subtypes of immune cells show regional differences in their distribution inside of the mouse molar tooth (Zhang et al., 2006). Most of the pulpal dendritic cells are coagulation factor 13a (FXIIIa)<sup>+</sup> (Nestle et al., 1993; Valladeau and Saeland, 2005) and can be further subdivided into a larger CD14<sup>+</sup>/CD68<sup>+</sup> group and a smaller CD14<sup>+</sup>/CD68<sup>+</sup>/CD1a<sup>+</sup> subpopulation (Okiji et al., 1997). Some HLA-DR<sup>+</sup> dendritic cells appear negative for FXIIIa/CD1a markers (Hahn and Liewehr, 2007). Dendritic cells are often identified at interfaces, including the border between pulp and odontoblast layer as well as along large blood vessels. Dendritic cells spend only a part of their time inside of the dental pulp. After local surveillance activity and detection of e.g., bacterial antigens, they travel to the lymph nodes via lymphatic vessels and present the antigens to T-lymphocytes (Okiji et al., 1997; Randolph et al., 2002; Hahn and Liewehr, 2007; Bhingare et al., 2014).

When a tooth loses its nerve supply, the numbers of immune cells drop. This raises various questions regarding interactions between local nerves and the immune system (Fristad et al., 1995). In line with this, dendritic cells increase in numbers as the density of dental nerves increases during caries progression (Sakurai et al., 1999).

In general, very little is known about when and how various immune cell populations arrive to the mouse teeth during development. For many of these dental immune cell types we still do not know their immediate and precise developmental origin although all of them are generated during late embryonic and postnatal haematopoiesis. Finally, it is not clear if there is any substantial difference in immune cell type composition between continuously growing incisors and molars. These issues require further investigations.

### Key papers:

- Hahn and Liewehr (2007).
- Farges et al. (2015).
- Perdiguero and Geissmann (2016).

## EVOLUTIONARY ASPECTS OF CELL TYPE HETEROGENEITY IN TEETH

Every tissue or organ has its evolutionary origin. The composition of a tissue, in terms of cell types, stands behind the overall functionality. Heterogeneity of cell types increases throughout the evolution in every functional entity. Novel cellular functions are elaborated, while older functions become more and more discretely partitioned to the specializing cells during increasing labor division as a function of evolutionary time (Arendt et al., 2016).

The key events of the origin of teeth are the elaboration of dentin (odontoblast) and enamel (ameloblast), and the development of epithelial-mesenchymal interactions that enable the construction of the morphogenetically complex entities.

Apparently, when it comes to the competence of the epithelium to engage mesenchyme into complex morphogenesis, teeth are not unique among the different epithelial appendages (Hughes et al., 2011). Indeed, various skin glands, hairs and feathers demonstrate a very conserved signaling and initiation mechanisms including involvement of the EDAR pathway or expression of Shh at the early steps (Pispa and Thesleff, 2003; Mikkola, 2011). Such an archetypical developmental program shared by several distinct appendages suggests their common origin from some prototypical gland-like structure. In line with this, differences in tooth histology and geometrical features between different species represent the outcomes from minor tinkering with signaling pathways rather than being derived from major genetic divergences (Tummers and Thesleff, 2009). A conserved pattern is seen not only in the morphological and/or molecular similarities between groups that have functional teeth (mammals, reptiles, amphibians or fishes) but also in recent birds despite the fact that they lost the ability to form teeth some 70–80 million years ago. Still, birds retain the evolutionary conserved tooth-forming pathways in both oral epithelium and ectomesenchyme. *In vitro* co-culture and *in vivo* transplantation experiments demonstrated that chick epithelium can initiate dental development when combined with mouse mesenchyme and vice versa (Wang et al., 1998; Mitsiadis et al., 2003). While the origin of epithelial-mesenchymal interaction can be logically envisioned and even experimentally tested in the future, the path leading to the emergence of fundamental cell types, such as odontoblasts or ameloblasts, is neither simple nor intuitive.

In light of this, the evolution of odontodes and the evolution of neural crest fates represent two important lines deserving a brief discussion.

Two different theories exist regarding the origin of tooth-forming epithelium (Soukup et al., 2008; Fraser et al., 2010). Historically, teeth were first considered to be some kind of external odontodes originating from the ectodermal epithelium. This “outside-in” theory was based on the structural

similarity between teeth and odontodes covering the bodies of jawless fishes. Indeed, odontodes often show analogous structural characteristics, including dentin that originates from ectomesenchyme and enameloid that closely resembles enamel of extant vertebrates. An opposing “inside-out” theory suggested that teeth originated from endodermal epithelium. It was based on findings that teeth-like structures were present deep in the pharynx even in the ancient jawless fishes (Soukup et al., 2008; Koussoulakou et al., 2009). By now, it seems rather likely that dentin and enamel as matrix types were elaborated during the early evolution of odontodes. This is supported by the example of *Psarolepis romeri*, an early Devonian bony fish, that had enamel-covered dermal odontodes and teeth covered with only dentin. The presence of enamel covering dentin as well as the similar situation with ganoin covering odontode scales suggest that such a composite structure preceded the combination of enamel and dentin in primitive teeth. *Lepisosteus oculatus* (the spotted gar) shows an epidermis-localized expression of enamel-specific genes. These genes are likely used to build ganoin—a matrix similar to enamel (Qu et al., 2015). In line with this, in another ancient stem osteichthian, *Andreolepis hedei*, the odontodes demonstrate highly regular growth mechanisms

similar to the actual dentition in gnathostomes (Qu et al., 2013). However, it does not clarify whether the odontoblast preceded the osteocyte as a cell type or if it was elaborated with the help of bone-mineralizing genetic programs co-opted by osteocytes.

Developmentally, odontoblasts, similar to osteocytes and dermal fibroblasts, originate from migratory multipotent cranial neural crest cells. At the same time, current consensus suggests that neural crest cells incrementally acquired different fates throughout evolution (Hall, 2013). Therefore, the emergence of odontoblasts could occur based on the prototypical innervated neural crest-derived sensory cells (Baker et al., 2008; Magloire et al., 2009) surrounded by rather chaotic mineralized matrix produced by them or other bone-specific cell types in the external armor. As for the origin of ameloblasts, the primary function of epidermal units could be the patterning of underlying mesenchyme and induction of only dentin-based odontodes (quite spread in extinct fishes). Such patterning of placode-forming epithelium could invent the unique enamel-forming gene expression program (Qu et al., 2015) and in addition to its signaling role start to produce the enamel or ganoin-based covering of dermal odontodes. The more ancient history and

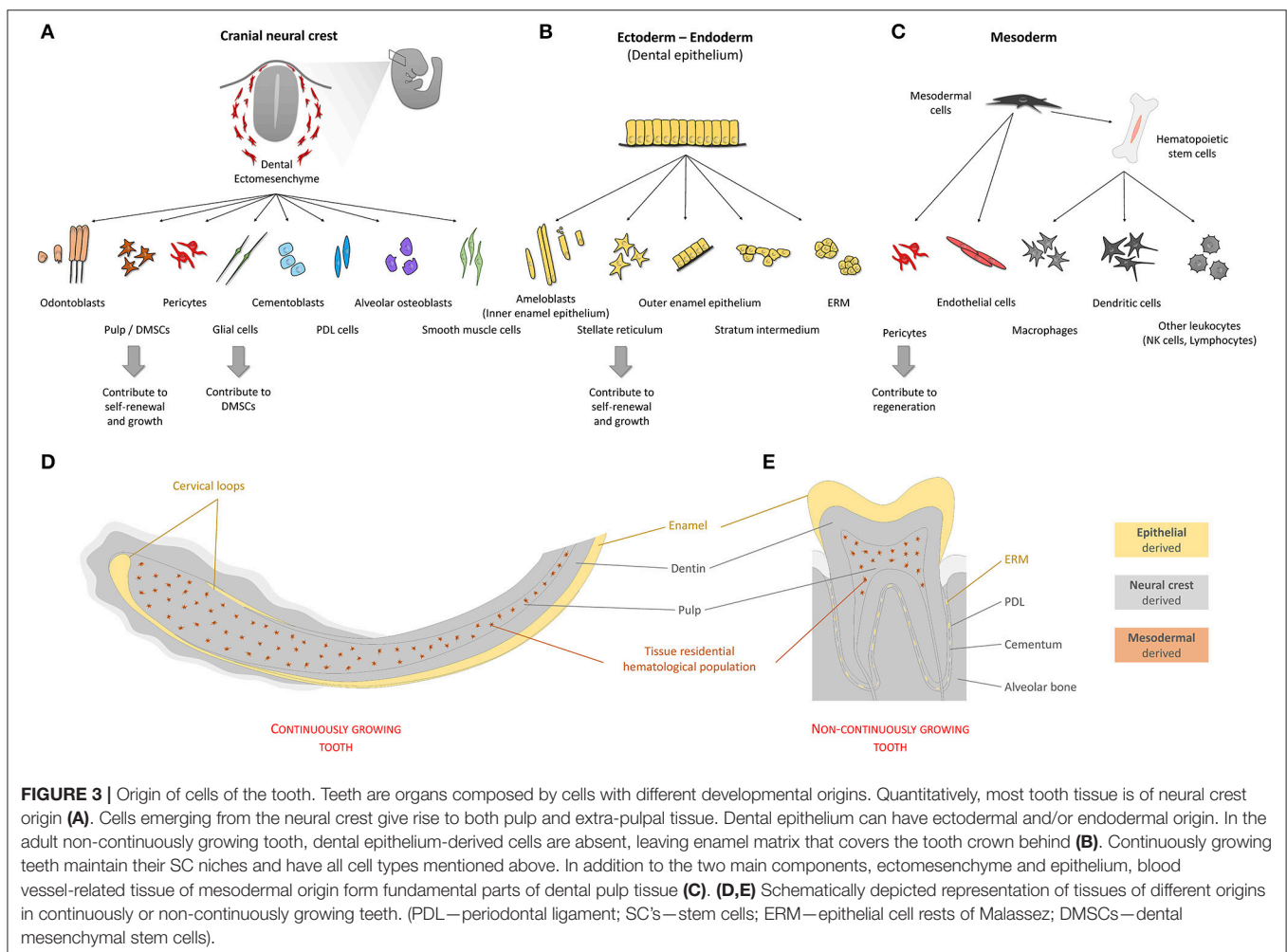


**FIGURE 3 |** Origin of cells of the tooth. Teeth are organs composed by cells with different developmental origins. Quantitatively, most tooth tissue is of neural crest origin (A). Cells emerging from the neural crest give rise to both pulp and extra-pulpal tissue. Dental epithelium can have ectodermal and/or endodermal origin. In the adult non-continuously growing tooth, dental epithelium-derived cells are absent, leaving enamel matrix that covers the tooth crown behind (B). Continuously growing teeth maintain their SC niches and have all cell types mentioned above. In addition to the two main components, ectomesenchyme and epithelium, blood vessel-related tissue of mesodermal origin form fundamental parts of dental pulp tissue (C). (D,E) Schematically depicted representation of tissues of different origins in continuously or non-continuously growing teeth. (PDL—periodontal ligament; SC’s—stem cells; ERM—epithelial cell rests of Malassez; DMSCs—dental mesenchymal stem cells).

the exact origin of the enamel-forming gene expression program should be studied further to deepen this area of investigation.

Over time, biting and chewing takes its toll, and teeth will inevitably deteriorate due to attrition, trauma and other insults. In order to compensate for this, different evolutionary strategies have emerged and accommodated for a gradual renewal of functional teeth. One way is to develop one or more novel generation/s of teeth. Based on the number of newly produced groups of teeth, species can be divided into mono-, di- and polyphyodonts. Some species have only one generation of teeth—*dentes decidui*—which is sufficient for the entire lifespan. Certain bats, shrews, seals and murid rodents belong to this group (van Nievelt and Smith, 2005; Jernvall and Thesleff, 2012). Humans, like most other mammals, have two generations of teeth. The first, *dentes decidui*, are later replaced by *dentes permanentes*. This strategy can be pushed to the extreme in case of polyphyodonts maintaining a postembryonic dental lamina capable of a continuous teeth renewal. This is in contrast to monophyodonts and diphyodonts, where the dental lamina is degraded after initiation of the primary and the secondary dentition, respectively (Buchtová et al., 2012; Gaete and Tucker, 2013). This type of tooth renewal is widespread among various vertebrates including reptiles, amphibians and fishes. *A. hedei*, the extinct stem osteichthyan, shows a very similar archetypical tooth shedding dynamics, which confirms the ancient nature of this mechanism (Chen et al., 2016).

An alternative way was provided by the emergence of the continuously growing (hypselodont) tooth. These teeth are capable to maintain their stem cell niches and can grow

throughout the whole lifespan of the animal. Such growing teeth are found in different species of rodents, lagomorphs, or tusk-bearing animals like elephants, boars, warthogs, walruses and even narwhals. This strategy would require a significant shift in heterogeneity of adult teeth, and the formation of epithelial as well as mesenchymal stem cell niches with associated coordinated amplification, fating and differentiation.

To summarize, manipulation of cell type composition, including residential progenitors and stem populations, appears as a cost-effective and highly flexible evolutionary strategy that can provide for any type of tooth renewal (Figure 3).

#### Key papers:

- Qu et al. (2015).
- Fraser et al. (2010).
- Soukup et al. (2008).
- Jernvall and Thesleff (2012).

## AUTHOR CONTRIBUTIONS

JK, IA, and KF: Framing the concept and structure, manuscript writing, approval of final manuscript. JK: Figures design. IA and KF: Editing and finalizing.

## ACKNOWLEDGMENTS

This work was supported by following grants: Ake Wiberg Foundation, Bertil Hallsten Foundation, ERC Consolidator grant (647844), Vetenskapsradet.

## REFERENCES

- AlShwaimi, E., Purcell, P., Kawai, T., Sasaki, H., Oukka, M., Campos-Neto, A., et al. (2009). Regulatory T cells in mouse periapical lesions. *J. Endod.* 35, 1229–1233. doi: 10.1016/j.joen.2009.06.006
- Arendt, D., Musser, J. M., Baker, C. V. H., Bergman, A., Cepko, C., Erwin, D. H., et al. (2016). The origin and evolution of cell types. *Nat. Rev. Genet.* 17, 744–757. doi: 10.1038/nrg.2016.127
- Bajaj, D., and Arola, D. (2009). Role of prism decussation on fatigue crack growth and fracture of human enamel. *Acta Biomater.* 5, 3045–3056. doi: 10.1016/j.actbio.2009.04.013
- Baker, C. V. H., O'Neill, P., and McCole, R. B. (2008). Lateral line, otic and epibranchial placodes: developmental and evolutionary links? *J. Exp. Zool. B Mol. Dev. Evol.* 310, 370–383. doi: 10.1002/jez.b.21188
- Balic, A., and Thesleff, I. (2015). Tissue interactions regulating tooth development and renewal. *Curr. Top. Dev. Biol.* 115, 157–186. doi: 10.1016/bs.ctdb.2015.07.006
- Beertsen, W., and Niehof, A. (1986). Root-analogue versus crown-analogue dentin: a radioautographic and ultrastructural investigation of the mouse incisor. *Anat. Rec.* 215, 106–118. doi: 10.1002/ar.1092150204
- Bhingare, A. C., Ohno, T., Tomura, M., Zhang, C., Aramaki, O., Otsuki, M., et al. (2014). Dental pulp dendritic cells migrate to regional lymph nodes. *J. Dent. Res.* 93, 288–293. doi: 10.1177/0022034513518223
- Buchtová, M., Stembírek, J., Glocová, K., Matalová, E., and Tucker, A. S. (2012). Early regression of the dental lamina underlies the development of diphyodont dentitions. *J. Dent. Res.* 91, 491–498. doi: 10.1177/0022034512442896
- Cao, Z., Zhang, H., Zhou, X., Han, X., Ren, Y., Gao, T., et al. (2012). Genetic evidence for the vital function of Osterix in cementogenesis. *J. Bone Miner. Res. Off. J. Am. Soc. Bone Miner. Res.* 27, 1080–1092. doi: 10.1002/jbmr.1552
- Charles, C., Hovorakova, M., Ahn, Y., Lyons, D. B., Marangoni, P., Churava, S., et al. (2011). Regulation of tooth number by fine-tuning levels of receptor-tyrosine kinase signaling. *Dev. Camb. Engl.* 138, 4063–4073. doi: 10.1242/dev.069195
- Chen, D., Blom, H., Sanchez, S., Tafforeau, P., and Ahlberg, P. E. (2016). The stem osteichthyan *Andreolepis* and the origin of tooth replacement. *Nature* 539, 237–241. doi: 10.1038/nature19812
- Chung, G., Jung, S. J., and Oh, S. B. (2013). Cellular and molecular mechanisms of dental nociception. *J. Dent. Res.* 92, 948–955. doi: 10.1177/0022034513501877
- Cox, B. N. (2013). How the tooth got its stripes: patterning via strain-cued motility. *J. R. Soc. Interface* 10:20130266. doi: 10.1098/rsif.2013.0266
- Diekwisch, T. G. (2001). The developmental biology of cementum. *Int. J. Dev. Biol.* 45, 695–706. doi: 10.1371/journal.pone.0074697
- Farges, J.-C., Alliot-Licht, B., Renard, E., Ducret, M., Gaudin, A., Smith, A. J., et al. (2015). Dental pulp defence and repair mechanisms in dental caries. *Mediators Inflamm.* 2015:e230251. doi: 10.1155/2015/230251
- Feng, J., Mantesso, A., De Bari, C., Nishiyama, A., and Sharpe, P. T. (2011). Dual origin of mesenchymal stem cells contributing to organ growth and repair. *Proc. Natl. Acad. Sci. U.S.A.* 108, 6503–6508. doi: 10.1073/pnas.1015449108
- Fraser, G. J., Cerny, R., Soukup, V., Bronner-Fraser, M., and Streelman, J. T. (2010). The odontode explosion: the origin of tooth-like structures in vertebrates. *BioEssays News Rev. Mol. Cell. Dev. Biol.* 32, 808–817. doi: 10.1002/bies.200900151
- Frazier-Bowers, S. A., Hendricks, H. M., Wright, J. T., Lee, J., Long, K., Dibble, C. F., et al. (2014). Novel mutations in PTH1R associated with primary failure of eruption and osteoarthritis. *J. Dent. Res.* 93, 134–139. doi: 10.1177/0022034513513588
- Fried, K., and Gibbs, J. L. (2014). “Dental pulp innervation,” in *The Dental Pulp. Biology, Pathology and Regenerative Therapies*. ed M. Goldberg (Heidelberg: New York, NY; Dordrecht; London: Springer), 75–96. doi: 10.1007/978-3-642-55160-4
- Fried, K., Sessle, B. J., and Devor, M. (2011). The paradox of pain from tooth pulp: low-threshold “algoneurons”? *Pain* 152, 2685–2689. doi: 10.1016/j.pain.2011.08.004

- Fristad, I., Heyeraas, K. J., Kvinnsland, I. H., and Jonsson, R. (1995). Recruitment of immunocompetent cells after dental injuries in innervated and denervated young rat molars: an immunohistochemical study. *J. Histochem. Cytochem.* 43, 871–879. doi: 10.1177/43.9.7543913
- Gaete, M., and Tucker, A. S. (2013). Organized emergence of multiple-generations of teeth in snakes is dysregulated by activation of Wnt/Beta-Catenin signalling. *PLoS ONE* 8:e74484. doi: 10.1371/journal.pone.0074484
- Hahn, C. L., Falkler, W. A., and Siegel, M. A. (1989). A study of T and B cells in pulpal pathosis. *J. Endod.* 15, 20–26. doi: 10.1016/S0099-2399(89)80093-7
- Hahn, C.-L., and Liewehr, F. R. (2007). Innate immune responses of the dental pulp to caries. *J. Endod.* 33, 643–651. doi: 10.1016/j.joen.2007.01.001
- Hall, B. K. (2013). *The Neural Crest in Development and Evolution*. Heidelberg: New York, NY; Dordrecht; London: Springer Science and Business Media.
- Harada, H., Kettunen, P., Jung, H. S., Mustonen, T., Wang, Y. A., and Thesleff, I. (1999). Localization of putative stem cells in dental epithelium and their association with Notch and FGF signaling. *J. Cell Biol.* 147, 105–120. doi: 10.1083/jcb.147.1.105
- Harada, H., and Ohshima, H. (2004). New perspectives on tooth development and the dental stem cell niche. *Arch. Histol. Cytol.* 67, 1–11. doi: 10.1679/aohc.67.1
- Harada, H., Toyono, T., Toyoshima, K., Yamasaki, M., Itoh, N., Kato, S., et al. (2002). FGF10 maintains stem cell compartment in developing mouse incisors. *Development* 129, 1533–1541.
- Huang, X., Bringas, P., Slavkin, H. C., and Chai, Y. (2009). Fate of HERS during tooth root development. *Dev. Biol.* 334, 22–30. doi: 10.1016/j.ydbio.2009.06.034
- Huang, X., Xu, X., Bringas, P., Hung, Y. P., and Chai, Y. (2010). Smad4-Shh-Nfic signaling cascade-mediated epithelial-mesenchymal interaction is crucial in regulating tooth root development. *J. Bone Miner. Res.* 25, 1167–1178. doi: 10.1359/jbmr.091103
- Hughes, M. W., Wu, P., Jiang, T.-X., Lin, S.-J., Dong, C.-Y., Li, A., et al. (2011). In search of the Golden Fleece: unraveling principles of morphogenesis by studying the integrative biology of skin appendages. *Integr. Biol.* 3, 388–407. doi: 10.1039/c0ib00108b
- Iwasaki, Y., Otsuka, H., Yanagisawa, N., Hisamitsu, H., Manabe, A., Nonaka, N., et al. (2011). *In situ* proliferation and differentiation of macrophages in dental pulp. *Cell Tissue Res.* 346, 99–109. doi: 10.1007/s00441-011-1231-5
- Izumi, T., Kobayashi, I., Okamura, K., and Sakai, H. (1995). Immunohistochemical study on the immunocompetent cells of the pulp in human non-carious and carious teeth. *Arch. Oral Biol.* 40, 609–614. doi: 10.1016/0003-9969(95)00024-J
- Jernvall, J., and Thesleff, I. (2000). Reiterative signaling and patterning during mammalian tooth morphogenesis. *Mech. Dev.* 92, 19–29. doi: 10.1016/S0925-4773(99)00322-6
- Jernvall, J., and Thesleff, I. (2012). Tooth shape formation and tooth renewal: evolving with the same signals. *Dev. Camb. Engl.* 139, 3487–3497. doi: 10.1242/dev.085084
- Juuri, E., Saito, K., Ahtiainen, L., Seidel, K., Tummers, M., Hochedlinger, K., et al. (2012). Sox2+ stem cells contribute to all epithelial lineages of the tooth via Sfrp5+ progenitors. *Dev. Cell* 23, 317–328. doi: 10.1016/j.devcel.2012.05.012
- Kaukua, N., Shahidi, M. K., Konstantinidou, C., Dyachuk, V., Kaukka, M., Furlan, A., et al. (2014). Glial origin of mesenchymal stem cells in a tooth model system. *Nature* 513, 551–554. doi: 10.1038/nature13536
- Khatibi Shahidi, M., Krivanek, J., Kaukua, N., Ernfors, P., Hladik, L., Kostal, V., et al. (2015). Three-dimensional imaging reveals new compartments and structural adaptations in odontoblasts. *J. Dent. Res.* 94, 945–954. doi: 10.1177/0022034515580796
- Kim, T. H., Bae, C. H., Lee, J. C., Ko, S. O., Yang, X., Jiang, R., et al. (2013).  $\beta$ -catenin is required in odontoblasts for tooth root formation. *J. Dent. Res.* 92, 215–221. doi: 10.1177/0022034512470137
- Klein, O. D., Lyons, D. B., Balooch, G., Marshall, G. W., Basson, M. A., Peterka, M., et al. (2008). An FGF signaling loop sustains the generation of differentiated progeny from stem cells in mouse incisors. *Development* 135, 377–385. doi: 10.1242/dev.015081
- Koussoulakou, D. S., Margaritis, L. H., and Koussoulakos, S. L. (2009). A curriculum vitae of teeth: evolution, generation, regeneration. *Int. J. Biol. Sci.* 5, 226–243. doi: 10.7150/ijbs.5.226
- Lesot, H., Hovorakova, M., Peterka, M., and Peterkova, R. (2014). Three-dimensional analysis of molar development in the mouse from the cap to bell stage. *Aust. Dent. J.* 59(Suppl. 1), 81–100. doi: 10.1111/adj.12132
- Li, J., Parada, C., and Chai, Y. (2017). Cellular and molecular mechanisms of tooth root development. *Development* 144, 374–384. doi: 10.1242/dev.137216
- Lin, Y., Cheng, Y.-S. L., Qin, C., Lin, C., D'Souza, R., and Wang, F. (2009). FGFR2 in the dental epithelium is essential for development and maintenance of the maxillary cervical loop, a stem cell niche in mouse incisors. *Dev. Dyn.* 238, 324–330. doi: 10.1002/dvdy.21778
- Liu, Y., Feng, J., Li, J., Zhao, H., Ho, T.-V., and Chai, Y. (2015). An Nfic-hedgehog signaling cascade regulates tooth root development. *Development* 142, 3374–3382. doi: 10.1242/dev.127068
- Luan, X., Ito, Y., and Diekwisch, T. G. H. (2006). Evolution and development of Hertwig's epithelial root sheath. *Dev. Dyn.* 235, 1167–1180. doi: 10.1002/dvdy.20674
- Lumsden, A. G., and Buchanan, J. A. (1986). An experimental study of timing and topography of early tooth development in the mouse embryo with an analysis of the role of innervation. *Arch. Oral Biol.* 31, 301–311. doi: 10.1016/0003-9969(86)90044-0
- Magloire, H., Couble, M.-L., Thivichon-Prince, B., Maurin, J.-C., and Bleicher, F. (2009). Odontoblast: a mechano-sensory cell. *J. Exp. Zool. B Mol. Dev. Evol.* 312B, 416–424. doi: 10.1002/jez.b.21264
- Marshall, D. R., Turner, S. J., Belz, G. T., Wingo, S., Andreansky, S., Sangster, M. Y., et al. (2001). Measuring the diaspora for virus-specific CD8+ T cells. *Proc. Natl. Acad. Sci. U.S.A.* 98, 6313–6318. doi: 10.1073/pnas.101132698
- Masopust, D., Vezys, V., Usherwood, E. J., Cauley, L. S., Olson, S., Marzo, A. L., et al. (2004). Activated primary and memory CD8 T cells migrate to nonlymphoid tissues regardless of site of activation or tissue of origin. *J. Immunol.* 172, 4875–4882. doi: 10.4049/jimmunol.172.8.4875
- Mikkola, M. L. (2011). The Edar subfamily in hair and exocrine gland development. *Adv. Exp. Med. Biol.* 691, 23–33. doi: 10.1007/978-1-4419-6612-4\_3
- Mitsiadis, T. A., Chéraud, Y., Sharpe, P., and Fontaine-Péru, J. (2003). Development of teeth in chick embryos after mouse neural crest transplantations. *Proc. Natl. Acad. Sci. U.S.A.* 100, 6541–6545. doi: 10.1073/pnas.1137104100
- Mukoyama, Y.-S., Gerber, H.-P., Ferrara, N., Gu, C., and Anderson, D. J. (2005). Peripheral nerve-derived VEGF promotes arterial differentiation via neuropilin 1-mediated positive feedback. *Dev. Camb. Engl.* 132, 941–952. doi: 10.1242/dev.01675
- Nait Lechguer, A., Kuchler-Bopp, S., Hu, B., Häikel, Y., and Lesot, H. (2008). Vascularization of engineered teeth. *J. Dent. Res.* 87, 1138–1143. doi: 10.1177/154405910808701216
- Nakamura-Ohshima, K., Watanabe, J., Kenmotsu, S., and Ohshima, H. (2003). Possible role of immunocompetent cells and the expression of heat shock protein-25 in the process of pulpal regeneration after tooth injury in rat molars. *J. Electron. Microsc. (Tokyo)* 52, 581–591. doi: 10.1093/jmicro/52.6.581
- Nakashima, K., Zhou, X., Kunkel, G., Zhang, Z., Deng, J. M., Behringer, R. R., et al. (2002). The novel zinc finger-containing transcription factor osterix is required for osteoblast differentiation and bone formation. *Cell* 108, 17–29. doi: 10.1016/S0092-8674(01)00622-5
- Nakatomi, M., Morita, I., Eto, K., and Ota, M. S. (2006). Sonic hedgehog signaling is important in tooth root development. *J. Dent. Res.* 85, 427–431. doi: 10.1177/154405910608500506
- Nedvetsky, P. I., Emmerson, E., Finley, J. K., Ettinger, A., Cruz-Pacheco, N., Prochazka, J., et al. (2014). Parasympathetic innervation regulates tubulogenesis in the developing salivary gland. *Dev. Cell* 30, 449–462. doi: 10.1016/j.devcel.2014.06.012
- Nestle, F. O., Zheng, X. G., Thompson, C. B., Turka, L. A., and Nickoloff, B. J. (1993). Characterization of dermal dendritic cells obtained from normal human skin reveals phenotypic and functionally distinctive subsets. *J. Immunol.* 151, 6535–6545.
- Northcutt, R. G., and Gans, C. (1983). The genesis of neural crest and epidermal placodes: a reinterpretation of vertebrate origins. *Q. Rev. Biol.* 58, 1–28. doi: 10.1086/413055
- Ohshima, H., Sato, O., Kawahara, I., Maeda, T., and Takano, Y. (1995). Responses of immunocompetent cells to cavity preparation in rat molars: an immunohistochemical study using OX6-monoclonal antibody. *Connect. Tissue Res.* 32, 303–311. doi: 10.3109/03008209509013738
- Okiji, T., Jontell, M., Belichenko, P., Bergenholtz, G., and Dahlström, A. (1997). Perivascular dendritic cells of the human dental pulp. *Acta Physiol. Scand.* 159, 163–169. doi: 10.1046/j.1365-201X.1997.584337000.x
- Ono, W., Sakagami, N., Nishimori, S., Ono, N., and Kronenberg, H. M. (2016). Parathyroid hormone receptor signalling in osterix-expressing mesenchymal

- progenitors is essential for tooth root formation. *Nat. Commun.* 7:11277. doi: 10.1038/ncomms11277
- Pang, Y. W., Feng, J., Daltoe, F., Fatscher, R., Gentleman, E., Gentleman, M. M., et al. (2016). Perivascular stem cells at the tip of mouse incisors regulate tissue regeneration. *J. Bone Miner. Res.* 31, 514–523. doi: 10.1002/jbmr.2717
- Perdiguer, E. G., and Geissmann, F. (2016). The development and maintenance of resident macrophages. *Nat. Immunol.* 17, 2–8. doi: 10.1038/ni.3341
- Pispa, J., and Thesleff, I. (2003). Mechanisms of ectodermal organogenesis. *Dev. Biol.* 262, 195–205. doi: 10.1016/S0012-1606(03)00325-7
- Qu, Q., Haitina, T., Zhu, M., and Ahlberg, P. E. (2015). New genomic and fossil data illuminate the origin of enamel. *Nature* 526, 108–111. doi: 10.1038/nature15259
- Qu, Q., Sanchez, S., Blom, H., Tafforeau, P., and Ahlberg, P. E. (2013). Scales and tooth whorls of ancient fishes challenge distinction between external and oral “teeth.” *PLoS ONE* 8:e71890. doi: 10.1371/journal.pone.0071890
- Rakian, A., Yang, W.-C., Gluhak-Heinrich, J., Cui, Y., Harris, M. A., Villarreal, D., et al. (2013). Bone morphogenetic protein-2 gene controls tooth root development in coordination with formation of the periodontium. *Int. J. Oral Sci.* 5, 75–84. doi: 10.1038/ijos.2013.41
- Randolph, G. J., Sanchez-Schmitz, G., Liebman, R. M., and Schäkel, K. (2002). The CD16<sup>+</sup> (FcyRIII<sup>+</sup>) subset of human monocytes preferentially becomes migratory dendritic cells in a model tissue setting. *J. Exp. Med.* 196, 517–527. doi: 10.1084/jem.20011608
- Rothová, M., Feng, J., Sharpe, P. T., Peterková, R., and Tucker, A. S. (2011). Contribution of mesoderm to the developing dental papilla. *Int. J. Dev. Biol.* 55, 59–64. doi: 10.1387/ijdb.103083mr
- Saito, K., Nakatomi, M., Ida-Yonemochi, H., Kenmotsu, S., and Ohshima, H. (2011). The expression of GM-CSF and osteopontin in immunocompetent cells precedes the odontoblast differentiation following allogeneic tooth transplantation in mice. *J. Histochem. Cytochem.* 59, 518–529. doi: 10.1369/0022155411403314
- Sakurai, K., Okiji, T., and Suda, H. (1999). Co-increase of nerve fibers and HLA-DR- and/or factor-XIIIa-expressing dendritic cells in dentinal caries-affected regions of the human dental pulp: an immunohistochemical study. *J. Dent. Res.* 78, 1596–1608. doi: 10.1177/00220345990780100401
- Seidel, K., Ahn, C. P., Lyons, D., Nee, A., Ting, K., Brownell, I., et al. (2010). Hedgehog signaling regulates the generation of ameloblast progenitors in the continuously growing mouse incisor. *Dev. Camb. Engl.* 137, 3753–3761. doi: 10.1242/dev.056358
- Sharpe, P. T. (2016). Dental mesenchymal stem cells. *Dev. Camb. Engl.* 143, 2273–2280. doi: 10.1242/dev.134189
- Skobe, Z., and Stern, S. (1980). The pathway of enamel rods at the base of cusps of human teeth. *J. Dent. Res.* 59, 1026–1032. doi: 10.1177/00220345800590060401
- Sloan, A. J., and Waddington, R. J. (2009). Dental pulp stem cells: what, where, how? *Int. J. Paediatr. Dent.* 19, 61–70. doi: 10.1111/j.1365-263X.2008.00964.x
- Smith, C. E. (1998). Cellular and chemical events during enamel maturation. *Crit. Rev. Oral Biol. Med.* 9, 128–161. doi: 10.1177/10454411980090020101
- Soukup, V., Epperlein, H.-H., Horáček, I., and Cerny, R. (2008). Dual epithelial origin of vertebrate oral teeth. *Nature* 455, 795–798. doi: 10.1038/nature07304
- Stern, I. B. (1964). An electron microscopic study of the cementum, Sharpey's fibers and periodontal ligament in the rat incisor. *Am. J. Anat.* 115, 377–409. doi: 10.1002/aja.1001150302
- Sun, L., Yang, C., Ge, Y., Yu, M., Chen, G., Guo, W., et al. (2014). *In vitro* three-dimensional development of mouse molar tooth germs in a rotary cell culture system. *Int. J. Paediatr. Dent.* 24, 175–183. doi: 10.1111/ipd.12057
- Thesleff, I., Keränen, S., and Jernvall, J. (2001). Enamel knots as signaling centers linking tooth morphogenesis and odontoblast differentiation. *Adv. Dent. Res.* 15, 14–18. doi: 10.1177/08959374010150010401
- Thesleff, I., and Tummers, M. (2008). “Tooth organogenesis and regeneration,” in *StemBook*, ed The Stem Cell Research Community (Cambridge, MA: Harvard Stem Cell Institute).
- Trulsson, M., and Johansson, R. S. (2002). Orofacial mechanoreceptors in humans: encoding characteristics and responses during natural orofacial behaviors. *Behav. Brain Res.* 135, 27–33. doi: 10.1016/S0166-4328(02)00151-1
- Tsuchiya, M., Sharma, R., Tye, C. E., Sugiyama, T., and Bartlett, J. D. (2009). Transforming growth factor-beta1 expression is up-regulated in maturation-stage enamel organ and may induce ameloblast apoptosis. *Eur. J. Oral Sci.* 117, 105–112. doi: 10.1111/j.1600-0722.2009.00612.x
- Tsuruga, E., Sakakura, Y., Yajima, T., and Shide, N. (1999). Appearance and distribution of dendritic cells and macrophages in dental pulp during early postnatal morphogenesis of mouse mandibular first molars. *Histochem. Cell Biol.* 112, 193–204. doi: 10.1007/s004180050407
- Tummers, M., and Thesleff, I. (2003). Root or crown: a developmental choice orchestrated by the differential regulation of the epithelial stem cell niche in the tooth of two rodent species. *Dev. Camb. Engl.* 130, 1049–1057. doi: 10.1242/dev.00332
- Tummers, M., and Thesleff, I. (2009). The importance of signal pathway modulation in all aspects of tooth development. *J. Exp. Zool. B Mol. Dev. Evol.* 312B, 309–319. doi: 10.1002/jez.b.21280
- Vahtokari, A., Aberg, T., Jernvall, J., Keränen, S., and Thesleff, I. (1996). The enamel knot as a signaling center in the developing mouse tooth. *Mech. Dev.* 54, 39–43. doi: 10.1016/0925-4773(95)00459-9
- Valladeau, J., and Saeland, S. (2005). Cutaneous dendritic cells. *Semin. Immunol.* 17, 273–283. doi: 10.1016/j.smim.2005.05.009
- van Nievelt, A. F. H., Smith, K. K. (2005). To replace or not to replace: the significance of reduced functional tooth replacement in marsupial and placental mammals. *Paleobiology* 31, 324–346. doi: 10.1666/0094-8373(2005)031[0324:TRONTR]2.0.CO;2
- Vidovic, I., Banerjee, A., Fatahi, R., Matthews, B. G., Dymont, N. A., Kalajzic, I., et al. (2017).  $\alpha$ SMA-expressing perivascular cells represent dental pulp progenitors *in vivo*. *J. Dent. Res.* 96, 323–330. doi: 10.1177/0022034516678208
- Wang, X.-P., Suomalainen, M., Felszeghy, S., Zelarayan, L. C., Alonso, M. T., Plikus, M. V., et al. (2007). An integrated gene regulatory network controls stem cell proliferation in teeth. *PLoS Biol.* 5:e159. doi: 10.1371/journal.pbio.0050159
- Wang, Y., Cox, M. K., Coricor, G., MacDougall, M., and Serra, R. (2013). Inactivation of Tgfb2 in Osterix-Cre expressing dental mesenchyme disrupts molar root formation. *Dev. Biol.* 382, 27–37. doi: 10.1016/j.ydbio.2013.08.003
- Wang, Y. H., Upholt, W. B., Sharpe, P. T., Kollar, E. J., and Mina, M. (1998). Odontogenic epithelium induces similar molecular responses in chick and mouse mandibular mesenchyme. *Dev. Dyn.* 213, 386–397. doi: 10.1002/(SICI)1097-0177(199812)213:4<386::AID-AJA4>3.0.CO;2-2
- Warshawsky, H. (1968). The fine structure of secretory ameloblasts in rat incisors. *Anat. Rec.* 161, 211–229. doi: 10.1002/ar.1091610207
- Xiong, J., Gronthos, S., and Bartold, P. M. (2013). Role of the epithelial cell rests of Malassez in the development, maintenance and regeneration of periodontal ligament tissues. *Periodontol.* 2000 63, 217–233. doi: 10.1111/prd.12023
- Xu, H., Snider, T. N., Wimer, H. F., Yamada, S. S., Yang, T., Holmbeck, K., et al. (2016). Multiple essential MT1-MMP functions in tooth root formation, dentinogenesis, and tooth eruption. *Matrix Biol.* 52–54, 266–283. doi: 10.1016/j.matbio.2016.01.002
- Yu, T., Volponi, A. A., Babb, R., An, Z., and Sharpe, P. T. (2015). Stem cells in tooth development, growth, repair, and regeneration. *Curr. Top. Dev. Biol.* 115, 187–212. doi: 10.1016/bs.ctdb.2015.07.010
- Zhang, J., Kawashima, N., Suda, H., Nakano, Y., Takano, Y., and Azuma, M. (2006). The existence of CD11c<sup>+</sup> sentinel and F4/80<sup>+</sup> interstitial dendritic cells in dental pulp and their dynamics and functional properties. *Int. Immunol.* 18, 1375–1384. doi: 10.1093/intimm/dx1070
- Zhao, H., Feng, J., Seidel, K., Shi, S., Klein, O., Sharpe, P., et al. (2014). Secretion of shh by a neurovascular bundle niche supports mesenchymal stem cell homeostasis in the adult mouse incisor. *Cell Stem Cell* 14, 160–173. doi: 10.1016/j.stem.2013.12.013
- Zheng, L., Ehardt, L., McAlpin, B., About, I., Kim, D., Papagerakis, S., et al. (2014). The tick tock of odontogenesis. *Exp. Cell Res.* 325, 83–89. doi: 10.1016/j.yexcr.2014.02.007

**Conflict of Interest Statement:** The authors declare that the research was conducted in the absence of any commercial or financial relationships that could be construed as a potential conflict of interest.

The reviewer PP and handling Editor declared their shared affiliation, and the handling Editor states that the process nevertheless met the standards of a fair and objective review.

Copyright © 2017 Krivanek, Adameyko and Fried. This is an open-access article distributed under the terms of the Creative Commons Attribution License (CC BY). The use, distribution or reproduction in other forums is permitted, provided the original author(s) or licensor are credited and that the original publication in this journal is cited, in accordance with accepted academic practice. No use, distribution or reproduction is permitted which does not comply with these terms.

## 5.5 Příloha E – Publikace číslo 5

### **Generation and characterization of DSPP- Cerulean/DMP1-Cherry reporter mice**

*Anushree Vijaykumar, Sean Ghassem-Zadeh, Ivana Vidovic-Zdrilic, Karren Komitas, Igor Adameyko, **Jan Krivanek**, Yu Fu, Peter Maye, Mina Mina*

## RESEARCH ARTICLE

# Generation and characterization of DSPP-Cerulean/DMP1-Cherry reporter mice

Anushree Vijaykumar<sup>1</sup>  | Sean Ghassem-Zadeh<sup>1</sup> | Ivana Vidovic-Zdrilic<sup>1</sup> |  
 Karren Komitas<sup>1</sup> | Igor Adameyko<sup>2,3</sup> | Jan Krivanek<sup>3,4</sup> | Yu Fu<sup>5</sup> | Peter Maye<sup>5</sup> |  
 Mina Mina<sup>1</sup> 

<sup>1</sup>Department of Craniofacial Sciences School of Dental Medicine, University of Connecticut, Farmington, Connecticut

<sup>2</sup>Department of Physiology and Pharmacology, Karolinska Institutet, Stockholm, Sweden

<sup>3</sup>Center for Brain Research, Medical University of Vienna, Vienna, Austria

<sup>4</sup>Department of Histology and Embryology, Faculty of Medicine, Masaryk University, Brno, Czech Republic

<sup>5</sup>Department of Reconstructive Sciences, School of Dental Medicine, University of Connecticut, Farmington, Connecticut

## Correspondence

Mina Mina, Division of Pediatric Dentistry, Department of Craniofacial Sciences, School of Dental Medicine, University of Connecticut Health, Farmington, CT 06030.

Email: mina@uchc.edu

## Funding information

National Institute of Health, Grant/Award Numbers: R01-DE016689, T90-DE022526

## Summary

To gain a better understanding of the progression of progenitor cells in the odontoblast lineage, we have examined and characterized the expression of a series of GFP reporters during odontoblast differentiation. However, previously reported GFP reporters (pOBCol2.3-GFP, pOBCol3.6-GFP, and DMP1-GFP), similar to the endogenous proteins, are also expressed by bone-forming cells, which made it difficult to delineate the two cell types in various in vivo and in vitro studies. To overcome these difficulties we generated DSPP-Cerulean/DMP1-Cherry transgenic mice using a bacterial recombination strategy with the mouse BAC clone RP24-258g7. We have analyzed the temporal and spatial expression of both transgenes in tooth and bone in vivo and in vitro. This transgenic animal enabled us to visualize the interactions between odontoblasts and surrounding tissues including dental pulp, ameloblasts and cementoblasts. Our studies showed that DMP1-Cherry, similar to *Dmp1*, was expressed in functional and fully differentiated odontoblasts as well as osteoblasts, osteocytes and cementoblasts. Expression of DSPP-Cerulean transgene was limited to functional and fully differentiated odontoblasts and correlated with the expression of *Dspp*. This transgenic animal can help in the identification and isolation of odontoblasts at later stages of differentiation and help in better understanding of developmental disorders in dentin and odontoblasts.

## KEYWORDS

bone, dentin matrix protein 1, dentin sialophosphoprotein, fluorescent protein reporters, Odontoblasts

## 1 | INTRODUCTION

Dentinogenesis is regulated by a single layer of highly differentiated postmitotic odontoblasts originating from the neural crest-derived cells of the dental papilla (Arana-Chavez & Massa, 2004; Kawashima & Okiji, 2016). The differentiation of odontoblasts from dental papilla cells involves several intermediate steps that are dependent on and regulated by epithelial signals (Lesot et al., 2001; Ruch, Lesot, & Begue-Kirn, 1995; Thesleff, Keranen, & Jernvall, 2001). During this process, dental

papilla in close proximity to the epithelial-mesenchymal interface first forms preodontoblasts that gradually differentiate into functional/secretory odontoblasts and eventually fully differentiated odontoblasts (Lesot et al., 2001; Ruch et al., 1995; Thesleff et al., 2001). In mice, the steps between the formation of preodontoblasts and highly differentiated odontoblasts are completed within 6–10 hr (Lesot et al., 2001; Ruch et al., 1995; Thesleff et al., 2001).

The formation of the mineralized matrix in dentin is similar to bone and requires Type I Collagen and noncollagenous proteins (NCPs). The

small integrin-binding ligand N-linked glycoprotein (SIBLING) family of proteins represents the most abundant group of NCPs in bone and dentin. The SIBLING family includes osteopontin (OPN), bone sialoprotein (BSP), dentin matrix protein 1 (DMP1), dentin sialophosphoprotein (DSPP), and matrix extracellular phosphoglycoprotein (MEPE) Fisher & Fedarko, 2003; Staines, MacRae, & Farquharson, 2012).

Although low levels of DSPP have been detected in other cells including bone-forming cells, (Prasad, Butler, & Qin, 2010), high levels of DSPP and DSP expression are the hallmark of odontoblast differentiation and are routinely used to distinguish differentiated odontoblasts from other cell types including osteoblasts (Prasad et al., 2010; Suzuki, Haruyama, Nishimura, & Kulkarni, 2012).

The *DSPP* gene encodes a single large precursor protein DSPP, which undergoes proteolytic cleavage forming dentin sialoprotein (DSP) and dentin phosphoprotein (DPP), representing the N-terminus and C-terminus of DSPP, respectively (MacDougall et al., 1997; Suzuki et al., 2012). These proteins have distinct roles in dentin mineralization. DSP regulates the initiation of dentin mineralization, and DPP plays a role in the maturation of mineralized dentin (Suzuki et al., 2012). The essential functions of DSPP in dentinogenesis were highlighted by the discovery of the linkage between multiple point mutations in the human *DSPP* gene with human dentinogenesis imperfecta (DGI) and dentin dysplasia (DD) (Prasad et al., 2010; Suzuki et al., 2012). Mice lacking DSPP and/or its processed fragments (DSP and DPP) also displayed severe dentin defects including a widened predentin along with a narrow and hypomineralized dentin (Prasad et al., 2010; Suzuki et al., 2012). In teeth, *Dspp*/DSPP is first expressed at low levels in secretory/functional odontoblasts and then at high levels in terminally differentiated odontoblasts (Prasad et al., 2010; Suzuki et al., 2012).

DMP1 is another member of the SIBLING family with essential roles in the mineralization of both dentin and bone (Fisher & Fedarko, 2003; Staines et al., 2012). Unlike DSPP, which is predominantly expressed at high levels in odontoblasts, DMP1 is also highly expressed by osteocytes, chondrocytes, and preosteoblasts (Qin, D'Souza, & Feng, 2007; Suzuki et al., 2012). In developing teeth, the expression of *Dmp1* is detected earlier than that of *Dspp*, and *Dmp1* null mice displayed abnormalities in dentin quite similar to those seen in *Dspp* null mice, though less severe (Ye et al., 2004). The levels of *Dspp* in *Dmp1* null mice were decreased as compared to wild-type (Ye et al., 2004), and the transgenic expression of *Dspp* rescued the tooth and alveolar bone defects of *Dmp1* KO mice (Qin et al., 2007). These observations together with the identification of DMP1-response elements in the *Dspp* gene suggested that the DMP1 transcription factor regulates DSPP expression in odontoblasts (Narayanan, Gajjeraman, Ramachandran, Hao, & George, 2006). Taken together, these studies clearly demonstrate the importance of both *Dspp* and *Dmp1* in the regulation of odontoblast differentiation and formation of mineralized dentin matrix.

To gain a better understanding of the progression of progenitor cells in the odontoblast lineage, we have examined and characterized the expression of a series of GFP reporters during odontoblast differentiation. These studies together have shown the stage-specific activation of these transgenes during odontoblast differentiation in vivo

and in vitro. pOBCol2.3-GFP and pOBCol3.6-GFP transgenes were activated at early stages of odontoblast differentiation (i.e., polarizing odontoblasts and prior to the expression of *Dmp1* and *Dspp*; Balic, Aguila, & Mina, 2010). DMP1-GFP was first activated in functional/secretory odontoblasts (cells expressing *Dmp1* and low levels of *Dspp*; Balic & Mina, 2011). All three transgenes (pOBCol2.3-GFP, pOBCol3.6-GFP, and DMP1-GFP) were also expressed at high levels in fully differentiated/mature odontoblasts, and their temporal and spatial patterns of expression mimicked those of endogenous transcripts and proteins (Balic et al., 2010; Balic & Mina, 2011).

However, these transgenes, similar to the endogenous proteins are also expressed by bone-forming cells (Kalajzic et al., 2002; Kalajzic et al., 2004). In bone, the pOBCol3.6-GFP transgene was expressed by pre- and early-osteoblasts, whereas pOBCol2.3-GFP and DMP1-GFP transgenes were expressed in mature osteoblasts and osteocytes (Kalajzic et al., 2002, 2004).

The expression of these transgenes in both tissues makes it difficult to delineate the two cell types in various in vivo and in vitro studies. To overcome these difficulties and to be able to distinguish between dentin and bone forming cells, we generated DSPP-Cerulean/DMP1-Cherry transgenic mice using a bacterial recombination strategy with the mouse BAC clone RP24-258g7. In this study, we have analyzed the temporal and spatial expression of both transgenes in the developing teeth and bone in vivo, and during in vitro mineralization in primary pulp cultures.

## 2 | RESULTS

### 2.1 | Expression of DSPP-Cerulean and DMP1-Cherry transgenes in developing teeth and alveolar bones in vivo

The patterns of expression of both transgenes were examined in three independent lines in developing teeth and alveolar bones. DMP1-Cherry and DSPP-Cerulean transgenes were not detected in the dental tissues during the initiation, bud, cap and early bell stages of tooth development (E10–18; data not shown). At the late bell stage (E19) DMP1-Cherry was expressed at low intensity in odontoblasts at the tip of the cusp of the first mandibular molar (data not shown). At the secretory stage of crown formation (P1–P6), DMP1-Cherry, and DSPP-Cerulean transgenes were expressed at high intensity in the entire layer of odontoblasts covering the dental pulp in the unerupted molars (Figure 1). DMP1-Cherry expression was also detected at high levels in osteoblasts and osteocytes within the alveolar bone (Figures 1A and 2A,D). DSPP-Cerulean was also detected transiently in the presecretory ameloblasts (Figure 1Ah,i).

In the erupted molars DMP1-Cherry and DSPP-Cerulean transgenes were co-expressed at high intensity in the entire layer of odontoblasts lining the crown and root (Figure 2C). DMP1-Cherry was expressed in osteocytes of the alveolar bones as well as cementoblasts (Figure 2C,D).

Developing incisors at all stages of development showed an apical to incisal gradient of expression of both transgenes. DMP1-Cherry

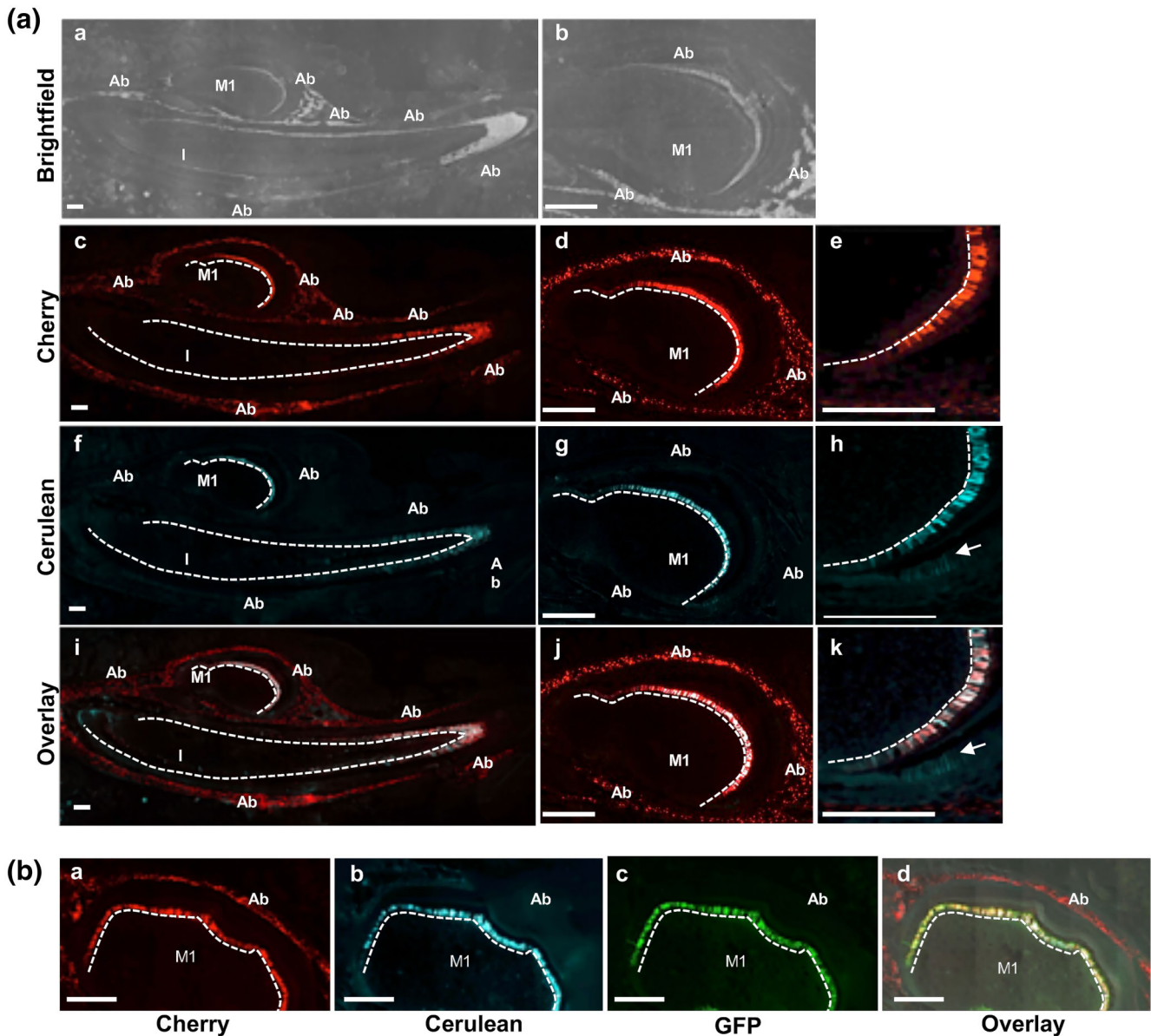


**FIGURE 1** Expression of DSPP-Cerulean and DMP1-Cherry transgenes in developing teeth and alveolar bone in vivo. (A) Representative images of sagittal sections through lower jaw at P6. Images are from the same section visualized under Bright field (a,b) and epifluorescent microscopy with filter cubes to detect Cherry (c-e) and Cerulean signals (f-h). Higher magnifications of areas containing first molars in Panel A are shown in b,d,e,g,h,j,k. DMP1-Cherry is detected in the odontoblasts lining the dental pulp of molars and incisors; as well as in the osteoblasts and osteocytes of the surrounding alveolar bone (c-e). DSPP-Cerulean is expressed in the odontoblasts of molars and incisors but not in the alveolar bone (f-h). Note the low levels of DSPP-Cerulean in ameloblasts in the cervical loop region (indicated by arrows in h and k). Also note the co-expression of DMP1-Cherry and DSPP-Cerulean in odontoblasts in incisor and molars (i-k). (B) Representative images of sagittal sections through the first molar and surrounding alveolar bone at P1. Images are from the same section visualized under epifluorescent microscopy with filter cubes to detect Cherry and Cerulean. Section in c was stained with anti-GFP antibody and visualized with filter cube for GFP. Note that DMP1-Cherry is detected in the odontoblasts and surrounding alveolar bone (a). DSPP-Cerulean is expressed in the odontoblasts of molars but not in the alveolar bone (b). The expression of GFP (c) is similar to DSPP-Cerulean (b). Also note the lack of GFP expression in the surrounding alveolar bone conforming the specificity of the antibody to Cerulean variant. Scale bars in all images = 200  $\mu$ m. In all images, the pulp chambers are denoted by dashed lines. Ab, alveolar bone; I, incisor; M1, first molar

and DSPP-Cerulean expression were not detected in the apical ends of the incisors, and were detected in odontoblasts at the midpoint and incisor tips (Figures 1A and 2A).

To ensure that all DSPP-Cerulean<sup>+</sup> cells (including possible low expressing cells) are visualized adequately, adjacent sections were also

processed for immunohistochemistry using anti-GFP antibody (Figure 1B). The anti-GFP antibody was raised against the N-terminal of GFP as an antigen and does not detect RFP proteins, dsRED or Cherry (Cell Biolabs, Inc. San Diego, CA). The absence of GFP staining in DMP1-Cherry<sup>+</sup> osteoblasts/osteocytes (Figure 1Bc) confirmed the

specificity of the antibody to Cerulean. The pattern of staining with anti-GFP antibody (GFP<sup>+</sup>) cells was very similar to the expression pattern of DSPP-Cerulean<sup>+</sup> cells in vivo (Figure 1Bb,c). The patterns of expression of these transgenes in developing teeth and alveolar bone were similar between the three lines (Figure S2).

## 2.2 | Interactions of DMP1-Cherry/DSPP-cerulean expressing cells with surrounding tissues

High resolution analysis of the adult (8 weeks old) mandibles with confocal microscopy revealed the morphological features of DMP1-

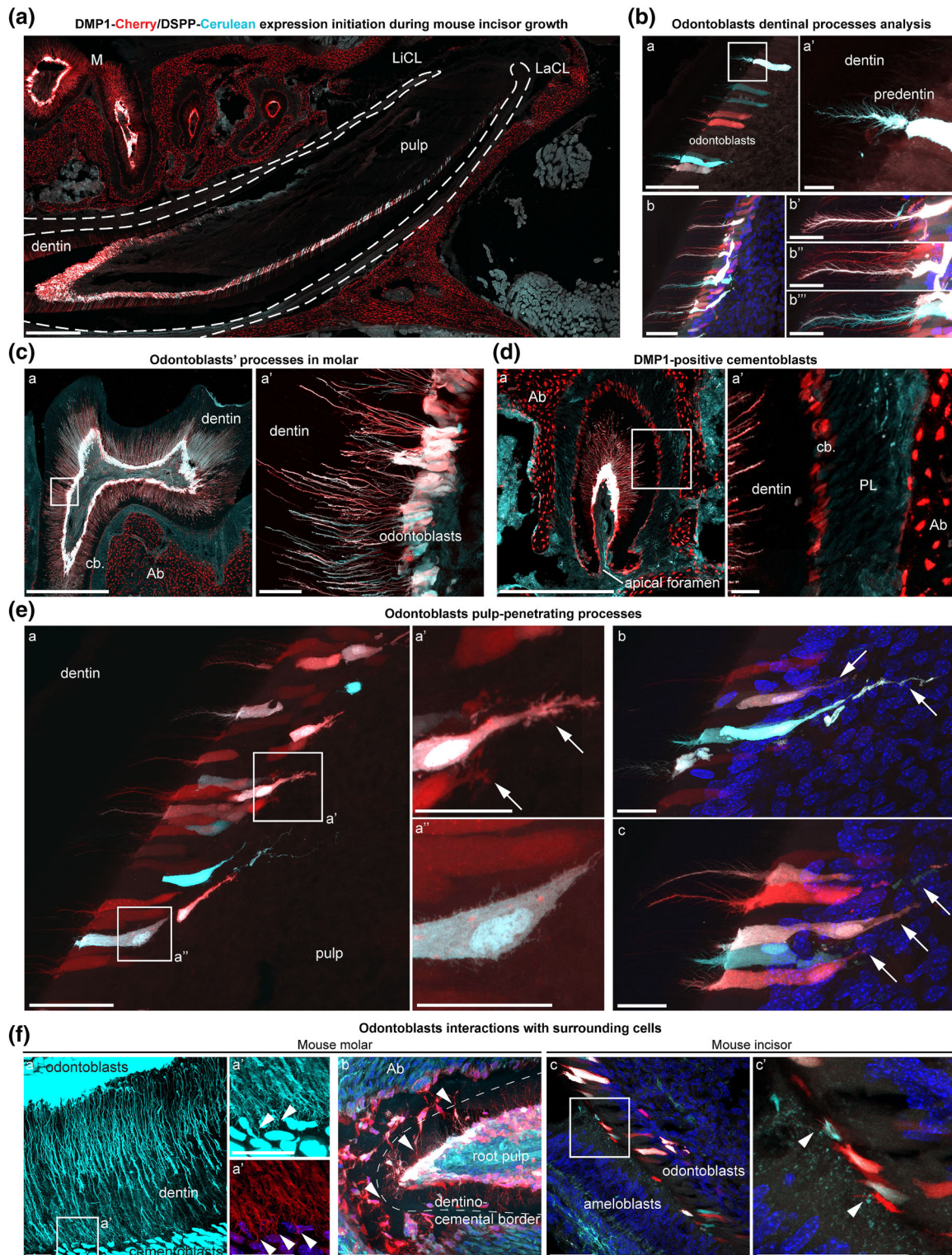


**FIGURE 2** Legend on next page

Cherry/DSPP-Cerulean<sup>+</sup> cells in incisors and molars (Figure 2). These studies showed the heterogeneity of the odontoblast layer containing DMP1-Cherry<sup>+</sup>, DSPP-Cerulean<sup>+</sup>, and DMP1-Cherry<sup>+</sup>/DSPP-Cerulean<sup>+</sup> cells (Figure 2B). All three types of cells extended long and branched processes from their apical ends into predentin and dentin (Figure 2B,C).

Confocal microscopy also revealed many fine structural details of odontoblast processes and contacts between the terminal branches of odontoblast process and surrounding tissues (Figure 2E,F). Odontoblasts extended many long and short branched processes from their basal ends into the subodontoblast region of dental pulp (Figure 2E). In addition, odontoblast processes from the apical ends extended toward cementum making close contacts with cementoblasts (Figure 2F). Prior to deposition of mineralized matrices in the incisor, short odontoblast processes penetrated the ameloblast layer (Figure 2F).

Thus, these studies provide structural details of odontoblast processes emanating from both apical and basal side of the odontoblasts. The thin processes that come in close proximity to ameloblasts prior to matrix deposition and the additional processes extending from the basal side of odontoblasts into dental pulp are consistent with results reported in PLP-CreERT2/R26YFP mouse (Khatibi Shahidi et al., 2015). These together provide additional support for the highly integrated cellular network of communication of odontoblasts with the pulp and other neighboring cells in teeth (Bleicher, 2014; Farahani, Simonian, & Hunter, 2011; Kawashima & Okiji, 2016; Khatibi Shahidi et al., 2015).

### 2.3 | Expression of DSPP-Cerulean and DMP1-Cherry transgenes during the mineralization of primary dental pulp cultures in vitro

The rapid transition and the close proximity of cells at different stages of differentiation in the developing teeth in vivo make it difficult to fully appreciate the stage-specific activation of these transgenes during odontoblast differentiation. To gain insight into differences in the stage of activation of these transgenes, the temporal and spatial expression of both, the DMP1-Cherry and DSPP-Cerulean transgenes was

examined during in vitro mineralization in primary pulp cultures. In these experiments, expression of the two transgenes were examined and correlated with the onset and subsequent growth of the Calcein Green-mineralized nodules in real time in the same live cultures over time.

In cultures, DMP1-Cherry expression was detected in a few cells at Day 7 (Figure 3). With the onset and subsequent growth of CG-stained mineralized matrix, there were continuous increases in the mean intensity of DMP1-Cherry (Figures 3A and 4A,B). DMP1-Cherry<sup>+</sup> cells were detected within CG-stained nodules and in areas between nodules (Figure 3A, overlay).

DSPP-Cerulean<sup>+</sup> cells were examined using filter cube for detection of Cerulean and after immunocytochemistry with anti-GFP antibodies (Figure 3B). DSPP-Cerulean<sup>+</sup> and DSPP-GFP<sup>+</sup> cells were not detected at early time point, and were first detected at Day 10 with subsequent increases thereafter. The cells expressing DSPP-Cerulean at low levels in vitro were more clearly identifiable with anti-GFP antibody staining (Figure 3B). A fraction of cells within the mineralized nodules co-expressed GFP<sup>+</sup> and DMP1-Cherry<sup>+</sup> (Figure 3B, overlay). DSPP-Cerulean<sup>+</sup> and GFP<sup>+</sup> cells were localized primarily within mineralized nodules (Figure 3C).

Changes in the percentage of DMP1-Cherry<sup>+</sup> and DSPP-Cerulean<sup>+</sup> cells in primary pulp cultures were examined by flow cytometry and immunocytochemistry, respectively (Figure 4C). Examination of unsorted cultures showed that freshly isolated pulp cultures contained about 14% DMP1-Cherry<sup>+</sup> cells (Figures 4C and S1C,D) but no DSPP-Cerulean<sup>+</sup>/GFP<sup>+</sup> cells (Figure 4C). The percentage of DMP1-Cherry<sup>+</sup> cells in the unsorted population decreased at Day 7 and followed by increases at Days 10 and 14. DSPP-Cerulean<sup>+</sup>/GFP<sup>+</sup> cells appeared at Day 10 and increased thereafter (Figure 4C).

The decrease in DMP1-Cherry<sup>+</sup> cells at Day 7 most likely reflects the nonproliferative nature or lack of survival of these postmitotic cells both in vivo and in vitro (Balic & Mina, 2011). Examination of cultures from FACS-sorted DMP1-Cherry negative population showed the absence of DMP1-Cherry<sup>+</sup> at Day 0 and continuous increases thereafter (Figure 4C).

**FIGURE 2** Detailed confocal-microscopy analysis of DMP1-Cherry/DSPP-Cerulean in adult 8 weeks old animals. (A) Sagittal section through the mandibular arch. Note the co-expression of DMP1-Cherry and DSPP-Cerulean in odontoblasts covering the dental pulp in incisor and molars. Note the increased expression of transgenes in apical-to-incisal direction. Also note the expression of DMP1-Cherry in osteoblasts and osteocytes of the alveolar bones. Scale bar = 500  $\mu$ m. (B) Odontoblast processes in incisor predentin and dentin during the early secretory stage. A higher magnification of odontoblasts in a showing cells expressing both transgenes (white), only DMP1-Cherry (red) and only DSPP-cerulean (blue). Note the elaborate branched odontoblast processes from all cells in predentin and dentin (b and b'). Scale bar in a,b = 50  $\mu$ m and in a', b'-b''' = 20  $\mu$ m. (C) Odontoblast processes in molars. Sagittal section through the adult (8 weeks old) mouse first molar showing co-expression of DMP1-Cherry and DSPP-Cerulean in odontoblasts and odontoblasts process (a). Inset a' shows the detailed image of the odontoblast layer and odontoblast processes in the region close to the cemento-enamel junction. Scale bar in C (a) = 500  $\mu$ m and in C (a') = 30  $\mu$ m. (D) Cross section through the apical part of the root from adult mouse molar (8 weeks old). Note the co-expression of DMP1-Cherry and DSPP-Cerulean in odontoblasts (a). Also note the expression of DMP1-Cherry in cementoblasts and alveolar bone. Inset a' shows expression of DMP1-Cherry in alveolar osteocytes and cementoblasts. Scale bars D (a) = 500  $\mu$ m, and in D (a') = 30  $\mu$ m. (E) Odontoblast processes and their interactions with pulp cells. (a-c) High magnifications of branched processes extending from basal end of the odontoblasts into dental pulp (all indicated by arrows) at different depths. Scale bar in E(a) = 50  $\mu$ m. Scale bar in E(a'-c) = 20  $\mu$ m. (F) Odontoblast processes and their interactions with surrounding mineralized cells. Root dentin is structurally interconnected with surrounding cementoblasts via dentinal tubules and its terminal branching region (a). Separated channels (Cherry/Cerulean) are shown in panel a'. Dentino-cemental border and multiple contacts between odontoblasts and cementoblasts of the apical molar root is shown on tilted cross section (b). In early developing odontoblasts, before the dentin synthesis is initiated, odontoblast processes contacting neighboring ameloblasts (c and c'). Scale bars: a,a' = 30  $\mu$ m and b, c, c' = 50  $\mu$ m. Ab, alveolar bone; cb, cementoblasts; LaCL, labial cervical loop; LiCL, lingual cervical loop; M, molar; and pl, periodontal ligament

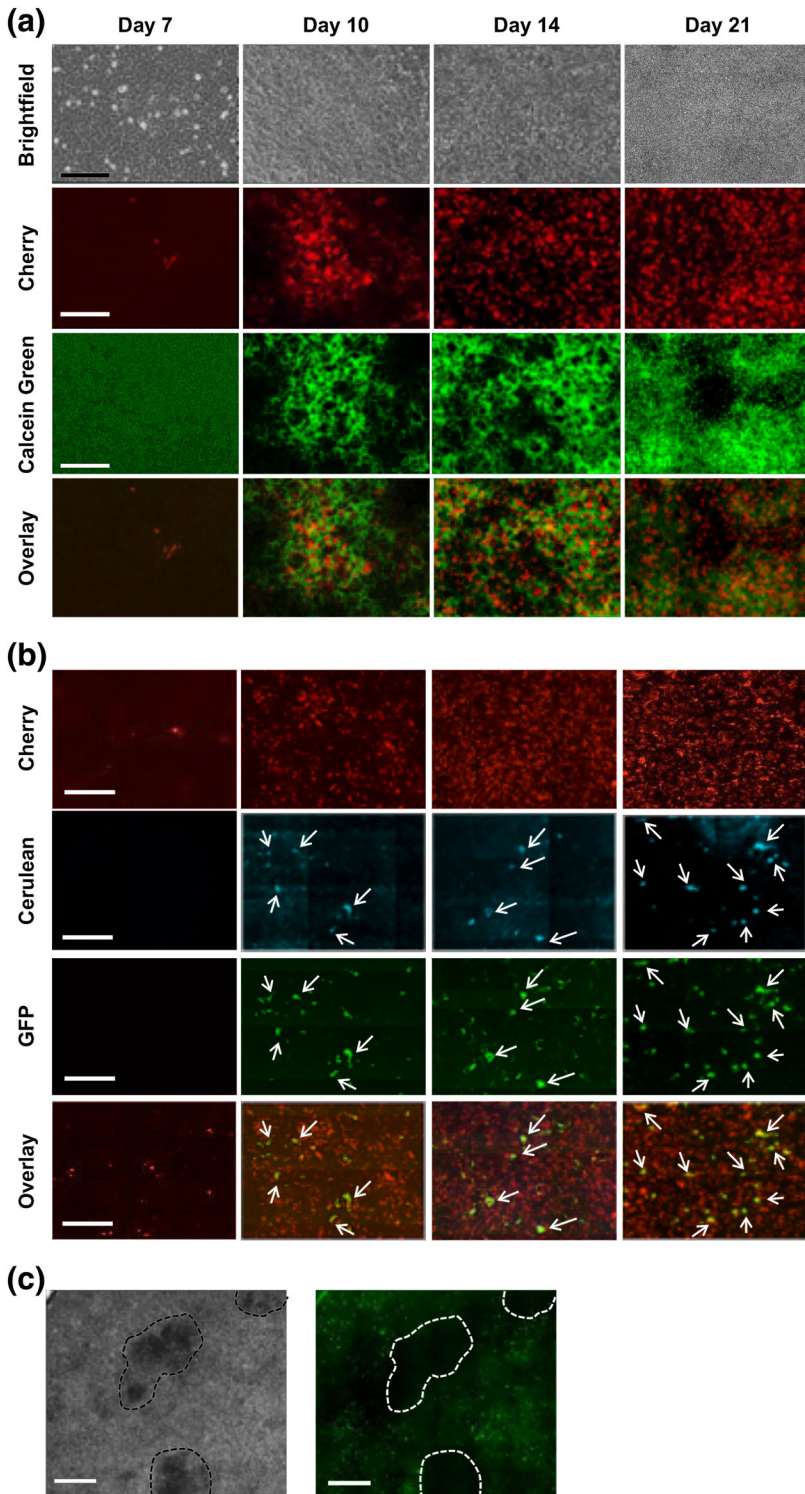


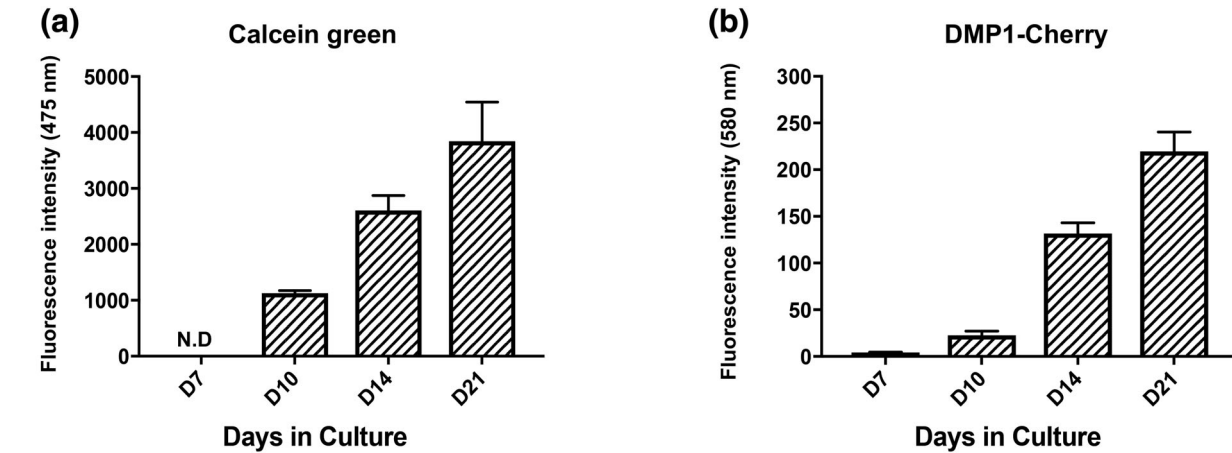
**FIGURE 3** Expression of DMP1-Cherry and DSPP-Cerulean transgenes during the in vitro mineralization of primary pulp cultures. (A) Expression of DMP1-Cherry transgene during in vitro mineralization of primary cultures derived from dental pulp. Representative images of pulp cultures at different time points analyzed under phase contrast, epifluorescent light using appropriate filters for detection of DMP1-Cherry and Calcein green. DMP1-Cherry is expressed in a few cells at Day 7. Between Days 10–14, DMP1-Cherry is expressed at high intensity in Calcein green-stained mineralized nodules. At these time points DMP1-Cherry expression is also detected in area between mineralized nodules. Scale bar: 200  $\mu$ m. (B) Representative images of pulp cultures at different time points analyzed under epifluorescent light using appropriate filters. These cultures were also stained with anti-GFP antibody. DSPP-Cerulean<sup>+</sup> and GFP<sup>+</sup> cells are first detected at Day 10 with increases thereafter. Note that anti-GFP antibody labeled cells that express DSPP-Cerulean at high and low levels. Also note the co-expression of GFP<sup>+</sup> and DMP1-Cherry<sup>+</sup> (indicated by arrows) in only fraction of cells in dental pulp cultures (row labeled Cherry-GFP). Scale bar: 200  $\mu$ m. (C) Bright field and epifluorescent images of a culture at Day 21 shows that labeled cells are detected only within mineralized areas (outside the dashed lines). Scale bar: 100  $\mu$ m

These studies showed continuous increases in the percentages of DMP1-Cherry<sup>+</sup>, DSPP-GFP<sup>+</sup>, and DMP1-Cherry<sup>+</sup>/DSPP-Cerulean<sup>+</sup> populations during in vitro mineralization of pulp cells. (Figure 4C). Time-lapse confocal imaging over 36 hr showed the transition of DMP1-Cherry<sup>+</sup> cells to DMP1-Cherry<sup>+</sup>/DSPP-Cerulean<sup>+</sup> cells (Figure S3).

The expression of these transgenes was also compared with the expression of endogenous *Dmp1* and *Dspp* by RT-PCR using primers listed in Figure S4A. The expression of transgenes was well

correlated with the expression of *Dmp1* and *Dspp*. Similar to endogenous expression of *Dmp1*, DMP1-Cherry was expressed at Day 7 with further increases till Day 21. *Dspp* and DSPP-Cerulean expression was detected later at Day 10, with further increases till Day 21 (Figure S4B).

These in vitro studies showed differences in the stage of activation of the transgenes during odontoblast differentiation in that the DMP1-Cherry<sup>+</sup> transgene is activated at an earlier developmental



**(c) Changes In the percentage of cells expressing transgenes**

Days of culture	FACS Analysis			Immunostaining
	% DMP1-Cherry <sup>+</sup> (unsorted culture)	% DMP1-Cherry <sup>+</sup> (Sorted cultures)	% DMP1-Cherry <sup>+/</sup> DSPP-Cerulean <sup>+</sup>	% DSPP-GFP <sup>+</sup> odontoblasts
D0	14.27 ± 1.14	0	0	0
D7	5.32 ± 0.84	0.83 ± 0.08	0	0
D10	27.7 ± 5.7	2.9 ± 0.39	2.38 ± 0.14	0.78 ± 0.31
D14	69.26 ± 3.72	18.15 ± 1.06	5.41 ± 1.42	4.43 ± 0.75
D21	-	-	-	5.29 ± 0.80

**FIGURE 4** Changes in the percentages of cells expressing transgenes. (A) Histogram showing changes in the intensity of Calcein green staining (absolute values) of primary cultures. Note the progressive increase in the intensity of Calcein green after Day 10. (B) Histograms showing progressive increase in the intensity of DMP1-Cherry expression during mineralization of primary pulp cultures. (c) The percentages of DMP1-Cherry<sup>+</sup> cells were examined in unsorted primary pulp cultures and FACS-sorted DMP1-Cherry<sup>-</sup> cultures. Cultures were processed for FACS analysis at various time points. The percentages of DSPP-Cerulean<sup>+</sup> and DSPP-GFP<sup>+</sup> cells were examined in unsorted primary pulp cultures by FACS analysis and immunostaining with anti-GFP antibody, respectively. Approximately 20,000–30,000 Hoechst<sup>+</sup> cells were counted from 10 to 40 different representative areas of the culture. Negative controls included primary BMSC cultures derived from the DSPP-Cerulean littermates stained with anti-GFP antibody and primary dental pulp cultures derived from the transgenic littermates without addition of anti-GFP antibody. The gating strategy for FACS analysis of DMP1-Cherry<sup>+</sup> and DSPP-Cerulean<sup>+</sup> cells are shown in Figure S4 was used. Results represent mean ± SEM of at least three independent experiments; ND, not detected

stage (i.e., functional odontoblasts) than DSPP-Cerulean transgene that is activated in fully differentiated odontoblasts.

## 2.4 | Expression of DSPP-Cerulean and DMP1-Cherry transgenes in calvaria, long bone in vivo and in primary BMSC and COB cultures in vitro

The specificity of the expression of these transgenes was also examined in bones and primary cultures derived from bone marrow stromal cells (BMSCs) and calvarial osteoblasts (COB) (Figure 5).

In calvaria and long bones isolated at P6, strong expression of DMP1-Cherry was detected in osteoblasts and osteocytes. DSPP-Cerulean was not detected in these tissues (Figure 5A).

In BMSC cultures, DMP1-Cherry<sup>+</sup> cells were first detected around Day 10 in discrete areas of CG-stained mineralization nodules

(Figure 5B). The number of cells expressing the transgene increased with more advanced stages of differentiation at Day 14.

In primary COB cultures, expression of DMP1-Cherry was first detected around Day 14 within the areas of CG-stained nodules (Figure 5C). The number of cells expressing the transgene increased further at Day 21. DSPP-Cerulean expression was not detected in BMSC and COB cultures (Figure 5B,C). These findings confirm that DSPP-Cerulean is exclusively expressed by odontoblasts.

## 3 | DISCUSSION

In our laboratory, we have characterized a series of transgenic mice, which express GFP under the control of tissue- and stage-specific promoters. However, the available animal models and different transgenes (pOBCol2.3-GFP, pOBCol3.6-GFP, and DMP1-GFP), like the

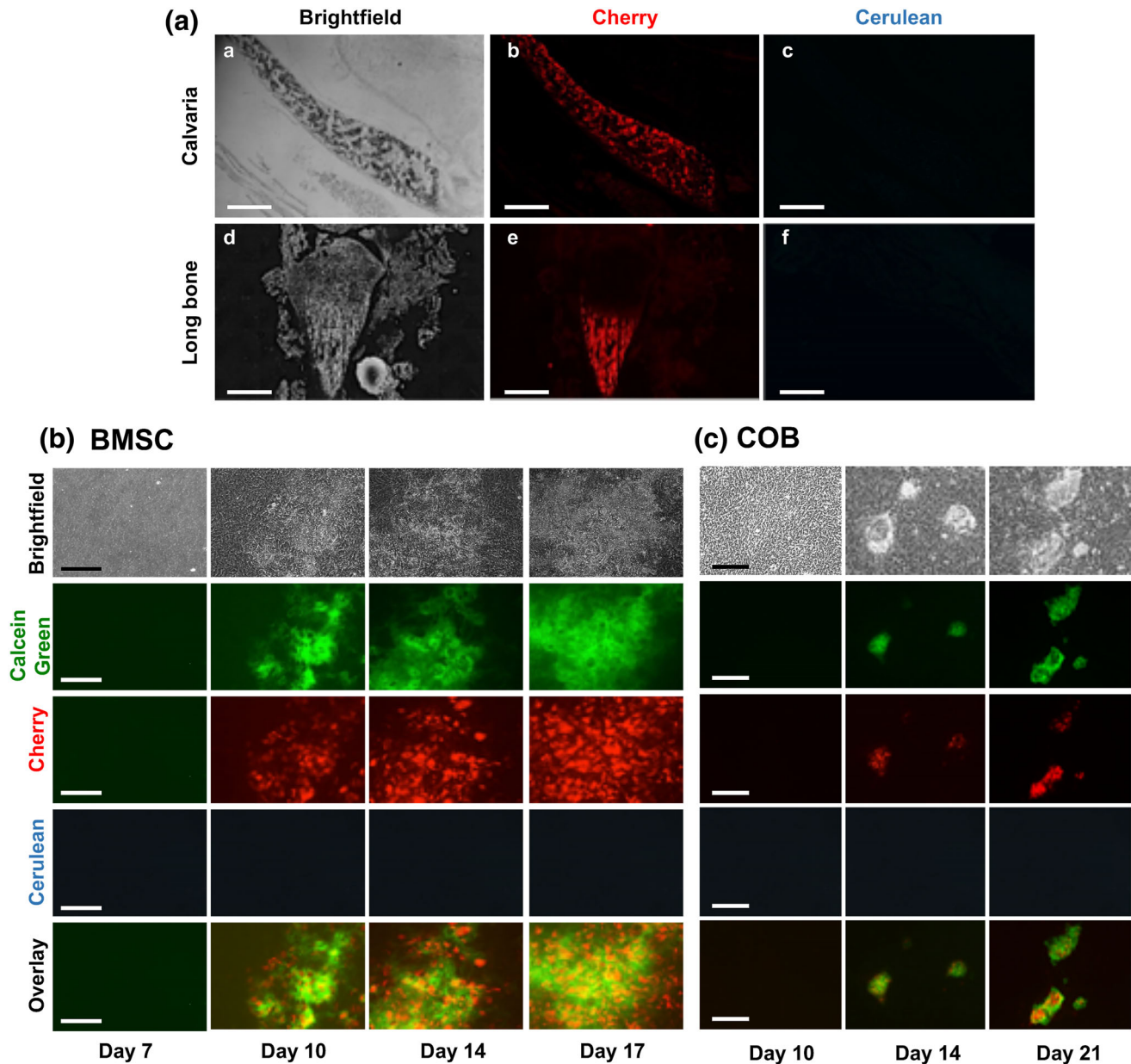


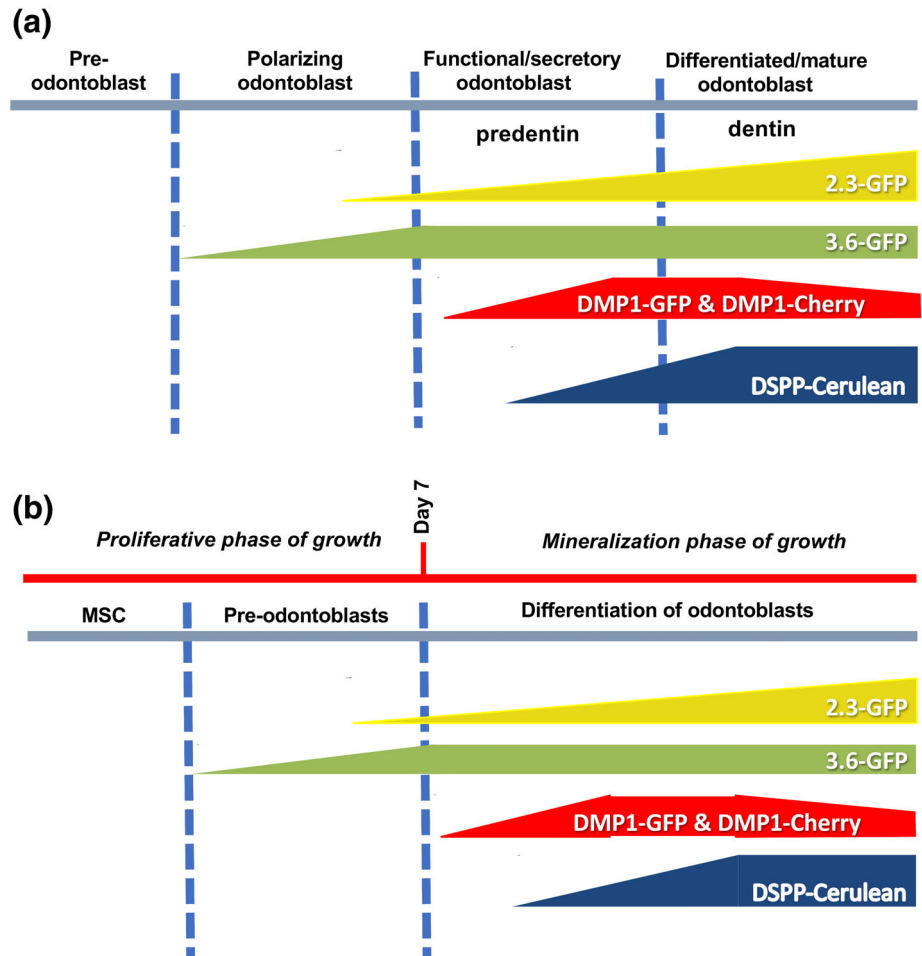
**FIGURE 5** Expression of DMP1-Cherry and DSPP-Cerulean transgenes in calvaria and long bone in vivo and primary cultures from BMSCs and COBs in vitro. (A) Representative images of sections through calvaria (a–c) and long bone (d–f) at P6. Images are from the same section visualized under epifluorescent microscopy with filter cubes to detect Cherry and Cerulean signals. DMP1-Cherry is expressed in the osteoblasts and osteocytes of calvaria and long bone (b,e). Note the lack of DSPP-Cerulean expression in these tissues (c,f). Scale bar: 200  $\mu$ m. (B) Representative images of cultures at various time points from bone marrow stromal cells (BMSCs). Note formation of Calcein green-stained nodules at Day 10. Also note increases in the Calcein green-stained areas at Days 14 and 17. Expression of DMP1-Cherry in the mineralized nodules was detected at Day 10 which progressively increased thereafter. Note the lack of expression of DSPP-Cerulean transgene in these cultures. Scale bar: 200  $\mu$ m. (C) Representative images of cultures at various time points from calvaria osteoblasts (COB) showing Calcein-green stained mineralized nodules at Days 14 and 21. DMP1-Cherry expression is detected in the mineralized nodules at Days 14 and 21. Note the lack of expression of DSPP-Cerulean in COB. Scale bar: 200  $\mu$ m

endogenous proteins, are expressed by bone-forming cells (Kalajzic et al., 2002, 2004), which in turn make it difficult to delineate the two cell types in various in vivo and in vitro studies. To overcome these difficulties and to be able to distinguish between dentin and bone forming cells we have generated DSPP-Cerulean/DMP1-Cherry transgenic mice.

Our in vivo and in vitro studies demonstrated that the DMP1-Cherry transgene was expressed by functional and fully differentiated odontoblasts (Figure 6), cementoblasts, osteoblasts and

osteocytes. The patterns of expression of this transgene is the same as the reported expression of endogenous *Dmp1* in various cell types (Qin et al., 2007) and DMP1-GFP (Balic & Mina, 2011). On the other hand, the DSPP-Cerulean transgene was expressed exclusively by odontoblasts identical to the endogenous expression of *Dspp*. These studies indicate that transgenes contain many of the cis-regulatory elements necessary for regulating faithful expression of DMP1 and DSPP in odontoblasts, cementum, and osteoblasts and osteocytes.

**FIGURE 6** Schematic representation of proposed stages of activation of transgenes during odontoblast differentiation in vivo and in vitro. (A) The expression of 3.6-GFP, 2.3-GFP, and DMP1-GFP transgenes during odontoblast differentiation in vivo are based on results reported by (Balic et al., 2010; Balic & Mina, 2011). DMP1-Cherry expression during odontoblast differentiation in vivo is similar to previously observed DMP1-GFP expression in functional odontoblasts with a lower intensity of expression in fully differentiated odontoblasts. DSPP-Cerulean is first detected at low levels in late functional odontoblasts with increases in fully differentiated odontoblasts. (B) Schematic representation of proposed stages of activation during the in vitro mineralization of dental pulp cultures. In these cultures preodontoblasts and odontoblasts are derived from mesenchymal stem cells



The stage-specific activation of these transgenes with the previously reported transgenic reporter animals (Balic et al., 2010; Balic & Mina, 2011), provide a panel of reporters that can help identify and isolate cells in odontogenic lineage at various stages of differentiation. This ability will bring a wealth of knowledge to help understand novel gene regulatory network involved in specification and progression of cells into odontoblasts lineage. In addition, these studies can lead to deciphering the underlying causes of dental congenital abnormalities and meaningful targeted therapies for affected patients.

## 4 | MATERIALS AND METHODS

### 4.1 | Generation of DSPP-Cerulean/DMP1-Cherry transgenic mice and analysis of the expression of transgenes in vivo

DSPP-Cerulean/DMP1-Cherry transgenic mice were generated using a bacterial recombination strategy with the mouse BAC clone RP24-258g7 as described previously (Gong, Yang, Li, & Heintz, 2002; Maye et al., 2009) and outlined in Figures S5 and S6. All mice were maintained in CD1 background.

Mandibular arches, long bones and calvaria at different stages were isolated from DSPP-Cerulean/DMP1-Cherry transgenic mice.

Tissues were fixed overnight in 4% paraformaldehyde, decalcified and processed for cryosectioning (Dyment et al., 2016).

Sections were examined and imaged using Zeiss Axio Observer Z1 inverted microscope using filter cubes optimized for the detection of Cherry Red Fluorescent Protein (HQ577/20 ex, HQ640/40 em, Q595lp beam splitter), Cerulean (ECFP, enhanced Cyan Fluorescent Protein; D436/20 ex, D480/40 em, Q455dclp beam splitter), Green Fluorescent Protein (GFP; HQ525/50ex, HQ 470/40 em, Q495lp beam splitter), and DAPI variants (AT350/50ex, ET460/50 em, T400lp beam splitter). The full-size images were obtained by scanning at high power followed by stitching the scans into a composite. Exposure times were adjusted for optimum imaging, and kept consistent throughout the various time points.

### 4.2 | Cell cultures, digital imaging, and epifluorescence analysis

Primary cultures from dental pulp, BMSC and COB were prepared from 5- to 7-day old hemizygous DSPP-Cerulean/DMP1-Cherry and nontransgenic mice (Sagomyants, Kalajzic, Maye, & Mina, 2015; Sagomyants & Mina, 2014).

Live cultures were first imaged for detection of various Fluorescent Proteins, and then processed for staining with anti-GFP Alexa Fluor 488 conjugated antibody (1:1,000 dilution, Molecular Probes,

Invitrogen; Sagomyants & Mina, 2014). The nuclei were stained with 1.0 µg/mL Hoechst 33342 dye (Invitrogen). Mineralization in these cultures was examined by Calcein Green staining (3 µg/mL in 2% NaHCO<sub>3</sub>, pH = 7.4; Wang, Liu, Maye, & Rowe, 2006). The mean fluorescence intensity of Calcein Green (CG) and DMP1-Cherry were measured using a multi-detection monochromator microplate reader (Safire<sup>2</sup>, Tecan, Research Triangle Park, NC; Sagomyants et al., 2015; Sagomyants & Mina, 2014). Calcein green staining was measured at 475/515-nm wavelength (excitation/emission) and at a gain of 40. Background fluorescence was measured with cultures grown in the absence of mineralization inducing reagents and these values were subtracted from respective CG measurements.

DMP1-Cherry intensity was measured at 580/610-nm wavelength (excitation/emission) and at a gain of 65. Background fluorescence for Cherry was measured with cultures from the nontransgenic littermates that lack fluorescent reporter expression, and these values were subtracted from respective Cherry measurements.

Quantification of DSPP-Cerulean<sup>+</sup> cells was performed by calculating the ratio of cells stained with anti-GFP antibody (DSPP-Cerulean<sup>+</sup> cells) to the total number of Hoechst<sup>+</sup> cells (Sagomyants et al., 2015; Sagomyants & Mina, 2014).

### 4.3 | Flow cytometric analysis and sorting

Cultures derived from DSPP-Cerulean/DMP1-Cherry transgenic and non-transgenic animals were processed for flow cytometric analysis at various days as described before (Sagomyants et al., 2015; Sagomyants & Mina, 2014). Cultures were also processed for flow cytometric analysis and sorting (FACS) sorting based on Cherry expression. Upon separation, reanalysis confirmed that the purity of isolated DMP1-Cherry<sup>+</sup> and DMP1-Cherry<sup>-</sup> populations were >98%. Live Cherry<sup>+</sup> and Cherry<sup>-</sup> cells were collected and re-plated at the same density as the primary cultures (8.75 × 10<sup>4</sup> cells/cm<sup>2</sup>). Cultures were grown for an additional 14 days and processed for FACS analyses, as described for unsorted cultures. The gating strategy for FACS analysis of DMP1-Cherry<sup>+</sup> and DSPP-Cerulean<sup>+</sup> cells as shown in Figure S1 was used.

### 4.4 | RNA extraction and analyses

Total RNA was isolated with TRIzol reagent (Invitrogen), and processed for gene expression analysis by real-time polymerase chain reaction analysis with primers specific for GAPDH, DSPP, DMP1 and different variants of GFP (Figure S3A).

### 4.5 | Time-lapse live imaging

Primary pulp cultures were analyzed by time-lapse confocal imaging to visualize the conversion of DMP1-Cherry<sup>+</sup> cells to DSPP-Cerulean<sup>+</sup> cells. Six to eight different positions of the well already expressing Cherry<sup>+</sup> cells were selected, followed by imaging over 36 hr using Zeiss 780 LSM equipped with a humidified imaging chamber maintained at 37C and 6% CO<sub>2</sub>. 20× images were taken using 561 nm laser for Cherry and 440 nm laser for Cerulean every 30 min over

36 hr. The images were converted to .mov video files and processed using ImageJ and Metamorph.

### 4.6 | Statistical analysis of data

was performed by GraphPad Prism 7 software using unpaired two-tailed Student *t*-test. Values in all experiments represented mean ± SEM of at least three independent experiments, and a \**P*-value ≤.05 was considered statistically significant.

### ACKNOWLEDGMENT

The authors thank all the individuals who provided reagents, valuable input, and technical assistance in various aspects of this study, including Barbara Rodgers, Xi Jiang, Dr. Ann Cowan, Dr. Evan Jellison, and UConn Health Flow Cytometry Core. This work was supported by grants from National Institute of Health (NIDCR) R01-DE016689 and T90-DE022526 grants.

### CONFLICT OF INTEREST

The authors declare no conflicts of interest with respect to authorship and/or publication of this article.

### ORCID

Anushree Vijaykumar  <https://orcid.org/0000-0002-9311-8715>

Mina Mina  <https://orcid.org/0000-0001-8252-4841>

### REFERENCES

- Arana-Chavez, V. E., & Massa, L. F. (2004). Odontoblasts: the cells forming and maintaining dentine. *The International Journal of Biochemistry & Cell Biology*, 36(8), 1367–1373. <https://doi.org/10.1016/j.biocel.2004.01.006>
- Balic, A., Aguila, H. L., & Mina, M. (2010). Identification of cells at early and late stages of polarization during odontoblast differentiation using pOBCol3.6GFP and pOBCol2.3GFP transgenic mice. *Bone*, 47(5), 948–958. <https://doi.org/10.1016/j.bone.2010.08.009>
- Balic, A., & Mina, M. (2011). Identification of secretory odontoblasts using DMP1-GFP transgenic mice. *Bone*, 48(4), 927–937. <https://doi.org/10.1016/j.bone.2010.12.008>
- Bleicher, F. (2014). Odontoblast physiology. *Experimental Cell Research*, 325(2), 65–71. <https://doi.org/10.1016/j.yexcr.2013.12.012>
- Dyment, N. A., Jiang, X., Chen, L., Hong, S. H., Adams, D. J., Ackert-Bicknell, C., ... Rowe, D. W. (2016). High-throughput, multi-image cryohistology of mineralized tissues. *Journal of Visualized Experiments*, (115). <https://doi.org/10.3791/54468>
- Farahani, R. M., Simonian, M., & Hunter, N. (2011). Blueprint of an ancestral neurosensory organ revealed in glial networks in human dental pulp. *The Journal of Comparative Neurology*, 519(16), 3306–3326. <https://doi.org/10.1002/cne.22701>
- Fisher, L. W., & Fedarko, N. S. (2003). Six genes expressed in bones and teeth encode the current members of the SIBLING family of proteins. *Connective Tissue Research*, 44(Suppl 1), 33–40 Retrieved from <https://www.ncbi.nlm.nih.gov/pubmed/12952171>

- Gong, S., Yang, X. W., Li, C., & Heintz, N. (2002). Highly efficient modification of bacterial artificial chromosomes (BACs) using novel shuttle vectors containing the R6Kgamma origin of replication. *Genome Research*, 12(12), 1992–1998. <https://doi.org/10.1101/gr.476202>
- Kalajzic, I., Braut, A., Guo, D., Jiang, X., Kronenberg, M. S., Mina, M., ... Rowe, D. W. (2004). Dentin matrix protein 1 expression during osteoblastic differentiation, generation of an osteocyte GFP-transgene. *Bone*, 35(1), 74–82. <https://doi.org/10.1016/j.bone.2004.03.006>
- Kalajzic, I., Kalajzic, Z., Kaliterna, M., Gronowicz, G., Clark, S. H., Lichtler, A. C., & Rowe, D. (2002). Use of type I collagen green fluorescent protein transgenes to identify subpopulations of cells at different stages of the osteoblast lineage. *Journal of Bone and Mineral Research*, 17(1), 15–25. <https://doi.org/10.1359/jbmr.2002.17.1.15>
- Kawashima, N., & Okiji, T. (2016). Odontoblasts: Specialized hard-tissue-forming cells in the dentin-pulp complex. *Congenit Anom (Kyoto)*, 56(4), 144–153. <https://doi.org/10.1111/cga.12169>
- Khatibi Shahidi, M., Krivanek, J., Kaukua, N., Ernfors, P., Hladik, L., Kostal, V., ... Fried, K. (2015). three-dimensional imaging reveals new compartments and structural adaptations in odontoblasts. *Journal of Dental Research*, 94(7), 945–954. <https://doi.org/10.1177/0022034515580796>
- Lesot, H., Lisi, S., Peterkova, R., Peterka, M., Mitolo, V., & Ruch, J. V. (2001). Epigenetic signals during odontoblast differentiation. *Advances in Dental Research*, 15, 8–13.
- MacDougall, M., Simmons, D., Luan, X., Nydegger, J., Feng, J., & Gu, T. T. (1997). Dentin phosphoprotein and dentin sialoprotein are cleavage products expressed from a single transcript coded by a gene on human chromosome 4. Dentin phosphoprotein DNA sequence determination. *The Journal of Biological Chemistry*, 272(2), 835–842 Retrieved from <https://www.ncbi.nlm.nih.gov/pubmed/8995371>
- Maye, P., Stover, M. L., Liu, Y., Rowe, D. W., Gong, S., & Lichtler, A. C. (2009). A BAC-bacterial recombination method to generate physically linked multiple gene reporter DNA constructs. *BMC Biotechnology*, 9, 20. <https://doi.org/10.1186/1472-6750-9-20>
- Narayanan, K., Gajjerman, S., Ramachandran, A., Hao, J., & George, A. (2006). Dentin matrix protein 1 regulates dentin sialophosphoprotein gene transcription during early odontoblast differentiation. *The Journal of Biological Chemistry*, 281(28), 19064–19071. <https://doi.org/10.1074/jbc.M600714200>
- Prasad, M., Butler, W. T., & Qin, C. (2010). Dentin sialophosphoprotein in biomineralization. *Connective Tissue Research*, 51(5), 404–417. <https://doi.org/10.3109/03008200903329789>
- Qin, C., D'Souza, R., & Feng, J. Q. (2007). Dentin matrix protein 1 (DMP1): new and important roles for biomineralization and phosphate homeostasis. *Journal of Dental Research*, 86(12), 1134–1141. <https://doi.org/10.1177/154405910708601202>
- Ruch, J. V., Lesot, H., & Begue-Kirn, C. (1995). Odontoblast differentiation. *The International Journal of Developmental Biology*, 39(1), 51–68.
- Sagomyants, K., Kalajzic, I., Maye, P., & Mina, M. (2015). enhanced dentinogenesis of pulp progenitors by early exposure to FGF2. *Journal of Dental Research*, 94(11), 1582–1590. <https://doi.org/10.1177/0022034515599768>
- Sagomyants, K., & Mina, M. (2014). Stage-specific effects of fibroblast growth factor 2 on the differentiation of dental pulp cells. *Cells, Tissues, Organs*, 199(5–6), 311–328. <https://doi.org/10.1159/000371343>
- Staines, K. A., MacRae, V. E., & Farquharson, C. (2012). The importance of the SIBLING family of proteins on skeletal mineralisation and bone remodelling. *The Journal of Endocrinology*, 214(3), 241–255. <https://doi.org/10.1530/JOE-12-0143>
- Suzuki, S., Haruyama, N., Nishimura, F., & Kulkarni, A. B. (2012). Dentin sialophosphoprotein and dentin matrix protein-1: Two highly phosphorylated proteins in mineralized tissues. *Archives of Oral Biology*, 57(9), 1165–1175. <https://doi.org/10.1016/j.archoralbio.2012.03.005>
- Thesleff, I., Keranen, S., & Jernvall, J. (2001). Enamel knots as signaling centers linking tooth morphogenesis and odontoblast differentiation. *Advances in Dental Research*, 15, 14–18. <https://doi.org/10.1177/08959374010150010401>
- Wang, Y. H., Liu, Y., Maye, P., & Rowe, D. W. (2006). Examination of mineralized nodule formation in living osteoblastic cultures using fluorescent dyes. *Biotechnology Progress*, 22(6), 1697–1701. <https://doi.org/10.1021/bp060274b>
- Ye, L., MacDougall, M., Zhang, S., Xie, Y., Zhang, J., Li, Z., ... Feng, J. Q. (2004). Deletion of dentin matrix protein-1 leads to a partial failure of maturation of predentin into dentin, hypomineralization, and expanded cavities of pulp and root canal during postnatal tooth development. *The Journal of Biological Chemistry*, 279(18), 19141–19148. <https://doi.org/10.1074/jbc.M400490200>

## SUPPORTING INFORMATION

Additional supporting information may be found online in the Supporting Information section at the end of this article.

**How to cite this article:** Vijaykumar A, Ghassem-Zadeh S, Vidovic-Zdrilic I, et al. Generation and characterization of DSPP-Cerulean/DMP1-Cherry reporter mice. *genesis*. 2019; e23324. <https://doi.org/10.1002/dvg.23324>

## **The development of dentin microstructure is controlled by the type of adjacent epithelium**

*Josef Lavicky, Magdalena Kolouskova, David Prochazka, Vladislav Rakultsev, Marcos Gonzalez-Lopez, Klara Steklikova, Martin Bartos, Anushree Vijaykumar, Jozef Kaiser, Pavel Pořízka, Maria Hovorakova, Mina Mina, **Jan Krivanek***

# The Development of Dentin Microstructure Is Controlled by the Type of Adjacent Epithelium

Josef Lavicky,<sup>1</sup> Magdalena Kolouskova,<sup>1</sup> David Prochazka,<sup>2</sup> Vladislav Rakultsev,<sup>1</sup> Marcos Gonzalez-Lopez,<sup>1</sup> Klara Steklikova,<sup>3,4</sup> Martin Bartos,<sup>5,6</sup> Anushree Vijaykumar,<sup>7</sup> Jozef Kaiser,<sup>2</sup> Pavel Pořízka,<sup>2</sup> Maria Hovorakova,<sup>3</sup> Mina Mina,<sup>7</sup> and Jan Krivanek<sup>1</sup>

<sup>1</sup>Department of Histology and Embryology, Faculty of Medicine, Masaryk University, Brno, Czech Republic

<sup>2</sup>Advanced Instrumentation and Methods for Materials Characterization, CEITEC Brno University of Technology, Brno, Czech Republic

<sup>3</sup>Institute of Histology and Embryology, First Faculty of Medicine, Charles University, Prague, Czech Republic

<sup>4</sup>Department of Cell Biology, Faculty of Science, Charles University, Prague, Czech Republic

<sup>5</sup>Institute of Dental Medicine, First Faculty of Medicine, Charles University, Prague, Czech Republic

<sup>6</sup>Institute of Anatomy, First Faculty of Medicine, Charles University, Prague, Czech Republic

<sup>7</sup>Department of Craniofacial Sciences School of Dental Medicine, University of Connecticut, Farmington, CT, USA

## ABSTRACT

Considerable amount of research has been focused on dentin mineralization, odontoblast differentiation, and their application in dental tissue engineering. However, very little is known about the differential role of functionally and spatially distinct types of dental epithelium during odontoblast development. Here we show morphological and functional differences in dentin located in the crown and roots of mouse molar and analogous parts of continuously growing incisors. Using a reporter (DSPP-cerulean/DMP1-cherry) mouse strain and mice with ectopic enamel (*Spry2*<sup>+/-</sup>; *Spry4*<sup>-/-</sup>), we show that the different microstructure of dentin is initiated in the very beginning of dentin matrix production and is maintained throughout the whole duration of dentin growth. This phenomenon is regulated by the different inductive role of the adjacent epithelium. Thus, based on the type of interacting epithelium, we introduce more generalized terms for two distinct types of dentins: cementum versus enamel-facing dentin. In the odontoblasts, which produce enamel-facing dentin, we identified uniquely expressed genes (*Dkk1*, *Wisp1*, and *Sall1*) that were either absent or downregulated in odontoblasts, which form cementum-facing dentin. This suggests the potential role of Wnt signalling on the dentin structure patterning. Finally, we show the distribution of calcium and magnesium composition in the two developmentally different types of dentins by utilizing spatial element composition analysis (LIBS). Therefore, variations in dentin inner structure and element composition are the outcome of different developmental history initiated from the very beginning of tooth development. Taken together, our results elucidate the different effects of dental epithelium, during crown and root formation on adjacent odontoblasts and the possible role of Wnt signalling which together results in formation of dentin of different quality. © 2021 The Authors. *Journal of Bone and Mineral Research* published by Wiley Periodicals LLC on behalf of American Society for Bone and Mineral Research (ASBMR).

**KEY WORDS:** TEETH; DENTIN; MICROSTRUCTURE; ODONTOBLAST; PROCESSES; ODONTOGENESIS; DENTINOGENESIS; INCISOR; MOLAR; WNT SIGNALING; LIBS

## Introduction

Teeth are highly specialized structures with an intricate inner architecture, positioned at the very beginning of the digestive system. They are important for food processing and essential for social interactions not only in humans but in other species as

well. Apart from the soft dental pulp, which is responsible for the maintenance of tooth viability, teeth are composed of three different types of calcified tissues: enamel, dentin, and cementum. The general shape, mechanical properties, and functions of teeth are determined by dentin, the most abundant and ontogenetically first developing hard dental tissue. Enamel, as the hardest

This is an open access article under the terms of the Creative Commons Attribution-NonCommercial License, which permits use, distribution and reproduction in any medium, provided the original work is properly cited and is not used for commercial purposes.

Received in original form June 5, 2021; revised form October 12, 2021; accepted November 8, 2021.

Address correspondence to: Jan Krivanek, PhD, Department of Histology and Embryology, Faculty of Medicine, Masaryk University, Brno, Czech Republic.

E-mail: jan.krivanek@med.muni.cz

Additional Supporting Information may be found in the online version of this article.

JL and MK contributed equally to this work.

*Journal of Bone and Mineral Research*, Vol. 37, No. 2, February 2022, pp 323–339.

DOI: 10.1002/jbmr.4471

© 2021 The Authors. *Journal of Bone and Mineral Research* published by Wiley Periodicals LLC on behalf of American Society for Bone and Mineral Research (ASBMR).

and the most calcified dental tissue, protects the most exposed part of the tooth — the crown. Cementum covers the root surface and, together with periodontal ligaments, maintains the anchoring of teeth in the adjacent alveolar bone. Dentin, in contrast to enamel, is a living tissue, which, alongside pulp, forms dentin-pulp complex.<sup>(1)</sup> This integrated functional unit maintains tooth homeostasis and enables the tooth to react to the outer environment.<sup>(2-6)</sup>

Odontoblasts are responsible for dentin development and maintenance of its viability and sensitivity. They are polarized, long-living cells positioned on the interface between the dental pulp and dentin itself.<sup>(7)</sup> Odontoblasts differentiate from ectomesenchyme after an orchestrated interaction with oral epithelium.<sup>(8,9)</sup> During tooth development, two basic types of oral epithelium can be distinguished: the enamel-forming epithelium and the epithelium, which plays a role in the development of the root. Enamel-forming oral epithelium in the crown gives rise to enamel-producing ameloblasts, while oral epithelium in the root forms Hertwig's epithelial root sheath (HERS), which does not produce any hard matrix and serves as an interactive partner for differentiating odontoblasts. After initiation of dentin production, HERS disintegrates into epithelial cell rests of Malassez (ERM).<sup>(8,10-13)</sup> This means that odontoblasts forming the crown and root dentin have a different interactive epithelial partner. The influence of oral epithelium on the determination of the different character of the adjacent dentin's microstructure and elemental composition has not yet been studied.

As odontoblasts lay down the dentin matrix, they are pushed back from the dental epithelium toward the dental pulp and leave behind a single, long process, which then persists inside the dentin matrix.<sup>(14)</sup> Odontoblasts' processes (also known as Tomes' fibers) are the key structural and functional components of dentin and make this tissue sensitive and able to react to the outer environment. This is particularly important in the process of tertiary dentinogenesis, a process that can be referred to as dental healing.<sup>(15,16)</sup> Odontoblasts contribute to sensing and reacting to increased tooth wear or dental caries by thickening the dental wall and thus prolonging the life span of teeth.<sup>(15)</sup> Interestingly, although dentin is a living tissue (similar to bone), once dentin is formed, it is not remodelled as it occurs in bone; therefore, dentin inner structure is determined during its formation.<sup>(17)</sup>

On the molecular level, the dentin matrix is formed by the calcification of the protein network, which is synthesized by the odontoblasts. This protein network is predominantly composed of collagen I fibrils but also several other non-collagenous proteins. Among the most abundant non-collagenous proteins belongs dentin sialophosphoprotein (DSPP) and dentin matrix acidic phosphoprotein 1 (DMP1), which serve as key mineralization centers.<sup>(8)</sup> Through the expression and phosphorylation of these proteins, odontoblasts regulate the rate of dentin matrix calcification.<sup>(18,19)</sup> Both proteins are highly expressed by odontoblasts.<sup>(20)</sup> Although, in contrast to DMP1, which is also expressed by other hard tissue-forming cells (osteoblasts/cytes, cementoblasts/cytes),<sup>(21,22)</sup> DSPP is specifically expressed within odontoblasts, which makes DSPP a unique molecular marker suitable for odontoblast detection and characterization. In this work, we focus on the differences between the microstructure of dentin in the crown (labial aspect of incisor) and the root (lingual aspect of incisor). Because we used genetically altered organisms, which have an ectopic enamel on the lingual aspect of mouse incisors, we are introducing more generalized terms: cementum-facing dentin and enamel-facing dentin.

Here we show, using different genetically altered animals and various methodological approaches, an unanticipated site-dependent microstructure of dentin in high detail. Our results show that the lingual and labial aspects of mouse incisors fully reflect the crown and root aspect in brachyodont teeth in the perspective of the microstructure of dentin and also the presence of cementum-forming cells in the periodontium. Further, we show a different gene expression pattern in odontoblasts on the labial and lingual aspect as well as the elemental composition and X-ray density in each type of dentin. Finally, using a mouse strain with ectopic enamel on the lingual aspect of the incisor, we confirm that the microstructure of dentin is dependent on the interaction with a different type of adjacent epithelium during development. Taken together, we hypothesize that the dentin microstructure is initially induced by the type of adjacent dental epithelium present during the beginning of odontoblast differentiation and influenced by Wnt signalling.

## Materials and Methods

### Animals

Animals used in this study included *DSPP<sup>Cerulean</sup>/DMP1<sup>Cherry</sup>* reporter mouse strain on CD-1 genetic background,<sup>(23)</sup> *Spry2<sup>+/-</sup>;Spry4<sup>-/-</sup>* mice<sup>(24,25)</sup> obtained by crossing the strains *Spry2*/ORF-null allele and *Spry4*/ORF-null allele (originally a kind gift from Dr Ophir Klein, San Francisco, UCSF<sup>(26,27)</sup>) on C57BL/6 genetic background, and C57BL/6 wild-type animals, which were used as controls. All animal experiments were approved by the Ministry of Education, Youth and Sports, Czech Republic (MSMT-8360/2019-2; MSMT-9231/2020-2; MSMT-272/2020-3) and performed according to international and local regulations. All mice were kept in a 12-hour light/dark cycle, 18°C to 23°C and 40% to 60% humidity. Animals had access to food and water *ad libitum*. Animals were genotyped using endpoint PCR utilizing transgene/mutation-specific primers. Both male and female mice were used. Adult (2-month-old) animals with suitable genotype were euthanized by isoflurane overdose (KDG9623, Baxter, Deerfield, IL, USA) and cervical dislocation and further utilized for experiments.

### Histological analysis

Mandibles and maxillae were carefully dissected, briefly washed in PBS, and fixed in 4% paraformaldehyde (pH 7.4) for 5 hours at 4°C. Fixed tissue was then decalcified in 10% EDTA (pH 7.4) for 10 days at 4°C. Samples were then processed either for cryosectioning or paraffin processing. Briefly, for cryosectioning, samples were incubated in 30% sucrose (Sigma-Aldrich, St. Louis, MO, USA; 16104) overnight at 4°C, washed twice in Tissue-Tek OCT Compound (Sakura Finetek Europe B.V., Alphen aan den Rijn, Netherlands; 4583) and embedded in fresh OCT. Samples used to obtain detail images were then sectioned to a thickness of 14 µm on cryostat Leica CM1860 (Leica Biosystems, Wetzlar, Germany). To obtain overview images of the mandible and maxilla of *DSPP<sup>Cerulean</sup>/DMP1<sup>Cherry</sup>*, samples were sectioned to a thickness of 40 µm using Kawamoto's tape (SECTION-LAB Co. Ltd., Hiroshima, Japan) on cryostat Leica CM1860 (Leica Biosystems). Samples embedded in paraffin were sectioned on a microtome (Leica SM2000R) to a thickness of 2 µm and processed as described further.

## In situ hybridization

For the in situ hybridization, RNAscope 2.5 HD Assay – RED (Advanced Cell Diagnostics, Newark, CA, USA; 322350) was utilized as described before.<sup>(28)</sup> The following probes were used: *Dkk1* (501921) and *Wisp1* (402521). Slides were counterstained with hematoxylin for 1 minute and mounted in Pertex medium (Histolab, Brea, CA, USA; 00801). Sections were imaged using Axio Imager 2 (Carl Zeiss AG, Jena, Germany).

## Immunostaining, confocal imaging, and image analysis

All cryosections were washed three times in PBS with 0.1% Tween 20 (Sigma-Aldrich, P1379). Sections from *DSPP<sup>Cerulean</sup>/DMP1<sup>Cherry</sup>* animals were stained with DAPI (Carl Roth, Karlsruhe, Germany; 6335.1) and mounted in VECTASHIELD Antifade mounting medium (Vector Laboratories, Burlingame, CA, USA; H-1000-10). Sections from wild-type and *Spry2<sup>+/-</sup>;Spry4<sup>-/-</sup>* animals were stained with Phalloidin-Alexa Fluor 488 (Cell Signaling Technology, Danvers, MA, USA; 8878S) diluted 1:100 in PBS (pH 7.4) overnight at 4°C. Sections were then subsequently stained with DAPI and mounted in 87.5% Glycerol (Penta CZ, Katovice, Czech Republic) diluted in PBS. For the detection of periostin (POSTN), sections from *DSPP<sup>Cerulean</sup>/DMP1<sup>Cherry</sup>* animals were stained with anti-POSTN antibody (Novus Biologicals, Littleton, CO, USA; NBP1-30042) diluted 1:200 overnight at 4°C. Subsequently, the sections were stained with donkey anti-rabbit secondary antibody conjugated with Alexa Fluor 647 (Thermo Fisher Scientific, Waltham, MA, USA; A31573) diluted 1:500 at room temperature for 2 hours. Sections were then stained with DAPI and mounted using VECTASHIELD Antifade mounting medium. For the analysis of the expression of odontoblast-specific markers, SALL1 antibody (Abcam, Cambridge, MA, USA; ab31526) and NFIC antibody (Novus, NBP2-37935) were used. SALL1 staining was performed on paraffin sections after pH 9 antigen retrieval (Agilent Dako, Santa Clara, CA, USA; S2367) at 95°C for 15 minutes. NFIC staining was performed on cryosections from wild-type animals without antigen retrieval. Sections were incubated with antibodies overnight at 4°C. Subsequently, donkey anti-rabbit secondary antibody conjugated with Alexa Fluor 568 (Thermo Fisher Scientific, A10042) diluted 1:800 was used, and nuclei were counterstained with DAPI (Carl Roth, 6335.1). Slides were then mounted in Fluoromount Aqueous Mounting Medium (Sigma-Aldrich, F4680). Sections were imaged using LSM880 confocal microscope (Carl Zeiss AG, Germany). Obtained data were then analyzed and exported using Imaris (Oxford Instruments, Abingdon, UK) and ZEN software (Carl Zeiss AG, Germany).

## Process straightness analysis

Segmentation was performed in Imaris using semiautomatic approach. Each of the randomly selected odontoblast processes (OPs) were traced using a single polyline. Dendrite straightness parameter was chosen for the quantification. This parameter is defined as the ratio between the length of the whole segmented polyline (OP) and the radial distance between the beginning and the end of the polyline. The value of the function is always equal to or smaller than 1 (a completely straight line has the straightness of 1). We compared 10 randomly chosen processes per each condition.

## Process width analysis

For the analysis of odontoblast process width, confocal images of the phalloidin-stained sagittal sections were used. Images were analyzed using Imaris software. The width of the processes was measured using the measure distance tool in the slice mode. The measurement was performed at the beginning of dentin (above the predentin) at the unified distance of 40 µm from the dentin-pulp edge. For each experimental condition, 85 individual processes were measured.

## Process number density analysis

The number density of processes was analyzed using coronal sections of dentin and from Z projections of sagittal sections of dentin obtained in the section mode of Imaris software. Subsequently, the processes were manually counted using ImageJ software, utilizing the point tool. The number of processes was counted on four unique regions of interest. All of the regions of interest used for the analysis contained at least 75 unique processes.

## Analysis of dentin fraction without the presence of the main process

The distance from the furthestmost point of processes main filament up to the enamel-dentin or cementum-dentin junction (= height of dentin without the presence of the main process) and total height of dentin in the corresponding place was measured using the measure distance tool in the slice mode of Imaris software. To obtain the fraction of dentin without the presence of the main process, the height of dentin without main OP was divided by the total dentin height. A total of 33 unique processes per experimental condition were analyzed.

## Analysis of the distribution of processes in dentin

The unified 10-µm-thick Z-stacks were created using ZEN Blue software's (Carl Zeiss AG) employing the image subset function. Z-stacks were exported as maximum-intensity projections using Imaris software. Subsequently, the images were analyzed in ImageJ software.<sup>(29)</sup> Binary single-channel images were produced using the threshold function. A 10×10 grid was overlaid over the image using the grid overlay plugin. Using the rectangle selection tool and the overlaid grid, 10 equal sectors (parallel with the dentin-pulp edge) were analyzed using the measure function. The area fraction parameter was then used for the final analysis. The analysis was performed on three images per experimental condition.

## Analysis of the distance from cervical loop to the first reporter expression

Sagittal sections containing the cervical loop region of incisors from maxillae and mandibles of the *DSPP<sup>Cerulean</sup>/DMP1<sup>Cherry</sup>* animals were analyzed. The distance from the apex of the cervical loops to the first odontoblast displaying either cerulean, cherry, or both signals above the background level was measured using the measure polyline tool in the slice mode in the Imaris software. The distance was measured both on the labial and lingual sides of the incisors. A total of eight sections (four animals, two sections each) were analyzed.

## Calcified matrix analysis

For the analysis of the elemental composition of the incisor and micro-CT analysis, wild-type Bl/6 animals were overdosed by isoflurane (KDG9623, Baxter), the mandibles and maxillae were then carefully dissected, briefly washed in PBS, and fixed in 4% paraformaldehyde (pH 7.4) overnight at 4°C. Fixed tissues were then dehydrated in ethanol (30%, 50%, 70%, 80%, 90%, 96%, 100%) in each solution three times for 10 minutes and subsequently embedded into epoxy adhesive LR White (Sigma-Aldrich, L9774). The blocks containing the embedded mandibles and maxillae were cut using a diamond saw and sections were polished using abrasive papers P1500 and P3000.

## Laser-induced breakdown spectroscopy (LIBS) analysis

The polished samples were placed in the interaction chamber, which is a part of the LIBS Discovery device (CEITEC BUT, Brno, Czech Republic). As the laser source Nd:YAG laser CFR-400 (Quantel, Lannion, France; 20 Hz, 532 nm, 10 ns) was employed. The laser pulse energy was controlled by a motorized attenuator (Eksma Optics, Vilnius, Lithuania) and was kept constant (30 mJ/pulse) throughout the experiment. The laser beam was focused on the sample surface with a glass triplet (Sill optics, DE,  $f = 32$  mm). The resulting spot size diameter was 30  $\mu\text{m}$ . Plasma radiation was collected using two UV-grade lenses with a total focal length of 75 mm and led via optical cable (400  $\mu\text{m}$ , Thorlabs, Newton, NJ, USA) to the entrance of a spectrometer (HR2000, Ocean Optics, Orlando, FL, USA). The precise timing of the experiment was controlled by the digital pulse generator (SyncRay, Lightigo, Brno, Czech Republic). The gate delay was set to 1.5  $\mu\text{s}$  and gate width to 50  $\mu\text{s}$ . All measurements were controlled by a computer equipped with LIBS control software (Lightigo). The spatial resolution for all measurements was determined by the laser spot size diameter and was set at 30  $\mu\text{m}$  in both directions. Obtained data were processed using the R software (R Foundation for Statistical Computing, Vienna, Austria).

## Micro-CT evaluation of dentin structure

Selected specimens (sectioned teeth in PMMA block) were scanned using desktop micro-CT SkyScan 1272 (Bruker microCT, Kontich, Belgium). Specimens were fixed on specimen holder and scanned under the following scanning parameters: 0.5  $\mu\text{m}$  pixel size, source voltage 60 kV, source current 166  $\mu\text{A}$ , 0.25 mm Al filter, rotation step of 0.1°, frame averaging = 2, 180° rotation, scanning time ~9 hours for each specimen. The flat-field correction was updated before each acquisition. Projection images were reconstructed into cross-section images using NRecon software (Bruker). 2D visualizations were achieved using DataViewer (Bruker).

The X-ray density of dentin was analyzed using ImageJ software. Briefly, five square, regularly distributed selections per enamel, enamel- and cementum-facing dentins, were analyzed using the measure function. Mean grey value was then used for the final analysis. A total of 25 selections per tissue type were analyzed (five images, five selections per tissue type each).

## Statistical analysis

Data were analyzed using Graph Pad Prism software (GraphPad Software, La Jolla, CA, USA). First, the normality of the data was assessed using Anderson-Darling (A2\*), D'Agostino-Pearson omnibus (K2), Shapiro-Wilk (W), Kolmogorov-Smirnov (distance)

tests, and QQ plots. If the data passed normality tests and  $F$  test to determine whether they have equal variances, a two-tailed  $t$ -test was used for the analysis. If the data did not pass normality tests, a two-tailed Mann-Whitney test was used to analyze the data. Subsequently, box plots and violin plots were constructed to visualize the obtained data. Box plots were made to display the interquartile range (25th to 75th percentile). Whiskers were used to indicate upper and lower extremes ( $1.5 \times$  interquartile range). Outliers were shown in red. When the number of data was less than 20, all points were shown. To visualize the data obtained from the analysis of the distribution of processes in dentin, the trend was traced through the medians of the respective regions with whiskers showing the whole range of values. The trends were tested using Pearson's linear correlation of medians from the individual data sets. This analysis was performed in MATLAB (MathWorks, Natick, MA, USA) programming language using a built-in linear of rank correlation (corr) function (testing a null hypothesis of no correlation against the alternative hypothesis of a nonzero correlation). The critical  $p$ -value for statistical significance was set to  $p = 0.05$ .

## Results

The microstructure of odontoblasts' processes in the crown and roots of molars is reflected by the labial and lingual aspects of incisors

To investigate the microstructure of OPs in different parts of mouse molars, we performed confocal microscopy analysis of the first molars of *DSPP<sup>Cerulean</sup>/DMP1<sup>Cherry</sup>* mice.<sup>(23)</sup> This mouse strain enables the visualization of odontoblast bodies and processes through the dual expression of fluorescent proteins constitutively expressed under the *DSPP* (cerulean) and *DMP1* (cherry) promoters. Three-dimensional confocal analysis of the first molars showed an entirely diverse structure of OPs in the crown and root part of the tooth (Fig. 1A–C). Processes in tooth crown dentin displayed smooth and straight morphology with thin and short secondary processes (branches of the main process). On the other hand, odontoblasts' processes in root dentin displayed complicated irregular morphology with longer and more pronounced secondary processes (Fig. 1B, C). To uncover if this phenomenon is also mirrored in the crown and root analogue of continuously growing teeth, we performed the same type of analysis in mouse incisors. Our analysis confirmed a consistent trend between processes found in both molar and incisor (Fig. 1D–F), supporting the crown analogue/root analogue theory (Fig. 1G). Mandibular incisors are in contrast to maxillary incisors more widely used in research.<sup>(28,30,31)</sup> To assess if different site-specific microstructure is reflected in dentin in both morphologically different incisors, we compared both incisors via the same approach and found an identical microstructural pattern (Fig. 2).

Enamel-forming epithelium controls the morphology of OPs in adjacent dentin

To investigate the induction role of different kinds of dental epithelium during early stages of hard-tissue formation, we took advantage of *Spry2<sup>+/-</sup>;Spry4<sup>-/-</sup>* mice, which are known for the presence of ectopic enamel on the lingual side of the incisors.<sup>(24,25)</sup> In contrast to the wild-type mouse in which the ameloblast layer is only present on the labial side, *Spry2<sup>+/-</sup>/Spry4<sup>-/-</sup>* mice display ameloblast layer on both labial and lingual sides. Additionally, the lingual cervical loop (LiCL) displays similar

## Dentin structure in molar and incisor: root (analogue) vs. crown (analogue)

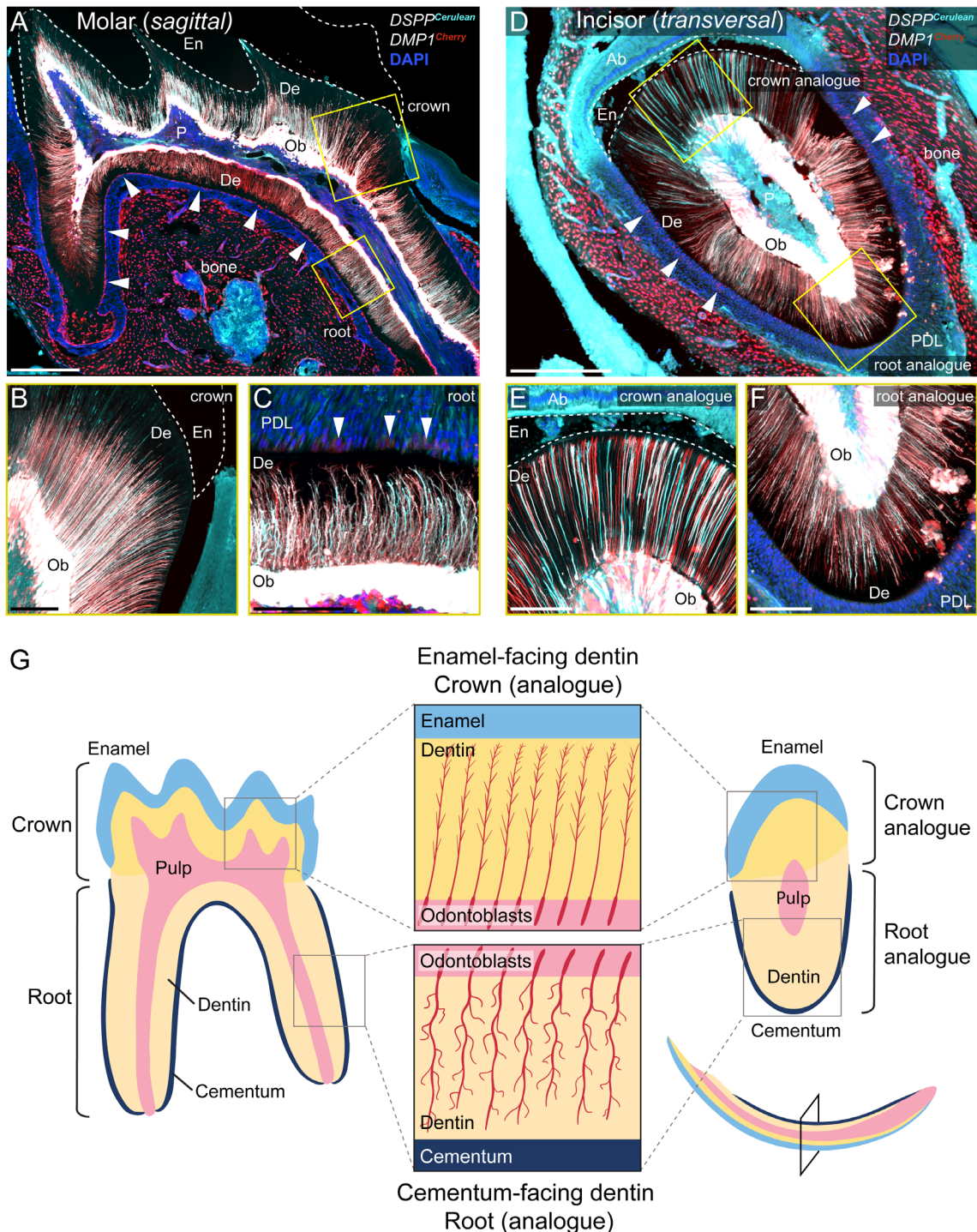


**Fig 1.** Dentin microstructure in molar and incisor: root (analogue) versus crown (analogue). Confocal images from thick, cleared histological sections from the *DSPP<sup>Cerulean</sup>/DMP1<sup>Cherry</sup>* mouse reporter strain show details of the microstructure of dentin with the focus on odontoblasts' processes in different parts of teeth. The sagittal section of the first molar (A) and transversal section of the mandibular incisor (D) show the structural similarities between these two types of teeth and the distribution of fluorescent proteins in the dental tissue and its close surroundings. Note the expression of *cherry* (DMP1) in odontoblasts but also bone-forming osteoblasts (cytes) and cementum-forming cementoblasts (cytes) on the surface of roots, while cerulean (DSPP) is expressed specifically by odontoblasts. Subsets of A and B show details of enamel-facing (crown/crown-analogue) dentin (B, E) and cementum-facing (root/root-analogue) dentin (C, F), respectively. Arrowheads highlight the presence of DMP1-expressing cementum-forming cells located around the root of molar and root analogue of incisors. Schematic visualization of the microstructure of dentin showing the same pattern in enamel-facing and cementum-facing aspects in both molars and incisors (G). Scale bars = 300  $\mu$ m (A, D), 100  $\mu$ m (B, C, E, F). Ab = alveolar bone; De = dentin; en = enamel; Ob = odontoblasts; P = pulp.

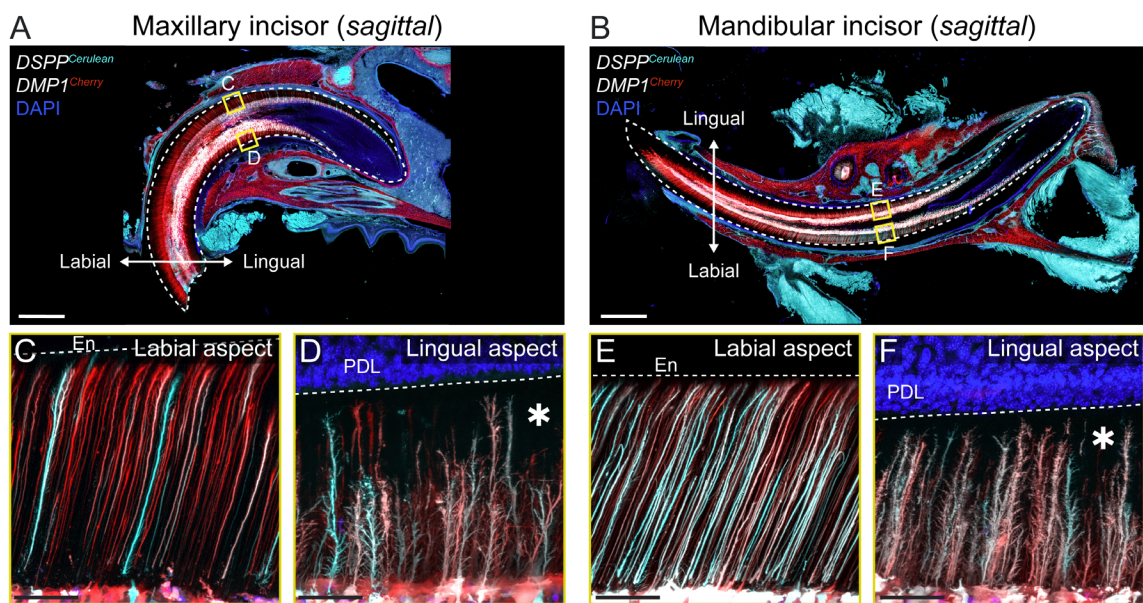


**Fig 2.** Mandibular and maxillary incisor dentin microstructure. Both upper and lower continuously growing incisors (A, B) show the same pattern in the labial (enamel-facing) (C, E) and lingual (cementum-facing) (D, F) odontoblast processes, respectively. White asterisks mark different microstructure of odontoblast processes in the lingual (cementum-facing) aspect of both mandibular and maxillary incisors. Scale bars = 1000  $\mu\text{m}$  (A, B) and 50  $\mu\text{m}$  (C–F) for details. En = enamel; PDL = periodontal ligaments.

morphology to the labial cervical loop (LaCL) (Fig. 6C, D); however, wild-type mice have an ameloblast layer only on the labial side and the lingual dental epithelium is disintegrated.<sup>(11)</sup> To visualize the morphology of OPs, we used the staining with Phalloidin-Alexa488, which specifically binds to actin<sup>(32)</sup> and enables the visualization of all cellular compartments in mineralized tissues. Confocal analysis of the phalloidin-stained sections from wild-type animals further confirmed the different structure of odontoblasts' processes in the labial and lingual aspects of the incisor (Fig. 3A), which coincided with our previous analysis of the *DSPP<sup>Cerulean</sup>/DMP1<sup>Cherry</sup>* strain (Fig. 1D–F; Fig. 2). However, in the *Spry2<sup>+/-</sup>;Spry4<sup>-/-</sup>* animals, where the ectopic ameloblast layer and enamel are also developed on the lingual aspect, the microstructure of OPs was the same as on the labial aspect of the incisor (Fig. 3A, B), displaying the same smooth and straight morphology. Their appearance, therefore, reflected the morphology of the OPs in the crown dentin of the molar (Fig. 1A, B). To further analyze differences in the morphology of OPs and specifically their terminal branching regions,<sup>(14)</sup> which are in contact with adjacent enamel or cementum, we first performed detailed microscopy focusing on the terminal part of OPs (Fig. 4A). Furthermore, we performed the segmentation of the processes and quantified their straightness (Fig. 4B, C).

Our results show similarities in the pattern among the OP endings (Fig. 4A) and whole-process morphology (Fig. 4B) in the enamel-facing dentin and cementum-facing dentin. These results are consistent in wild-type molars, maxillary, and mandibular incisors, using *DSPP<sup>Cerulean</sup>/DMP1<sup>Cherry</sup>* animals or phalloidin staining in wild-type and *Spry2<sup>+/-</sup>;Spry4<sup>-/-</sup>* animals (Fig. 4). The morphology of OPs in all enamel-facing dentins was highly similar. In the case of cementum-facing dentins, OPs in both maxillary and mandibular incisors displayed highly similar morphology. In the molars, OPs in the cementum-facing dentin displayed thinner and more twisting morphology when compared with the incisors (Fig. 4A).

To uncover the morphology and distribution of cementum-forming cherry<sup>+</sup> (DMP1-expressing) cells in maxillary and mandibular incisors and to compare this pattern to molar roots, we analyzed the periodontal space on the lingual aspects of both types of incisors using *DSPP<sup>Cerulean</sup>/DMP1<sup>Cherry</sup>* mouse strain (Fig. S1). Our data show that the structure of periodontal space on the labial aspect of the incisor resembles the situation in the molar. However, in the more distal parts, just a seldom presence of DMP1-expressing cementoblasts was observed. This enabled us to establish universal terms cementum-facing and enamel-facing dentin.

#### Quantifications of labial and lingual dentin differences

To quantify these differences, we performed segmentation and analysis of the individual processes. Quantification of processes' straightness shows that in the *DSPP<sup>Cerulean</sup>/DMP1<sup>Cherry</sup>* strain's molar crown dentin, OPs display the mean straightness of  $0.96 \pm 0.02$  (a straight line has the straightness of 1), while the OPs in the root dentin display the straightness of  $0.90 \pm 0.04$  (Fig. 4C). OPs in the labial (with enamel) dentin of mandibular incisor display the straightness of  $0.99 \pm 0.01$  and the OPs on the lingual (without enamel) side display  $0.98 \pm 0.01$ . In the maxillary incisor, the OPs of the labial (enamel-facing) side showed the straightness of  $0.98 \pm 0.01$ , while on the lingual (cementum-facing) side, OPs displayed  $0.95 \pm 0.02$ . In the wild-type maxillary incisor stained with phalloidin, OPs of the labial side displayed the straightness of  $0.98 \pm 0.01$ . The OPs on the lingual side displayed, on the other hand, the straightness of  $0.90 \pm 0.05$ . Finally, the OPs of the *Spry2<sup>+/-</sup>;Spry4<sup>-/-</sup>* animals displayed on the labial (enamel-facing) side the straightness of  $0.99 \pm 0.01$  and  $0.99 \pm 0.00$  on the lingual (ectopic enamel-facing) side.

To further highlight the differences in the features of odontoblast processes and corresponding dentins, we analyzed confocal images of labial (enamel-facing) and lingual (cementum-facing) dentins of wild-type animals and labial (enamel-facing) and lingual (ectopic enamel-facing) dentins of *Spry2*<sup>+/-</sup>; *Spry4*<sup>-/-</sup> animals (Fig. 5). The analysis of OP's width showed that processes localized on the labial-side dentins of wild-type mice (both mandibular and maxillary) and maxillary *Spry2*<sup>+/-</sup>; *Spry4*<sup>-/-</sup> incisors were significantly thinner ( $p < 0.0001$ ) than the processes located in the corresponding lingual-side dentins (Fig. 5A). Interestingly, the width of the OPs located in the lingual (ectopic enamel-facing) dentin of the *Spry2*<sup>+/-</sup>; *Spry4*<sup>-/-</sup> maxillary incisor was significantly lower compared with its lingual wild-type counterpart (Fig. 5A).

Analysis of the number density of the processes showed that the processes on the labial sides of the incisors have significantly higher density than processes on the lingual side of all analyzed conditions, including the ectopic enamel-facing lingual dentin of *Spry2*<sup>+/-</sup>; *Spry4*<sup>-/-</sup> animals (Fig. 5B). Comparison of wild-type and *Spry2*<sup>+/-</sup>; *Spry4*<sup>-/-</sup> process density showed no significant change ( $p = 0.0532$ ) between the lingual sides of the incisors.

To quantify the changes of the dentin quality in relation to the OPs, we analyzed the relative fraction of dentin height without the presence of the main process (Fig. 5C) and the distribution of all processes in different types of dentins (Fig. 5D). The fraction of the dentin without the presence of the main process was significantly larger ( $p < 0.0001$ ) in the lingual (cementum-facing) dentin than in the labial (enamel-facing) dentins of wild-type mandibular and maxillary incisors. In contrast to this, the fraction

of the labial and lingual dentins of the maxillary incisor of the *Spry2*<sup>+/-</sup>; *Spry4*<sup>-/-</sup> animals showed similar values ( $p < 0.7462$ ), which fully reflects the altered situation in the lingual (ectopic enamel-facing) dentin and show high similarity induced by the changed type of dental epithelium. The differences between the lingual sides of maxillary incisors of wild-type and *Spry2*<sup>+/-</sup>; *Spry4*<sup>-/-</sup> animals were also significant (Fig. 5C).

To quantify the density and distribution of all OPs (including side branches) in the enamel-facing and cementum-facing dentins, we analyzed the OP density in 10 different regions, beginning at the predentin up to the outermost dentin (Fig. 5D; Fig. S2). Pearson's correlation between the lingual and labial dentins was calculated using medians of each of the data points (Fig. 5D). Our analysis shows distinct trends of the area fraction in labial and lingual dentin of mandibular ( $R = 0.6165$ ,  $p = 0.0802$ ) and maxillary ( $R = 0.2612$ ,  $p = 0.46$ ) incisors of wild-type animals. In contrast to wild types, the analyses of labial and lingual dentins in *Spry2*<sup>+/-</sup>; *Spry4*<sup>-/-</sup> maxillary incisor show correlating trends ( $R = 0.8697$ ,  $p = 0.0011$ ), which further confirms our hypothesis about the inductive function of the type of attached dental epithelium during development. The plots of Pearson's correlations are shown in Fig. S3.

All performed quantifications further support our hypothesis of the different microstructure of cementum-facing and enamel-facing dentin. Most interestingly, the lingual, ectopic enamel-facing dentin of the *Spry2*<sup>+/-</sup>; *Spry4*<sup>-/-</sup> animal displayed similar patterns of OPs compared with its labial counterpart. This confirms a different inductive role of ameloblast-forming dental epithelium and non-ameloblast-forming dental epithelium on adjacent dentin microstructure.

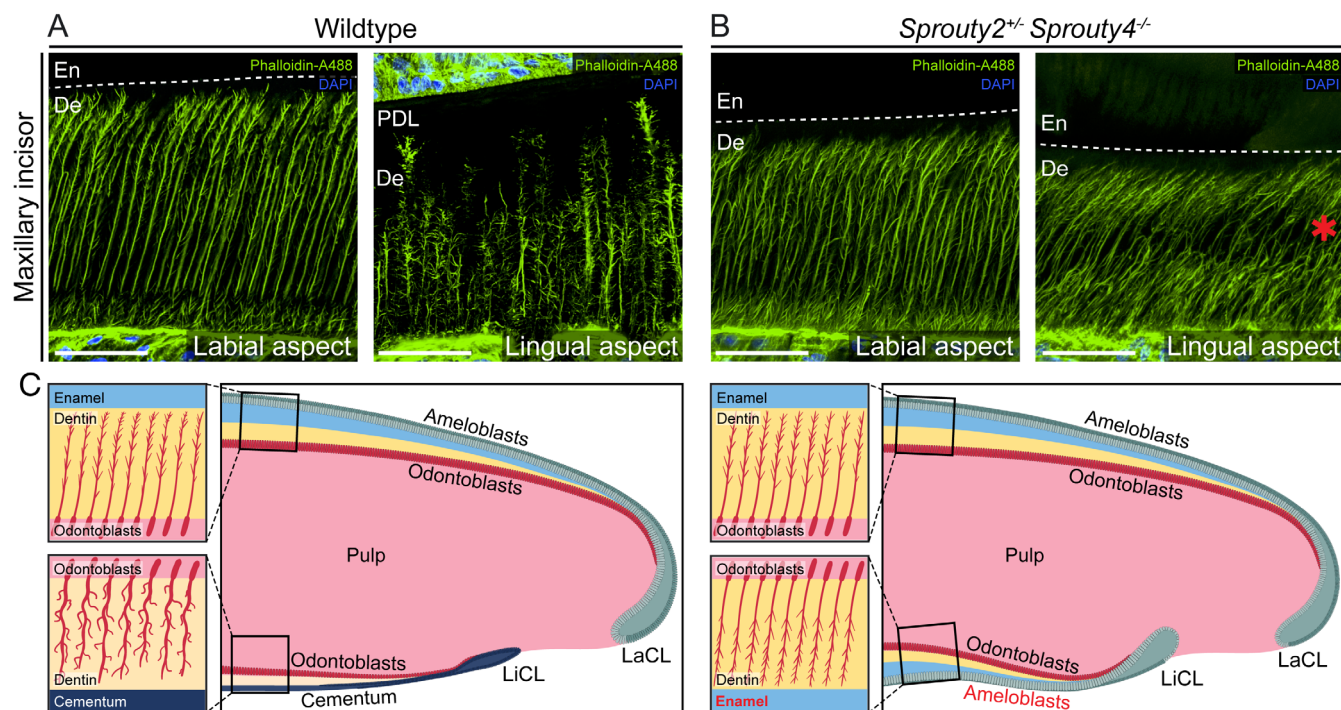


**Fig 3.** Dentin adjacent to ectopically developed enamel shows altered microstructure. Confocal images of the labial and lingual aspect of maxillary incisors stained with Phalloidin-Alexa488 show the different microstructure of OPs on the labial and lingual aspect of incisor in wild-type animals (A) and similar microstructure on both aspects in maxillary incisor of *Spry2*<sup>+/-</sup>; *Spry4*<sup>-/-</sup> animals (B) having ameloblasts and enamel on both sides of the tooth. (C) Schematic drawing reflecting the influence of different dental epithelium on dentin development. Red asterisk shows the altered morphology of OPs in dentin adjacent to ectopic enamel on the lingual aspect of the maxillary incisor in *Spry2*<sup>+/-</sup>; *Spry4*<sup>-/-</sup>. Scale bars = 50  $\mu$ m. En = enamel space; LaCL = labial cervical loop; LiCL = lingual cervical loop; PDL = periodontal ligament.

## Microstructure of odontoblast processes of enamel-facing and cementum-facing dentin

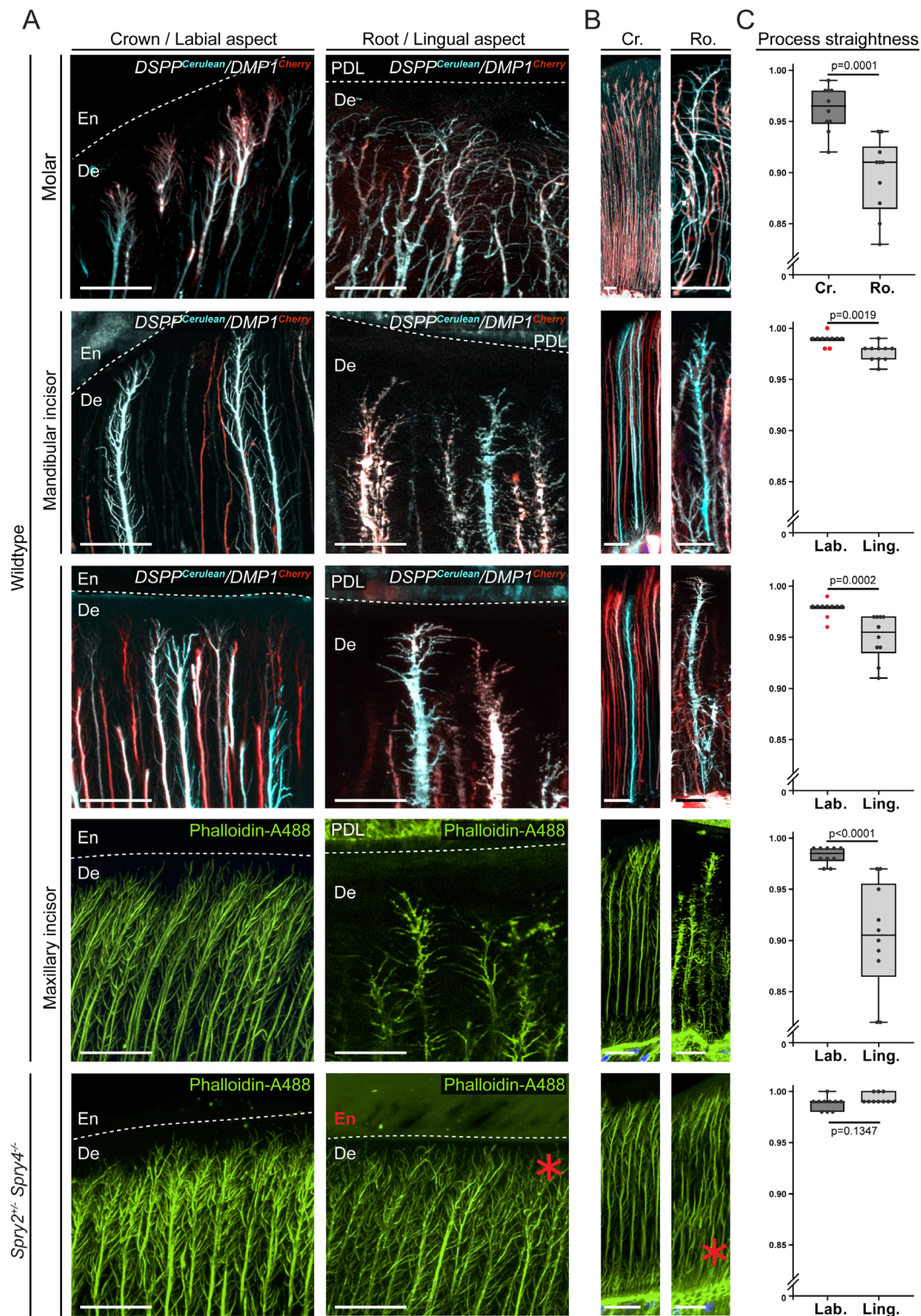


**Fig 4.** Analysis of odontoblasts' terminal branching regions and processes straightness in enamel-facing and cementum-facing dentin. Confocal images of histological sections from *DSPP<sup>Cerulean</sup>/DMP1<sup>Cherry</sup>*, wild-type, and *Spry2<sup>+/-</sup>;Spry4<sup>-/-</sup>* animals stained with Phalloidin-Alexa488 with a special emphasis on the terminal branching regions relating to the first formed dentin adjacent to enamel and cementum, respectively (A). Details on the process morphology are shown in (B) and quantifications straightness of the processes in (C). Red asterisks show the altered morphology of OPs in dentin adjacent to ectopic enamel on the lingual aspect of the maxillary incisor in *Spry2<sup>+/-</sup>;Spry4<sup>-/-</sup>*. Scale bars = 20  $\mu$ m. Cr = crown (analogue); en = enamel/enamel space; Lab. = labial side; Ling. = lingual side; PDL = periodontal ligament; Ro = root (analogue).



## Early polarization and differentiation of odontoblasts in enamel and cementum-facing dentin

To further investigate an early odontoblast's differentiation and dentin morphogenesis, we analyzed the (pre)odontoblast-epithelium interphase close to the labial and lingual cervical loops in wild-type and *Spry2*<sup>+/-</sup>;*Spry4*<sup>-/-</sup> animals (Fig. 6). We show that the presence of differentiating preameloblasts stimulates adjacent preodontoblasts to synchronous polarization and more consistent generation of OPs, resulting in the generation of highly tubular dentin (Fig. 6A, C, D). Conversely, the emerging dentin adjacent to the lingual aspect of the wild-type incisor shows almost atubular structure, likely resulting from more asynchronous polarization of odontoblasts suggested by the uneven distribution of odontoblast nuclei (Fig. 6B). These findings suggest an early patterning effect of the adjacent dental epithelium type on the future microstructure of the whole dentin matrix.

To investigate differences in the timing of odontoblast differentiation between the labial and lingual side of the tooth, we measured the distance of first DSPP- and/or DMP1-expressing

(cerulean and cherry fluorescent protein-expressing, respectively) odontoblast from the apex of each cervical loop in *DSPP*<sup>Cerulean</sup>/*DMP1*<sup>Cherry</sup> animals (Fig. 7). In the mandibular incisor, the distance to the first cerulean-positive, cherry-positive, and both reporter-expressing odontoblast was significantly longer on the lingual side when compared with the labial side (Fig. 7A, B). In the maxillary incisor, the differences in the distances were greatly reduced, but the distances on the lingual side were still significantly longer for all three measured features (Fig. 7C, D). These data suggest that the differentiation into functional odontoblasts is faster on the labial side of the incisor.

## Molecular differences of odontoblasts on the labial and lingual aspect of mouse incisor

To address molecular differences of odontoblasts on the labial and lingual aspect, we performed in situ hybridization (ISH) and immunohistochemical (IHC) expression analysis of selected odontoblast-specific genes. First, we analyzed the expression of two Wnt-signaling related genes, *Dkk1* and *Wisp1*, using ISH.

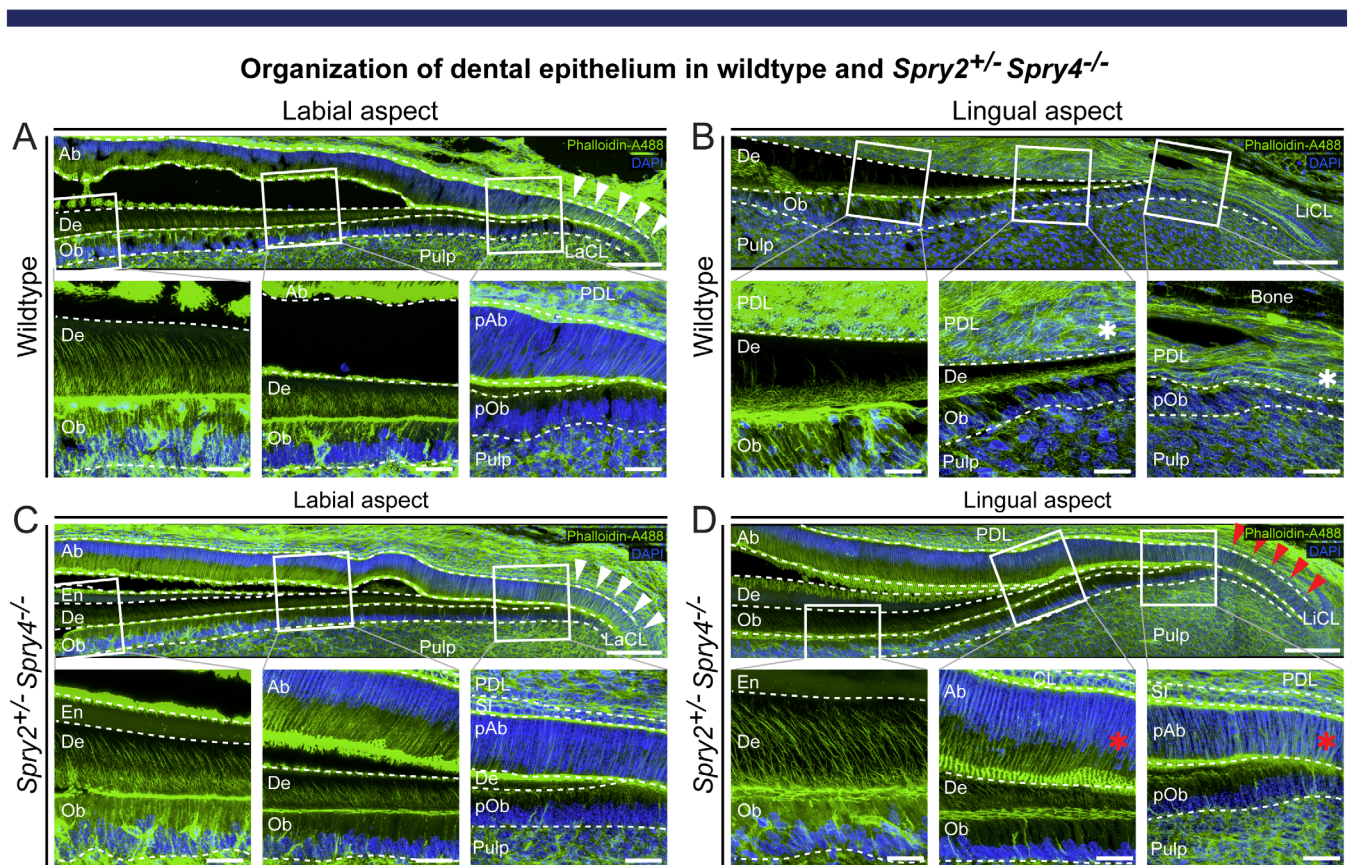


**Fig 6.** Early polarization of odontoblast and dentin patterning. Confocal images of histological sections from maxillary incisors of wild-type and *Spry2*<sup>+/-</sup>;*Spry4*<sup>-/-</sup> animals stained with Phalloidin-Alexa488 (green) and DAPI (blue). Each panel contains an overview image of the early differentiating area where preodontoblasts polarize and differentiate. Highlighted subsets show details of differentiation. In the wild-type mouse, epithelium at the labial aspect gives rise to (pre)ameloblasts (highlighted with white arrowheads A), whereas at the lingual aspect, preameloblasts are not formed and the epithelium is being disintegrated (B). In contrast to this, the enamel-forming ameloblast epithelium is formed by both labial and lingual cervical loops of *Spry2*<sup>+/-</sup>;*Spry4*<sup>-/-</sup> incisors. Ectopic, (pre)ameloblastic epithelium is marked with red arrowheads. Asterisks highlight the difference between the structure of wild-type and *Spry2*<sup>+/-</sup>;*Spry4*<sup>-/-</sup> lingual cervical loop highlighting different interacting partners of the respective (pre)odontoblasts. Note faster polarization of odontoblasts induced by adjacent epithelium with ameloblasts at the labial aspect of wild-type and both aspects of *Spry2*<sup>+/-</sup>;*Spry4*<sup>-/-</sup> incisors (A, C, D). Scale bars = 100 μm (cervical loop tile scans), 25 μm (details). Ab = ameloblasts; pAb = preameloblasts; De = dentin; En = enamel space; LaCL = labial cervical loop; LiCL = lingual cervical loop; Ob = odontoblasts; pOb = preodontoblasts; P = pulp; PDL = periodontal ligament.

Strong expression of *Dkk1* was localized in preodontoblasts exclusively on the labial side of the incisors (Fig. 8A, B). On the lingual side, only weak spots of positive signal were found. *Wisp1* expression was also located predominantly on the labial side of the incisors with the expression being consistent even in older odontoblasts (Fig. 8C, D). On the lingual side, a weaker signal was found only close to the cervical loop. Similar to this, we observed a specific and strong nuclear signal of SALL1 (IHC) in the odontoblasts on labial sides of the incisors (Fig. 8E, F). On the lingual side, the nuclear signal of Sall1 was only slightly above the level of the background and started further from the cervical loop apex. Nuclear signal of NFIC was found in the pulp cells surrounding both cervical loops (Fig. 8G, H). NFIC was also expressed in odontoblasts and subodontoblastic cells on both sides of the incisors. The signal found in odontoblasts did, however, diminish further from the cervical loops.

### Analysis of element composition and dentin density

To further investigate whether the differences in the morphology of the OPs are connected to the different composition of key elements of the dentin matrix, we performed laser-induced breakdown spectroscopy (LIBS) analysis on the established model of mouse incisor. The spectroscopic analysis provided semiquantitative information on the spatial distribution of calcium and magnesium in mandibular and maxillary mouse incisors on transversal sections. The methodology of elemental mapping by LIBS has been previously described.<sup>(33,34)</sup> The

analysis was performed on the ground, polished sections from the distal part of the maxillary and mandibular incisors (Fig. 9A).

The relative contents of calcium and magnesium were plotted as a function of the measurement position. It was observed that calcium was most abundant in the enamel in contrast to magnesium, which was detected in higher amounts in dentin (Fig. 9A). Focusing on the dentin, we detected a higher amount of calcium in the dentin facing the enamel in both mandibular and maxillary incisors. Magnesium showed uneven distribution within the dentin matrix being slightly more present in the enamel-facing dentin in the mandibular incisor.

Additionally, principal component analysis (PCA) of the LIBS data was performed to further highlight more complex relationships of the elemental composition of incisors. The utilization of PCA in LIBS has already been thoroughly described previously.<sup>(35)</sup> Principal component (PC) scores were plotted on a map with respect to the original spectra position. The resulting patterns were afterwards compared with the original teeth structure knowing the correlation between PC scores and the original samples. The respective PC loadings were investigated to yield information about the contribution of individual elements. Most interesting information was observed in PC1 and PC3 presented in Fig. 9B and Figs. S3 and S4. Analysis of loadings (Fig. S4) showed the highest contribution of Ca followed by Mg to PC1. In other words, the higher the PC score means the higher the intensity of the spectral line and hence the content of the respective element. Conversely, in PC3, higher values resulted from the high intensity of calcium and low intensity of magnesium. PCA suggested a trend of enamel-facing dentin being different in

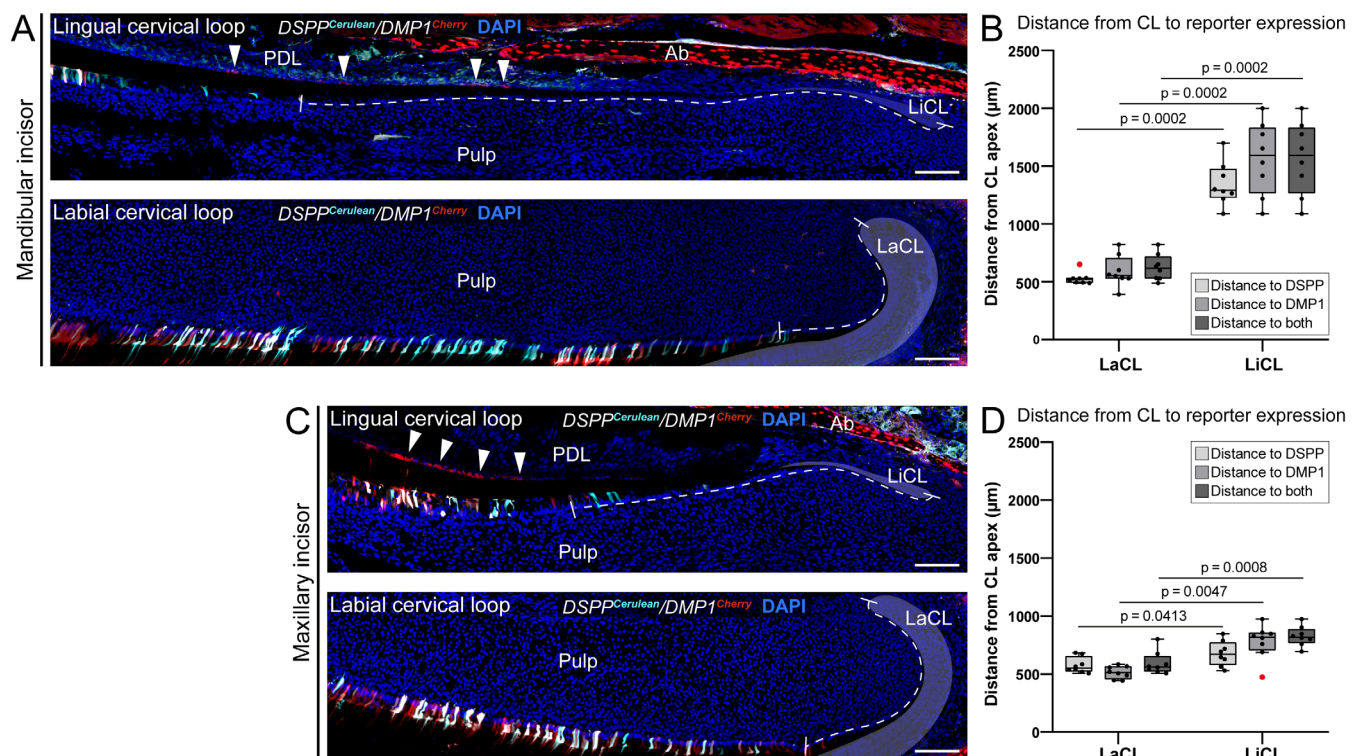


**Fig 7.** Reporter expression distance analysis. Analysis of images taken from *DSSP<sup>Cerulean</sup>/DMP1<sup>Cherry</sup>* mandibular (A) and maxillary (C) incisor's apical regions. The distance from the apex of the cervical loop to the first cell expressing fluorescent protein: DSSP (cerulean), DMP1 (cherry), or both were measured and results were compared between the lingual and labial aspects (B, D). Scale bars = 200 µm. Arrows indicate cementoblasts. Ab = alveolar bone; LaCL = labial cervical loop; LiCL = lingual cervical loop; PDL = periodontal ligament.

elemental composition from the opposing, cementum-facing dentin (Fig. 9B; Fig. S4). This phenomenon was more pronounced in the case of the mandibular incisor.

Based on the above-mentioned results, the PC1 and PC3 scores were cross plotted (Fig. S4) and data points clustered by using *k*-means clustering (5 clusters). Each cluster was assigned a color and the respective colors were subsequently presented in the

picture as a function of position (Fig. 9C). Cluster 1 corresponds to enamel, clusters 2 and 3 correspond to both cementum-facing dentin and alveolar bone. Cluster 5 corresponds to resin in which the samples were embedded and soft tissues. Finally, cluster 4 specifically designates enamel-facing dentin.

Finally, to assess the dentin X-ray density in different regions of dentin, we utilized the micro-CT analysis of wild-type maxillary

## Molecular differences in odontoblasts on the labial and lingual aspect of mouse incisors

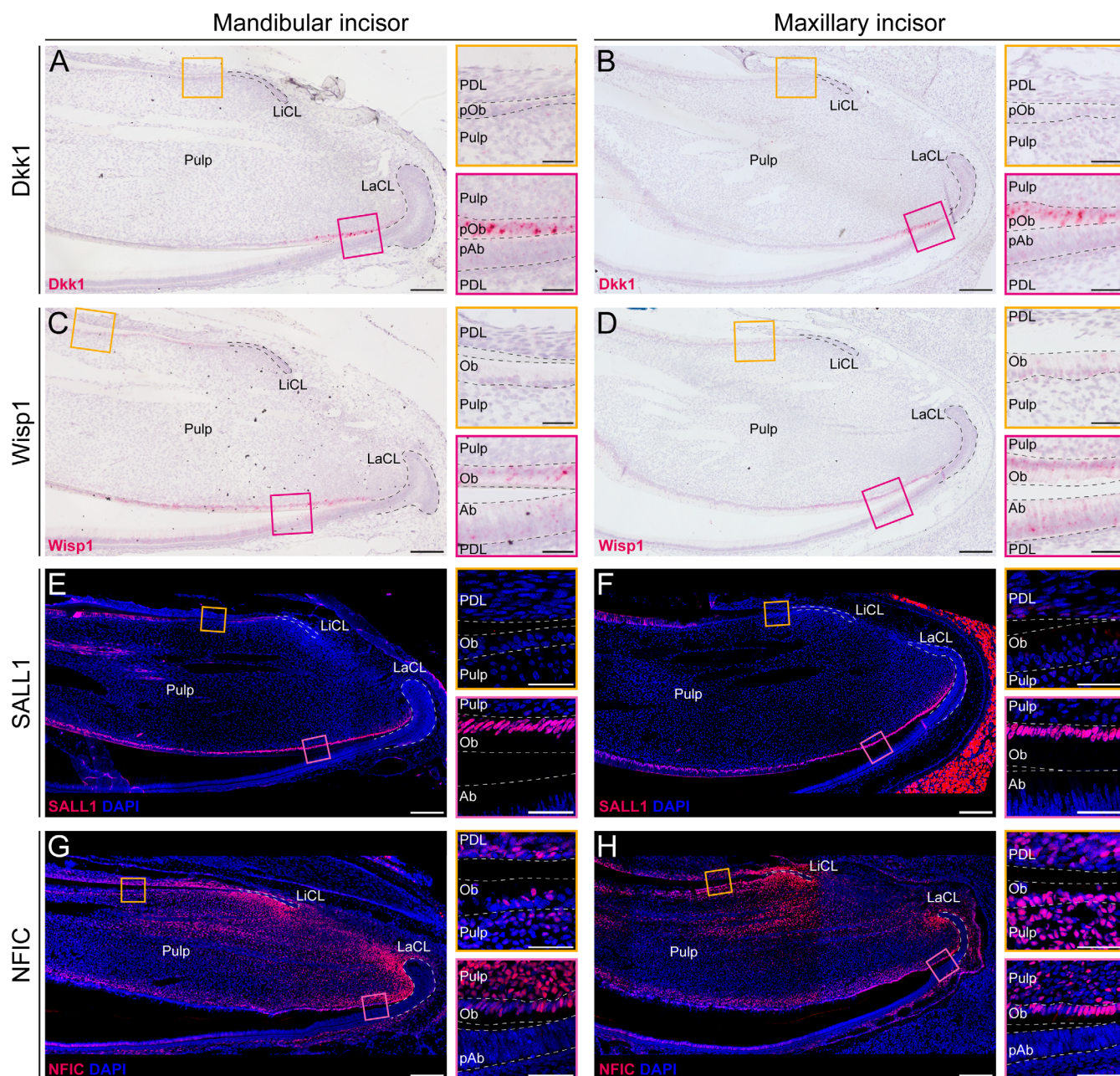
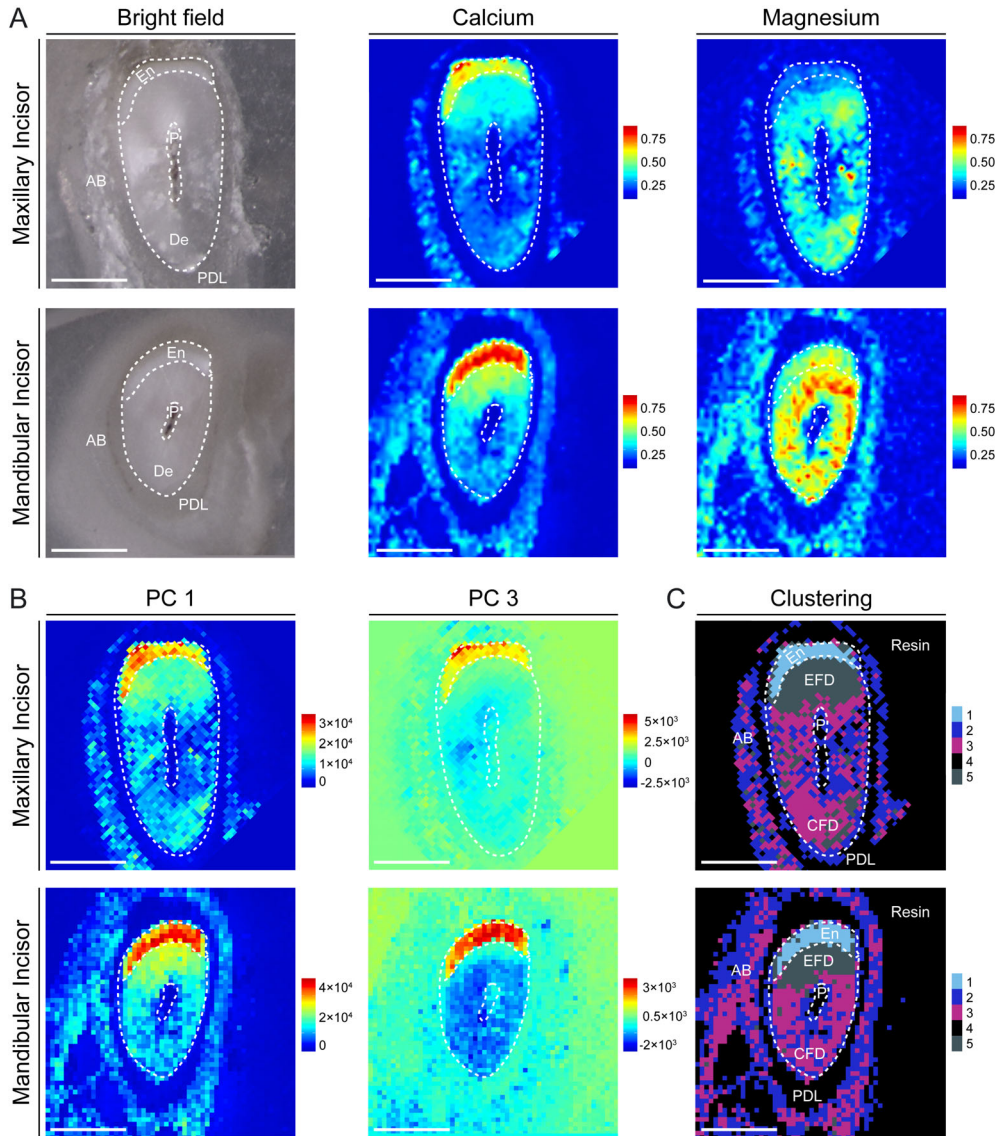


**Fig 8.** Molecular differences of odontoblasts on the labial and lingual aspect of mouse incisor. Analysis of selected odontoblast-specific molecular markers shows a different expression pattern on the labial and lingual aspect of both mandibular and maxillary incisors. In situ hybridization of *Dkk1* (A, B) and *Wisp1* (C, D) shows a specific expression only in odontoblasts on the labial aspect of the incisor. Similar to this, the immunohistochemical staining of SALL1 shows the same expression pattern (E, F), while the immunohistochemical staining of previously shown NFIC (G, H) did not show a different expression on labial and lingual aspects. Scale bars = 200  $\mu$ m (overview images) and 50  $\mu$ m (details). LaCL = labial cervical loop; LiCL = lingual cervical loop; Ab = ameloblasts; pAb = preameloblasts; Ob = odontoblasts; pOb = preodontoblasts; PDL = periodontal ligament.

## LIBS analysis of element composition of wildtype incisors



## Micro-CT analysis of X-ray density of wildtype incisors

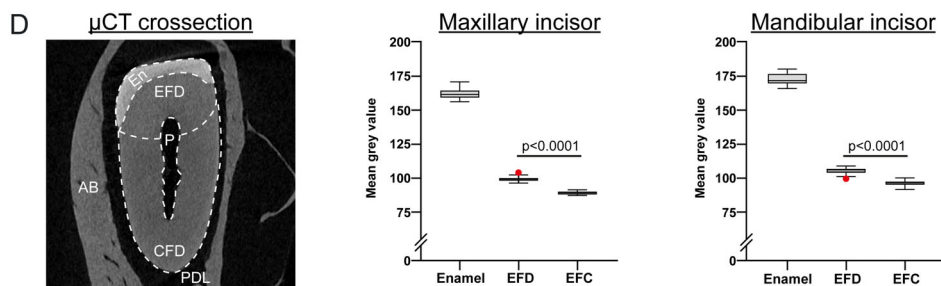


**Fig 9.** Analysis of elemental composition and dentin density. Brightfield images (left) of ground sectioned, polished teeth sections and subsequent analyses (right) represent heat maps showing the relative amount of calcium and magnesium on the transversal section from the distal part of the mandibular and maxillary incisor (A). The function of position plots of principal component analysis (B) and *k*-means clustering from the PCA (D). Micro-CT analysis of dentin density in EFD and CFD of mandibular and maxillary incisors (C) ( $n = 25$ ). Graphs also plot the grey mean values of enamel to enable the comparison between dentin and enamel. Scale bars = 500  $\mu$ m. AB = alveolar bone; CFD = cementum-facing dentin; EFD = enamel-facing dentin; En = enamel; PDL = periodontal ligament.

and mandibular incisor (Fig. 9D). Although the differences between the enamel-facing (EFD, labial) and cementum-facing (CFD, lingual) dentins are faint, the analysis of mean gray value of these two regions has shown significantly higher values in EFD ( $p < 0.0001$ ) in both mandibular and maxillary incisor.

## Discussion

Microstructure, chemical composition, and development of dentin and odontoblasts have been extensively studied topics for many decades. This tissue gives the tooth its shape and specific mechanical and sensory properties. Here we expand the knowledge about dentin microstructure and composition and provide evidence for differences in the microstructure of dentin secreted by odontoblasts facing dental epithelium during early hard-tissue formation. Furthermore, we show differential expression of several odontoblast-specific genes that may control the observed differences in dentin and odontoblast structure.

Because dentin is not remodelled, the complete developmental history of dentin is sealed in the inner structure of this hard matrix. The morphology of dentinal tubules then reflects the development of odontoblasts and visualization of dentin microstructure provides us with a detailed history of the dentinogenesis itself.<sup>(14,36)</sup> Our data show that the type of dental epithelium influences the adjacent preodontoblasts in a different manner, which results in different microstructure and elemental composition of the adjacent dentin controlled by the very beginning of its formation.

It was shown before that dentin in root and crown differs on several levels including the composition of phosphoproteins, levels of calcification, speed of crystal growth, and mechanical properties.<sup>(18,19,37)</sup> However, only a limited number of research studies focus on the morphology of the dentinal tubules and their functional components—odontoblast processes.<sup>(14,36,38)</sup> Using *DSPP<sup>Cerulean</sup>/DMP1<sup>Cherry</sup>* mouse strain, we were able to map the three-dimensional morphology of odontoblast processes in an unprecedented detail. First, we described a significantly different OPs morphology within the crown and roots of mouse molars. Furthermore, our results show that this phenomenon is reflected in the incisors, which are structurally and developmentally different. Importantly, we show that the inner microstructure of dentin is changed when the type of adjacent epithelium changes its function. Our findings suggest that the predetermination of dental epithelium controls the structure of OPs by controlling the differentiation of the adjacent odontoblasts. Our results are consistent when comparing different types of teeth (both molars and incisors) and different inbred strains (CD1 and BI/6 background). Functional analysis on animals with ectopic enamel on the lingual aspect of maxillary incisors (using *Spry2<sup>+/-</sup>;Spry4<sup>-/-</sup>* animals) enabled us to make a conclusion of enamel-facing and cementum-facing predetermination of dentin microstructure. Important to note is that the phenotype of *Spry2<sup>+/-</sup>;Spry4<sup>-/-</sup>* animals is highly variable with incomplete penetrance. We observed the presence of ectopic enamel only in a few maxillary incisors (which were used for the analysis), but no mandibular incisors with ectopic enamel were observed. Comparing the microstructure of maxillary and mandibular incisors using *DSPP<sup>Cerulean</sup>/DMP1<sup>Cherry</sup>* animals provided us with identical results regarding the microstructure of OPs. This, together with the results obtained from the analysis of *Spry2<sup>+/-</sup>;Spry4<sup>-/-</sup>* maxillary incisor, serves as adequate proof of principle.

It had been shown that cementum is present on the lingual aspect of rodent incisors.<sup>(39)</sup> The development of cementoblasts and cementum in continuously growing incisors is still not fully understood.<sup>(39-41)</sup> Our results confirm the presence of DMP1-expressing cementoblasts in the periodontal space attached to the lingual side of dentin. Periodontal ligaments in periodontal space were visualized by POSTN staining for greater clarity (Fig. S1).<sup>(28)</sup> The structure of the cementoblast layer and periodontal space in the incisors displayed the same pattern as in molar roots. This enabled us to establish universal terms cementum-facing and enamel-facing dentin. DMP1-expressing cementoblasts were preferentially found in the more apical region on the incisor lingual aspect. In the more distal parts, just a seldom presence of DMP1-expressing cementoblasts was observed. This might show that the activity of cementum-forming cells is limited mostly to the apical region and later their activity decreases.

To quantify the observed differences between the OPs found in enamel-facing and cementum-facing dentin, we at first chose straightness. This parameter was chosen because of its independence on the length of the process, which naturally varies because of changing dentin height. The observed trend showed that in the enamel-facing dentin, the OPs have straighter (straightness value closer to 1) morphology when compared with the cementum-facing dentin. Although the general trend of cementum-facing and enamel-facing microstructure of OPs was similar in all observed conditions and samples, minor differences can be observed in OP morphology comparing incisors and molars.

The overall larger differences in the straightness of the two different classes of OPs in the molar may be caused by the temporal separation of the production of the crown and root dentin. Conversely, the smaller differences in the incisors may be caused by synchronous deposition of the dentin matrix, which has to accommodate for the abrasion of the tip of the incisor. Furthermore, the small, though still statistically significant, differences between the OPs in the mandibular incisor may be in part caused by less pronounced curvature of the incisor when compared with the maxillary incisor in which the OPs have a larger difference between the two sides.

Moreover, in mouse incisors, we analyzed the OP's width, number density, the dentin quality by measuring the fraction of dentin height without the presence of the main process and the analysis of the distribution of all processes in different regions of dentin. All these data have consistently shown statistically significant differences in all aspects between the labial and lingual sides of wild-type mandibular and maxillary incisors. Additionally, the analysis of dentin in *Spry2<sup>+/-</sup>;Spry4<sup>-/-</sup>* maxillary incisors has shown that dentin facing an ectopically present enamel on the lingual aspect of the incisor is in most of the observed aspects more similar to dentin on the labial side. This further confirms the inductive role of different kinds of dental epithelium on dentin microstructure. Interestingly, the number density of processes in *Spry2<sup>+/-</sup>;Spry4<sup>-/-</sup>* displayed the same trend as observed in wild-type animals. This suggests that this feature of dentin is determined by a different mechanism, which is independent of the inductive role of the ameloblastic epithelium.

Previous studies performed on rat incisors report that in mandibular incisors the enamel-facing odontoblasts display production of predentin that exceeds that of the cementum-facing odontoblasts.<sup>(18)</sup> Furthermore, it has been reported that the conversion of cementum-facing predentin into dentin is faster than

in the enamel-facing dentin. Thus, the speed of dentin growth might cause a change of OP morphology as a secondary effect.

Based on these previous observations, we decided to investigate the possible differences in the early odontoblast differentiation and dentin production. To do so, we focused on the cervical regions of the incisors. Our results show that the distinct morphology of OPs on labial and lingual sides of wild-type incisors is established during the early odontoblast differentiation. Interestingly, on the lingual side, the odontoblasts polarize further from the cervical loop and only a few of them leave their processes in the newly formed dentin. This paired with the analysis of the relative fraction of dentin height without the presence of the main process suggests a more asynchronous differentiation of odontoblast without the presence of ameloblastic epithelium. This is further supported by the fact that in both analyses the *Spry2*<sup>+/-</sup>; *Spry4*<sup>-/-</sup> lingual dentin displays the same trends as the labial dentin.

To further investigate the rate of differentiation of odontoblasts, we analyzed the expression of the reporters in *DSpp*<sup>Cerulean</sup>/*DMP1*<sup>Cherry</sup> mice. Our results go in line with the aforementioned trends. Odontoblasts on the lingual side start to express *Dspp* and *Dmp1* further from the cervical loop, which suggests slower odontoblast differentiation in the absence of ameloblastic epithelium.

Although we observed a consistent phenotype in all analyzed features and conditions, the precise molecular signalling responsible for a different dentin production and microstructure is, however, still unknown. One of the mechanisms that might have a role in this process is RUNX2 and Wnt signalling, which has been shown to have a differential role and effect on adjacent dental mesenchyme in the crown and root dental epithelium.<sup>(42)</sup> Our results support these findings and suggest that Wnt signalling likely plays an important role in dentin patterning. Two Wnt pathway-related genes (*Dkk1* and *Wisp1*) showed robustly different expression patterns in odontoblasts on the labial and lingual aspects of mouse incisor. Moreover, SALL1, a newly identified transcription factor present during odontoblast development,<sup>(28)</sup> showed the same pattern and was predominantly expressed in odontoblasts on the labial side. Recently, SALL1 has been found to be an interacting partner of RUNX2 and was shown to increase the accessibility of cis-regulatory elements inside the *Runx2* locus.<sup>(43)</sup> Interestingly, the knockdown of *Sall1* in murine dental pulp cells in vitro have reduced their odontoblastic differentiation and also inhibited calcification.<sup>(43)</sup> This might coincide with the slower odontoblast differentiation and reduced amount of calcium in the lingual dentin and also its lesser X-ray density in vivo.

Even though it was previously shown that NFIC plays an important role in dental mesenchyme during the growth of molar roots,<sup>(44-46)</sup> we did not observe a clear difference in the expression of this protein on the labial and lingual side of mouse incisor, suggesting it has a different role in incisor renewal than in the extensively studied molar development.<sup>(44-46)</sup> Further investigation needs to be performed to answer precise molecular pathways controlling divergent dentin development.

To investigate the elemental composition of the calcified matrix in each type of dentin, we performed LIBS analysis focused on calcium and magnesium content. We uncovered characteristic regionalization of these two elements distinguishing a cementum-facing and enamel-facing dentin on the elemental level. Previous studies, which used microindentation as one of the methodologies, suggested that in the rat incisor, the enamel-facing dentin is harder, which is caused by a higher

amount of calcium and lower amount of magnesium and vice versa for the cementum-facing dentin.<sup>(47)</sup> It has been further connected to the fact that the enamel-facing dentin matrix displays larger calcospherites, which result from slower calcification, which is likely regulated by the larger ratio of highly phosphorylated phosphoproteins. Cementum-facing dentin then displays smaller calcospherites, resulting from faster calcification likely regulated by a larger ratio of slightly phosphorylated phosphoproteins.<sup>(47)</sup> Authors then attribute the higher amount of magnesium in the cementum-facing dentin as a result of faster calcification, which produced apatite with lower purity (polluted with magnesium).<sup>(18,19,37)</sup> Contrary to the research performed on the rat model, we have found that in the mouse mandibular incisor, the intensity of magnesium signal is slightly elevated in the enamel-facing region of the tooth, and thus reflecting the distribution of calcium, which was, however, much more distinct. In the case of the maxillary incisor, magnesium was more evenly distributed, and its signal displayed lesser intensity compared with the mandibular incisor. The calcium distribution in the maxillary incisor, however, precisely reflected the calcium distribution in the mandibular incisor and therefore was more concentrated in the enamel-facing dentin. Additionally, we employed PCA analysis and *k*-means clustering of the PCA scores. PCA can reveal differences in multidimensional data, express the difference numerically (by scores of respective principal components), and describe the importance of each part of multidimensional data for a particular principal component (PC). In our case, by employing the PCA, we were able to discriminate specific parts of the transversal section of mouse teeth not only based on the relative change of selected elements but also on their complex relationship. The PCA plots and the *k*-means clustering obtained from the PCA data, therefore, highlight the fact that the labial and lingual dentins are distinct when it comes to the composition of the two important elements. Our findings concerning the X-ray density of labial and lingual dentins go in line with previous work on the topic, as it was previously shown that root dentin is less dense than the average value of dentin density.<sup>(48,49)</sup>

Taken together, we summarize that the distinct inner structure of dentin is, from the very beginning of its development, controlled by the type of the adjacent epithelium, and we hypothesize that it is responsible for the different mechanical properties of dentin. Our data also suggest that the different dentin microstructure is controlled by Wnt signalling in odontoblasts. This new insight into the connection between dentin development, function, structure, and composition will be important for future research focused on dental patterning or organogenesis based on epithelial-mesenchymal interactions.

## Disclosures

All authors state that they have no conflicts of interest.

## Acknowledgments

JK was supported by the Grant Agency of Masaryk University (MUNI/H/1615/2018) and by funds from the Faculty of Medicine MU to junior researcher. JL was supported by the Grant Agency of Masaryk University (MUNI/IGA/1532/2020) and is a Brno PhD Talent Scholarship Holder, funded by the Brno City Municipality. MH and KS were supported by the Grant Agency of the Czech Republic (21-041785). PP gratefully acknowledges the support

of the Czech Grant Agency under the project 20-19526Y. MH, KS, and MB were supported by Charles University and the Czech Ministry of Education, Youth and Sports (Progres Q25 and Q29).

We thank Adela Lochmanova for her help taking care of the mice colony and Katarina Mareckova for her help with histological analysis. Our special thanks go to Karel Novotny (Faculty of Science, Masaryk University) and Anna Konecna (CEITEC, Brno University of Technology), who helped with the initial LIBS analysis, and Petr Zaunstöck (Faculty of Science, Masaryk University) for his help with the polishing of samples used for LIBS analysis. Furthermore, we also thank Daniel Kovac for his help with statistical analysis. We acknowledge the core facility CELLIM of CEITEC supported by the Czech-Bioluminescence large RI project (LM2018129 funded by MEYS CR) for their support with obtaining scientific data presented in this paper.

Authors' roles: JKr planned and performed experiments, analyzed the data and wrote the manuscript. JL performed experiments, analyzed the data and wrote the manuscript. MK, DP, VL, MGL, KS, MB, AV, PP, MH, MM performed experiments and analyzed the data. JKa analyzed data.

## Peer Review

The peer review history for this article is available at <https://publons.com/publon/10.1002/jbmr.4471>.

## Data Availability Statement

The data that supports the findings of this study are available in the supplementary material of this article

## References

1. Pashley DH. Dynamics of the pulpo-dentin complex. *Crit Rev Oral Biol Med.* 1996;7(2):104-133.
2. Cho YS, Ryu CH, Won JH, et al. Rat odontoblasts may use glutamate to signal dentin injury. *Neuroscience.* 2016;29(335):54-63.
3. Lee Y-L, Liu J, Clarkson BH, Lin C-P, Godovikova V, Ritchie HH. Dentin-pulp complex responses to carious lesions. *Caries Res.* 2006;40(3):256-264.
4. Lin M, Luo ZY, Bai BF, Xu F, Lu TJ. Fluid mechanics in dentinal microtubules provides mechanistic insights into the difference between hot and cold dental pain. *PLOS One.* 2011;6(3):e18068.
5. Veerayuthwilai O, Byers MR, Pham T-TT, Darveau RP, Dale BA. Differential regulation of immune responses by odontoblasts. *Oral Microbiol Immunol.* 2007;22(1):5-13.
6. Won J, Vang H, Kim JH, Lee PR, Kang Y, Oh SB. TRPM7 mediates mechanosensitivity in adult rat odontoblasts. *J Dent Res.* 2018;97(9):1039-1046.
7. Arana-Chavez VE, Massa LF. Odontoblasts: the cells forming and maintaining dentine. *Int J Biochem Cell Biol.* 2004;36(8):1367-1373.
8. Balic A, Thesleff I. Chapter seven—tissue interactions regulating tooth development and renewal. *Curr Top Dev Biol.* 2015;115:157-186.
9. Thesleff I, Sharpe P. Signalling networks regulating dental development. *Mech Dev.* 1997;67(2):111-123.
10. Bae C-H, Kim T-H, Chu J-Y, Cho E-S. New population of odontoblasts responsible for tooth root formation. *Gene Expr Patterns.* 2013;13(5):197-202.
11. Xiong J, Gronthos S, Bartold PM. Role of the epithelial cell rests of Malassez in the development, maintenance and regeneration of periodontal ligament tissues. *Periodontol.* 2000;63:217-233.
12. Yamashiro T, Zheng L, Shitaku Y, et al. Wnt10a regulates dentin sialophosphoprotein mRNA expression and possibly links odontoblast

- differentiation and tooth morphogenesis. *Differentiation.* 2007;75(5):452-462.
13. Krivanek J, Adameyko I, Fried K. Heterogeneity and developmental connections between cell types inhabiting teeth. *Front Physiol.* 2017;8:376.
14. Khatibi Shahidi M, Krivanek J, Kaukua N, et al. Three-dimensional imaging reveals new compartments and structural adaptations in odontoblasts. *J Dent Res.* 2015;94(7):945-954.
15. Smith AJ, Cassidy N, Perry H, Begue-Kirn C, Ruch J-V, Lesot H. Reactionary dentinogenesis. *Int J Dev Biol.* 1995;39(1):273-280.
16. Smith AJ, Scheven BA, Takahashi Y, Ferracane JL, Shelton RM, Cooper PR. Dentine as a bioactive extracellular matrix. *Arch Oral Biol.* 2012;57(2):109-121.
17. Couve E, Osorio R, Schmachtenberg O. The amazing odontoblast: activity, autophagy, and aging. *J Dent Res.* 2013;92(9):765-772.
18. Beertsen W, Niehof A. Root-analogue versus crown-analogue dentin: a radioautographic and ultrastructural investigation of the mouse incisor. *Anat Rec.* 1986;215(2):106-118.
19. Steinfors J, van den Bos T, Beertsen W. Differences between enamel-related and cementum-related dentin in the rat incisor with special emphasis on the phosphoproteins. *J Biol Chem.* 1989;264(5):2840-2845.
20. Simon S, Smith AJ, Lumley PJ, et al. Molecular characterization of young and mature odontoblasts. *Bone.* 2009;45(4):693-703.
21. Sun Y, Gandhi V, Prasad M, et al. Distribution of small integrin-binding ligand, N-linked glycoproteins (SIBLING) in the condylar cartilage of rat mandible. *Int J Oral Maxillofac Surg.* 2010;39(3):272-281.
22. Toyosawa S, Okabayashi K, Komori T, Ijuhin N. mRNA expression and protein localization of dentin matrix protein 1 during dental root formation. *Bone.* 2004;34(1):124-133.
23. Vijaykumar A, Ghassem-Zadeh S, Vidovic-Zdrilic I, et al. Generation and characterization of DSPP-cerulean/DMP1-cherry reporter mice. *Genesis.* 2019;57:e23324.
24. Boran T, Peterkova R, Lesot H, Lyons DB, Peterka M, Klein OD. Temporal analysis of ectopic enamel production in incisors from sprouty mutant mice. *J Exp Zool B Mol Dev Evol.* 2009;312B(5):473-485.
25. Klein OD, Lyons DB, Balooch G, et al. An FGF signaling loop sustains the generation of differentiated progeny from stem cells in mouse incisors. *Development.* 2008;135(2):377-385.
26. Klein OD, Minowada G, Peterkova R, et al. Sprouty genes control diastema tooth development via bidirectional antagonism of epithelial-mesenchymal FGF signaling. *Dev Cell.* 2006;11(2):181-190.
27. Shim K, Minowada G, Coling DE, Martin GR. Sprouty2, a mouse deafness gene, regulates cell fate decisions in the auditory sensory epithelium by antagonizing FGF signaling. *Dev Cell.* 2005;8(4):553-564.
28. Krivanek J, Soldatov RA, Kastriiti ME, et al. Dental cell type atlas reveals stem and differentiated cell types in mouse and human teeth. *Nat Commun.* 2020;11(1):4816.
29. Schneider CA, Rasband WS, Eliceiri KW. NIH Image to ImageJ: 25 years of image analysis. *Nature Methods.* 2012;9(7):671-675. <https://doi.org/10.1038/nmeth.2089>
30. An Z, Sabalic M, Bloomquist RF, Fowler TE, Streelman T, Sharpe PT. A quiescent cell population replenishes mesenchymal stem cells to drive accelerated growth in mouse incisors. *Nat Commun.* 2018;9(1):1-9.
31. Harada H, Kettunen P, Jung H-S, Mustonen T, Wang YA, Thesleff I. Localization of putative stem cells in dental epithelium and their association with notch and Fgf signaling. *J Cell Biol.* 1999;147(1):105-120.
32. Bleckert A, Photowala H, Alford S. Dual pools of actin at presynaptic terminals. *J Neurophysiol.* 2012;107(12):3479-3492.
33. Limbeck A, Brunnbauer L, Lohninger H, et al. Methodology and applications of elemental mapping by laser induced breakdown spectroscopy. *Anal Chim Acta.* 2021;22(1147):72-98.
34. Modlitbová P, Pořízka P, Kaiser J. Laser-induced breakdown spectroscopy as a promising tool in the elemental bioimaging of plant tissues. *TrAC Trends in Analytical Chemistry.* 2020;122:115729. <https://doi.org/10.1016/j.trac.2019.115729>
35. Pořízka P, Klus J, Képeš E, Prochazka D, Hahn DW, Kaiser J. On the utilization of principal component analysis in laser-induced breakdown spectroscopy data analysis, a review. *Spectrochim Acta Part B Atomic*

- Spectroscopy. 2018;148:65-82. <https://doi.org/10.1016/j.sab.2018.05.030>
36. Li C, Jing Y, Wang K, et al. Dentinal mineralization is not limited in the mineralization front but occurs along with the entire odontoblast process. *Int J Biol Sci.* 2018;14(7):693-704.
  37. Mishima H, Kozawa Y, Sakae T. Two patterns of calcification in rat and rabbit incisor dentin. In Suga S, Nakahara H, eds. *Mechanisms and phylogeny of mineralization in biological systems.* Tokyo: Springer Japan; 1991 pp 223-227.
  38. Shuhaibar N, Hand AR, Terasaki M. Odontoblast processes of the mouse incisor are plates oriented in the direction of growth. *Anat Rec.* 2020;304(8):1820-1827.
  39. Foster BL, Soenjaya Y, Nociti FH, et al. Deficiency in acellular cementum and periodontal attachment in Bsp null mice. *J Dent Res.* 2013;92(2):166-172.
  40. Imhof T, Balic A, Heilig J, et al. Pivotal role of tenascin-W (-N) in post-natal incisor growth and periodontal ligament remodeling. *Front Immunol.* 2021;11:608223.
  41. Tummers M, Thesleff I. Observations on continuously growing roots of the sloth and the K14-Eda transgenic mice indicate that epithelial stem cells can give rise to both the ameloblast and root epithelium cell lineage creating distinct tooth patterns. *Evol Dev.* 2008;10(2):187-195.
  42. Wen Q, Jing J, Han X, et al. Runx2 regulates mouse tooth root development via activation of WNT inhibitor NOTUM. *J Bone Miner Res.* 2020;35(11):2252-2264.
  43. Lin Y, Xiao Y, Lin C, et al. SALL1 regulates commitment of odontoblast lineages by interacting with RUNX2 to remodel open chromatin regions. *Stem Cells.* 2021;39(2):196-209.
  44. Huang X, Xu X, Bringas P, Hung YP, Chai Y. Smad4-Shh-Nfic Signaling Cascade-Mediated Epithelial-Mesenchymal Interaction is Crucial in Regulating Tooth Root Development. *J Bone Miner Res.* 2010;25(5):1167-1178. <https://doi.org/10.1359/jbmr.091103>
  45. Kim T-H, Bae C-H, Yang S, Park J-C, Cho ES. Nfic regulates tooth root patterning and growth. *Anat Cell Biol.* 2015;48(3):188-194.
  46. Liu Y, Feng J, Li J, Zhao H, Ho T-V, Chai Y. An Nfic-hedgehog signaling cascade regulates tooth root development. *Development.* 2015;142(19):3374-3382.
  47. Steinfort J, Deblauwe BM, Beertsen W. The inorganic components of cementum- and enamel-related dentin in the rat incisor. *J Dent Res.* 1990;69(6):1287-1292.
  48. Gradl R, Zanette I, Ruiz-Yaniz M, et al. Mass density measurement of mineralized tissue with grating-based X-ray phase tomography. *PLOS One.* 2016;11(12):e0167797.
  49. Manly RS, Hodge HC, Ange LE. Density and refractive index studies of dental hard tissues: II. Density distribution curves 1,2. *J Dent Res.* 1939;18(3):203-211.

## 5.7 Příloha G – Publikace číslo 7

# **Rapid isolation of single cells from mouse and human teeth**

*Jan Krivanek, Josef Lavicky, Thibault Boudierlique, Igor Adameyko*

# Rapid Isolation of Single Cells from Mouse and Human Teeth

Jan Krivanek<sup>1</sup>, Josef Lavicky<sup>1</sup>, Thibault Boudierlique<sup>2</sup>, Igor Adameyko<sup>2,3</sup>

<sup>1</sup> Department of Histology and Embryology, Faculty of Medicine, Masaryk University <sup>2</sup> Department of Molecular Neuroimmunology, Centre for Brain Research, Medical University of Vienna <sup>3</sup> Department of Physiology and Pharmacology, Karolinska Institute

## Corresponding Authors

Jan Krivanek

jan.krivanek@med.muni.cz

Igor Adameyko

igor.adameyko@meduniwien.ac.at

## Citation

Krivanek, J., Lavicky, J., Boudierlique, T., Adameyko, I. Rapid Isolation of Single Cells from Mouse and Human Teeth. *J. Vis. Exp.* (), e63043, doi:10.3791/63043 (2021).

## Date Published

October 27, 2021

## DOI

10.3791/63043

## URL

jove.com/video/63043

## Introduction

Single-cell RNA sequencing is a powerful tool for deciphering *in vivo* cell population structure, hierarchy, interactions, and homeostasis<sup>1,2</sup>. However, its results strongly depend on the first step of this advanced analysis - the preparation of a single-cell suspension of perfect quality out of the complex, well-organized tissue. This encompasses keeping cells alive and preventing unwanted, artificial changes in gene expression profiles of the cells<sup>3,4</sup>. Such changes might lead

to the inaccurate characterization of population structure and misinterpretation of the collected data.

Specific protocols for the isolation out of a wide range of tissues have been developed<sup>5,6,7,8</sup>. They usually employ mechanical dissociation in combination with further incubation with various proteolytic enzymes. These typically include trypsin, collagenases, dispases, papain<sup>6,7,8,9</sup>, or commercially available enzyme mixtures such as Accutase,

## Abstract

Mouse and human teeth represent challenging organs for quick and efficient cell isolation for single-cell transcriptomic or other applications. The dental pulp tissue, rich in the extracellular matrix, requires a long and tedious dissociation process that is typically beyond the reasonable time for single-cell transcriptomics. For avoiding artificial changes in gene expression, the time elapsed from euthanizing an animal until the analysis of single cells needs to be minimized. This work presents a fast protocol enabling to obtain single-cell suspension from mouse and human teeth in an excellent quality suitable for scRNA-seq (single-cell RNA-sequencing). This protocol is based on accelerated tissue isolation steps, enzymatic digestion, and subsequent preparation of final single-cell suspension. This enables fast and gentle processing of tissues and allows using more animal or human samples for obtaining cell suspensions with high viability and minimal transcriptional changes. It is anticipated that this protocol might guide researchers interested in performing the scRNA-seq not only on the mouse or human teeth but also on other extracellular matrix-rich tissues, including cartilage, dense connective tissue, and dermis.

Tryple, etc.<sup>5</sup>. The most critical part affecting the transcriptome quality is enzymatic digestion. It was shown that prolonged incubation with enzymes at 37 °C influences the gene expression and causes the upregulation of many stress-related genes<sup>10, 11, 12, 13</sup>. The other critical parameter of the isolation process is its overall length, as it has been shown that cell transcriptomes change after the tissue ischemia<sup>14</sup>. This protocol presents an efficient protocol for gentle isolation of single cells from mouse and human teeth, faster than other, previously utilized protocols for isolation of cells from complex tissues<sup>5, 6, 9, 11, 13, 15, 16</sup>.

This protocol presents how to quickly dissect soft tissue from the hard tooth and prepare a single-cell suspension suitable for scRNA-seq. This method employs only one centrifugation step and minimizes the effect of unwanted transcriptional changes by reducing the tissue handling and digestion time and keeping the tissue and cells at 4 °C most of the time. The procedure showcases the isolation of cells from mouse incisors, molar, and human wisdom teeth as an example, but principally should work for other teeth in various organisms. The complete protocol is schematically visualized in **Figure 1**. This protocol has been recently used to generate a dental cell type atlas obtained from mouse and human teeth<sup>1</sup>.

## Protocol

All animal experiments were performed according to the International and local regulations and approved by the Ministry of Education, youth and sports, Czech Republic (MSMT-8360/2019-2; MSMT-9231/2020-2; MSMT-272/2020-3). This protocol was tested with both male and female wildtype C57BL/6 and CD-1 mice and with genetically modified Sox10::iCreER<sup>T2</sup> mice<sup>17</sup> (combined with various reporter systems) on a C57BL/6 background. Experiments with human samples were performed with the

approval of the Committees for Ethics of the Medical Faculty, Masaryk University Brno & St. Anne's Faculty Hospital in Brno, Czech republic.

## 1. Experimental set-up and preparation of solutions

### 1. Instrument set-up

1. Cool down the centrifuge to 4 °C.
2. Heat the incubation chamber to 37 °C.
3. Start the Fluorescence-activated cell sorting (FACS) machine and set all the temperatures of the sorter (including collection tube holder) to 4 °C. Perform the instrument quality control, set the drop delay.
4. Set the preliminary gating strategy and perform the test sorting.

**NOTE:** When using FACS, use the 100 µm nozzle.

### 2. Prepare the solutions (steps 1.2.1-1.2.3).

1. Wash solution: Prepare fresh 2% FBS (Fetal Bovine Serum) in HBSS (Hanks' Balanced Salt Solution).
2. Digestion mixture: Prepare fresh collagenase P (3 U/mL) fully dissolved in HBSS.
3. Optional: Prepare fresh HBSS + BSA (0.04%) and chill analytical grade methanol in a -20 °C freezer for storing single-cell suspension at -80 °C.

**NOTE:** Step 1 needs to be performed before the start of the experiment. The composition of the utilized solutions is summarized in **Supplementary Table 1**.

## 2. Preparation of experimental animal/s and human tooth

1. Prepare the experimental animals (mouse).

1. Euthanize the mouse according to the local regulations; e.g. by anaesthetics overdose as described previously<sup>1</sup>.

**CAUTION:** Regulations for humane euthanizing of experimental animals varies locally. Always follow valid local regulations.

2. Immediately proceed to the tissue dissection step (step 3).

**NOTE:** If the tissue from the experimental animals cannot be dissected immediately (e.g., because of transfer from animal housing facility), place the experimental animals on ice and perform tissue dissection as soon as possible. To obtain more cells from mouse molar pulps, use younger (6 weeks and less) animals. With increasing age, the size of dental pulp decreases. Mouse incisors mostly keep their structure with increasing age so animals of various ages can be used for tissue dissection.

2. Prepare the human tooth

**NOTE:** Human teeth were extracted for a clinically relevant reason. Every diagnosis was treated individually, and an experienced dental surgeon always performed the tooth extraction.

1. Put the freshly extracted tooth immediately into a 50 mL tube with ice-cold HBSS and keep the tube on ice until further processing.

**NOTE:** Using retained wisdom teeth from patients until age 25-30 is recommended for the highest cell yield.

### 3. Tissue dissection

1. Hold the experimental animal behind its head, looking on the ventral aspect of its head so that the tail points away.

2. Using small, sharp scissors, quickly remove the skin from the mandible to expose the mandibular arch, the soft tissue between each half of the mandibles, and the adjacent facial muscles.

1. Make a deep cut from each side of the mandible; firstly, through m. masseter along the buccal side of the mandible up to the temporomandibular joint, and then along the inner part of each half of the mandible through the base of the oral cavity (see **Supplementary Figure 1**).

3. Cut all the muscles and ligaments along the mandible up to the temporomandibular joint from both outside and inside of the oral cavity.

**NOTE:** Avoid cutting bones. This might damage the most apical part of the incisor.

4. Grasp the mandible using bent tip tweezers and remove it. Then, split the dissected mandible into two halves with scissors by cutting through mandibular symphysis (see **Supplementary Figure 1**).

5. Use an industrial low lint wipe to chafe the remaining soft tissue from each half of the mandible. After both parts of the mandible are cleaned, place them into a pre-prepared Petri dish with ice-cold HBSS.

**NOTE:** From this point forward, work on ice. Further dissection of mouse incisors and molars is performed under a stereomicroscope with a black background.

6. Mouse mandibular incisors

1. For the dissection of mandibular incisors, remove the alveolar ridge with all three molars and transversally crack the mandibular arch in the place corresponding to the position between the first and second molar.

**NOTE:** A sharp scalpel blade no. 11 and tweezers are used to perform this step (see **Table of Materials**).

2. Carefully pull the incisor out of the rest of the dental socket.

**NOTE:** If successful, the extracted incisor will contain intact apical parts, including epithelial tissue with complete cervical loops.

3. If needed, remove the remaining fragments of bone still attached to the incisor with tweezers and a scalpel.
4. Place the dissected incisors into fresh, ice-cold HBSS and dissect the tissue of interest: cervical loop, dental pulp, or other parts of the tooth.
5. Place the dissected soft tissue into a droplet of fresh, ice-cold HBSS in the middle of a 10 cm Petri dish. Keep on ice.

#### 7. Mouse mandibular molars

1. For dissecting mandibular molars, completely remove the alveolar ridge from the rest of the mandible using a scalpel blade.
2. Move the dissected alveolar crest into fresh, ice-cold HBSS in a Petri dish and carefully remove all the remaining fragments of alveolar bones attached to the roots.
3. Place the dissected molars without alveolar bone into fresh, ice-cold HBSS. To expose the pulp, start to remove parts of the dentin from the apical side using fine, sharp tip tweezers until you reach the pulp cavity.
4. Once the pulp cavity is reached, carefully dissect dental pulp using a pair of sharp tip tweezers and

place the soft tissue of the dental pulp into a droplet of fresh, ice-cold HBSS in the middle of a 10 cm Petri dish kept on ice.

**NOTE:** Since mouse molar pulps are extremely small, adapt magnification on the stereomicroscope accordingly.

#### 8. Human tooth

1. Wash human tooth once again in ice-cold HBSS to remove the remaining blood.
2. Place the tooth into three thick-walled sterile plastic bags and use a cast iron benchtop engineer's vise to crack the tooth. Use vise jaws with a flat surface to avoid penetrating the bags.
3. Slowly tighten the vise until you hear the tooth cracking; remove it from the bags and place it into fresh, ice-cold HBSS in a Petri dish.
4. Using two tweezers, take out the dental pulp, clean it from all the remnants of hard tissue and place it into one droplet of ice-cold HBSS in the middle of a 10 cm Petri dish kept on ice.

**CAUTION:** Human tissue might potentially be infectious. When working with human tissue, use protective equipment to avoid direct contact with the tissue.

### 4. Preparation of single-cell suspension

1. Prepare a 15 mL tube with 2.5 mL of digestion mixture composed of Collagenase P (3 U/mL) fully dissolved in HBSS. Keep the solution on ice until use.

**NOTE:** Always use freshly prepared Collagenase P; do not freeze the aliquots. Collagenase P activity varies from batch-to-batch. Check the activity of your batch before diluting. Collagenase P is activated by calcium, whose

amount is already sufficient in the lyophilized powder. Therefore, it is unnecessary to enrich the enzyme mix with calcium. Collagenase P is not inactivated by FBS but can be inactivated by chelating agents (e.g., Ethylenediaminetetraacetic - EDTA). Stopping the dissociation process is ensured by diluting the Collagenase P in Wash solution (2% FBS in HBSS). It has been shown that adding FBS increases cell viability and the final number of cells after sorting<sup>18</sup>.

2. Using a round-shaped scalpel blade no. 10, cut the tissue in all directions into the smallest possible pieces. Reaggregate the tissue pieces in the middle of the droplet and repeatedly cut the tissue aggregates using a round-shaped (No. 10) scalpel blade. Repeat this process several times until the material is sufficiently minced.

3. Transfer the shredded tissue pieces using a 1 mL pipette tip into the prepared digestion mixture.

**NOTE:** In the case of a larger number of animals being processed at once, split the tissue into several tubes with Collagenase P. The maximum amount per tube are pulps obtained from approximately 10 mouse incisors. In the case of molars, where pulps are much smaller, the number of processed pulps can be increased adequately. When using human teeth, use a maximum of 2-3 pulps per tube, depending on the pulp size.

4. Place the tube into a 37 °C preheated incubator with a shaker. Tilt the tube inside the shaker to an angle of 60° and set the speed to 150-200 rpm to ensure constant suspension movements inside the tube.

5. Vigorously triturate the suspension every 3-4 min with a 1 mL pipette tip to disintegrate all the clumps.

**NOTE:** With time, the clumps will become smaller and softer until they almost disappear.

6. In total, incubate for 15-20 min. At the end of the incubation, triturate for the last time, and then slowly add ice cold Wash solution to a final volume of 12 mL.

7. Remove the remaining clumps or pieces of calcified tissue by filtering the suspension using a 50 µm cell strainer.

8. Take 10-20 µL of the filtered cell suspension and count the cells during centrifugation using a cell counting chamber (Hemocytometer). Centrifuge for 5 min at 300 x g at 4 °C. Remove the supernatant using a 10 mL serological pipette.

**NOTE:** If the number of cells is limited that cannot be counted in diluted suspension, skip the cell counting and use all the cells for further processing.

9. Optional: Proceed for fixation and storage<sup>21</sup>.

1. Re-suspend the pellets (up to 10<sup>7</sup> cells) in 100 µL of HBSS + BSA (0.04%).

2. Add 400 µL of chilled methanol and mix slowly.

3. Incubate the cell suspension for 15 min on ice.

4. Store at -80 °C until processed (no longer than 1 month).

10. Resuspend the pellet in the Wash solution. Aim for 700-1200 cells/µL of the Wash solution.

11. Keep the tube on ice until further processing.

**NOTE:** If necessary, perform the fixation and storage at -80 °C. However, immediate processing of the cell suspension for scRNA-seq is recommended. Further steps will depend based on the single-cell RNA seq protocol. When the scRNA-seq protocol uses a microfluidic system (some sc-RNA-seq companies do), load the cells based on the manufacturer's guidelines either directly or after cell sorting.

12. For FACS, proceed to step 5.

## 5. Fluorescence-activated cell sorting (FACS)

1. Before sorting, prepare the cell sorting instrument.
  1. Cool down the whole system to 4 °C, perform the instrument quality control, set the drop delay and the voltage of the deflection plates. Put collection tubes in the collection tube holder.
 

**NOTE:** To avoid additional centrifugation steps resulting in an inevitable cell loss, sort cells into a microtube (1.5 mL) with a small amount (25-50 µL) of the Wash solution.
2. Optional: perform viability staining before FACS.
  1. Add Propidium iodide into cell suspension before FACS to a final concentration 0.5 µg/mL and incubate for 15 min at 4 °C.
3. Load the sample into the cell sorter. Set a strict gating strategy to remove cell debris, doublets, and dead cells. Sort the cells into a prepared tube or multi-well plates. An example of a gating strategy is shown in **Figure 2**.
 

**NOTE:** To minimize manipulation steps and accelerate the protocol, applying a strict gating strategy is recommended (suggested in **Figure 2**) rather than using a viability staining. To separate the immune cells from the isolated population, CD45 antibody staining can be performed. To perform this, resuspend cell suspension in 100 µL of staining solution (PBS + 2% FBS + anti-CD45-APC conjugated antibody 1/100 dilution). Incubate for 15 min on ice protected from light and perform FACS directly.

## Representative Results

Exemplary isolation of single cells was performed from two mandibular incisors from one 6-week-old C57BL/6 mouse male. Following this protocol, a single-cell suspension was prepared, and subsequently, single-cell sequencing was performed. The prepared single-cell suspension was analyzed and sorted using FACS (**Figure 2**). Firstly, the FSC-A (forward scatter, area) and SSC-A (side scatter, area) plotting was applied, and an appropriate gating strategy was used to select a population with expected size and granularity to filter out cell debris and cell doublets or aggregates (**Figure 2A**). This selected population (P1), counting 38% of all events, was further used, and FSC-A and FSC-H (forward scatter, height) parameters were applied to remove the remaining cell doublets (**Figure 2B**). The population without cell doublets (P2) counting 95% of P1 can be subsequently used for scRNA-seq. Alternatively, additional gating can be used to select the population of interest (e.g., expression of fluorescent proteins or live/dead staining). To check the number of live/dead cells in the final suspension, the PI (propidium iodide) staining was performed (**Figure 2C**). The P3 population containing PI<sup>-</sup> (living) cells was 98.4% out of the parent P2 population and 35.5% out of the total events. The total number of filtered out, dead (PI<sup>+</sup>) cells was 1887.

The final number of cells obtained without viability staining suitable for RNA-seq (P2) counted 118,199 cells from two mouse incisor pulps. This means the number of almost 60,000 living cells from one mandibular incisor.

To clarify the number of immune cells in the final single-cell suspension, two approaches were used. Firstly, the CD45 antibody staining and subsequent FACS analysis were used. As a complementary method, the total number of

immune cells (CD45+) in scRNA-seq data was analysed. FACS analysis showed 14.44% of CD45+ cells (13.20% alive and 1.24% dead) (**Figure 3A**). Analysis of scRNA-seq data showed 10.90% of CD45-expressing cells (**Figure 3B**). The decrease of CD45+ cells in scRNA-seq data can be caused by additional thresholding during scRNA-seq analysis.

These representative data on the example of mouse incisor show that the given protocol in combination with strict gating

strategy is efficient in obtaining a high number of cells out of a single mouse tooth without the necessity of additional use of viability staining. The ratio of immune (CD45+) cells was minor (13.2%). Moreover, it was previously shown that the immune cells are essential in maintaining tooth homeostasis, so removing them from scRNA-seq analysis during the FACS would be counterproductive in some applications.

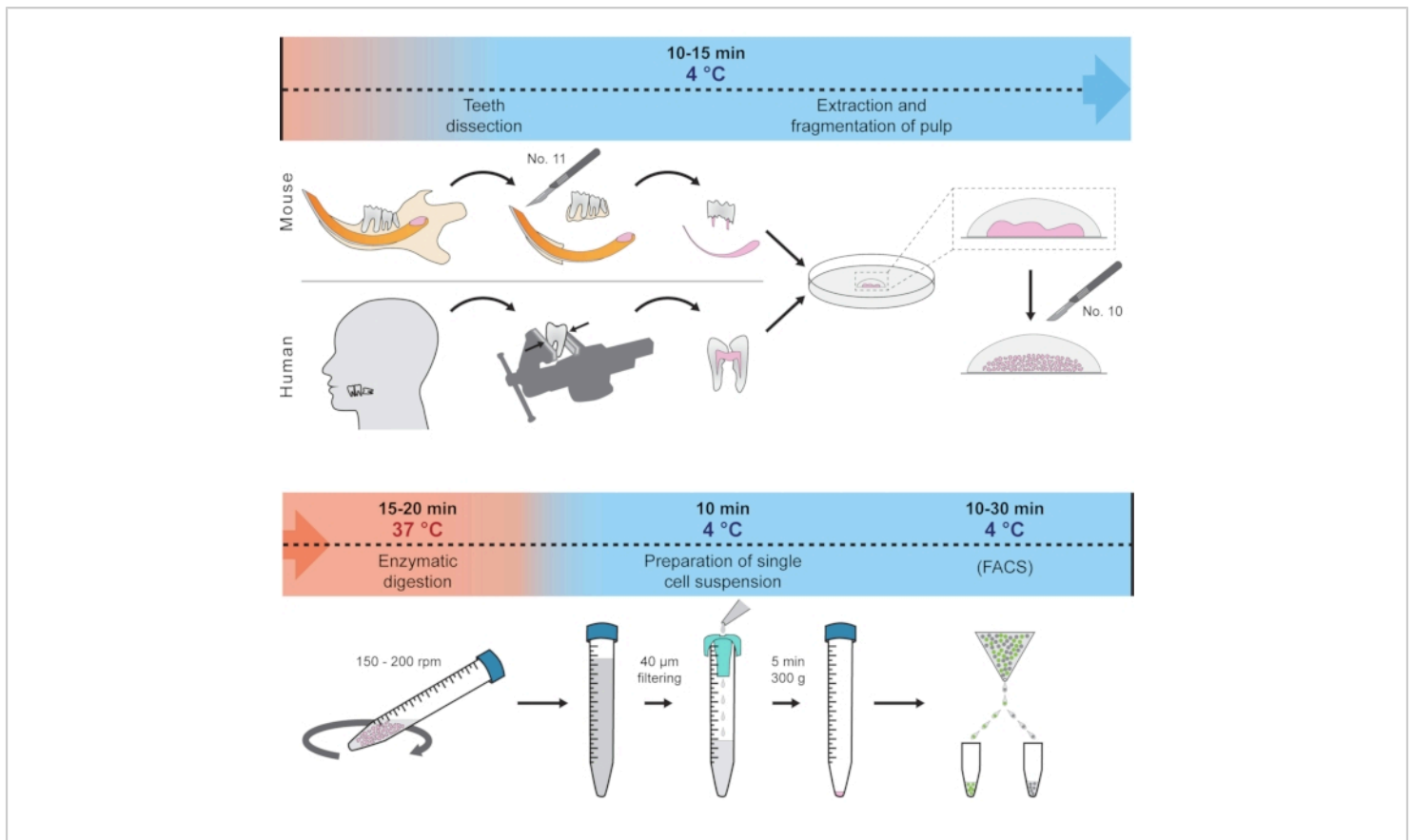


**Figure 1: Schematic representation of the protocol.** Different steps, including temperature conditions and expected time, are represented to prepare single-cell suspension from mouse and human teeth. [Please click here to view a larger version of this figure.](#)

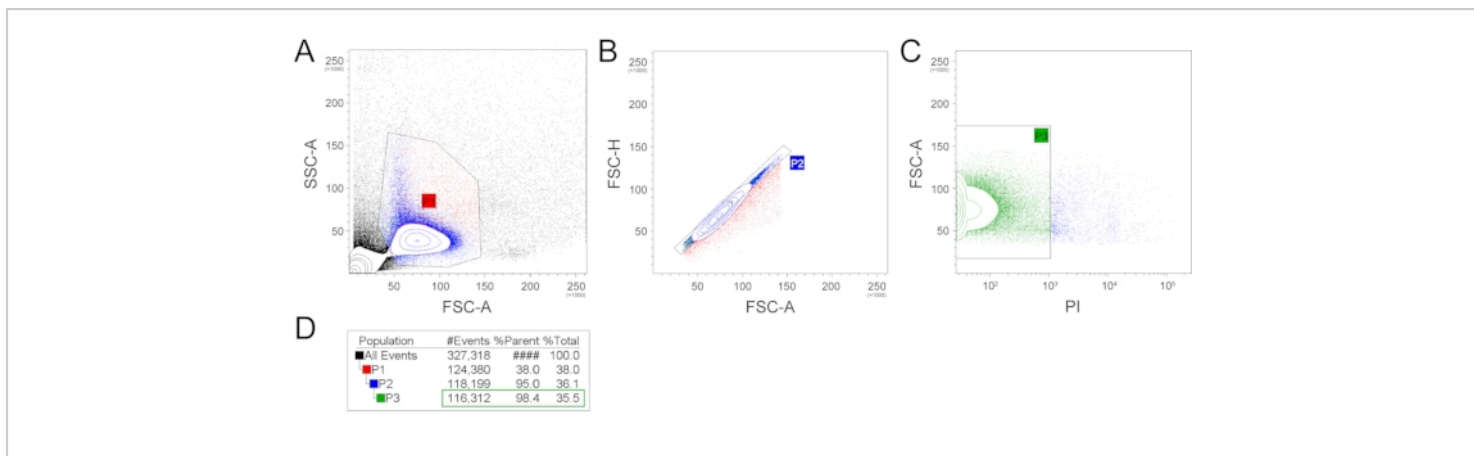


**Figure 2: Example of the gating strategy.** FSC-A and SSC-A gating was used to produce the P1 gate, reflecting the cell population with expected size and granularity and filtering out the cell and extracellular matrix debris and most large events (A). Subsequently, the P1 population was plotted in FSC-H and FCS-A plot, which filtered out cell doublets (B). This P2 population was then analyzed for the presence of dead cells by propidium iodide (C). The number of events/cells per gate are represented in (D). (FSC-A - forward scatter, area; SSC-A - side scatter, area; FSC-H - forward scatter, height; PI - propidium iodide). [Please click here to view a larger version of this figure.](#)

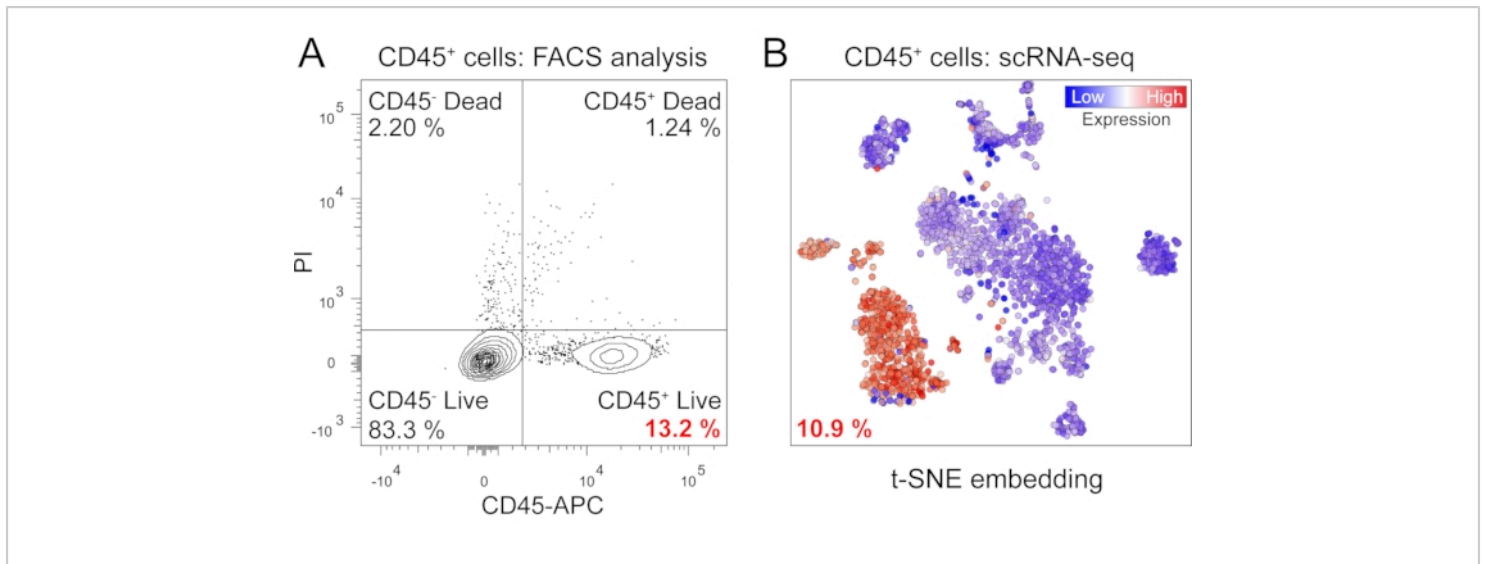


**Figure 3: Quantification of the immune cells.** Quantification of the immune cells was performed by FACS analysis of cells stained with anti-CD45 antibody and Live/Dead analysis using propidium iodide staining (A). Further quantification of immune cells was performed during scRNA-seq analysis (B). (CD45-APC - anti-CD45 allophycocyanin conjugated antibody; PI - propidium iodide; t-SNE - t-distributed stochastic neighbor embedding). [Please click here to view a larger version of this figure.](#)

**Supplementary Figure 1: Overview of the mandible dissection process.** Dashed lines illustrate suggested cuts. TMJ - temporomandibular joint, m. masseter - musculus masseter. [Please click here to download this File.](#)

**Supplementary Table 1: The compositions of the solutions used in the study.** [Please click here to download this Table.](#)

## Discussion

Studying teeth and bones on the cellular or molecular level is generally challenging since cells forming these tissues are surrounded by different kinds of hard matrices<sup>19</sup>. One of the main goals for performing single-cell RNA-seq on dental tissue is the need to obtain cells of interest fast and without any artificial changes in their transcriptomes. To accomplish this, a highly efficient protocol suitable for

isolating cells from mouse and human tooth pulps was developed, which allows for quick generation of single-cell suspensions for all transcriptomic applications. This was ensured by fast tissue isolation, minimizing the steps of tissue and cell manipulations, and streamlining the mechanical and enzymatic digestion.

The most critical steps of this protocol are fast tissue processing and adequate single-cell suspension preparation<sup>8,9</sup>. A manual approach is used to obtain dental pulps without utilizing a dental drill or other heat-generating devices. Overheating may cause an artificial expression of heat shock proteins and other genes, ultimately leading to the analyzed gene expression patterns being unrepresentative of the original tissue<sup>20</sup>. Manual tissue harvesting may be a challenging step that will likely need some training beforehand. The pulp is then cut into small pieces and

enzymatically digested at 37 °C. Except for the 15-20 min of enzymatic digestion, the whole protocol is performed at 4 °C. The tissue processing and especially the enzymatic digestion were minimized to the shortest possible time since more prolonged incubation at 37 °C can cause changes in gene expression patterns<sup>10</sup>. Mechanical removing of the dentin is recommended before enzymatic digestion. Dentin and the pulp-attached predentin contain a large amount of collagen, and its excessive presence might decrease the effectiveness of the digesting solution. After being removed from the body (or death of organisms), it was shown that cells start to modify their gene expression patterns quickly<sup>12</sup>. Therefore, cell isolation and processing should be carried out as fast as possible. The current protocol reduces the processing time to 35-45 min from isolating the tissue (euthanizing animal) to preparing single-cell suspension.

One alternative modification of this technique is cell preservation for later use. This is achieved by methanol fixation. Methanol-fixed cell suspension can be stored for up to 1 month at -80 °C, as described in the protocol<sup>21</sup>. However, whenever possible, perform scRNA-seq directly, since it was shown that the single-cell data from methanol-fixed single-cell suspensions might suffer from increased expression of stress-related genes and contamination with ambient RNA<sup>22</sup>. This step might need additional modification according to the manufacturer's protocols.

Before the first application of this protocol, performing several validation steps are recommended to test the technique. From our experience, we suggest testing the aforementioned critical steps of the protocol. Additionally, we suggest testing the effectiveness of the collagenase P solution and testing the handling of the tissue dissociation step. Specifically, around the first 5 min after the initiation of collagenase P incubation,

the pieces of tissue should aggregate together. This is a common situation. Aggregates are disintegrated every 3-4 min using a 1 mL pipette, and with increasing time, they should become smaller until barely visible.

Furthermore, it is recommended to perform cell counting in a cell counting chamber before centrifugation and before and after filtering to detect possible cell losses due to suboptimal supernatant removal. If the final single-cell suspension needs to be purified, FACS can be used. Cell sorting enables not only to remove debris or dead cells but importantly enables to enrich final suspension with fluorescently labeled cells<sup>13,19</sup>. To avoid shear stress or clogging of the cell sorter, a wide nozzle (85 µm or 100 µm) is used. This will further improve the viability of the sorted cells.

This technique was designed and tested on both mouse and human teeth. The major limiting factor is the small number of cells in the reduced dental pulps of the teeth of older mice (molars) and humans. Suppose a larger number of cells need to be obtained or cells from the teeth of older patients are to be acquired. One possible solution is to process a higher number of teeth and merge them into a single batch, subsequently processed as one sample.

Living cells of human dental pulp were firstly isolated more than twenty years ago using an enzyme mixture of collagenase I and dispase<sup>23</sup>. Since then, isolations of dental pulp cells became widely utilized, and several techniques have been used<sup>5,6,7,8</sup>. The critical significance of the method presented here is the adaption of all isolation steps to make the isolation fast and gentle to ensure the high quality of the final cell suspension for scRNA-seq. Higher cell yield can be obtained by more prolonged incubation with enzymes. This protocol provides an efficient solution for quickly obtaining single cells from mouse and human teeth of suitable quality

for single-cell RNA-sequencing. This technique is expected to be widely used for other tissues or organisms with just slight technical modifications.

## Disclosures

Authors declare no conflicts of interest.

## Acknowledgments

J.K. was supported by the Grant Agency of Masaryk University (MUNI/H/1615/2018) and by funds from the Faculty of Medicine MU to junior researcher. J.L. was supported by the Grant Agency of Masaryk University, (MUNI/IGA/1532/2020) and is a Brno Ph.D. Talent Scholarship Holder - Funded by the Brno City Municipality. T.B. was supported by the Austrian Science Fund (Lise Meitner grant: M2688-B28). We thank to Lydie Izakovicova Holla and Veronika Kovar Matejova for their help with the obtaining of human teeth. Finally, we thank Radek Fedr and Karel Soucek for their kind assistance with FACS sorting.

## References

1. Krivanek, J. et al. Dental cell type atlas reveals stem and differentiated cell types in mouse and human teeth. *Nature Communications*. **11** (1), 4816 (2020).
2. Soldatov, R. et al. Spatiotemporal structure of cell fate decisions in murine neural crest. *Science*. **364** (6444) (2019).
3. Machado, L., Relaix, F., Mourikis, P. Stress relief: emerging methods to mitigate dissociation-induced artefacts. *Trends in Cell Biology*. **0** (0) (2021).
4. Nguyen, Q. H., Pervolarakis, N., Nee, K., Kessenbrock, K. Experimental considerations for single-cell RNA sequencing approaches. *Frontiers in Cell and Developmental Biology*. **6** (2018).
5. Chiba, Y. et al. Single-cell RNA-sequencing from mouse incisor reveals dental epithelial cell-type specific genes. *Frontiers in Cell and Developmental Biology*. **8** (2020).
6. Debnath, S. et al. Discovery of a periosteal stem cell mediating intramembranous bone formation. *Nature*. **562** (7725), 133-139 (2018).
7. Kanton, S., Treutlein, B., Camp, J. G. Chapter 10 - Single-cell genomic analysis of human cerebral organoids. *Methods in Cell Biology*. **159**, 229-256 (2020).
8. Price, F. D. et al. Inhibition of JAK-STAT signaling stimulates adult satellite cell function. *Nature Medicine*. **20** (10), 1174-1181 (2014).
9. van den Brink, S. C. et al. Single-cell sequencing reveals dissociation-induced gene expression in tissue subpopulations. *Nature Methods*. **14** (10), 935-936 (2017).
10. O'Flanagan, C. H. et al. Dissociation of solid tumor tissues with cold active protease for single-cell RNA-seq minimizes conserved collagenase-associated stress responses. *Genome Biology*. **20** (1), 210 (2019).
11. van Velthoven, C. T. J., de Morree, A., Egner, I. M., Brett, J. O., Rando, T. A. Transcriptional profiling of quiescent muscle stem cells in vivo. *Cell Reports*. **21** (7), 1994-2004 (2017).
12. Miyawaki-Kuwakado, A. et al. Transcriptome analysis of gene expression changes upon enzymatic dissociation in skeletal myoblasts. *Genes to Cells*. **26** (7), 530-540 (2021).
13. Mattei, D. et al. Enzymatic dissociation induces transcriptional and proteotype bias in brain cell

- populations. *International Journal of Molecular Sciences*. **21** (21), 7944 (2020).
14. Ferreira, P. G. et al. The effects of death and post-mortem cold ischemia on human tissue transcriptomes. *Nature Communications*. **9** (1), 490 (2018).
  15. He, W., Ye, J., Xu, H., Lin, Y., Zheng, Y. Differential expression of  $\alpha 6$  and  $\beta 1$  integrins reveals epidermal heterogeneity at single-cell resolution. *Journal of Cellular Biochemistry*. **121** (3), 2664-2676 (2020).
  16. Machado, L. et al. In situ fixation redefines quiescence and early activation of skeletal muscle stem cells. *Cell Reports*. **21** (7), 1982-1993 (2017).
  17. Laranjeira, C. et al. Glial cells in the mouse enteric nervous system can undergo neurogenesis in response to injury. *The Journal of Clinical Investigation*. **121** (9), 3412-3424 (2011).
  18. Song, X. et al. Improved strategy for jet-in-air cell sorting with high purity, yield, viability and genome stability. *FEBS Open Bio*. **11** (9), 2453-2467 (2021).
  19. Greenblatt, M. B., Ono, N., Ayturk, U. M., Debnath, S., Lalani, S. The unmixing problem: A guide to applying single-cell RNA sequencing to bone. *Journal of Bone and Mineral Research*. **34** (7), 1207-1219 (2019).
  20. Charlebois, D. A., Hauser, K., Marshall, S., Balázsi, G. Multiscale effects of heating and cooling on genes and gene networks. *Proceedings of the National Academy of Sciences*. **115** (45), E10797-E10806 (2018).
  21. Chen, J. et al. PBMC fixation and processing for Chromium single-cell RNA sequencing. *Journal of Translational Medicine*. **16** (1), 198 (2018).
  22. Denisenko, E. et al. Systematic assessment of tissue dissociation and storage biases in single-cell and single-nucleus RNA-seq workflows. *Genome Biology*. **21** (1), 130 (2020).
  23. Gronthos, S., Mankani, M., Brahimi, J., Robey, P. G., Shi, S. Postnatal human dental pulp stem cells (DPSCs) in vitro and in vivo. *Proceedings of the National Academy of Sciences of the United States of America*. **97** (25), 13625-13630 (2000).